CONF-811087--

DE82 019828

CONF-811087

Proceedings of the Fourth Symposium on the Physics and Technology of Compact Toroids

Held at Lawrence Livermore National Laboratory October 27-29, 1981

R. F. Post

W. C. Turner

Editors

Lawrence Livermore National Laboratory

Manuscript Date: June 11, 1982

LAWRENCE LIVERMORE LABORATORY
University of California • Livermore, California • 94550

Available from: National Technical Information Service • U.S. Department of Commerce
5285 Port Royal Road • Springfield, VA 22161 • $15.00 per copy • (Microfiche $3.50)

DISTRIBUTION OF THIS DOCUMENT IS UNLIMITED

CONTENTS

Page

PROGRAM 1

REVIEW OF SYMPOSIUM 3

POSTER SESSIONS 9

SYMPOSIUM PAPERS 13

I. Field Reversed Theta Pinch-Theory 13

I-1. The Analytical and Numerical Calculations of Field Reversed Theta Pinch Equilibria Based on a Generalized Hill's Vortex Model (D. V. Anderson, J. H. Hammer, D. C. Barnes) 15

I-2. An Integral Poloidal Flux Squared Invariant Model of the Relaxation of a Field Reversed Theta Pinch (J. E. Brandenburg) 19

I-3. Rotational Instabilities in the FRC: Results of Hybrid Simulations (D. S. Harned) 24

I-4. Equilibrium and Power Balance Constraints on a Quasi-Static, Ohmically-Heated FRC (K. F. McKenna, D. J. Rej, M. Tuszewski) 28

I-5. Nonadiabatic Scattering and Transport at the Spindle Cusp (R. W. Moses, D. W. Hewett) 32

I-6. Ion Kinetic Effects on the Tilt Mode in FRCs (J. L. Schwarzmeier, C. E. Seyler, D. C. Barnes) 35

I-7. Quasistatic Evolution of Compact Toroids (A. G. Sgro, R. L. Spencer, C. Lilliequist) 39

I-8. Multiple Solutions of a Free Boundary FRC Equilibrium Problem in a Metal Cylinder (R. L. Spencer, D. W. Hewett) 43

I-9. Plasma Transport Modeling of a Field-Reversed Theta Pinch (L. C. Steinhauer, R. D. Milroy, A. L. Hoffman) 47

I-10. Particle Transport in Field Reversed Configurations (M. Tuszewski, R. K. Linford, J. Lipson, A. G. Sgro) 51

CONTENTS (continued)

Page

II. Field Reversed Theta Pinch Experiment 55

II-1. Initial Operation of FRX-C 57
(W. T. Armstrong, R. R. Bartsch, J. C. Cochrane, R. W. Kewish, M. Haworth, R. K. Linford, J. Lipson, K. F. McKenna, D. J. Rej, E. G. Sherwood, R. E. Siemon, M. Tuszewski)

II-2. Compact Toroid Formation Using Barrier Fields and Controlled Reconnection in the TRX-1 Field Reversed Theta Pinch 61
(A. L. Hoffman, W. T. Armstrong)

II-3. Onset Time of n = 2 Rotational Instability of FRC Plasma 65
(Y. Nogi, S. Shimamura, Y. Osanai, K. Saito, K. Yokoyama, S. Shiina, S. Hamada, H. Yoshimura, T. Minato, M. Tanjyo, S. Okada, Y. Ito, S. Ohi, S. Goto, T. Ishimura, H. Ito, Y. Aso, S. Himeno, K. Hirano, C. Wu)

II-4. Reconnection Studies in a Low-Compression Theta Pinch 69
(E. Sevillano, F. L. Ribe, H. Meuth)

III. Spheromak - Theory 73

III-1. Analytic Model of Radiation-Dominated Decay of a Compact Toroid 75
(S. P. Auerbach)

III-2. A Theory of the Relaxation of Finite Beta Toroidal Plasmas 79
(J. E. Brandenburg)

III-3. Compressible MHD Fluctuations 84
(E. Hameiri, H. A. Rose)

III-4. Current Drive, Heating and Fueling by Compact Torus Injection 88
(J. H. Hammer, C. W. Hartman)

III-5. A New Type of Collective Accelerator 91
(C. W. Hartman, J. H. Hammer)

III-6. MHD Simulation and the Implication in Reactor Concept of Merging Spheromaks 102
(M. Katsurai, K. Katayama, T. Sato)

CONTENTS (continued)

Page

III-7. Resistive MHD Stability Calculations of Force-Free Spheromak Configurations (A. I. Shestakov, N. J. O'Neill) 106

III-8. Numerical Simulation of a Beam Heated Compact Torus (D. E. Shumaker, B. McNamara, W. C. Turner) 110

III-9. Numerical Simulation of the Energy Balance in the Proto S-1C Spheromak (Y. C. Sun, S. C. Jardin, D. Heifetz, M. Yamada, D. E. Post) 114

III-10. Formation and Merging of Spheromaks and Formation of FRC (T. Sato, S. Otsuka, K. Araki) 118

IV. Spheromak - Experiment 123

IV-1. Plasma Impurity Control Studies in CTX (C. W. Barnes, I. Henins, H. W. Hoida, T. R. Jarboe, R. K. Linford, J. Marshall, A. R. Sherwood, M. Tuszewski) 125

IV-2. Metallic Liner, Electrode Material, and Stabilization Coil Studies in the PS-1 Experiment (H. Bruhns, C. Chin-Fatt, Y. P. Chong, A. W. DeSilva, G. C. Goldenbaum, H. R. Griem, G. W. Hart, R. A. Hess, R. Shaw) 129

IV-3. Properties of Spheromaks Generated by a Magnetized Coaxial Source (H. W. Hoida, I. Henins, T. R. Jarboe, R. K. Linford, J. Lipson, J. Marshall, D. A. Platts, A. R. Sherwood, M. Tuszewski) 133

IV-4. Spheromak Experiments in Proto S-1C (A. Janos, S. Cowley, H. Hsuan, S. Paul, C. Skinner, F. Wysocki, M. Yamada) 137

IV-5. Creation of a Spheromak by a Conical Theta-Pinch (K. Kawai, Z. A. Pietrzyk) 142

IV-6. RF Heating Plans for CTX (S. O. Knox, B. L. Wright) 145

CONTENTS (continued)

		Page
IV-6.	MHD Stability Studies in the Proto S-1 A/B Device (C. Munson, A. Janos, M. Newhouse, F. Salberta, F. Wysocki, M. Yamada)	149
IV-7.	A New Approach to Controlling Impurity Contamination of a Plasma-Gun-Produced Compact Torus (R. F. Post, W. C. Turner)	153
IV-8.	Beta II Compact Torus Experiment - Plasma Equilibrium and Power Balance (W. C. Turner, D. S. Prono, C. W. Hartman, J. Taska, G. C. Goldenbaum, E. H. A. Granneman)	158
IV-9.	Experiments on CT Merging in the CTCC-1 (K. Watanabe, K. Ikegami, M. Nishikawa, A. Ozaki, N. Satomi, T. Uyama)	164
V.	General	169
V-1.	Traveling Mirror Adiabatic Compressor (P. M. Bellan)	171
V-2.	Analytic Field Reversed Mirror Equilibrium With an Electric Field (J. K. Boyd)	174
V-3.	Present Status of REB Ring Studies at Institute of Plasma Physics, Nagoya University (M. Hasegawa, A. Mohri, K. Narihara, Y. Tomita, J. Tsuzuki)	178
V-4.	Anomalous Diffusion in Toroidal Plasma (N. A. Krall)	182
V-5.	MeV and GeV Prospects for Producing a Large Ion Layer Configuration for Fusion Power Generation (J. R. McNally, Jr.)	231
V-6.	Propagation of Intense Charge-Neutral Ion Beams in Magnetic Fields (S. Robertson, H. Ishizuka, W. Peter, N. Rostoker)	233
V-7.	Generation of a Compact Torus with a μ-s Rotating Relativistic Electron Beam (G. Saenz)	237

CONTENTS (continued)

Page

V-8. The Prototype Moving-Ring Reactor 241
(A. C. Smith, Jr., C. P. Ashworth, K. E. Abreu, D. M. Woodall, G. A. Carlson, W. S. Neef, Jr., H. H. Fleischmann, W. Grossman, Jr., T. Kammash, K. R. Schultz, C. P. C. Wong, D. K. Bhadra, R. L. Creedon, E. T. Cheng, G. R. Hopkins)

V-9. Review of Japanese CT Studies 245
(K. Watanabe)

CONFERENCE ATTENDEES 249

PROGRAM

Tuesday, October 27, 1981

9:00 - 9:05 am	T. K. Fowler - Welcoming Remarks
9:05 - 9:20 am	R. F. Post - Fusion vs Field Reversal or Fusion Via Field Reversal?
9:20 - 10:05 am	M. Tuszewski - Review of Reversed Field Theta Pinch Experiments
10:05 - 10:20 am	Discussion
10:20 - 10:40 am	Break
10:40 - 11:25 am	D. Schnack - Review of Reversed Field Theta Pinch Theory
11:25 - 11:40 am	Discussion
11:40 - 12:30 pm	T. Watanabe - Review of Japanese Compact Torus Program
12:30 - 2:00 pm	Lunch
2:00 - 4:00 pm	Poster Session A: Spheromak Theory, Field-Reversed Theta Pinch Experiments, Particle Beams and Rings
4:00 - 5:00 pm	MFE Facility tours
5:00 - 6:00 pm	Wine and cheese reception

Wednesday, October 28, 1981

9:00 - 9:40 am	G. C. Goldenbaum - Review of Spheromak Experiments
9:40 - 9:55 am	Discussion
9:55 - 10:35 am	J. H. Hammer - Spheromak Theory Review
10:35 - 10:50 am	Discussion
10:50 - 11:10 am	Break
11:10 - 11:50 am	S. Jardin - Stability Studies of Spheromaks
11:50 - 12:05 pm	Discussion
12:05 - 1:00 pm	J. DiMarco - Review of Recent Reversed Field-Pinch Results
1:00 - 2:00 pm	Conference luncheon
2:00 - 4:00 pm	Poster Session B: Spheromak Experiments, Field-Reversed Theta Pinch Theory

Thursday, October 29, 1981

9:00 - 9:45 am	S. Robertson - Review of Application of Particle Beams to Compact Tori
9:45 - 10:00 am	Discussion
10:00 - 10:20 am	Break
10:20 - 11:25 am	D. Post - Impurity Radiation Issues in Short Time Scale Experiments
11:25 - 11:40 am	Discussion
11:40 - 12:25 pm	N. Krall - Review of Anomalous Transport in Toroidal Devices
12:25 - 12:40 pm	Discussion
12:40 pm	Conference Wrap-up

REVIEW OF THE FOURTH SYMPOSIUM ON THE PHYSICS AND TECHNOLOGY OF COMPACT TOROIDS

R. F. Post

Hosted by the Lawrence Livermore National Laboratory, the Fourth Symposium on the Physics and Technology of Compact Toroids took place on the 27-29 October 1981. Attendees, numbering 80, heard 10 review papers in three morning plenary sessions, and interacted in two afternoon poster sessions where some 45 contributions were presented. There were 7 participants from overseas, including 6 scientists from Japan, and 1 from West Germany. Immediately following the Symposium, a two-day Joint U.S./Japan workshop on compact toroid research was held.

The review papers were chosen by the Program Committee with two objectives in mind: First, to inform the attendees of the state of the compact torus art, in experiment and in theory, in the two mainline approaches to compact torus research--the field-reversed theta pinch and the spheromak configuration. Second, to provide in-depth reviews by acknowledged experts of related fields (e.g. the reversed-field Z pinch) and/or common concerns (for example, particle transport) of interest to compact torus researchers.

In the first category, review papers by M. Tuszewski (LANL) and by D. Schnack (LANL) covered experiments and theory, respectively, in reversed-field theta pinch research. Of particular interest in these studies is the elucidation of the long-duration, grossly-stable regimes there encountered, the existence of which is in apparent disagreement with the predictions of fluid (MHD) theory. The entities that we refer to here might be described as "elongated Hill's vortices," reversed-field configurations characterized by the total absence of toroidal field components. Finite orbit effects may be able to explain both the existence of these grossly stable regimes, and aspects of their behavior at termination, when the plasma typically exhibits a rapidly-growing elliptical ($m = 2$) rotational mode. Probably related also is the observation of non-classical rates of cross-field transport, apparently explainable in terms of the so-called "lower hybrid" mode, driven by steep field gradients near the separatrices, the steepness of the gradient being associated with the small size of the present experimental plasmas.

Again in the first category, the review papers by G. Goldenbaum (U. Maryland), J. Hammer (LLNL), and S. Jardin (PPPL) covered experimental (G. G.) and theoretical (J. H. and S. J.) work to date on spheromak plasmas. Here the good news is that the configurations achieved are seen to adhere closely to the (favorable) predictions of the theory of so-called "Taylor minimum-energy states," exhibiting remarkable and controllable grossly stable behavior, both in their formation and their subsequent gross behavior. The bad news is that in apparently every such experiment electron temperatures are low (10 to 20 eV), being dominated by impurity radiation losses. As a consequence, magnetic field energy decay lifetimes (some hundreds of microseconds) are severely limited. This conclusion was verified by direct measurement of radiation losses, and by correlations with preliminary measures (discharge charging) aimed at reducing the impurity levels.

A review paper was also given (T. Watanabe) covering compact torus research in Japan. It was evident from this paper that this field of fusion research is growing rapidly in Japan, with results coming already from new experiments. Of particular interest was the report of the merging of compact torus plasmas, a technique which could possibly lead to a means for continuously maintaining such entities.

In the second category of review papers, subjects of general interest, the four papers given included: A review of reversed-field Z-pinch work (J. DiMarco, LANL); a review of the application of particle beams to compact torus research (S. Robertson, Irvine); a general discussion of impurity radiation issues (D. Post, PPPL); and a review of the theory of anomalous transport in toroidal devices (N. Krall, Jaycor).

(J. DiMarco) In that they seek a minimum-energy state, reversed-field Z-pinches, such as the ZT-40 at LANL, share physics with spheromaks; in that their plasmas are large aspect ratio entities of toroidal rather than spherical topology, they do not. Nevertheless, the transport processes involved in each may turn out to be similar. Determining whether or not this is the case, however, we must await the impurity clean-up of spheromak plasmas, a condition now adequately achieved in ZT-40 at LANL, greatly aided by the circumstances that, relative to impurity radiation rates, heating energy inputs are much higher than is presently the case in spheromak plasmas.

(S. Robertson) Particle beams have played a role in fusion research since its earliest days. Their earliest entry into the subject of field-reversed plasmas come through work on the ASTRON concept of Christofilos. Since those early experiments new techniques have appeared, in particular high current electron and ion diode generators, that benefit both the ASTRON concept and newer ones. In the Cornell experiment of Fleischmann and co-workers, field-reversing ASTRON-type electron rings, recently translated and magnetically compressed, have been studied. Most recently it has been found possible to embed these rings in a background plasma within which diamagnetic currents have been induced, leading to field-reversed entities that consist of a mixture of circulating high energy electrons and of currents carried in the background plasma. Attention is also being given to the possibility of creating such hybrid particle ring-plasma entities with energetic ions derived from pulsed diode generators. In work at Irvine it has been shown that very high current ion beams can be transported across a magnetic field (and, presumably, into a field-reversed configuration). The technique, involving the presence of space-charge neutralizing electrons and the production of a transverse electric field by polarization, may become important for the creating and/or sustaining of field-reversed plasma entities.

(D. Post) Owing in large part to interest in the subject stimulated by impurity problems in tokamaks, the physics of impurity radiation is by now well understood. Computer codes are now available to model almost any situation of interest in fusion research. These codes, applied to compact torus experiments, provide additional confirmation that their present performance is limited by power losses to impurity radiation, which is clamping the electron temperature and thereby shortening the magnetic field decay time through attendant ohmic losses in the plasma.

(N. Krall) A central issue for all toroidal confinement systems is that of cross-field transport, known to be anomalous in virtually all such systems. A starting point for the theoretical treatment of anomalous transport is the quasi-linear theory. In the context of field-reversed systems, this formalism has been applied with success to the case of the reversed-field theta pinch. Here the unstable wave during the transport is taken to be the lower hybrid wave. As shown by Linford and Hamasaki, the analysis yields a scaling for confinement times varying as R^2/a_i, plasma radius (to max density) squared, divided by mean ion gyroradius. This scaling seems to fit the experimental results well, over a range of $40 \leq R^2/a_i \leq 120$ cm ($25 \leq \tau \leq 65$ μs). Whether this scaling will continue to longer values of the scaling parameters, allowing thereby much larger τ values, is of course not yet known.

In the regimes one expects other sources of anomalous transport to occur, such as resistive interchanges, and trapped electron modes may have relevance. These have, of course, been studied extensively in connection with tokamak theory. How they will apply to compact toroids is not at this time clear. What is clear, however, is that one cannot a priori assume that anomalous transport will necessarily be negligible in such systems. It is, therefore, fortunate that one need not achieve anything approaching classical transport rates to achieve adequate confinement for fusion purposes in a compact torus system: There is a "margin of safety."

In the poster sessions the papers submitted spanned the spectrum of compact torus research. A random selection includes:

- Studies of the onset time of rotational instabilities in a FRC plasma (T. Nogi et al., Nihon University, Japan).
- Initial operation of FRX-C (the new LANL compact torus facility) (W. T. Armstrong, et al., LANL).
- Analytic model of radiation-dominated decay of a compact toroid (S. Auerbach, LLNL).
- Spheromak experiments in Proto. S-1C (M. Yamada et al., PPPL).
- Particle transport in field-reversed configurations (M. Tuszewski, LANL).

Considering the totality of the poster papers, and comparing them broadly with the work reported in the previous (Third) Symposium, some evident advances can be seen, both in experiment and in theory. In spheromak experiments a much better understanding of the tilting and shifting instabilities and their control has been gained. At the same time the essential role played by impurity radiation losses in limiting lifetimes has been made clear, and has been confirmed by theory and by computer code calculations. In field-reversed theta-pinch research new facilities have been brought into operation, and a better experimental understanding has been gained of the limits on lifetime of the plasma entities, including plausible theoretical scaling laws. More generally, it appears that the ground work has now been laid for the next round of improvements in the performance of compact torus systems, improvements that could include a major increase in the electron temperature and, presumably therefore, the lifetime of spheromak plasmas.

As noted earlier, the Symposium was followed by a Joint U.S./Japan Workshop on Compact Torus research. The mode of the workshop was, by definition, less structured leaving more time for detailed discussion. Highlights from the workshop included:

- A discussion of the very interesting Japanese work on the merging of two spheromak configurations
- Recent Cornell work on hybrid electron ring-plasma field-reversed configurations, including experiments on inducing circulating currents in the plasma.

Summarizing the week's activities, it can be fairly said that compact torus research has, in its newer areas, graduated from a purely exploratory phase to one of more clearly defined goals, with progress toward those goals already being made. In the older approaches, such as that of particle rings and the reversed-field theta pinch, new facilities are appearing, and with them, improved understanding of the physics issues involved. Specifically, the stability of particle ring-plasma hybrids is being explored both theoretically and experimentally (Cornell); the radial transport and rotational instability of reversed-field theta pinches is being explored, both in the U.S. (LANL and Math Sciences N.W) and in Japan (Nihon University). Perhaps of greatest significance is the fact that it is now being widely recognized that MHD stable field-reversed configurations of a variety of forms can exist and that these configurations could have a very important role to play in the development of fusion power, particularly with respect to their intrinsic size advantage and their potential with respect to fusion systems employing advanced fuels.

POSTER SESSIONS

Poster Session A: 2:00 - 4:00 Tuesday, October 27

A-1. Initial Operation of FRX-C
(W. T. Armstrong, R. R. Bartsch, J. C. Cochrane, R. W. Kewish, M. Hayworth, R. K. Linford, J. Lipson, K. F. McKenna, D. J. Rej, E. G. Sherwood, R. E. Siemon, M. Tuszewski)

A-2. Compact Toroid Formation Using Barrier Fields and Controlled Reconnection in the TRX-1 Field Reversed Theta Pinch
(A. L. Hoffman, W. T. Armstrong)

A-3. Onset Time of n = 2 Rotational Instability of FRC Plasma
(Y. Nogi, S. Shimamura, Y. Osanai, K. Saito, K. Yokoyama, S. Shiina, S. Hamada, H. Yoshimura, T. Minato, M. Tanjyo, S. Okada, Y. Ito, S. Ohi, S. Goto, T. Ishimura, H. Ito, Y. Aso, S. Himeno, K. Hirano)

A-4. Reconnection Studies in a Low-Compression Theta Pinch
(E. Sevillano, F. L. Ribe, H. Meuth)

A-5. Current Drive, Heating and Fueling by Compact Torus Injection
(J. H. Hammer, C. W. Hartman)

A-6. A New Type of Collective Accelerator
(C. W. Hartman, J. H. Hammer)

A-7. Compressible MHD Fluctuations
(E. Hameiri, H. A. Rose)

A-8. Drift Orbits in Spheromak Configurations
(H. Biglari, M. Bensadoun, H. H. Fleischmann)

A-9. Resistive MHD Stability Calculations of Force-Free Spheromak Configurations
(A. I. Shestakov, N. J. O'Neill)

A-10. Numerical Simulation of the Energy Balance in the Proto S-1C Spheromak
(Y. C. Sun, S. C. Jardin, D. Heifetz, M. Yamada, D. E. Post)

A-11. Quasistatic Evolution of Compact Toroids
(A. G. Sgro, R. L. Spencer, C. Lilliequist)

A-12. Numerical Simulation of a Beam Heated Compact Torus
(D. E. Shumaker, B. McNamara, W. C. Turner)

A-13. A Theory of the Relaxation of Finite Beta Toroidal Plasmas
(J. E. Brandenburg)

A-14. Analytic Model of Radiation-Dominated Decay of a Compact Toroid
(S. P. Auerbach)

A-15. Particle Transport in Field Reversed Configurations
(M. Tuszewski, R. K. Linford, J. Lipson, A. G. Sgro)

A-16. MHD Simulation and the Implication in Reactor Concept of Merging Spheromaks
(M. Katsurai, K. Katayama, T. Sato)

A-17. Formation and Merging of Spheromaks and Formation of FRC
(T. Sato, S. Otsuka, K. Araki)

A-18. The Prototype Moving-Ring Reactor
(A. C. Smith, Jr., G. A. Carlson, H. H. Fleischmann, C. P. C. Wong)

A-19. Traveling Mirror Adiabatic Compressor
(P. M. Bellan)

A-20. Induction of Large Plasma Currents in Electron Rings-Hybrid CT Configuration
(R. Jaykumar, D. Taggart, M. R. Parker, H. H. Fleischmann)

A-21. Propagation of Intense Charge-Neutral Ion Beams in Magnetic Fields
(S. Robertson, H. Ishizuka, W. Peter, N. Rostoker)

A-22. CT Formation with Electron Beams
(J. D. Sethian, K. A. Gerber, A. W. DeSilva, A. E. Robson)

A-23. Investigation of a 1 μs Relativistic Electron Beam Injected Into a Toroidal Magnetic Field
(G. Saenz, A. Fisher)

A-24. MeV and GeV Prospects for Producing a Large Ion Layer Configuration for Fusion Power Generation
(J. R. McNally, Jr.)

Poster Session B: 2:00 - 4:00 Wednesday, October 28

B-1. MHD Stability Studies in the Proto S-1 A/B Device
(C. Munson, A. Janos, M. Newhouse, E. Salberta, F. Wysocki, M. Yamada)

B-2. Spheromak Experiments in Proto S-1C
(A. Janos, S. Cowley, H. Hsuan, S. Paul, C. Skinner, F. Wysocki, M. Yamada)

B-3. Experiments on CT Merging in the CTCC-1
(K. Watanabe, K. Ikegami, M. Nishikawa, A. Ozaki, N. Satomi, T. Uyama)

B-4. Beta II Compact Torus Experiment - Plasma Equilibrium and Power Balance
(W. C. Turner, D. S. Prono, C. W. Hartman, J. Taska, G. C. Goldenbaum, E. H. A. Granneman)

B-5. A New Approach to Controlling Impurity Contamination of a Plasma-Gun-Produced Compact Torus
(R. F. Post, W. C. Turner)

B-6. Properties of Spheromaks Generated by a Magnetized Coaxial Source
(H. W. Hoida, I. Henins, T. R. Jarboe, R. K. Linford, J. Lipson, J. Marshall, D. A. Platts, A. R. Sherwood, M. Tuszewski)

B-7. Plasma Impurity Control Studies in CTX
(C. W. Barnes, I. Henins, H. W. Hoida, T. R. Jarboe, R. K. Linford, J. Marshall, A. R. Sherwood, M. Tuszewski)

B-8. RF Heating Plans for CTX
(S. O. Knox, B. L. Wright)

B-9. Metallic Liner, Electrode Material, and Stabilization Coil Studies in the PS-1 Experiment
(H. Bruhns, C. Chin-Fatt, Y. P. Chong, A. W. DeSilva, G. C. Goldenbaum, H. R. Griem, G. W. Hart, R. A. Hess, R. Shaw)

B-10. Creation of a Spheromak by a Conical Theta-Pinch
(K. Kawai, Z. A. Pietrzyk)

B-11. The Analytical and Numerical Calculations of Field Reversed Theta Pinch Equilibria Based on a Generalized Hill's Vortex Model
(D. V. Anderson, J. H. Hammer, D. C. Barnes)

B-12. Analytic Field Reversed Mirror Equilibrium With an Electric Field
(J. K. Boyd)

B-13. An Integral Poloidal Flux Squared Invariant Model of the Relaxation of a Field Reversed Theta Pinch
(J. E. Brandenburg)

B-14. Ion Kinetic Effects on the Tilt Mode in FRCs
(J. L. Schwarzmeier, C. E. Seyler, D. C. Barnes)

B-15. Multiple Solutions of a Free Boundary FRC Equilibrium Problem in a Metal Cylinder
(R. L. Spencer, D. W. Hewett)

B-16. Equilibrium and Power Balance Constraints on a Quasi-Static, Ohmically-Heated FRC
(K. F. McKenna, D. J. Rej, M. Tuszewski)

B-17. Plasma Transport Modeling of a Field-Reversed Theta Pinch
(L. C. Steinhauer, R. D. Milroy, A. L. Hoffman)

B-18. Particle Transport in Field-Reversed Configuration
(M. Tuszewski, R. K. Linford, J. Lipson, A. G. Sgro)

B-19. Rotational Instabilities in the FRC: Results of Hybrid Simulations
(D. S. Harned)

B-20. Nonadiabatic Scattering and Transport at the Spindle Cusp
(R. W. Moses, D. W. Hewett)

I. FIELD REVERSED THETA PINCH THEORY

The Analytical and Numerical Calculations of Field Reversed Theta Pinch Equilibria Based on a Generalized Hill's Vortex Model

D. V. Anderson
National Magnetic Fusion Energy Computer Center
Lawrence Livermore National Laboratory
Livermore, California

J. H. Hammer
Mirror Program
Lawrence Livermore National Laboratory
Livermore, California

D. C. Barnes
Institute for Fusion Studies
University of Texas
Austin, Texas

We have been investigating methods for numerically extending the analytic solutions of field reversed theta pinch equilibria so that the results may be used in various stability and dynamics studies. We have used generalizations of elliptical Hill's vortex equilibria which accomodate separatrices with more rectangular shapes and which allow plasma to exist outside the separatrix. Although the equilibria are specified analytically inside the plasma surface, numerical techniques are required to generate the solution in the vacuum region. Two computer codes have been used in sequence. The first determines a set of external coils and their currents so that they match the known coil field inside the plasma. Then, given this coil field, we compute the contribution from the plasma currents to the fields in the vacuum region.

Extensions of Berk, Hammer, and Weitzner (BHW) Analytical Equilibria

A generalization of Hill's vortex type equilibria has been given by Berk, Hammer, and Weitzner.[1] For flux surfaces inside the separatrix the flux function is specified by

---

Work performed under the auspices of the U. S. D. O. E. by the Lawrence Livermore National Laboratory under contract number W-7405-ENG-48 and by the University of Texas under contract number DE-FG-80-ET-53088.

$$\psi = \psi_0\left(-\frac{x^2}{2} - \sum_{n=1}^{N} A_n \sum_{q=1}^{n} \frac{(-1)^q x^{n-q+1} z^{2q-2}}{g(n,q)}\right)$$

where

$$x = \frac{1}{2}\left(\frac{r}{r_{sep}}\right)^2$$

and

$$g(n,q) = (n - q)!(n - q + 1)!(2q - 2)!2^{n-q}$$

By specifying the elongation of the separatrix, by requiring the shape of the separatrix near the midplane to vary like $r = z^{2(N-1)}$ and by the requirement that $\psi = 0$ at the separatrix, we obtain N linear equations to determine the N unknowns A_n. These are solved by the code SEECOD.

Model Solved in the code SEECOD

From the forms given above for the flux ψ we may compute the current density as follows:

$$J_\theta = \frac{1}{r}\Delta^{*}\psi = + \frac{1}{r}\psi_0\frac{r\partial}{8\partial r}\left(\frac{1\partial}{r\partial r}\left(\frac{r^4}{r_{sp}^4}\right)\right)$$

or

$$J_\theta = ar; \qquad a = \frac{\psi_c}{r_{sp}^4}\frac{1}{r_{sp}^4}$$

Thus we recover the same form for the current density as in the usual Hill's vortex case. We are interested in determining the fields from the external sources (the coils) and we obtain them by subtracting out the plasma portion. The contribution given by the plasma currents may be written

$$\psi(r,z)_{plas} = \frac{r}{\pi}\int\frac{r'dr'dz'}{((r+r')^2 + (z-z')^2)^{1/2}}ar'\left(\left(\frac{2}{m} - 1\right)K(m) - \frac{2}{m}E(m)\right)$$

where

$$m = \frac{4rr'}{(r+r')^2+(z-z')^2}$$

and K, E are the complete elliptic integrals of the first and second kind. Evaluation of this integral is accomplished numerically in the SEECOD program. Then trivially

$$\psi_{coil} = \psi_{anal} - \psi_{plas}$$

gives a representation of the coil fields within the plasma boundary. To find ψ_{coil} outside the plasma boundary and to find the required external currents, we try to match ψ_{coil} to that produced by an external assortment of current carrying hoops. For convenience we take them all cenetered and aligned along the axis of symmetry and put them all at the same radius $r = r_{coil}$. Axially the coils are uniformly spaced at intervals Δz starting at $\Delta/2$ and ending at $(N - 1/2)\Delta z$. Also an identical set is used for $z < 0$. The fields of these coils are given by complete elliptic integrals. A least squares formulation is used to determine a set of coil currents which best matches the analytically determined ψ_{coil}. These currents give us enough information to regenerate the equilibria with the numerical equilibrium solver CYLEQ as described below.

The BHW model described here had assumed the plasma boundary to be the separatrix. We note that all of the equations given here are still valid if we take the boundary to be a flux surface outside the separatrix. In extending the plasma boundary the model becomes at the same time more realistic and more tractable: Realistic in the sense that plasma is observed on open flux surfaces in the experiments. Tractable in the sense that at least two of the stability codes applied to these results usually breakdown if the plasma pressure goes to zero at the separatrix.

Equations solved by CYLEQ

In the numerical equilibria to be computed it is convenient to partition the flux function according to the current sources which generate it--namely the coils and the plasma. So we use

$$\psi_{tot} = \psi_{plas} + \psi_{coil}.$$

ψ_{coil} is determined from the complete elliptic integrals at every grid point. ψ_{plas} is obtained by solving the plasma part of Ampere's law

$$\Delta\psi_{plas} = \frac{\partial^2\psi_{plas}}{\partial z^2} + \frac{\partial^2\psi_{plas}}{\partial r^2} - \frac{1}{r}\frac{\partial\psi_{plas}}{\partial r} = -rJ_\theta(r).$$

Far field boundary conditions are accurately represented on the relatively close-in boundaries by using the multipole expansion to obtain ψ_{plas} from the moments of the plasma current density. *Details of the code are given elsewhere.*[2]

We have computed (or if you will re-computed) the BHW equilibria over both the plasma and vacuum regions. *This provides the initial conditions for stability studies like those being described by* Shestakov[3] at this meeting. Several flux profiles are shown here for analytical BHW equilibria that extend to the separatrix for various rectangularities (z^2, z^4, and z^6). We also show the extension of the BHW equilibria to the outer flux surfaces again for the same rectangularities.

References

1. Herbert L. Be[illegible], James H. Hammer, and Harold Weitzner, *Phys. Fluids* **24**, 1758, (1981).

2. David V. Anderson and Daniel C. Barnes, *J. Comput. Phys.* **42**, 288 (1981).

3. A. I. Shestakov, *Private Communication*

An Integral Poloidal Flux Squared Invariant Model of the Relaxation of a Field Reversed Theta Pinch*

John Brandenburg
Lawrence Livermore National Laboratory
University of California, P.O. Box 5511
Livermore, CA 94550

The formation of a Field Reversed Theta Pinch (FRTP) has several distinct stages[1]. The plasma first forms a radial equilibrium after an initial radial shock. It is then observed to reconnect at the ends forming a closed field line configuration and then shock axially as it contracts to a final equilibrium length. A quiescent period then follows, lasting several hundred sound transit times. In this paper a model called the "Sonic Bath" is proposed, wherein the closed field line plasma is assumed to form an unstable intermediate equilibrium after the axial contraction. This intermediate equilibrium relaxes through shear Alfven turbulence driven by micro-tearing modes that saturate. The closed field line plasma then relaxes to a state of minimum magnetic energy, subject to a constraining invariant, whereas the thermodynamic energy of the plasma is constant due to the non-compressional turbulence. The shear alfven waves couple to magneto-sonic waves, which can freely leave the closed field lines, which in turn are absorbed in a bath of plasma assumed present on the open field lines during the relaxation period, thus removing the excess energy. A near perfectly conducting, adiabatic plasma without toroidal field is assumed to exist inside a perfectly conducting chamber. Small energy changes and flux losses and weak turbulence are assumed for this model.

According to Drake et al.[2], micro-tearing modes in shear free systems will saturate at a level that depends on geometric factors only:

$$\frac{\delta B}{B} = \frac{\rho_e}{a} = \gamma \sqrt{\beta} \tag{1.1}$$

where β, the plasma Beta, is near one and γ is a constant not depending on magnetic field strength, and where a is a scale length of resistivity gradients in the plasma.

Assuming that the shear Alfven waves are converted to magneto-sonic waves at some singular surface and lost, we can write the total energy loss as:

$$\Delta W \cong \frac{\delta B^2}{8\pi} C_s \, 2\pi a \ell \tau \tag{1.2}$$

* Work performed under the auspices of the U.S. Department of Energy by the Lawrence Livermore National Laboratory under contract number W-7405-ENG-48.

where C_s is the sound speed and where τ is the duration of the bath:

$$\tau \cong \frac{1}{C_s} \tag{1.3}$$

a sound transit time. Therefore, using our saturation scaling we obtain

$$\Delta W = \frac{\delta B^2}{8\pi} 2\pi a \ell^2 = \frac{B^2}{8\pi} \gamma^2 2\pi a \ell^2 = W_i \gamma^2 2 \frac{1}{a} \tag{1.4}$$

So we obtain an approximately fractional energy loss:

$$W_f = \epsilon W_i \quad , \quad \frac{\partial \varepsilon}{\partial H} = 0 \tag{1.5}$$

where W_i and W_i are the magnetic energies of the intermediate and final equilibrium.

Assuming near perfect conductivity, non-compressional turbulence, and the axisymmetry of the intermediate state, plus the assumption of Taylor that resistivity will destroy all but one global MHD invariant of the plasma we obtain the Lagrange multiplier minimization problem for the magnetic energy:

$$\partial W + \lambda \ \delta I = 0 \tag{1.6}$$

with the invariant:

$$I = \int \Phi^N \, d\tau \tag{1.7}$$

where N can be any number. By using the condition that $d\Phi$ vanish on a conducting wall, we obtain the equation for the relaxed field. We can integrate this equation by parts and with a vanishing surface term on the seperatrix and obtain:

$$W_f = \lambda \ I \tag{1.8}$$

as the magnetic energy on closed field lines in the relaxed state. Therefore, the relaxation process with invariant I takes the system to a final state where the energy is just the invariant times some constant of the process. However, the scaling of the invariant with the flux is not known, we will now use the fractional energy loss scaling to uniquely specify the invariant.

It is always possible to define:

$$W_i = \lambda_0 I \tag{1.9}$$

Since energy changes are small we can write the relaxation as a linear transformation in some variable: σ.

$$W_f = (\lambda_0 - \delta\sigma) \ I \tag{1.10}$$

Now this linear transformation must have the property that it leaves I unchanged and also the total system energy, H, unchanged. That is: *the relaxation process only redistributes the total system energy but does not change it.* Therefore, σ is a symmetry variable for H:

$$\frac{\partial H}{\partial \sigma} = \frac{\partial \sigma}{\partial H} = 0 \qquad (1.11)$$

and so we have:

$$\frac{\partial \varepsilon}{\partial H} = \delta\sigma \frac{\partial}{\partial H}\left(\frac{1}{\lambda_o}\right) = \delta\sigma \frac{\partial}{\partial H}\left(\frac{I}{W_i}\right) = 0 \qquad (1.12)$$

Therefore, I must scale as $W_{i,f}$ with H.

$$I = \int \Phi^2 \, dx^3 \qquad (1.13)$$

This invariant was first suggested by Leaf Turner[4] for turbulence in incompressible conducting fluids, on the basis that it might be "rugged".

We then have for the relaxed magnetic field equation:

$$\nabla \cdot \left(\frac{\nabla\Phi}{r^2}\right) = 2\lambda\Phi \qquad (1.14)$$

This is just the Grad-Shafronov equation for $P = \alpha\Phi^2$.

The solution to Grad-Shafronov equation for our relaxed magnetic field has been worked out generally (Wietzner[5]) and consists of Coulomb wave functions. In the FRTP experiments the resulting plasmas are long and thin so that we may neglect the variation in z. In this limit we have:

$$\Phi = \Phi_a \sin(\pi \frac{r^2}{a^2}) \qquad (1.15)$$

The Sonic Bath model, because it does not have large energy changes, does not involve large flux losses. In order to compare the parameters of the Sonic Bath derived equilibrium we must assume that large flux losses observed in experiments occur during the radial implosion period preceding the sonic bath relaxation. Since experiments with small ratios of bias to final field have the largest flux losses and because for total flux loss:

$$\frac{\Phi_i}{\Phi_w} = \frac{B_b}{B_v} \qquad (1.16)$$

where Φ_w and Φ_l are the flux at the wall and flux lost respectively.

The experiment with the largest flux losses and smallest ratio of B_b to B_f was done at NRL[1], where $B_b/B_f = .07$. For an intermediate equilibrium theory flux losses will be insensitive to the ratio of vortex radius to wall radius, r_v/r_w. Therefore, we can write:

$$\frac{\Phi_b}{\Phi_w} = \frac{\Phi_f}{\Phi_w} + \frac{\Phi_l}{\Phi_w} \cong \frac{\Phi_f}{\Phi_w} + .07 \tag{1.17}$$

and plot a curve of values from our infinite length solution and from experiments.

We also can add a gauge transform to the theory and find a new invariant to give finite pressure on the separatrix. A density profile, assuming uniform temperature, is given for the gauge transformed invariant model. Both models give similar curves of r_v/r_w versus Φ_b/Φ_w. Elsewhere in this proceedings this invariant model is generalized to include toroidal fields.

I would like to thank Steve Auerbach, Leaf Turner, Jim Hammer and Herb Berk for many helpful discussions and suggestions. I would also like to thank Richard F. Post for his encouragement of the research.

References

1. R. Linford, "Proposal for FRX-C and Multiple Cell Compact Torus Experiments", LA-8045-P.

2. J. F. Drake, N. T. Gladd, C. S. Liu, and C. L. Chang, Phys. Rev. Letters, 39, 460 (1977).

3. J. B. Taylor, "Relaxation of Toroidal Plasma and Generation of Reverse Magnetic Fields," Phys. Rev. Letters, 33, 19 (1974) p. 1139.

4. Leaf Turner, LANL, unpublished.

5. B. Wietzner, H. L. Berk, and J. H. Hammer, UCRL-85338, submitted to Phys. Fluids.

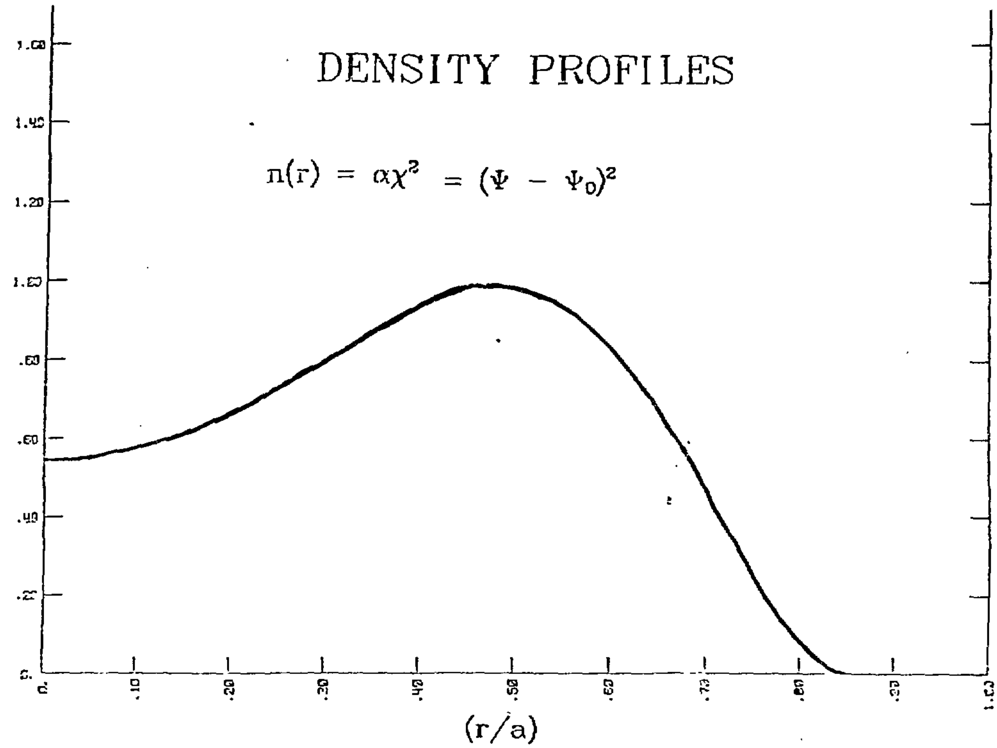
DENSITY PROFILES
$n(r) = \alpha\chi^2 = (\Psi - \Psi_0)^2$
(r/a)

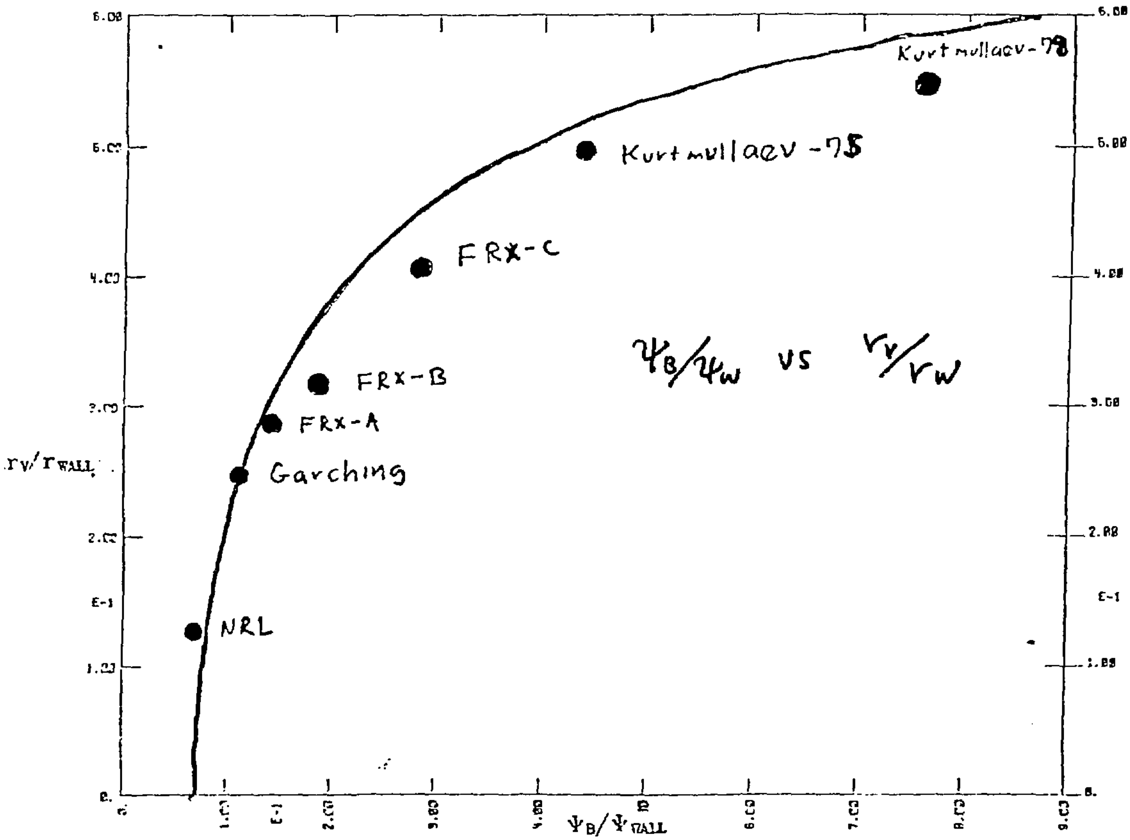
Kurtmullaev-78
Kurtmullaev-75
FRX-C
FRX-B
FRX-A
Garching
NRL
Ψ_B/Ψ_W vs r_v/r_w
r_V/r_{WALL}
Ψ_B/Ψ_{WALL}

ROTATIONAL INSTABILITIES IN THE FRC: RESULTS OF HYBRID SIMULATIONS

Douglas S. Harned*

Electronics Research Laboratory
University of California, Berkeley
Berkeley, CA 94720

Simulations of rotational instabilities in the Field Reversed Configuration (FRC) using our quasineutral hybrid simulation code, AQUARIUS, have shown that m = 2 instabilities can occur for levels of ion rotation well below thresholds predicted by previous theory.[1,2]

AQUARIUS is a fully nonlinear, two-dimensional simulation code. No axial variation is allowed (i.e., $k_z = 0$). Ions are treated as particles and electrons are considered to be a massless fluid. The electric and magnetic fields are described by the Darwin (nonradiative) version of Maxwell's equations. Square conducting wall boundaries are used. We assume that the plasma is initially in a rotating rigid rotor equilibrium, with parameters similar to those of FRC experiments after ion spin-up has occurred. Any unstable mode will be naturally excited by the thermal noise in the initial equilibrium.

We define Ω_i to be the mean ion rotation frequency, Ω_e to be the mean electron rotation frequency, and $\Omega_* \equiv \Omega_e - \Omega_i$ to be the relative drift frequency. As in previous papers,[1,2] we use the parameter $\alpha \equiv -\Omega_i/\Omega_*$ and the parameter β_0, the "beta-on-axis," defined by $\beta_0 \equiv 8\pi n(0)T_i/B_0^2$. T_i is the ion temperature, $T_i = m_i v_t^2/2$, and B_0 is the external magnetic field. For nonreversed theta pinch equilibria our simulations show similar behavior to that predicted by finite Larmor radius (FLR) theory.[1] No instabilities have been observed for $\alpha < 1.0$ and for larger values of α

*Current address: Los Alamos National Laboratory, Los Alamos, New Mexico 87545 growth rates are comparable to those predicted by Freidberg and Pearlstein[1] and by Seyler.[2]

For reversed (FRC) equilibria we find unstable $m = 2$ modes in a range previously thought to be stable, $\alpha < 1.0$. Figure 1 shows growth rates for the $m = 2$ mode as a function of α. For the results of Fig. 1, $\Omega_* = 0.05\ \omega_{ci}$ and field-reversal is 60%, i.e., $|B_z(0)/B_0| = 0.6$. For $\alpha = 0.0$, in this case, 60% field-reversal corresponds to $\beta_0 = 0.65$. We fix $|B_z(0)/B_0|$ rather than β_0 because this is consistent with measurements in the PIACE experiment at Osaka[3] in which $|B_z(0)/B_0|$ does not change significantly during the plasma lifetime, indicating that β_0 decreases as spin-up occurs. The entire range of α shown in Fig. 1 is predicted to be stable by FLR theory. These new results, with low unstable values of α, are consistent with measurements of carbon impurity rotation in FRX-B.[4] The maximum radial perturbation in the unstable modes of our FRC simulations has been found to occur near the field null, where resonant ion effects would be strongest. This is in contrast to the nonreversed case where the maximum perturbation is near the plasma edge. Our results are an indication that, as in other configurations,[5] the destabilizing contribution of resonant ions[2] may prevent absolute finite Larmor radius stabilization from occurring.

An example of a long simulation run showing nonlinear behavior is shown in Fig. 2. At long times both the real part of the frequency and the growth rate are found to decrease. These observations are consistent with both the PIACE and FRX-B experiments.

We have varied β_0 to see the effect of profiles that are more sharply peaked near the field null. Simulations show that decreasing β_0 (i.e., reduced compression) increases the growth rate of the $m = 2$ mode for a fixed value of α. However, this result should not imply shorter lifetimes for reduced compression cases since as β_0 is reduced it should take longer for spin-up to reach a given value of α. Simulations have also shown that for low values of β_0 there exist unstable modes with $m > 2$.

The most recent results from AQUARIUS have been with increased values of $S \equiv R/\rho_i$, where R is the major radius and ρ_i is the ion Larmor radius in the external magnetic field. Our FRX-B simulations used $S \sim 10$. For cases where $S = 31$, similar to FRX-C, we find much lower growth rates. This is presumed to be due to a reduction in the destabilizing resonant ion effects. For a case with $\alpha = 1.0$, $|B_z(0)/B_0| = 0.82$, and $\Omega_* = 0.005\ \omega_{ci}$, the $m = 2$ growth rate is found to be $\gamma = 0.0026\ \omega_{ci}$ and the $m = 3$ growth rate $\gamma = 0.0072\ \omega_{ci}$. These are approximately a factor of ten lower than for FRX-B parameters. These results indicate that the plasma lifetime should increase for larger values of S, not only because of the expected reduction in spin-up, but also because of a reduction in the growth rates of rotational instabilities.

References

1. J. P. Freidberg and L. D. Pearlstein, Phys. Fluids 21, 1207 (1978).

2. C. E. Seyler, Phys. Fluids 22, 2324 (1979).

3. S. Ohi, et al., Proc. of Third Symposium on Physics and Technology of Compact Toroids (Los Alamos, 1980).

4. R. K. Linford, et al., *Proc. of Seventh IAEA Conf. (Innsbruck, 1978).*

5. C. E. Seyler and J. P. Freidberg, Phys. Fluids 23, 331 (1980).

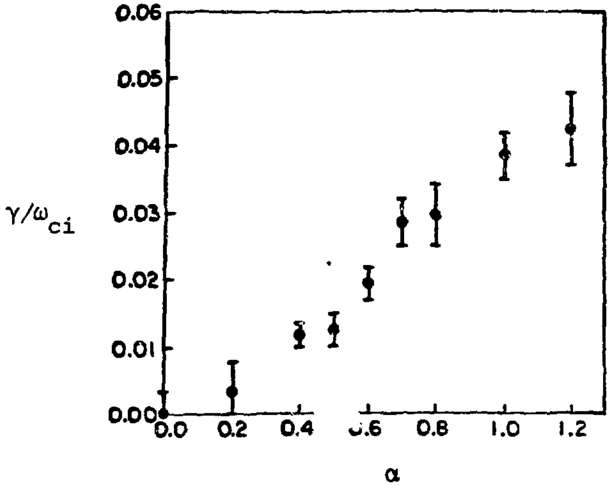

Fig. 1. Growth rates obtained from simulation for the m = 2 mode as a function of α. $|B_z(0)/B_0| = 0.6$ and $\Omega_* = 0.05\ \omega_{ci}$. β_0 varies from 0.41 for $\alpha = 1.2$ to 0.65 for $\alpha = 0.0$.

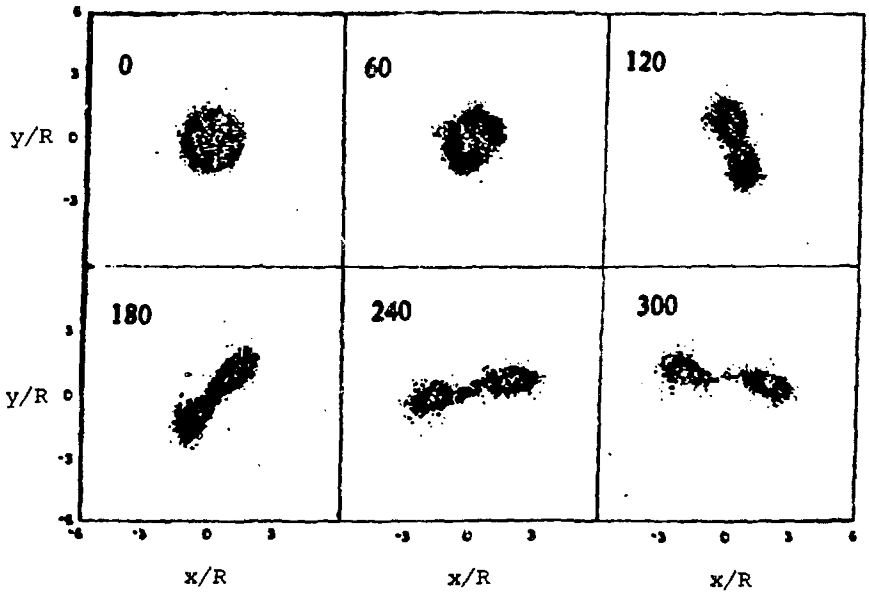

Fig. 2. Particle positions in the r − θ plane for an FRC with $\alpha = 1.0$, $\beta_0 = 0.49$, and $\Omega_* = 0.05\ \omega_{ci}$ at time intervals of 60 ω_{ci}^{-1}, from t = 0 to t = 300 ω_{ci}^{-1}. These frames correspond to 1.6 μs intervals for FRX-B parameters.

EQUILIBRIUM AND POWER BALANCE CONSTRAINTS ON A QUASI-STATIC, OHMICALLY-HEATED FRC

K. F. McKenna, D. J. Rej and M. Tuszewski
Los Alamos National Laboratory
Los Alamos, New Mexico 87545

I. Introduction

In present experiments, FRC's (field-reversed configurations) are generated on "dynamic" time scales, using pulsed high-power theta-pinch technology [1] which does not easily extrapolate to reactor-size devices. The attractiveness of FRC reactor scenarios would be enhanced by the development of quasi-static (i. e. formation time >> Alfven time) formation techniques requiring moderate power levels. In this report the quasi-static formation of FRC plasmas is analytically investigated.[2,3] The set of equations which yield the time evolution of the ohmically-heated-plasma parameters, under the constraints of radial equilibrium and plasma energy losses, are presented. Subject to the simplifying assumptions used in the model, this equation set is completely general and would apply to any ohmically-heated FRC. A sample calculation is presented in which the FRC azimuthal current, I_θ, is generated by the rotating-magnetic-field (RMF) technique.[4]

II. Governing Equations

An infinitely long, ohmically-heated FRC is considered. The electron and ion energy balance equations for a unit volume of the plasma are,

$$\frac{3}{2}\frac{d}{dt}(nkT_e) = \eta J_\theta^2 - P_{rad} - \frac{3}{2}nk\left[\frac{(T_e - T_i)}{\tau_{eq}} + \frac{T_e}{\tau_{Ee}}\right] \tag{1a}$$

$$\frac{3}{2}\frac{d}{dt}(nkT_i) = \frac{3}{2}nk\left[\frac{(T_e - T_i)}{\tau_{eq}} - \frac{T_i}{\tau_{Ei}}\right], \tag{1b}$$

where the resistivity, η, is assumed classical. $P_{rad} = n(t)\sum F_z n(0) L_z$, is the radiation power due to the initial fraction F_z of impurity element z with the cooling rate, L_z, as computed by Post, et. al.[5]. τ_{eq} is the electron-ion equilibration time. τ_{Ei} and τ_{Ee} are the ion and electron thermal energy confinement times respectively, with $\tau_{Ej} = \xi_j \tau_{jj}(r_w/2\rho_j)^2$ where, $\xi_j = 1$ for classical conduction losses and $\xi_j < 1$ for losses greater than classical, τ_{jj} is the species self-collision time, r_w is the wall radius, and ρ_j is the gyroradius at the separatrix.

The radial distribution of particle density, n, and azimuthal current density, j_θ, are specified by assuming rigid-rotor profiles, $n = n_{max}\,\mathrm{sech}^2 K[(r/r_o)^2 - 1]$ where r_o is the magnetic axis, and $j_\theta = ne\omega r$. It is further assumed that the FRC is contained within a flux-conserving wall of radius r_w, so that $r_s \simeq r_w$, where $r_s = \sqrt{2}r_o$ is the separatrix radius. Taking $K \simeq 2$, conservation of particles yields $n_{max} \simeq 2n_o$ where n_o is the initial fill density. The radial equilibrium constraint requires

$$n_{max}\,k(T_e + T_i) = B_w^2/2\mu_o, \tag{2}$$

where the magnetic field at the wall, B_w, is constrained through Ampere's law by the FRC azimuthal current,

$$B_w = -\frac{\mu_o}{2}\int_o^{r_w} j_\theta\,dr. \tag{3}$$

Ohmic dissipation results in FRC heating on relatively long time scales. This presents the possibility of "puff-gas injection" during the heating process. In anticipation of the example calculation given in section III, the fill density, n_o, is allowed to increase uniformly with temperature as,

$$n_o(t) = n_o(0)\left[(T_e + T_i)/T_e(0)\right]^{1/(2\gamma+1)} , \qquad (4)$$

where $\gamma > 0$, $T_e(0)$ and $n_o(0)$ are the electron temperature and density at time $t = 0$, and $T_i(0) \simeq 0$. Temperature is assumed to be independent of radius. The equations which result from integrating Eqs. 1a and 1b over the plasma volume, using the above expressions, can be solved to yield the time evolution of the plasma parameters for a given r_w, γ, and the initial equilibrium conditions, $T_e(0)$, $n_o(0)$ and $j_\theta(0)$.

III. Example Numerical Calculation ; FRC's Formed by the RMF Technique

Figure 1 illustrates the RMF generation of an FRC. This technique has been successfully demonstrated in small-scale devices.[4,6,7] According to Blevin and Thonemann,[4] the electrons are tied to the rotating field lines, of magnitude B_o, resulting in a rigid-rotor current density distribution ($j_\theta = ne\omega r$) when, $\omega_{ce} > \omega > \omega_{ci}$ and $\nu_{ei}/\omega_{ce} < 1$, where ω is the rotating-field frequency, ω_{ce} and ω_{ci} are the electron and ion cyclotron frequencies (with respect to B_o) and ν_{ei} is the electron-ion collision frequency.

Integrating j_θ over radius yields, $I_\theta \propto \omega n_o$ for the total equilibrium current. This current can be maintained by programming in time the rotating-field frequency, ω, and/or n_o through puff-gas injection. Allowing $\omega \propto n_o^{\gamma}$, the radial equilibrium constraints require that $n_o(t)$ vary with temperature as shown in Eq. 4, and so

$$\omega = \omega(0)\left[(T_e + T_i)/T_e(0)\right]^{\gamma/2(\gamma+1)} , \qquad (5)$$

where $\omega(0)$ is the value of ω at $t = 0$. Note that as $\gamma \to \infty$, $n_o(t) \to n_o(0)$ (i.e., no gas injection) and $\omega \propto (T_e + T_i)^{1/2}$.

The numerical results of Hugrass and Grimm,[8] show that the rotating field can penetrate and be sustained within the plasma if the penetration condition is satisfied, $\nu_{ei} r_w/\omega_{ce}\delta \leq 1$, where δ is the classical skin depth. Taking, from past experimental results,[6] $\omega = 5\omega_{ci}$ which sets an upper bound on B_o, and using Eqs. 4 and 5 it can be shown[2] that the penetration condition has the functional form,

$$\frac{\nu_{ei}}{\omega_{ce}}\frac{r_w}{\delta} = F\left\{n_o(0),\ \omega(0),\ T_e(0),\ r_w,\ (1 + T_i/T_e)/(T_e/T_e(0))^{\lambda}\right\} \qquad (6)$$

where $\lambda = [(\gamma/2 - 1)/(2\gamma + 1)] + 3/4$. If $F \leq 1$ at $t = 0$, then for $\gamma > 1/8$ the penetration condition is satisfied for all time t. Thus, the bounds on γ are $1/8 \leq \gamma \leq \infty$. The initial rotating field frequency, $\omega(0)$, is obtained from the combination of the Eqs. 2 and 3 evaluated at $t = 0$, and can be written as,

$$\omega(0) = C_1\ [T_e(0)/n_o(0)]^{1/2}/r_w^{2}, \qquad (7)$$

where C_1 is a constant. Substuting Eq. 7 into Eq. 6, evaluated at $t = 0$, yields,[2] for the initial fill density,

$$n_o(0) = C_2\ [T_e(0)/r_w^{2}]^{4/5}, \qquad (8)$$

where C_2 is a constant.

For the initial conditions $T_e(0) = 2$ eV, $T_i(0) \approx 0$ and $r_w = 40$ cm, Eqs. 7 and 8 give $\omega(0) = 1.3 \times 10^5$ rad/sec and $n_o(0) = 1.5 \times 10^{12}$ cm^{-3} respectively. The solution of Eqs. 1a and 1b for $\gamma = \infty$ (constant fill density) and $\gamma = 1/8$ (maximum rate of gas injection), for the above set of conditions, is plotted in Fig. 2. Radiation and transport losses have been neglected so these curves give the upper bounds on T_e and T_i, assuming classical resistivity. The corresponding $n_o(t)$ and $\omega(t)$ for this case are shown in Fig. 3. Although gas injection results in a somewhat lower T_e, it is technologically advantageous in view of the significantly smaller increase in rotating field frequency, ω, than required without gas injection. The effect of impurity radiation is shown in Fig. 4, where T_e is given for $\gamma = 1/8$ and oxygen impurity fractions, ranging from 0 to 15% of the initial fill density. The relatively weak effect of radiation on the temperature time history is attributable to the low initial density $n_o(0)$. The scaling of T_e with wall radius is displayed in Fig. 5 for various times. As can be seen, the time required to ohmically heat quasi-statically formed FRC's to temperatures of fusion interest increases with the device radius squared. Figures 6 and 7 show the effects of cross-field thermal conduction on the electron temperature time-history for $r_w = 40$ cm, $\gamma = 1/8$, and 2% oxygen impurity. Electron thermal conduction losses many times faster than classical can be tolerated (Fig. 6.). However, ion thermal transport (Fig. 7.) only about a factor of two greater than classical is sufficient to clamp T_e at uninteresting values; a 1-D model is required to adequately investigate this effect. For the $\gamma = \infty$ (constant density) case, ion energy transport is unimportant since the low initial density results in a characteristic electron-ion equilibration time that greatly exceeds the ohmic heating time (see Fig. 2).

REFERENCES

1. W. T. Armstrong, R. K. Linford, J. Lipson, D. A. Platts and E. G. Sherwood, Phys. Fluids, to be published.
2. K. F. McKenna, Los Alamos Scientific Laboratory LA-9024-MS, 1981.
3. K. F. McKenna, D. J. Rej, and M. Tuszewski, to be published.
4. H. A. Blevin and P. C. Thonemann, Nucl. Fusion Suppl. Part I, 55 (1962).
5. D. E. Post, R. V. Jenson, C. B. Tarter, W. H. Grasberger, and W. A. Lokke, At. and Nucl. Dat. 20, 397 (1977).
6. P. S. Davenport, G. Francis, W. Miller, and A. F. Taylor, U.K.A.E.A. Culham report CLM-R65, 1966.
7. W. N. Hugrass, I. R. Jones, K. F. McKenna, M. G. R. Phillips, R. G. Storer and H. Tuczek, Phys. Rev. Lett. 44, 1676 (1980).
8. W. N. Hugrass and R. C. Grimm, The Flinders University of South Australia report FUPH-R-166, 1980.

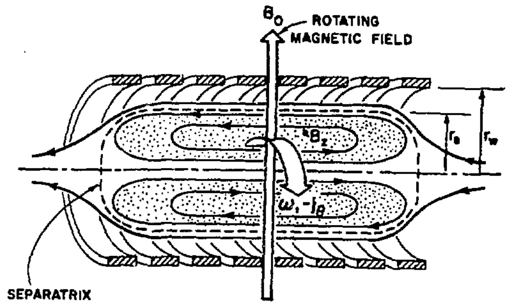

FIGURE 1.

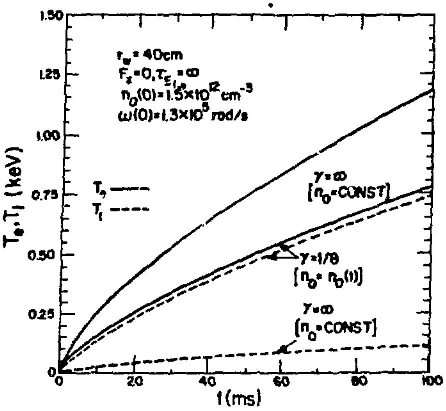

FIGURE 2.

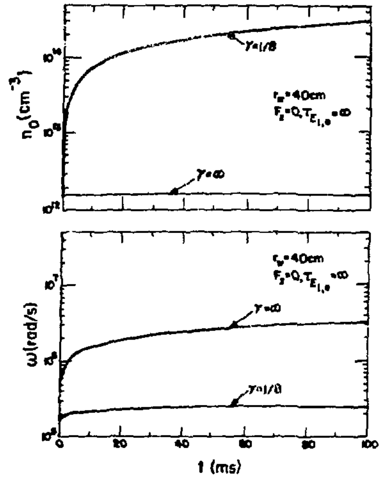

FIGURE 3.

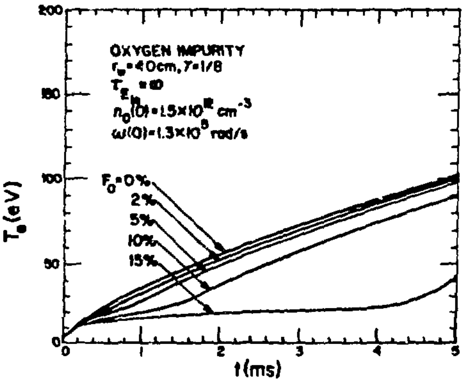

FIGURE 4.

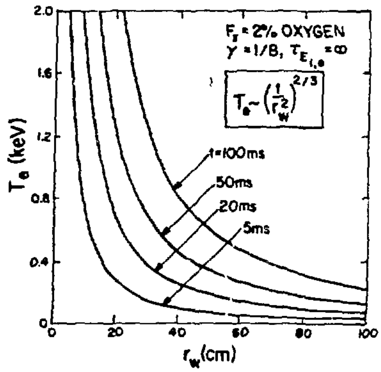

FIGURE 5.

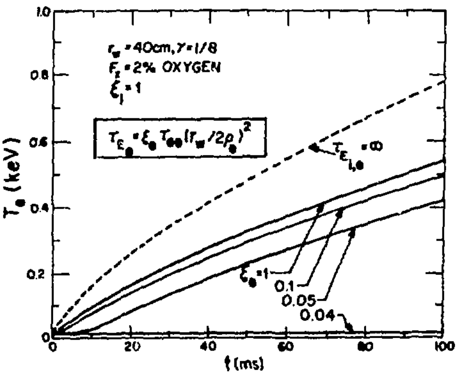

FIGURE 6.

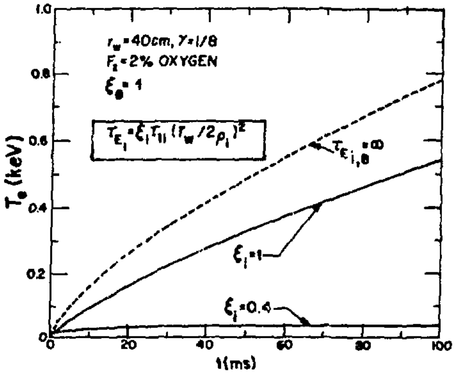

FIGURE 7.

NONADIABATIC SCATTERING AND TRANSPORT AT THE SPINDLE CUSP

R. W. Moses and D. W. Hewett
Los Alamos National Laboratory
Los Alamos, New Mexico 87545

When magnetohydrodynamics is used to describe plasma flow across a separatrix to open field lines, the transport is modeled by a diffusion equation with a sink for particles on the open lines. In that case, it is assumed that plasma is carried to and from the separatrix by diffusive processes. The purpose of this note is to discuss the nonadiabatic processes occurring at a spindle cusp to transfer plasma across a separatrix. After an ion is delivered to the vicinity of the separatrix by diffusion it enters the spindle cusp and will skip back and forth across the separatrix, producing a structured transport not seen with MHD.

To illustrate the motion of ions across a separatrix, let us consider a cylindrical magnetic field of the form

$$B_r(r,z) = -\frac{\partial A_\theta}{\partial z} \quad ,$$

$$B_z(r,z) = \frac{1}{r}\frac{\partial (rA_\theta)}{\partial r} \quad . \tag{1}$$

The magnetic flux passing through any circle concentric with the axis and having radius r is

$$\psi = 2\pi r A_\theta(r,z) \quad .$$

Since B_z changes sign at $z = 0$, ψ must also have odd parity at $z = 0$ and is defined by

$$\psi > 0 \text{ for } z < 0 \text{ and } r > 0 \quad ,$$

$$\psi = 0 \text{ for } z = 0 \text{ and/or } r = 0 \quad ,$$

$$\psi < 0 \text{ for } z > 0 \text{ and } r > 0 \quad . \tag{2}$$

Therefore, a simplified spindle separatrix is defined by the z axis and $z = 0$ plane. The Lagrangian of a particle in this field with an azimuthally symmetric electrostatic potential, ϕ, is

$$L = \frac{1}{2} mv^2 - q\phi + qA_\theta v_\theta \quad . \tag{3}$$

The canonical angular momentum is

$$p_\theta = mr^2\dot{\theta} + qrA_\theta \tag{4}$$

We note that p_θ is a constant of the motion since $\frac{\partial L}{\partial \theta} = 0$. Let us define the ψ value for any particle as $\psi(r_g,z_g)$ where the guiding center moves on a surface (r_g,z_g) as long as the magnetic moment, $\mu = T_\perp/B$, is preserved in adiabatic motion.

After some brief manipulations one can express p_θ as a function of ψ and μ for particles in adiabatic motion near the axis

$$p_\theta = \frac{q}{2\pi} \psi - \frac{m}{q} \mu \quad , \ z < 0$$

$$p_\theta = \frac{q}{2\pi} \psi + \frac{m}{q} \mu \quad , \ z > 0 \quad . \tag{5}$$

Eq. (5) is consistent with the simultaneous invariance of p_θ, ψ, and μ away from the spindle point, $r = z = 0$. However, only p_θ is invariant in the vicinity of the spindle point. Equations (2) and (5) lead to the following restrictions on p_θ

$$p_\theta > -\frac{m}{q} \mu_M \text{ for } z < 0 \quad ,$$

$$p_\theta < \frac{m}{q} \mu_M \text{ for } z > 0 \quad . \tag{6}$$

where μ_M is the maximum magnetic moment that can be anticipated for particles of given kinetic energy. Consequently there is a range of flux surfaces between which particles may freely scatter at the spindle cusp

$$-\frac{2\pi m}{q^2} \mu_M < \psi < \frac{2\pi m}{q^2} \mu_M \quad . \tag{7}$$

For example, an ion coming from the left, $z < 0$, with ψ satisfying Eq. (7) may cross the separatrix and move along the positive z axis or be deflected away from the axis near the $z = 0$ plane. In time the same ion may be mirrored back to the spindle cusp and repeat the "scattering" as long as Eq. (7) is satisfied.

In conclusion, we have identified a collisionless process that can trannsfer ions and electrons across a separatrix at a spindle cusp. This "scattering" has a limited range of penetration into the plasma, given by Eq. (7) in flux coordinates. Since the range in ψ is proportional to the particle mass, ions will be scattered over a much wider region than electrons. Electron transport will be governed primarily by standard diffusive processes but a significant new factor has been added to ion transport in a spindle cusp.

Computer codes are being written to elucidate this nonadiabatic particle behavior near the spindle cusp. We expect to extend these concepts of particle scattering across the cusp plane by using a more realistic flux profile. We can then realistically quantify the scattering process by actually following individual particle orbits through the static cusp region. Particle and angular momentum transport probabilities through the cusp region can be determined in this way.

ION KINETIC EFFECTS ON THE TILT MODE IN FRCs

J. L. Schwarzmeier, Los Alamos National Laboratory,

C. E. Seyler, Cornell University

D. C. Barnes, Institute for Fusion Studies, University of Texas

Theory[1–3] and simulations[3–4] have shown that field reversed configurations (FRC's) should be unstable magnetohydrodynamically to the tilting mode, yet tilting seldom is seen in the experiments. Profile effects (within MHD) and ion finite larmor radius (FLR) effects have been proposed to explain the observed stability of FRC's. The present work seeks to test both of these effects.

I. Model

Here we employ the dispersion functional[5] form of the Vlasov-fluid model, and then expand in two small quantities: a.) $\varepsilon = r_L/a << 1$ (small larmor radius) and b) $\delta = a/b << 1$ (highly elongated equilibria). The two-dimensional nature of the equilibrium is retained exactly, and to leading order in ε and δ we retain FLR effects, parallel kinetic effects, and resonant particles.

The linearized equations of motion have the form[6]

$$\Delta(\vec{\xi}^*, \vec{\xi}) = -2\delta W + 2\omega^2 K + \omega F - R(\omega) = 0 \quad , \qquad (1)$$

where δW is the incompressible MHD potential energy, K is the Vlasov-fluid kinetic energy, F is the FLR term, and $R(\omega)$ contains the parallel kinetic effects and resonant particles. In the Vlasov-fluid model the displacement $\vec{\xi}$ has two components: $\vec{\xi} = \xi_\theta(s,\psi)\hat{\theta} + \xi_n(s,\psi)\hat{n}$, where $\hat{n} = \hat{\theta} \times \hat{b}$, $\hat{b} = \vec{B}/B$, ψ is the poloidal flux function, and s is the arclength along a flux contour. A significant reduction in the dimensionality of the problem to be solved is accomplished by a) requiring that the largest term in $R(\omega)$ be made to vanish, and b) using the result from MHD[3] that δW is minimized by an axial shift, $\xi_z(\psi)$, for highly elongated elliptical equilibria. These observations lead to the forms

$$\xi_n(s,\psi) = \hat{B}_r(s,\psi)\xi_z(\psi) \qquad (2)$$

and

$$\xi_\theta(s,\psi) = ir^2 B_r(s,\psi)\xi_z'(\psi)/n \quad , \tag{3}$$

where $\hat{B}_r(s,\psi) = \sin\ \alpha = \hat{n}\cdot\hat{z}$, and the integer n in Eq. (3) is the toroidal mode number. The only unknown in Eq. (2) and Eq. (3) is the function $\xi_z(\psi)$. This is a vast simplification over the original problem.

The result of substituting Eq. (2) and Eq. (3) in Eq. (1) is

$$\Delta(\xi_z^*,\xi_z) = \int_{\psi_{vor}}^{\psi_{sep}} d\psi\ \left\{d_1(\psi,\omega)|\xi_z|^2 + d_2(\psi,\ \omega)|\xi_z'|^2\right\} \quad , \tag{4}$$

where both d_1 and d_2 are of the form

$$d_j(\psi,\omega) = \int ds\ \tilde{d}_j(s,\psi,\omega)/B(s,\psi). \tag{5}$$

The form Eq. (4) results when we take into account the leading order contribution of the parallel kinetic effects in $R(\omega)$, but drop the resonant particle terms in $R(\omega)$. The variation of Δ in Eq. (4) leads to the ordinary differential equation

$$d_2(\psi,\omega)\xi_z'' + d_2'(\psi,\omega)\xi_z' - d_1(\psi,\omega)\xi_z = 0 \quad , \tag{6}$$

where ψ is the independent variable.

II. MHD Results

Magnetohydrodynamic simulations show that the tilt mode is internal, $\xi_z(\psi_{sep}) = 0$. Therefore, we only require equilibrium solutions that are realistic inside the separatrix. Convenient control over equilibrium profiles is provided by the Berk, Hammer, Weitzner[7] solution for $\psi(r,z)$. These solutions are designed so that the "flatness" of the flux contours can be adjusted by a parameter p, where

$$\lim_{\substack{z\to o\\ r\to r_{sep}}} \psi(r,z) \sim z^p.$$

$p = 2$ is a Hill's vortex and $p \gg 1$ is a race track-like equilibrium.

The MHD portion of our code has been benchmarked against the linear MHD simulation code of Shestakov. For a particular run of Shestakov,[8] we have the following comparison of the e-folding time of an unstable tilt mode:

$\gamma^{-1} = 2\mu sec$ (Shestakov)

$\gamma^{-1} = 2.3\mu sec$ (present work)

The main effect to be studied in an MHD context is how the flatness of the flux contours affects the growth of the tilt mode. Figure 1 shows the growth rate from MHD versus the flatness parameter p of the Berk, Hammer, Weitzner solution. The conclusion is the stability of the tilt mode is enhanced significantly by making the equilibrium more race track-like. Additional runs have to be made for larger p, and verification of the current results have to be performed to determine whether or not the tilt mode can be stabilized by profile effects alone.

III. FLR Effects

With MHD regularity conditions in the current model, the FLR term in Eq. (1) diverges at the vortex due to a breakdown in the assumption that $\varepsilon \ll 1$. For instance, near the field null the ion orbits are no longer cycloidal with $\Omega_{ci} \gg \Omega_d$, where Ω_d is the (cross field) azimuthal drift frequency. The model is being ammended to make the transition from cycloidal to betatron orbits, and soon we will be able to investigate more correctly the effect of FLR.

References

1. M. N. Rosenbluth and M. N. Bussac, Nuclear Fusion, 19, 489 (1979).
2. J. R. Cary, IFSR#10, March (1981).
3. D. C. Barnes, C. E. Seyler, and D. V. Anderson, Symposium on Compact Toruses and Energetic Particle Injection, Princeton, NJ, Dec., (1979).
4. A. I. Shestakov, D. D. Schnack, and J. Killeen, Symposium on Compact Toruses and Energetic Particle Injection, Princeton, NJ, Dec., (1979).
5. K. R. Symon, C. E. Seyler, and H. R. Lewis, submitted to Journal of Plasma Physics.
6. C. E. Seyler and D. C. Barnes, Phys. of Fluids, (1981).
7. H. Berk, J. Hammer, and H. Weitzner, Phys. of Fluids, 24, 1758 (1981).
8. A. I. Shestakov, J. Killeen, and D. D. Schnack, submitted to Jour. of Comp. Phys., 1981.

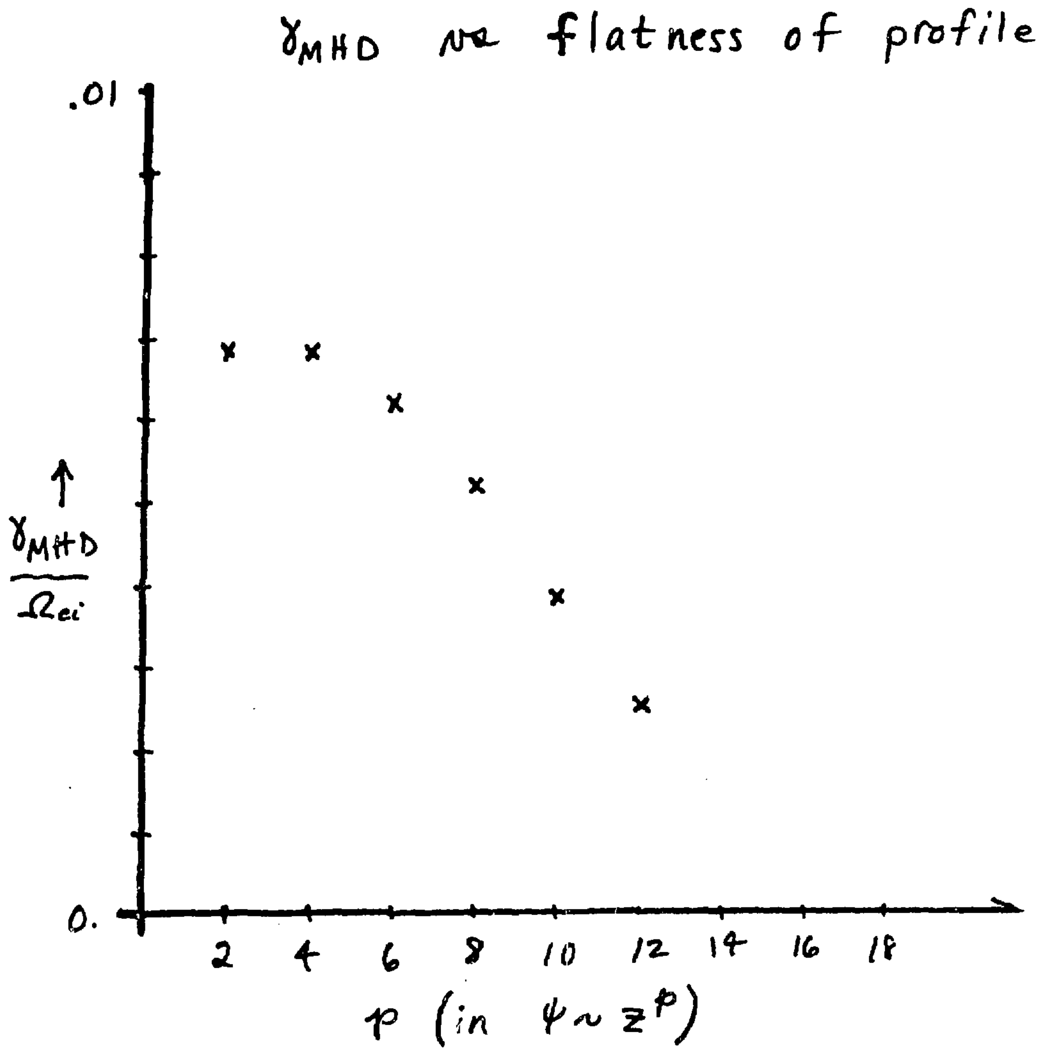

Figure 1

MHD growth rate versus flatness of the equilibrium profile.

QUASISTATIC EVOLUTION OF COMPACT TOROIDS

A. G. Sgro, R. L. Spencer, and C. Lilliequist
Los Alamos National Laboratory
Los Alamos, New Mexico 87545

We should like to present some results of our simulations of the post formation evolution of compact toroids. The simulations were performed with a 1-1/2 D transport code. Such a code makes explicit use of the fact that the shapes of the flux surfaces in the plasma change much more slowly than do the profiles of the physical variables across the flux surfaces. Consequently, assuming that the thermodynamic variables are always equilibrated on a flux surface, one may calculate the time evolution of these profiles as a function of a single variable that labels the flux surfaces. Occasionally, during the calculation these profiles are used to invert the equilibrium equation to update the shapes of the flux surfaces. In turn, these shapes imply certain geometric cofficients, such as $A = \langle 1/r^2 \rangle$, which contain the geometric information required by the 1-D equations.

Compact toroids have the feature that the separatrix touches the axis of symmetry, which implies that some of the geometric cofficients are singular. Thus, the transport equations and the surface averaged equilibrium equation are singular PDEs and ODEs. We have expressed these equations in terms of nonsingular variables that are appropriate combinations of the singular variables and other variables which go to zero at the separatrix. We made two checks of the accuracy of our algorithm. First, we inverted the equilibrium equations on a 129 x 145 grid on which we resolved 40 flux contours. An analytic solution for $\psi(r,z)$ was available and we found that the numerical flux surface variables agreed with those derived from the analytic solution to better than 0.1%. Also, we compared the results of a 21 cell 1-D diffusion calculation with an analytic solution and found agreement to better than 3%.

A certain fraction of the gun-injected compact toroid shots (up to 50%) show an oscillation about the minimum energy force-free state. In Fig. 1, the toroidal field on the axial midplane at r = .6*R and the poloidal field at the midplane on the major axis are plotted as functions of time. The solid lines are the experimental results. We also plot the ratio of these fields and indicate, by a dotted line, the value this ratio would have in the minimum energy force-free state. At early times this ratio oscillates on the rapid MHD timescale of a few μs. At about 50 μs, it settles down to the minimum energy value and then evolves away from this value on the resistive timescale (50-100 μs). This resistive evolution is terminated by MHD activity that drives this ratio back to the value in the minimum energy state. Afterwards, it again evolves on the resistive timescale.

We simulate the resistive timescale evolution of the experiment. The observed temperature is about 10 eV, which implies that the experimental beta is low. Therefore, the computations were done for a beta of zero. We initialize the code with the (analytically known) minimum energy configuration, indicated by the leftmost x in the three plots of Fig. 1. The computational results at various times are indicated by the subsequent x's. The computations follow the experiment reasonably well. Of course, the code does not follow the MHD relaxation, so we stopped plotting the x's when the experiment relaxed.

In Fig. 2 we plot the computed radial profiles of toroidal and poloidal field at the axial midplane at various times. These plots show that the plasma evolves resistively away from the minimum energy state towards one in which the toroidal field and the toroidal current are peaked on the magnetic axis. The relaxation occurs between 50 and 100 μs.

In conclusion, the computational algorithm consistently handles the singularities due to the separatrix touching the major axis. We find that in a certain fraction of the shots, the plasma evolves at low beta toward a state in which the toroidal field and toroidal current are peaked on the major axis. It then relaxes back to the minimum energy state on a hydrodynamic timescale.

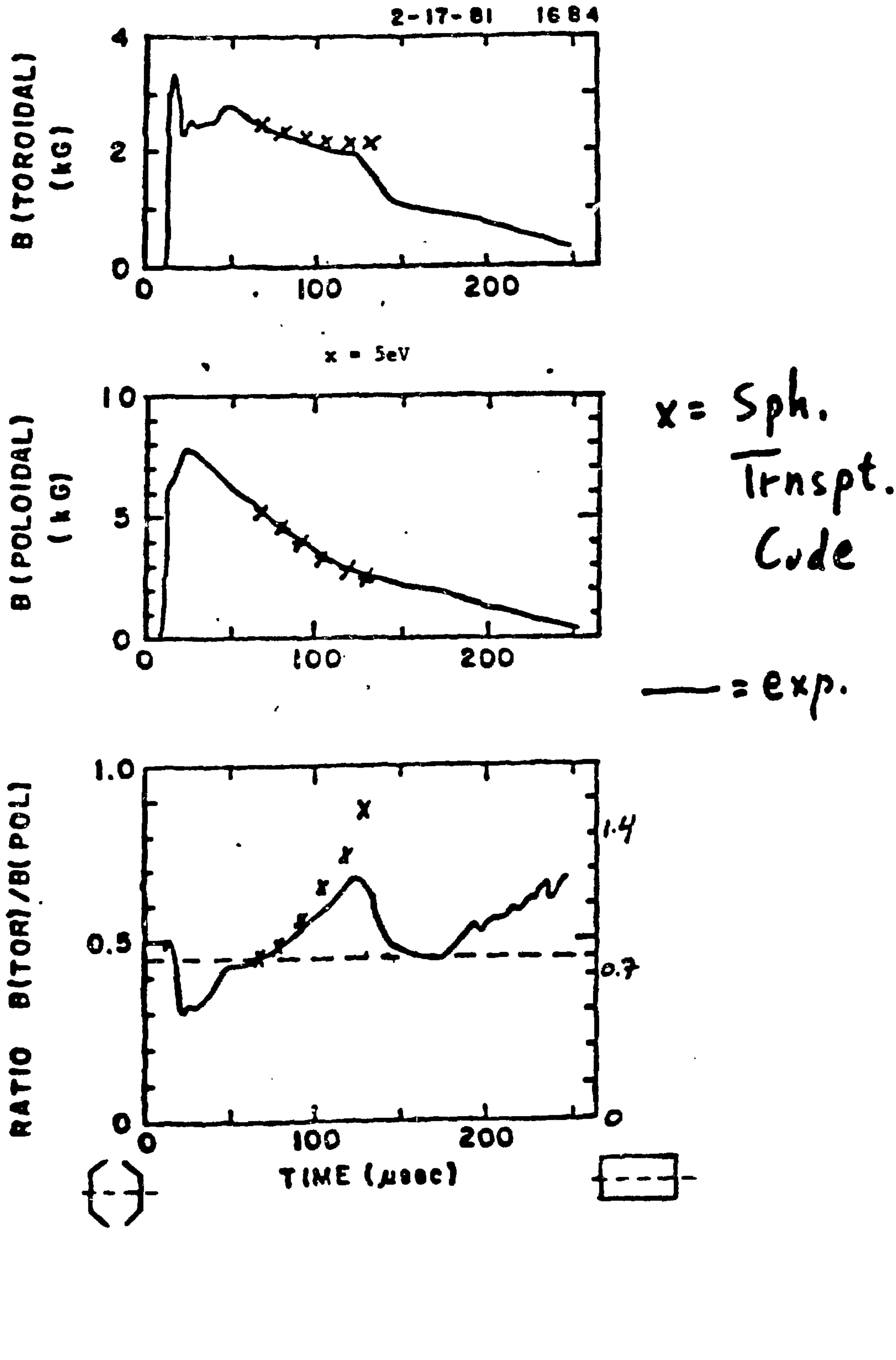
2-17-81 1684
B (TOROIDAL) (kG)
x = 5eV
B (POLOIDAL) (kG)
x = Sph. Trnspt. Code
— = exp.
RATIO B(TOR)/B(POL)
TIME (μsec)

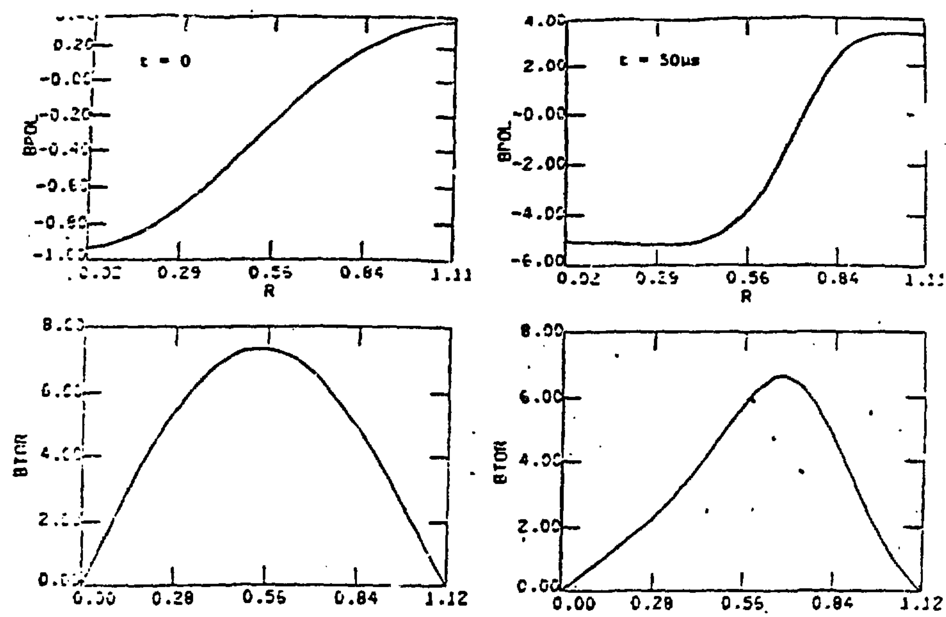

Spheromak Transport Code Results

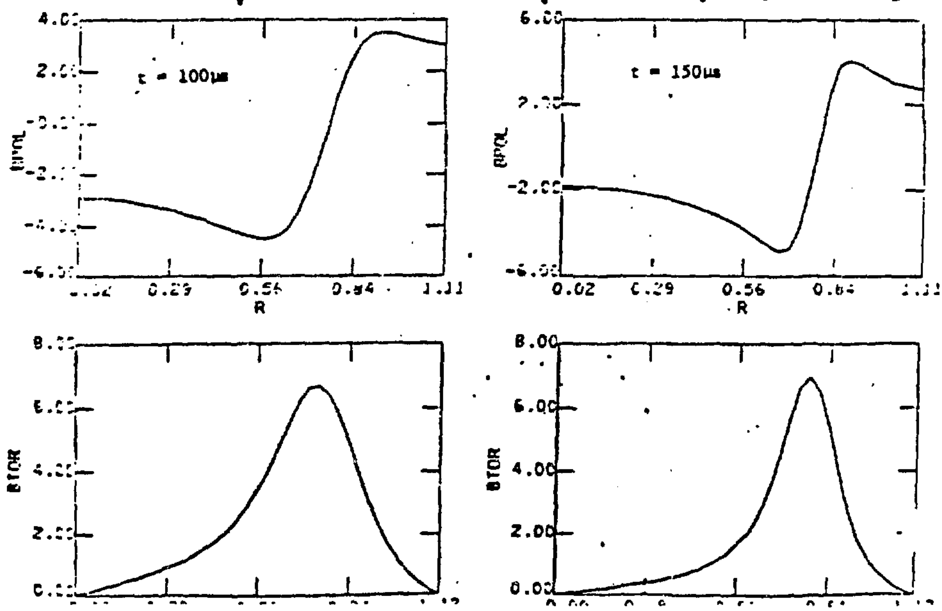

MULTIPLE SOLUTIONS OF A FREE BOUNDARY FRC EQUILIBRIUM PROBLEM IN A METAL CYLINDER

Ross L. Spencer and Dennis W. Hewett
University of California
Los Alamos National Laboratory
Los Alamos, NM 87545

I. INTRODUCTION

Field reversed theta pinch experiments routinely produce very prolate plasma equilibria; magnetohydrodynamic equilibrium codes do not. Since the experimental plasmas seem to be stable against the tilting-instability that is predicted for moderately elongated equilibria, it has been conjectured that the observed stability is due to exaggerated elongation. It has been difficult to test this hypothesis because long equilibria have been difficult to compute. Previous calculations have indicated that such equilibria might exist[1-4], but none of these computed equilibria has been completely satisfactory.

We present a new approach to the computation of FRC equilibria that avoids the previously encountered difficulties. For arbitrary pressure profiles it is computationally expensive, but for one special pressure profile the problem is simple enough to require only minutes of Cray time; it is this problem that we have solved. We solve the Grad-Shafranov equation, $\Delta^{*}\psi = -r^2 p'(\psi)$, in an infinitely long flux conserving cylinder of radius a with the boundary conditions that $\psi(a,z) = -\psi_w$ and that $\partial\psi/\partial z = 0$ as $|z|$ approaches infinity. The pressure profile is $p'(\psi) = cH(\psi)$ where c is a constant and where H(x) is the Heaviside function. We have found four solutions to this problem: There is a purely vacuum state, two z-independent plasma solutions, and an r-z-dependent plasma state. These last three solutions are obtained only if the constant c is greater than a certain critical value; for c smaller than this lower limit the three plasma solutions cease to exist. At the critical value of c the two z-independent solutions coalesce, and at a slightly higher value of c the two-dimensional solution and one of the z-independent solutions coalesce. It is near this second value of c that elongated equilibria are obtained. This means that the elongated equilibria are found near a bifurcation point of the solution set, a notoriously difficult region in which to compute. This probably explains why elongated solutions have been so difficult to find.

II. ONE-DIMENSIONAL SOLUTIONS

Except for the trivial vacuum solution, $\psi = -\psi_w r^2/a^2$, the z-independent solutions are the simplest to find. An elementary calculation yields

$$\psi = \begin{cases} \frac{1}{2}r^2\left(b - \frac{1}{2}cr^2 \right), & r < r_{sep} \\ -\frac{1}{2}br^2 + d, & r_{sep} < r < a \end{cases} \tag{1}$$

$$\text{where} \quad b = \frac{a^2 c}{8}\left[1 \pm \left(1 - \frac{32\psi_w}{ca^4} \right)^{1/2} \right], \tag{2}$$

and where $d = 2b^2/c$ and $\psi = 0$ at $r_{sep} = 2\sqrt{b/c}$. Note that there are two possible solutions; these two solutions are realized only if b is real, i.e. only if $c \geq 32\psi_w/a^4$. Figure 1 displays the $\psi = 0$ radius as a function of c. The upper solution in this figure is a high trapped flux solution that compresses the vacuum flux against the wall as c becomes large. The lower solution in this figure is a low trapped flux solution that is squeezed to the axis by the vacuum flux as c becomes large. The presence of a value of c below which no equilibria exist is explained by noting that the toroidal current density is given by $j_\theta = -crH(\psi)$. If c is too small, there is not enough current density to produce field reversal, and no solutions of the model problem are possible. This same argument should apply to any two-dimensional solutions as well, so we expect in any family of equilibria parameterized by c to encounter a lower limit in c below which no equilibria exist.

III. A TWO-DIMENSIONAL SOLUTION

From studies of Hill's vortex equilibria done by us (and independently by John Boyd), we know there is at least one two-dimensional family of solutions parametrized by c. With ψ given by the Hill's vortex formula inside the separatrix, a matching vacuum field outside the separatrix may be constructed by means of ellipsoidal coordinates. For both prolate and oblate Hill's vortices, the matching vacuum field has mirror coils at infinity, but for the spherical Hill's vortex, the field lines at infinity are straight. This spherical solution is given by

$$\psi = \begin{cases} \frac{3}{4}B_0 r^2\left(1 - \frac{r^2+z^2}{\rho_0^2}\right), & r^2+z^2 < \rho_0^2 \\ -\frac{1}{2}B_0 r^2\left[1 - \left(\frac{\rho_0^2}{r^2+z^2}\right)^{3/2}\right], & r^2+z^2 \geq \rho_0^2 \end{cases} \tag{3}$$

where $\rho_0 = \sqrt{15B_0/2c}$ and where B_0 is the uniform magnetic field at infinity. This solution will be obtained in the model problem when the plasma radius becomes very small so that the cylindrical wall is effectively very far away, i.e., when c is very large. This means there exists a two-dimensional family of solutions whose large c limit is given by Eq. (3) (B_0 is replaced by $2\psi_w/a^2$). As c is decreased, the equilibria should become larger and finally approach a final state at some critical value of c.

We tried to compute these larger equilibria by finite difference methods on a mesh, but ran into difficulties. We conjecture that the sharp-edged current distribution and the free-boundary non-linearity in the problem were what caused our iteration methods to converge to states that were not in fact equilibria. To overcome these difficulties we completely reformulated the problem. Using the Green's theorem for Δ^*, the Grad-Shafranov equation may be inverted to obtain the equation

$$\psi = -\int G(r,r',z,z')p'(\psi)\, r'dr'dz' + \frac{1}{2\pi}\int \psi \frac{\partial G}{\partial r'}\frac{da'}{r'^2} \tag{4}$$

where G satisfies $\Delta^* G = r\delta(r-r')\delta(z-z')$ and $G = 0$ if $r,r' = a$. The Green's function is given by the expression

$$G(r,r',z,z') = \frac{rr'}{\pi}\int_0^\infty \cos k(z-z')I_1(kr)I_1(kr')\frac{K_1(ka)}{I_1(ka)}dk - \frac{\sqrt{rr'}}{2\pi}Q_{1/2}\left(\frac{r^2+r'^2+(z-z')^2}{2rr'}\right) \tag{5}$$

Formulating the problem this way has the advantage that it is not necessary to compute finite differences across the separatrix where the current density may be discontinuous; the integration is taken over the region where there is current and the Green's function takes care of the vacuum field. Doing the integrations accurately requires a fine mesh; if a general pressure profile were used, iteration would be necessary to find ψ inside the separatrix, and this method might be very expensive. But for our model problem, there is no ψ dependence on the right-hand side of Eq. (4) except for the shape of the separatrix. Since the separatrix is given by $\psi = 0$, Eq. (4) can be used to obtain the following non-linear equation for the separatrix.

$$c\int_{\Omega} G\, r'dr'dz' \;+\; \psi_w \frac{r^2}{a^2} \;=\; 0 \qquad (6)$$

where Ω is the region in the $r'-z'$ plane bounded by the separatrix. We do the integrations in spherical coordinates and represent the separatrix as an expansion in even-order Legendre polynomials as follows.

$$\rho(x) \;=\; \Sigma_{n=1}^{N}\, a_n P_{2n}(x) \qquad (7)$$

where $\rho(x)$ is the spherical radius of the separatrix at the polar angle $\theta = \cos^{-1}(x)$. The problem is solved when the a_n's are determined.

When Eq. (6) is solved for very large c the small radius spherical solution is recovered. As c is decreased the solutions remain practically spherical until the radius of the solution at z=0 becomes greater than about .6a; as c is decreased further, the solutions become prolate and racetrack-like in shape. As c approaches the value $36\psi_w/a^4$, the elongation becomes infinite, and the two-dimensional solution branch connects with the one-dimensional high-trapped-flux solution branch. The significance of this value of c is that the only one-dimensional solution that satisfies the average-beta condition of Barnes[5] is the high-trapped-flux solution at $c = 36\psi_w/a^4$. Figure 2 shows the separatrix shapes for a sequence of values of c approaching the critical value, Fig. 3 shows the elongation of the solutions as a function of c, and Fig. 4 shows the flux plot of a long equilibrium. Note that the elongation is sharply singular at the critical value of c; only in a narrow region in c are long equilibria obtained. Since these elongated equilibria lie near a bifurcation point, it should be a very delicate matter to compute them by standard numerical methods.

We have found up to four solutions of our model problem given a value of c. There may be other solution branches, but this two-dimensional branch contains elongated racetrack equilibria of the type observed in experiments.

This work was performed under the auspices of the U.S.D.O.E.

REFERENCES

1. H. L. Berk, J. H. Hammer, and H. Weitzner, Phys. Fluids 24, 1758 (1981).
2. R. N. Byrne and W. Grossman in Proceedings of the Third Symposium on Physics and Technology of Compact Toroids in the Magnetic Fusion Energy Program, (Los Alamos Scientific Laboratory, Los Alamos, New Mexico, 1980), pg. 138.
3. D. V. Anderson and J. H. Hammer, private communication.
4. R. Christian, private communication.
5. D. C. Barnes, C. E. Seyler, and D. V. Anderson in Proceedings of the US-Japan Joint Symposium on Compact Toruses and Energetic Particle Injection, (Plasma Physics Laboratory, Princeton, New Jersey, 1979), pg. 110.

FIGURE CAPTIONS

Fig. 1 The ψ=0 radius is displayed as a function of c for the one-dimensional solution of the model problem. The dot on the upper branch locates the point where the two-dimensional solutions connect with the one-dimensional solutions.

Fig. 2 The separatrix shapes for a sequence of values of ca^4/ψ_w are shown: (a) 60, (b) 40, (c) 36.4, (d) 36.07.

Fig. 3 The elongation, z_{sep}/r_{sep}, is displayed as a function of c.

Fig. 4 A flux plot for the case ca^4/ψ_w = 36.07 is shown.

Figure 1

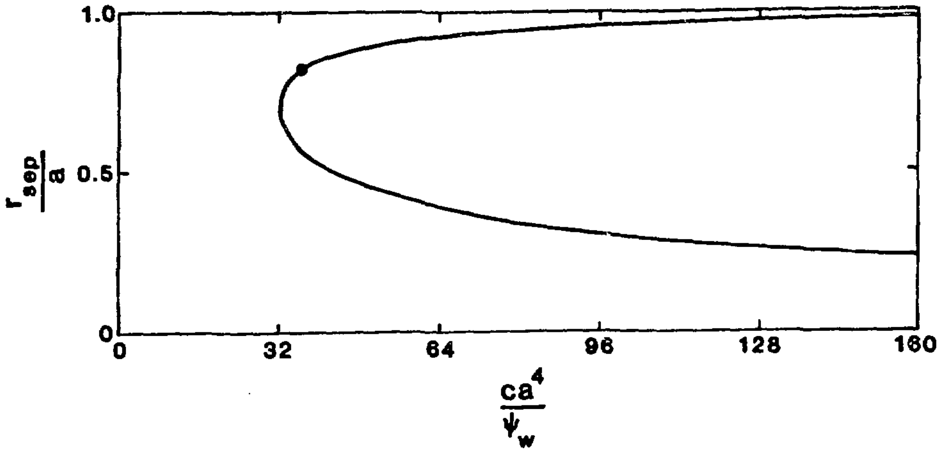

Figure 2

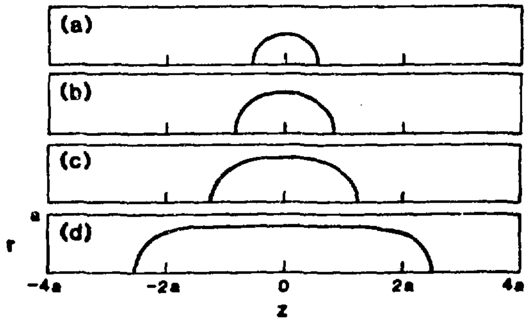

Figure 3

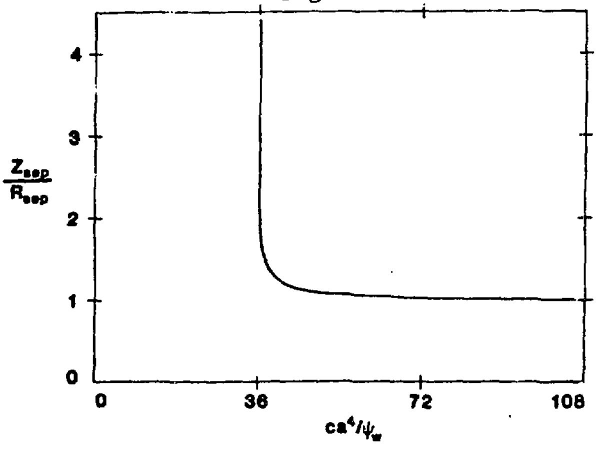

Figure 4

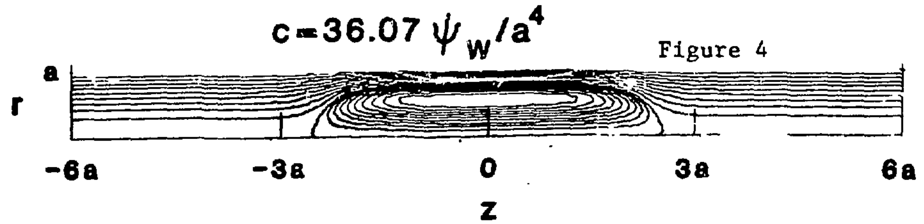

PLASMA TRANSPORT MODELLING OF A FIELD-REVERSED THETA PINCH

by

Loren C. Steinhauer, Richard D. Milroy, and Alan L. Hoffman
Mathematical Sciences Northwest, Inc.

I. Introduction

Although most of the work on field-reversed theta pinches has emphasized plasma formation and stability, increased attention has been focussed lately on transport processes. On the FRX-A and -B experiments,[1] the observed particle confinement times, $\tau_N = 30 - 50$ μsec, are somewhat lower than expected for classical resistivity. Therefore turbulent mechanisms, in particular the lower hybrid drift (LHD) instability, have been identified as possible causes of the anomalous transport. Theoretical calculations[2,3] based on an estimated particle diffusivity for the LHD mode predict τ_N consistent with the experiment. However, the decay of the magnetic configuration, represented by the loss of poloidal magnetic flux, has not been adequately addressed. Previous calculations either ignored flux loss or assumed classical resistivity at the magnetic axis since the LHD diffusivity vanishes at that point.

We have considered the loss of poloidal flux, ϕ_p, that can be inferred from experiment. Although ϕ_p cannot be measured directly, it[4] and the ion inventory inside the separatrix, N, can be inferred from external loop measurements and single chord interferometry if a two dimensional equilibrium is assumed. Figure 1 shows the time histories of ϕ_p and N from the TRX-1 experiment described in paper A2. Clearly τ_ϕ and τ_N are comparable, suggesting that flux loss is also anomalous.

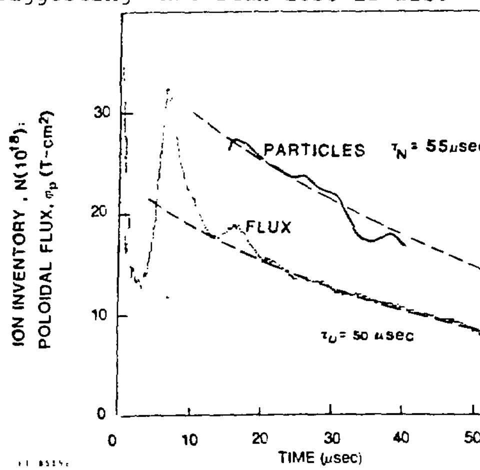

Figure 1. Time Histories of Inferred Ion Inventory and Poloidal Flux on TRX-1 Shot 1867 (15 mTorr Fill Pressure)

II. Plasma Model

We have developed a plasma formulation which describes both particle and flux loss and thus serves as an interpretive tool in determining the actual resistivity. The plasma is assumed to be in equilibrium in both the radial (radial pressure balance) and axial[1] ($\bar{\beta} = 1 - x^2/2$) directions. It is elongated, axisymmetric, and uniform in the axial direction in the region between two "sharp" ends (Figure 2). The radial profile is "two-dimensional" in that the pressure is constant on a flux surface. Uniform temperature is assumed. Finally, on open field lines, endloss is represented as a particle sink $-n/\tau_s$ where τ_s is the end streaming time.

Given these assumptions, it is possible to solve the transport problem on a reduced domain in radius, $R \leqslant r$. The effect of both particle inventory and diffusion in the inner region, $0 \leqslant r < R$ is accounted for by a correction factor applied in the diffusion velocity in the outer closed line region, $R \leqslant r \leqslant r_s$.

Figure 2. Magnetic Field Configuration

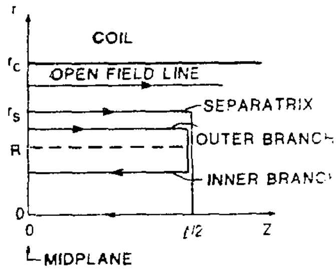

A. Quasi-steady profile model. The "simplest" solution is found by assuming a quasi steady radial profile. This allows time dependent bulk parameters, e.g., vacuum magnetic field, separatrix radius, and length, but assumes a nearly constant normalized radial structure. Then the diffusion equation reduces, by a separation of variables procedure, to an ordinary second order differential equation. The open field line region is solved analytically by assuming strictly steady behavior in that region: that result is applied as a boundary condition at r_s. The earlier method of Tuszewski and Linford[3] is similar except that they assumed a strictly steady radial profile (constant r_s, magnetic field) and thus ruled out flux loss *a priori*. This method calculates the instantaneous decay times τ_ϕ and τ_N.

B. Time-dependent calculation. A second approach is to numerically solve the time dependent equations in a magnetic flux coordinate system. The same numerical procedure is applied to both open and closed field line regions. The problem is initialized using a pre-specified initial profile (usually rigid rotor). The profile then evolves in time as the configuration decays. The time history of global parameters (ϕ_p, N, r_s, ℓ, and excluded flux) are followed as a function of time for comparison with experimental data. The quasi-steady and time-dependent methods were compared to determine the accuracy of the quasi-steady assumption. The decay times were quite close, within 10 percent, even for a rapidly decaying plasma.

III. Interpretation of Recent Experiments

We calculate the transport for plasma conditions, Table I, comparable to those in the FRX-B and TRX-1 experiments. The resistivity is the sum of classical, η_c, and LHD (wave energy bound), η_a, each multiplied by adjustable factors, f_c and f_a.

Table I

Bulk Parameters Relevant to FRX-B and TRX-1

parameters:	
vacuum magnetic field	= 0.55 T
ion temperature	= 200 eV
electron temperature	= 110 eV
r_c	= 12.5 cm
ℓ	= 75 cm

For a radius appropriate to FRX-B (R = 3.7 cm) and $f_c = f_a = 1$, the calculated particle loss time is close to experiment, $\tau_N \cong 40$ µsec, but τ_ϕ = 600 µsec which is far too long ($\tau_\phi \cong 50$ µsec was inferred from external loop data). Thus the simple "classical plus LHD" resistivity fails to match the experiment. Increasing the anomalous coefficient, f_a, has little effect on τ_ϕ, and in fact increases it. However, increasing f_c causes τ_ϕ to drop rapidly: for $f_c \cong 5$, $\tau_\phi \cong 45$ µsec and $\tau_N \cong 28$ µsec, in much better agreement with experiment.

This is evidence for an anomalous mechanism in addition to the LHD mode (which causes no anomalous flux loss).

Figure 3 shows radial profiles for a combination which gives good agreement with both τ_ϕ and τ_N. Note that the drift parameter v_D/v_i is depressed substantiall near the magnetic axis in contrast to rigid rotor like profiles. The consequent flattening of ∇B is characteristic of race track like equilibria.

Figure 3. Radial Profiles for Parameters of Table I with R = 3.7 cm; Resistivity is 4 x classical + 1/2 x LHD; and the Endloss Rate on Open Field Lines is Reduced by 1/2. For these assumptions, τ_ϕ = 54 μsec, τ_N = 40 μsec.

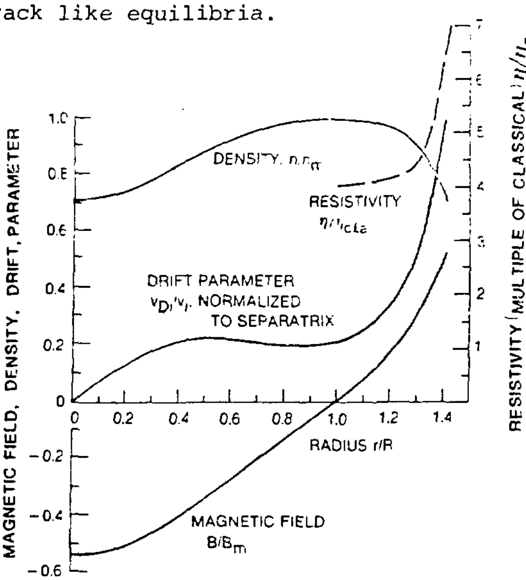

Suppose the same resistivity as assumed in Figure 3 is applied in a larger radius example relevant to plasmas produced in TRX-1, R = 4.7 cm. Then τ_N increases by a factor of 3.6 (to 145 μsec) and τ_ϕ increases by 1.6 (to 90 μsec). However, inspection of Figure 1 shows that the decay times are actually much shorter. Evidently, the resistivity combination of Figure 3 is not universal. In fact, f_c must be raised to about 8 and f_a to 1 to produce the τ_ϕ, τ_N shown in Figure 1.

Another resistivity form with classical plus LHD plus a "bump" localized near the magnetic axis was applied using the time-dependent model. This simulates turbulence localized near the field null which was conjectured to be an alternative explanation for the rapid flux loss. For an 8 x classical bump, ∇B was dramatically flattened near R, driving τ_ϕ rapidly toward large values. In view of this unrealistic behavior localized turbulence near the magnetic axis seems to be ruled out.

Finally, an alternative axial structure to that of Figure 2 was considered using the time-dependent model. The closed flux lines were assumed to have equal elongation (length ÷ radial width) rather than equal length. This resembles a Hill's vortex, in contrast to the equal length case which is closer to a race track. The alteration had little effect on τ_N but doubled τ_ϕ as a result of a more extreme depression of ∇B near R. This seems less realistic because reduced ∇B is characteristic of a race track and not a Hill's vortex.

IV. Conclusions

Two plasma transport models have been devised to interpret the decay of field-reversed configurations. The quasi-steady profile and the time-dependent computation agree quite closely. A resistivity form of classical plus LHD grossly underestimates the poloidal flux loss rate. The "classical" contribution must be enchanced by a factor of 4 to 8 to get the proper τ_ϕ. This indicates the presence of additional non LHD turbulence. The radial profiles exhibited a flattening of ∇B near the magnetic axis, a feature characteristic of race track equilibria. A resistivity form adding a spatial "bump" near the magnetic axis was also studied in order to simulate localized turbulence in that region. This form predicted very long τ_ϕ and thus was regarded as unrealistic. Finally, an alternative axial profile closer to that of Hill's vortex equilibria was considered. This change produced even more ∇B flattening near the magnetic axis. This is inconsistent with Hill's vortex equilibria (no ∇B flattening) and suggests that the plasma naturally seeks out race track like equilibria.

Acknowledgements This work was supported by USDOE Contract No. DE-AC06-80ER53098

References

1. W.T. Armstrong, et al., Los Alamos Scientific Laboratory, Report LA-UR-80-158 (1980); to be published.

2. S. Hamasaki and N.A. Krall, in Proceedings of the Third Symposium on the Physics and Technology of Compact Toroids in the Magnetic Fusion Energy Program, Los Alamos Scientific Laboratory, Report LA-8700-C (1980), p. 152.

3. M. Tuszewski and R.K. Linford, Los Alamos Scientific Laboratory, Report LA-UR-81-2319 (1981); to be published.

4. A.L. Hoffman, R.D. Milroy, and L.C. Steinhauer, to be published.

5. H.L. Berk, et al., Phys. Fluids 24, 1758 (1981).

Particle Transport in Field Reversed Configurations

M. Tuszewski, R. K. Linford, J. Lipson and A. G. Sgro

1. Introduction

A field reversed configuration (FRC) is a compact toroid that contains no toroidal field. These plasmas are observed to be grossly stable[1] for about 10-100 μsec. The lifetimes appear limited by an n = 2 rotational instability which may be caused by particle loss.[2] Particle transport is therefore an important issue for these configurations. We investigate particle loss with a steady-state, 1-D model which approximates the experimental observation[1] of elongated FRC equilibrium with about constant separatrix radius.

2. Steady-state particle transport model

We consider an FRC with a 2-D (r,z) elongated equilibrium confined inside a straight cylindrical conducting wall. The balance between plasma and magnetic field pressures in this geometry imposes[1]

$$\langle\beta\rangle = 1 - \frac{1}{2} x_s^2 \quad , \tag{1}$$

where $\langle\beta\rangle$ is the average $\beta = P/(B_o^2/2\mu_o)$ over the separatrix volume. B_o is the external magnetic field and x_s is the ratio of separatrix to conducting wall radius. The constraint of Eq. (1) applies to any axial (z) position on the elongated portion of the FRC. We neglect end effects and consider a 1-D model where 2-D effects are included by using Eq. (1) as a condition on the radial profile. We assume a steady state where particle loss across the separatrix is balanced by a source of particles from axial contraction. We assume uniform temperatures T_e and T_i, as suggested by the experimental data.[1] We further assume complete MHD stability and neglect self-consistent radial electric fields as well as flux annihilation at the field null. The steady-state radial diffusion equation is given by

$$\frac{1}{r}\frac{d}{dr}(r\Gamma) = \begin{cases} +\,n/\tau_\ell & r < r_s \\ -\,n/\tau_\parallel & r > r_s \end{cases} \quad , \tag{2}$$

where τ_ℓ is the time constant of the axial contraction and $\tau_\parallel$ is the particle confinement time on open field lines. We take $\tau_\parallel = \ell/2v_s$, where v_s is the sound speed and ℓ is the length of the FRC to model present experiments where particles steadily flow along open field lines, without any end-plugging. We assume, from experimental observation,[1] that ℓ is about 70% of the coil length. In addition to Eq. (1), the second constraint on the radial profile comes from matching at the separatrix the particle fluxes from the closed and open field line regions. To satisfy this boundary condition, it is useful to introduce an auxiliary variable w with

$$[d\beta/dr]_{r_s} = -\beta_s/w\rho_{io} \quad , \tag{3}$$

where β_s is the plasma β on the separatrix. The quantity w is just the ratio of the gradient length at the separatrix to the vacuum ion gyroradius ρ_{io}. The condition $r\Gamma(r_s-) = r\Gamma(r_s+)$ determines the value of w. The particle confinement time τ is defined as $N/2\pi r_s\Gamma_s$, where N is the number of particles per unit axial length within the separatrix and $2\pi r_s\Gamma_s$ is the radial flux of particles at the separatrix, per second and per unit axial length.

We take $r\Gamma = (r\Gamma)_C + (r\Gamma)_{LHD}$ where $(r\Gamma)_C$ is the classical (Spitzer) particle flux and $(r\Gamma)_{LHD}$ corresponds to anomalous transport from the Lower Hybrid Drift (LHD) instability saturated by wave energy bound.[3] A quantitatively similar saturation level is obtained from electron resonance broadening.[4] Other saturation mechanisms such as ion trapping[5] yield higher saturation levels for the cases of interest in this work. It is found that typical FRC radial profiles have a classical core near the field null ($r = R$) and an anomalous region in the vicinity of the separatrix. The particle confinement times τ, determined by LHD transport, will be shown to be in good agreement with the experimental data.[1] On the other hand, classical transport yields lifetimes which do not fit the experimental data. Integrating Eq. (2) from $r = o$ to $r = r_s$, and using Eq. (3), one obtains

$$\tau = 4\,\frac{(m_i/\pi m_e)^{1/2}}{(1 + T_e/T_i)\omega_{cio}} \cdot \frac{(1 - \beta_s)^{3/2}\langle\beta\rangle}{\beta_s} \cdot S \cdot w^3 \quad , \tag{4}$$

where $S = R/\rho_{io}$. Integrating Eq. (2) from $r = r_s$ to $r = r_w$, assuming an exponential tail for the pressure profile on open field lines, using Eq. (4) and particle flux continuity at the separatrix, one obtains

$$w^4 = (\ell S/8\, r_s) \cdot (\pi m_e/m_i)^{1/2} \cdot (1 + T_e/T_i)^{1/2} \,/\, (1 - \beta_s)^{3/2} \quad . \tag{5}$$

For given m_e/m_i, T_e, T_i, B_o, r_w, ℓ, x_s, and for a given choice of w, Eq. (2) is integrated numerically for $r \leq r_s$, with the constraints of Eqs. (1) and (3). This determines the value of β_s, which in turn determines w with Eq. (5). By iterative procedure, the self-consistent values of w and β_s are found and the confinement time τ is obtained from Eq. (4). The details of this calculation are contained in Reference 6.

3. Confinement times for FRX-B and FRX-C parameters

We consider recent experimental data of the FRX-B device,[7] and the FRX-C parameters as projected from a scaling code.[8] Those parameters and the theoretical values of τ, β_s and w are given in Table I for each case. The values of τ are also plotted in Fig. 1 as function of the variable R^2/ρ_{io}. We observe from Fig. 1 that the theoretical values of τ for the FRX-B device are comparable to the experimental values of the stable periods which are also indicated in Fig. 1. This is consistent with the theoretical picture of plasma spin-up linked to particle transport.[2] The empirical scaling $\tau(\mu sec) \sim 0.6\, R^2/\rho_{io}$ derived from the FRX-B results[9] is also indicated on Fig. 1. The theoretical points are in good agreement with this scaling, perhaps suggesting a somewhat stronger scaling $\tau \sim 0.8\, R^2/\rho_{io}$. Within the uncertainties of the experimental data and of the transport theory, there is good agreement between experiment, the LHD theory in this paper, and the numerical results of Hamasaki,[9] who first suggested the R^2/ρ_{io} scaling. We observe from Fig. 1 that this scaling appears to approximately fit the projected performance of the FRX-C device. One should also note that this scaling only applies for deuterium ions. For other ion species, Eq. (4) shows a scaling of τ as m_i rather than the $m_i^{-1/2}$ dependence suggested by the R^2/ρ_{io} scaling.

4. Scaling of the LHD transport

We investigate the scaling of τ with the three parameters, S, x_s, and w, that control the radial β profiles. These parameters usually vary simultaneously, but in order to test the sensitivity of τ to each of them, we vary only one parameter on a given scaling, keeping the other two constant.

The scaling with S corresponds approximately to the cases of Table I and Fig. 1 since, for these data, the variations of x_s, w, and B_o are small. The numerical results suggest $\tau \sim R^2/\rho_{io}$, which is the empirical scaling discussed in the previous section. In addition to this observed R^2/ρ_{io} scaling, the model predicts increased confinement time with increases in the values of x_s and w.

It may be desirable to form FRC's with values of x_s closer to unity in order to minimize pressure gradients, as suggested by Eq. (1). We consider the FRX-C cases of Table I and vary x_s from 0.45 to 0.8, while keeping r_w, S, w, T_e, and T_i constant. The results of this scaling, given in Fig. 2, yield the approximate scaling $\tau \sim x_s^{3.3}$, so that an increase in τ up to a factor of seven may be obtained.

It is conceivable to improve the open field line confinement $\tau_{\parallel}$ by some end-plugging technique or by plasma injection. A corresponding increase in w may be obtained. We vary w for the FRX-C cases of Table I, at constant S and x_s. The results, given in Fig. 3, suggest $\tau \sim w^{1.6}$ and an increase of w from 1 to 3 yields about a factor of 6 increase in τ. Furthermore, increasing w decreases the value of the drift parameter v_d/v_i at the separatrix. This may greatly reduce anomalous transport if a different saturation mechanism such as ion trapping[5] is relevant in the weak drift parameter regime.

5. Comparison of various boundary conditions at the separatrix.

It has been shown above that the determination of the radial profile at the separatrix is crucial to the FRC confinement scaling. The detailed physics of this profile may involve two-fluid, electric field, electron temperature gradient and finite-orbit effects. In particular, it is of interest to evaluate the contribution to the pressure on open field lines of guiding centers inside the separatrix which are assumed not to suffer end loss. A 1-D transport code[9] is being used to compare various loss rates on open field lines that estimate this guiding center contribution. First, $\partial n/\partial t = n/\tau_{\parallel}$ is used, where $\tau_{\parallel} = \ell/2v_s$. This corresponds to the free streaming model of this paper. Second, an ad hoc reduction in loss rate is used with $\partial n/\partial t = (n/\tau_{\parallel}) \cdot \{1 - \exp[-(r - r_s)^2/\rho_{io}^2]\}$. Third, the contribution of guiding centers inside the separatrix is calculated, and the loss rate on open field lines is decreased accordingly. This work is in progress.

References

1. W. T. Armstrong, R. K. Linford, J. Lipson, D. A. Platts, and E. G. Sherwood, Phys. Fluids (to be published).
2. D. C. Barnes and C. E. Seyler, in Proceedings of the US-Japan Joint Symposium on Compact Toruses and Energetic Particle Injection, Princeton, (1979), p. 110.
3. R. C. Davidson and N. A. Krall, Nucl. Fusion 17, 1313 (1977).
4. S. P. Gary, Phys. Fluids 23, 1193 (1980).
5. H. V. Fahrbach, W. Köppendörfer, M. Munich, J. Neuhauser, H. Röhr, G. Schramm, J. Sommer, and E. Holzhauer, Nucl. Fusion 21, 257 (1981).
6. M. Tuszewski and R. K. Linford, "Particle Transport in Field Reversed Configurations," Los Alamos National Laboratory report LA-UR-81-2319 (1981) (submitted to Phys. Fluids).
7. J. Lipson, W. T. Armstrong, J. C. Cochrane, K. F. McKenna, E. G. Sherwood, and M. Tuszewski, Appl. Phys. Lett. 38 680 (1981).
8. R. E. Siemon and R. R. Bartsch, Third Symposium on Physics and Technology of Compact Toroids in the Magnetic Fusion Energy Program, Los Alamos 1980, Los Alamos National Laboratory report LA-8700-C (1981), p. 172.
9. S. Hamasaki and N. A. Krall, Conference Record IEEE International Conference on Plasma Science, Montreal (1979) 5E10.

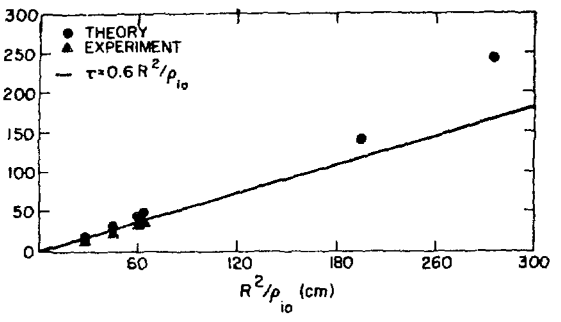

Figure 1
Scaling of τ with R^2/ρ_{io} for the FRX-B and C devices.

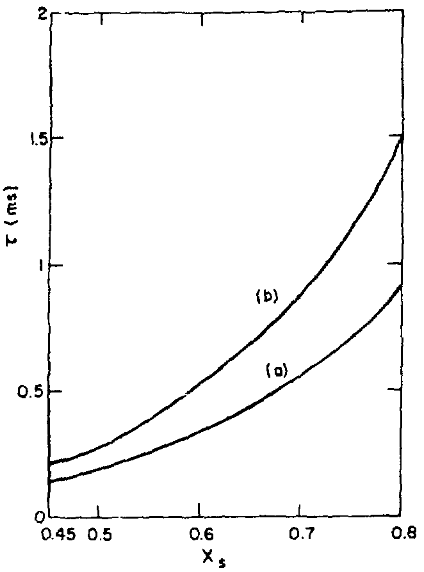

Figure 2
Scaling of τ with x_s
(a) FRX-C, S = 27
(b) FRX-C, S = 36

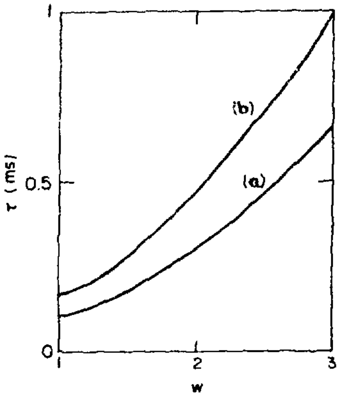

Figure 3
Scaling of τ with w
(a) FRX-C, S = 27
(b) FRX-C, S = 36

TABLE I

EXPERIMENTAL AND NUMERICAL FRC DATA

Device	P_o (mTorr)	x_s	S	T_i (eV)	T_e (eV)	β_s	w	τ (μs)
FRX-B	9	.44	7.1	870	150	.54	1.04	17
(r_w = 12.5 cm)	17	.42	12.2	430	150	.50	1.19	28
	29	.47	14.5	390	150	.44	1.15	42
	41	.45	16	270	150	.43	1.21	48
FRX-C	20	.45	27	500	150	.32	1.23	141
(r_w = 22.5 cm)	40	.48	36	250	150	.28	1.31	243

II. FIELD REVERSED THETA PINCH EXPERIMENT

Initial Operation of FRX-C*

W. T. Armstrong, R. R. Bartsch, J. C. Cochrane, R. W. Kewish,
M. Haworth**, R. K. Linford, J. Lipson, K. F. McKenna,
D. J. Rej, E. G. Sherwood, R. E. Siemon, and M. Tuszewski
Los Alamos National Laboratory
Los Alamos, NM 87545

Introduction

FRX-C is a field-reversed theta pinch recently placed into operation. It is designed to increase the stable lifetime of the field-reversed configuration (FRC) by increasing the size a factor of two (eight in volume) over the previous FRX-A & B experiments.[1] The near term objectives include: 1) determine the scaling of the FRC with size and clarify the mechanism(s) that limit confinement of an FRC, 2) investigate the MHD stability of FRCs with larger size relative to an ion gyro radius, and 3) generate FRCs with temperatures in the 0.1 to 1.0 keV range and densities in the range of 10^{15} to 10^{16} cm^{-3}. The machine was placed into operation on September 2, 1981. Preliminary results are given below based on a limited number of plasma discharges (42).

Description of the FRX-C Experiment[2,3]

The FRX-C theta-pinch coil has a 45-cm diameter and 2-m length. The main bank that generates the fast-rising field for implosion heating and FRC formation uses Scyllac technology. The capacitors are connected to the coil at two feed slots so that twice the dc charge voltage is applied to the coil. At maximum main-bank dc charge voltage (55 kV) the amplitude of the fast rising field is ~ 15 kG with a quarter period of 5 μs. The e-folding decay time of the crowbarred waveform following the peak of the magnetic field is ~ 300 μs, as required to study expected confinement times of 100 μs or more. An initial slow-rising reversed-bias field is applied before preionization and application of the main bank. In initial experiments the bias has typically been about 2 kG, but studies are planned with various bias levels up to about 5 kG. A vacuum magnetic field waveform typical of the initial operation is shown in Fig. 1. Electrical parameters of the experimental hardware are listed in Table I and a detailed description is contained in Ref. 2. The vacuum system has a base pressure of 2×10^{-8} torr and consists of a 40-cm diameter, 3.6-m long quartz discharge tube, stainless steel vacuum hardware, and two cryo pumps.

The initial experiments have utilized a ringing theta pinch to generate the PI plasma as was done on earlier experiments.[1] The PI discharge occurs approximately 20 μs prior to the main bank and is preceeded by two low-level rf discharges (~ 35 MHz) that provide seed electrons. A z-pinch preionization system is also planned to permit flexibility in the experiment. Passive mirrors are used at each end of the theta-pinch coil to aid the reconnection process. At present an on-axis mirror ratio of 6% results from a 5% reduction in coil radius that extends 16 cm at each end.

FRC Parameters

The present limited parameter set is compared with the predictions of a semi-empirical FRC scaling code[3] (used in the design of FRX-C) in Fig. 2. The good agreement of predicted and observed parameters supports the code predictions of parameters at other operating conditions. The data obtained for

*Work supported by the U.S. Department of Energy.

**Present address: Auburn University, Auburn, Alabama.

the single operating condition presently studied are summarized in Table II. The inferred ratio of major radius to ion gyro-radius is ~ 26 (referenced to the external field). The achievement of an increase in this quantity over past smaller experiments (the device FRX-B achieved values in the range of 7-18) is important in assessing the scaling of FRC stability and transport properties.

The diagnostics presently incorporated on FRX-C include an axial array of compensated field probes to determine the separatrix profile, a side-on 3.4-μm interferometer, a C-V Doppler broadening measurement for T_i, and an end-on framing camera. Early azimuthal asymmetry in the FRC formation, associated with the theta-pinch preionizer and the radial implosion, is indicated by end-on framing photographs. However, the FRC is observed to regain azimuthal symmetry in ~ 10 μs after main bank firing. More serious axial asymmetries associated with reconnection and axial contraction are observed in the separatrix profile data. The data suggest shot-to-shot variation in FRC length (50 to 150 cm) and axial position. Short, displaced FRCs may result in less-than-optimum lifetimes. Changes in the mirror configuration and initial plasma conditions are planned to further aid symmetric, reproducible reconnection.

Additional diagnostics are being developed for future operation. Single-point Thomson scattering for T_e is being installed. Neutron and proton yield measurements are planned for T_i, as well as O-VII Doppler broadening measurements for T_i. The redundant temperature measurements will aid interpretation of C-V and O-VII impurity radiation measurements (dependent on equilibration with deuterium) and clarify interpretation of nuclear yield measurements (sensitive to the tail of the ion distribution function). Detailed density measurements are planned through a multipoint, nonspectrally-resolved Thomson scattering diagnostic, an end-on cine-holographic interferometer, and additional side-on interferometry. The Thomson scattering diagnostic will provide an axial density profile to be used in identifying internal tearing, as well as the ellipticity of the flux surfaces. The holographic interferometer will provide radial density profiles needed to ascertain FRC transport and equilibrium properties. Collective scattering measurements of CO_2 laser light from plasma fluctuations in the separatrix region are also planned in the study of anomalous radial transport.[4]

Critical Issues

The principal objectives of the FRX-C experiment are to establish the scalings of FRC stability and transport with increased plasma and coil size. Previous theoretical work indicated a large rotational velocity must be exceeded to induce the rotational instability.[5] Recent theoretical work suggests instability may occur at lower rotational velocities but with slow growth rates consistent with experimental quiescent periods.[6] Past experimental evidence[1] has supported a possible causality between particle transport and rotational acceleration. More recent experimental work has shown some contribution of end-shorting to rotational acceleration.[7] Finally, continuing analysis of particle transport dominated by the lower-hybrid-drift instability suggests improvement in confinement with increased plasma radius.[8]

These various issues will be initially addressed on FRX-C by varying the particle inventory and closed flux to ascertain the basic confinement and stability scaling with respect to smaller devices. The present FRX-C data is too limited to impact on these issues. However, without optimized operation, FRCs formed on FRX-C have stable periods, which are substantially longer (~ 2 times longer) than FRCs formed on the smaller FRX-B device with similar densities, temperatures, and fields.[1]

References

1. W. T. Armstrong, R. K. Linford, J. Lipson, D. A. Platts, and E. G. Sherwood, Phys. Fluids (to be published Nov. 1981).
2. R. W. Kewish, Jr., R. R. Bartsch, and R. E. Siemon, "Engineering Design of the FRX-C Experiment," 9th Symposium for Engineering Problems of Fusion Research, (Chicago 1981).
3. R. E. Siemon and R. R. Bartsch, "Scaling Laws for FRC Formation and Predicition of FRX-C Parameters," Proc. of the Third Symposium on the Physics and Technology of Compact Toroids, Los Alamos, 1980, Los Alamos National Laboratory Report LA-8700-C (March 1981), p. 172.
4. H. U. Fahrbach, et al., Nucl. Fusion 21, 257 (1981).
5. C. E. Seyler, Phys. Fluids 22, 2324 (1979).
6. D. S. Harned, "Rotational Instabilities in the Field-Reversed Theta Pinch - Results of Hybrid Simulations," 23rd Annual Meeting of the Division of Plasma Physics, A.P.S., Vol. 26, No. 7, 2Q7, (New York, 1981), p. 882.
7. Y. Aso, Ch. Wu, S. Himeno, S. Yamaguchi, and K. Hirano, Compact Toroid Workshop, A3, (Osaka, 1981), p. 21.
8. M. Tuszewski and R. K. Linford, "Particlc Transport in Field Reversed Configurations," submitted to Phys. Fluids (1981).

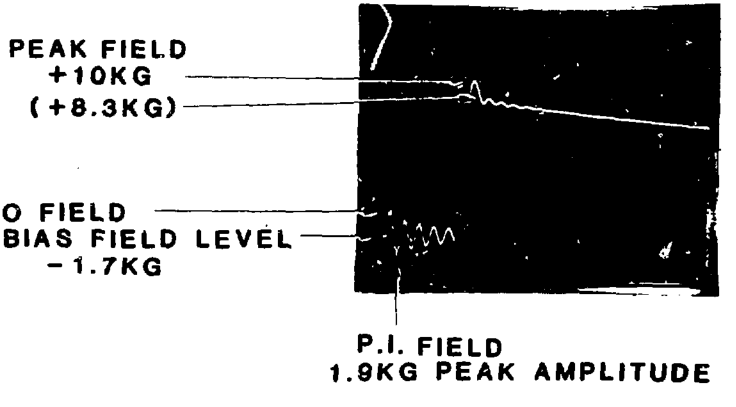

Fig. 1. The FRX-C vacuum magnetic field waveform (10 μs per division).

TABLE I: FRX-C MACHINE PARAMETERS

Coil Dimensions	
Diameter	.45 m
Length	2.0 m
End Mirror Ratio	1.06
Magnetic Field	
Typical Amplitude	10 kG
Risetime ($\tau_{1/4}$)	5 μs
Decay (L/R)	300 μs
Main Capacitor Bank	
No. of Capacitors (2.8 μf)	140
Stored Energy (55 kV)	600 kJ
Bias Bank	
No. of Capacitors (170 μf)	60
Stored Energy (10 kV)	500 kJ
Maximum Field	5 kG
Theta Preionization Bank	
No. of Capacitors (0.7 μf)	16
Stored Energy (50 kV)	14 kJ
Typical Field	1.9 kG
Frequency	200 kHz

TABLE II: FRC PARAMETER SUMMARY

Fill Pressure	20 mtorr
Main Bank Charge Voltage	42 kV
Bias Field	1.5 kG
Plasma Parameters at t ~ 30 μsec:	
Equilibrium field	7.4 kG
Separatrix Radius	~12 cm
FRC Length	~100 cm
Trapped Flux Fraction	~25%
Density (interferometry)	~4 x 10^{15} cm^{-3}
T_e+T_i (pressure balance)	~400 eV
T_i (Carbon V)	~200-300 eV
Stable Lifetime	70-100 μs

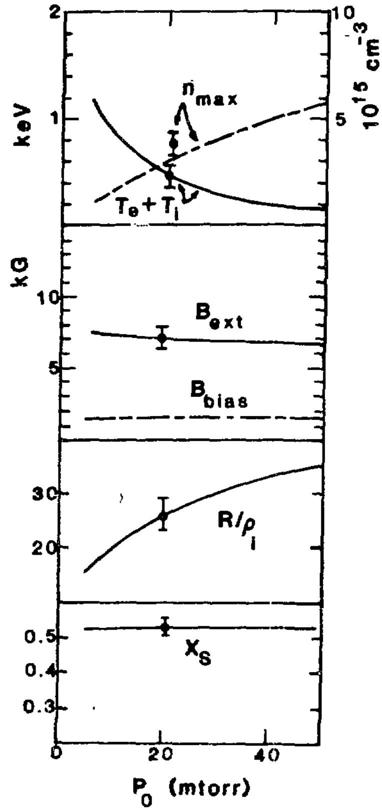

Fig. 2. A comparison of code predicted FRC parameters (lines) with FRX-C data (points). Error bars represent shot-to-shot variations.

COMPACT TOROID FORMATION
USING BARRIER FIELDS AND CONTROLLED RECONNECTION
IN THE TRX-1 FIELD REVERSED THETA PINCH

Alan L. Hoffman and W.T. Armstrong
Mathematical Sciences Northwest, Inc.

TRX-1 is a new 20 cm diameter, 1-m long field reversed theta pinch with a magnetic field swing of 10 kG in 3 μsec. It employs z discharge preionization and octopole barrier fields to maximize flux trapping on first half cycle operation. Cusp coils are used at the theta pinch ends to delay reconnection and fast mirror coils are used to trigger reconnection at a time designed to maximize axial heating efficiency and toroid lifetime. These controls are designed to study toroid formation methods which are claimed to be especially efficient by Russian experimenters.[1] Studies have been conducted on flux trapping efficiency, triggered reconnection, and equilibrium and lifetime.

1. Flux Trapping

Most experiments have been carried out using a low axial discharge current of 15 kA in a varistor damped half cycle lasting 5 μsec. In the presence of a bias field, plus mirror fields at the ends to direct the discharge along the tube walls, an annular discharge is formed which produces a very low preionization level and no measurable impurities. Figure 1 shows a calculation of the ionization level before and during a theta pinch implosion.

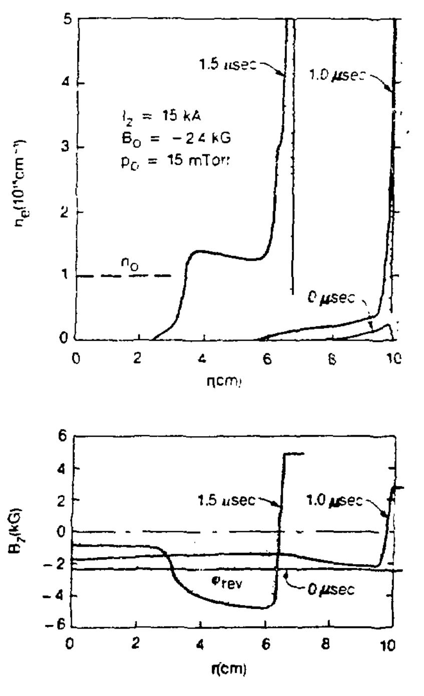

Figure 1. Flux Trapping Calculation for Low Annular Preionization

Cross tube interferometry and end-on visible photography confirm this qualitative behavior. Only a 25 percent ionization level is produced in a 2 cm annulus, and full ionization does not occur until the radial implosion reaches the axis. Nevertheless, reasonable flux trapping and nearly complete sweep-up is measured. At a 2.4 kG bias level about 40 percent of the initial flux remains at the external field zero crossing point, and 20 percent after a toroid is formed in axial equilibrium.

The above values can be increased by 50 percent by doubling the preionization current. Figure 2 shows measurements at a 30 kA axial discharge current of the reverse flux at the zero crossing point, and of the diamagnetic signal once radial equilibration occurs. Data is shown with and without barrier fields of about a 2 kG level at the tube walls. The barrier fields only increase flux trapping at the highest initial reverse bias flux levels. They also increase flux trapping for the large flux values produced by second half cycle operation, they significantly reduce the level of carbon impurities, and they tend to broaden the imploding sheath and eliminate radial bouncing. These are exactly the same effects noted by the Kurtmullaev group.[1]

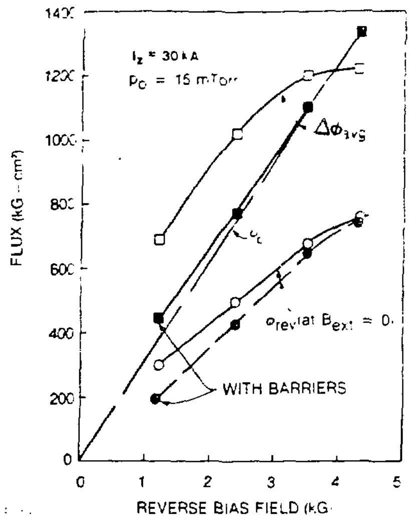

Figure 2. Flux Trapping Measurements at High Preionization Current

2. Triggered Reconnection

It has been found that experimentally measured data on the reconnection time could be exactly duplicated by MHD calculations[2] if the level of internal flux were correctly accounted for. Through the use of the cusp fields, reconnection could be delayed for about 6 μsec at a 2.4 kG reverse bias level. Figure 3 shows diamagnetic signal profiles both with and without triggered reconnection. Triggered reconnection occurs about 2 μsec after triggering the end mirrors, which also have 3 μsec risetimes but produce at least 50 percent higher field than the theta pinch. Early triggering results in an axial implosion occurring near peak field, and large diamagnetic signals. Imploding area waves and large radial excursions on central impact are predicted by MHD calculations, and are clearly seen in the experimental measurements.

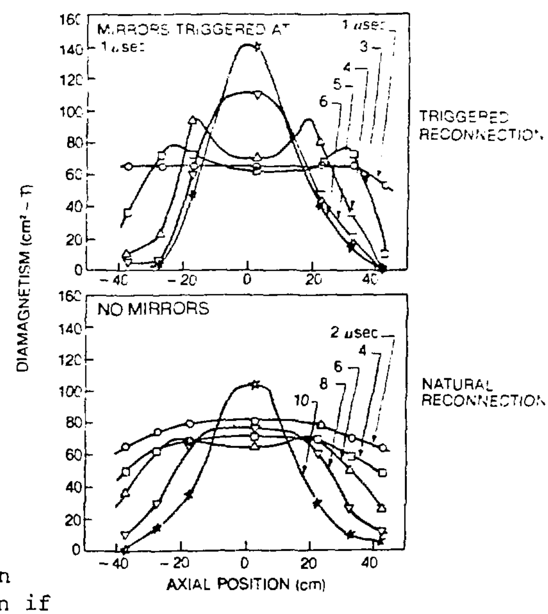

Figure 3. Experimental Diamagnetism Profiles During Triggering and Implosion

Careful Temperature measurements have not yet been made, but the ion temperature is about 150 eV before the axial implosion and about 200 eV afterward. These temperatures are considerably higher than would be produced by a non reversed theta pinch implosion and adiabatic compression.

Natural reconnection generally does not occur as symmetrically as shown on Figure 3, and almost always results in toroid ejection out one end. The axial implosion is weaker due to the lower magnetic field present after crowbarring the theta pinch capacitor bank. Reconnection can only be held off for the length of time shown if barrier fields are employed. Without barrier fields, tearing occurs well away from the theta pinch ends. The reconnection or tearing time can be characterized by the time at which the peak central diamagnetic signal occurs. This time is shown on Figure 4 as a function of initial reverse bias field for cases where the mirror coils are not energized. Internal field probes show that the peak axial implosion occurs about 3 μsec after full reconnection at the ends. Natural reconnection is seen to occur earlier as the internal flux is increased, in agreement with simple MHD modeling of plasma driven out of the reconnection region by $\vec{J} \times \vec{B}$ forces. The effects of barrier fields on reducing internal tearing tendencies is most likely due to a broader current sheet profile, but residual azimuthal field components could also be a factor.

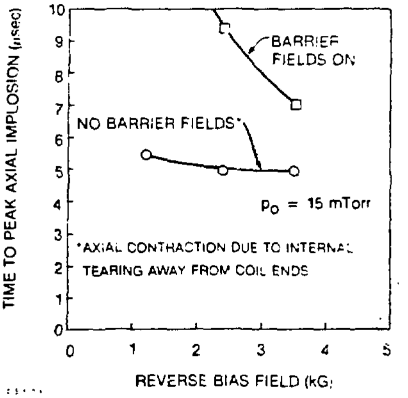

Figure 4. Natural Reconnection Time Dependence on Internal Flux

3. Equilibrium and Lifetime

Once the dynamic phases of radial and axial compression are complete, the resultant toroid will seek an equilibrium governed by radial and axial force balance, and flux conservation. For elongated field reversed configurations (FRC) the plasma shape will be determined by the ratio of internal to external flux, and the total plasma energy. This shape is only weakly dependent on exact profiles; the separatrix radius r_s, and length, ℓ_s, scale approximately as

$$r_s \propto (\phi_{rev}/B)^{1/3} \tag{1}$$

$$\ell_s \propto NT/(\phi_{rev}^{2/3}\ B^{4/5}) \tag{2}$$

where N is the total number of ions, T is the average temperature, ϕ_{rev} is the internal flux and B is the external field. Loss of internal flux then results in a decreased radius and increased length. Loss of particles results in decreasing length with no change in radius. In TRX-1, B does not change greatly during the life of the FRC.

Figure 5 shows measured diamagnetic signal profiles during the decay phase of a field reversed configuration. Figure 6 shows time dependent details of the diamagnetic signal, external field, 2271 Å CV radiation, and chordwise integrated electron density at the center of the theta pinch. The separatrix radius $r_s \simeq r_{\Delta\phi} = \sqrt{\Delta\phi/\pi B}$ is also plotted, and can be compared with the effective coil radius of 12.5 cm. Before a rotating m=2 instability destroys the configuration at 45 μsec, the most noticeable decay is in diamagnetic signal, rather than FRC length. This implies that internal flux loss is at least as important a loss mechanism as particle loss. Based on the data in Figures 5 and 6, plus Equations (1) and (2) assuming constant temperature, the flux loss time is

50 μsec and particle loss time is 55 μsec. The implications of this with respect to the radial extent of anomalous resistivity is discussed in paper B19.

Figure 5. Equilibrium Measurements

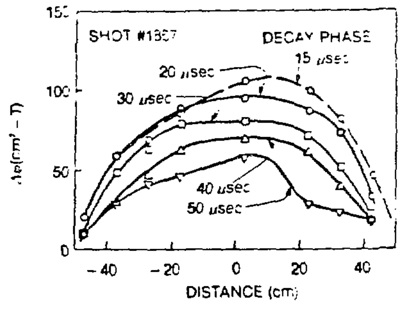

Figure 6. Central Flux, Density and Radiation Measurements

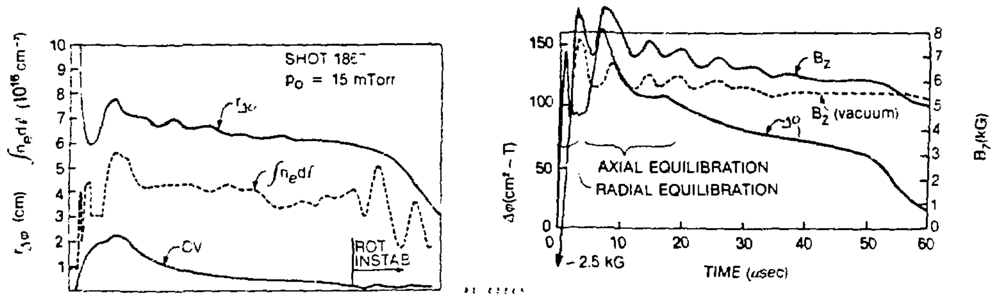

References

1. A.G. Es'kov, et al., in Plasma Physics and Controlled Thermonuclear Research, Vol. II, (IAEA, Vienna, 1978), p. 187.

2. R.D. Milroy, to be published.

ONSET TIME OF n=2 ROTATIONAL INSTABILITY OF FRC PLASMA

Y.Nogi, S.Shimamura, Y.Osanai, K.Saito, K.Yokoyama, S.Shiina, S.Hamada and H.Yoshimura
College of Science and Technology, Nihon University, Tokyo

Y.Aso, Ch.Wu,* S.Himeno** and K.Hirano
Institute of Plasma Physics, Nagoya University, Nagoya

T.Minato, M.Tanjyo, S.Okada, Y.Ito, S.Ohi, S.Goto, T.Ishimura and H.Itô
Plasma Physics Laboratory, Osaka University, Osaka

§ 1 Introduction

Confinement time of a field reversed configuration (FRC) plasma produced by a theta pinch has been prolonged till nearly 100 μsec.[1] At the end of the confinement phase almost FRC plasmas excite a n=2 rotational instability and touch a vacuum tube wall. Although Freidberg and Pearlstein determined the stability threshold for Ω/Ω_* (Ω is the angular frequency of the rotation and Ω_* is the ion diamagnetic frequency)[2], the cause of the rotation is understood poorly. There are two most promising mechanisms of the rotation in recent time. One is that the carrying away of angular momentum from the plasma due to ion diffusion across the separatrix causes the remaining plasma to rotate in the proper direction.[3] Computer simulations of a one-dimensional transport model of Hamasaki, where the quasi-linear diffusion coefficient for the lower hybrid drift instability is used, have indicated a scaling law concerning to the particle loss.[4] The half-life time for particle containment in a fixed coil radius has such a scale as

$$\tau_s(N/2) \sim R^2/\rho_i ,$$

where R is the major radius and ρ_i is the ion gyroradius at the separatrix. Past experimental works of FRX-A and B at Los Alamos National Laboratory appeared to be consistent with his scaling law.[5] On the other hand, Steinhauer proposed another mechanism, that is, end shorting effect on open field lines.[6] The plasma is spun up by viscous force associated with the rotation of the open field lines plasmas which are driven by end shorting currents. He derived a scaling law of the stable time which depends sensitively on aspect ratio. For low aspect ratio regime in which almost present experiments are included, the stable time is

$$\tau_s(\mathrm{end}) \sim LN^{5/4}T_i^{1/2}/B_e\Psi_p ,$$

where L is the distance between the end walls, N is the ion line density, B_e is the external field and Ψ_p is the poloidal flux. Some experiments showed good tendency to the parameters in the scaling law. Azimuthal magnetic field inferred from this axial shorting current has been observed by Thomas and Ekdahl.[7,8] These experiments, however, are standard theta pinches which have no reversed bias field.

Many experimental data will be needed to clear the mechanism of the rotation. Present paper shows recent results of FRC plasma experiments at three

* On leave from the Institute of Physics, Academia Sinica, Peking, China
** On leave from Energy Conversion Research Institute, Hokkaido University

laboratories in Japan; Nihon University, Nagoya University and Osaka University. After discussions of our data with their scaling laws, we propose a new one, which is suitable to account for the stable times of many FRC plasmas.

§ 2 Experimental Apparatus

The machine parameters are shown in Table 1. We describe briefly the remarkable points of each machine. In NUCTE (Nihon University), FRC is produced by a standard θ-pinch method except the preheating, which is used z-current ringing in the bias field.[9] In STP-L (Nagoya University), the preionized plasma is injected by two small coaxial guns and the preheating is done by standard θ-discharge. The machine has quasi-static guide field (GF) of 2.7 m long at both ends of the main coil.[10] In PIACE (Osaka University), two theta pinch guns which are located close to both ends of a main coil are used to generate counter streaming plasmas in the guide field.[11] The fully ionized plasma is compressed by the main coil in the reversed bias mode. Ion temperature of the produced plasma is very high (~1 keV).

Table 1

		Coil L (m)	Coil R (cm)	Tube R (cm)	Main Field B_{max} (kG)	Main Field τ (μs)	Bias Field (kG)
Nihon Univ.	NUCTE-I	2	8	5.7	10	40	-0.7
	NUCTE-II	"	"	6.9	"	"	"
Nagoya Univ.	STP-L	1.5	6	5.1	10	27	-0.5
Osaka Univ.	PIACE-I	1	5	4	20	45	-3.2
	PIACE-II	"	7.5	6	14	75	-2.0

§ 3 Measurement Methods

The ion temperature of the plasma T_i is inferred from the Doppler broadening of the CV 2271 Å line. The electron temperature T_e is measured by Thomson scattering of a ruby laser. The average electron density $\bar{n}_e$ is obtained by $\int n_e dr/2r_s$, where r_s is a separatrix radius in the axial midplane. The r_s and the plasma length ℓ_p are obtained from the excluded flux loop signals. An image converter camera is used to observe the macroscopic behavior of the plasma.

§ 4 Experimental Data and Discussions

All experimental data are listed in Table 2. The blanks in the Table mean that the values are not gotten at present.

Since the Hamasaki's scaling law is given in a fixed coil radius, it is not correct to compare with the different size machine data together. So only NUCTE is suitable to discuss the correlation with it. Although the R^2/ρ_i law has been confirmed by varing the bank energy and the filling pressure of the deuterium gas at LANL, we are trying to investigate it by means of different approaches, which are to know mass and R^2 dependences. For this purpose deuterium and hydrogen gases are prepared in NUCTE I, and the discharge tube in NUCTE I is replaced by a 20% larger bore tube in NUCTE II. The experimental results show $\tau(D_2)/\tau(H_2)=\sim 1.4$ as shown in Table 2. However, the ratio of R^2/ρ_i calculated from T_i, $R(\sim r_s/\sqrt{2})$ and B is $\tau(D_2)/\tau(H_2)=\sim 0.6$. The difference suggests that mass dependence is included in the proportional coefficient of the scaling law. The R effect is now under investigation.

	Gas	Ti (keV)	Te (eV)	ne (10^{15} cm^{-3})	lp (cm)	rs (cm)	τ diamag (μs)	τ stable (μs)
NUCTE-I	H_2	0.08	110	2.5	80-120	2.5	40-45	20-25
"	D_2	0.13	"	2.0-2.5	"	"	50-60	30-35
NUCTE-II	D_2					2.7-3.0	60-70	35-40
STP-L (without GF)	D_2	0.35	100	5	40-80	1.8	20	20
" (with GF)	D_2	0.45	140	"	"	"	30	30
PIACE-I	D_2	1.0	200-250	6	30-40	1.5	15-25	8-10
PIACE-II (High Comp.)	D_2	0.8		5.5	"	3.1	30-35	15-18
" (Low Comp.)	D_2	0.4		2.5	60	3.7	45	15-25

Table 2

The Steinhauer's scaling has many parameters. Some of them are easy to measure experimentally and some are not. Especially, the poloidal flux in the plasma is the most difficult to observe. It seems to be a future problem to discuss the experimental data with this scaling law.

We have tried to create a new scaling law to be able to explain all our data. So the parameters which contribute greately to τ_s is picked out. Since the experimental values have broadenings due to experimental error, reproducibilty and temporal transition of the plasma in the stable time, their average are used. For example, $\bar{n}_e=2.3\times10^{15}$cm^{-3}, $\bar{\ell}_p$=100 cm and $\bar{r}_s$=2.5 cm in NUCTE I(D_2). The fittest scaling law is

$$\tau_s = C_1\bar{n}_e\bar{r}_s\bar{\ell}_pL$$

as shown in Fig.1. As R_c (coil radius) is seemed to be proportional to r_s, this relation can be transformed into $\tau_s=C_2N_eL/R_c$, where N_e is a total electron number included in the separatrix and L/R_c is an aspect ratio of the main coil. The remarkable points of this scaling law are that τ_s does not depend on the temperature and the magnetic field strength. This scaling law suggests that the slender machine is preferable to the FRC plasma, provided the volume of the machine is constant. Mass dependence may be included in C_1. As there are few experiments using hydrogen gas, we can not assert how function of m is suitable.

Next work is to mark other experimental data down in Fig.1. Eberhagen and Grossmann's experiment agrees well with our scaling law, where τ_s=20μsec,

$\overline{r}_s$=1.75 cm, $\overline{n}_e$=2x10^{16}cm^{-3}, $\overline{\ell}_p$=35 cm (estimated value) and L=70 cm.[12] However, Es'kov's experiment is not on the extended line of our scaling law to 100 μsec.[1] As we don't know a set of the data in order to calculate $\overline{n}_e\overline{r}_s\overline{\ell}_p$ on FRX-A and B, their points are not plotted in the figure.

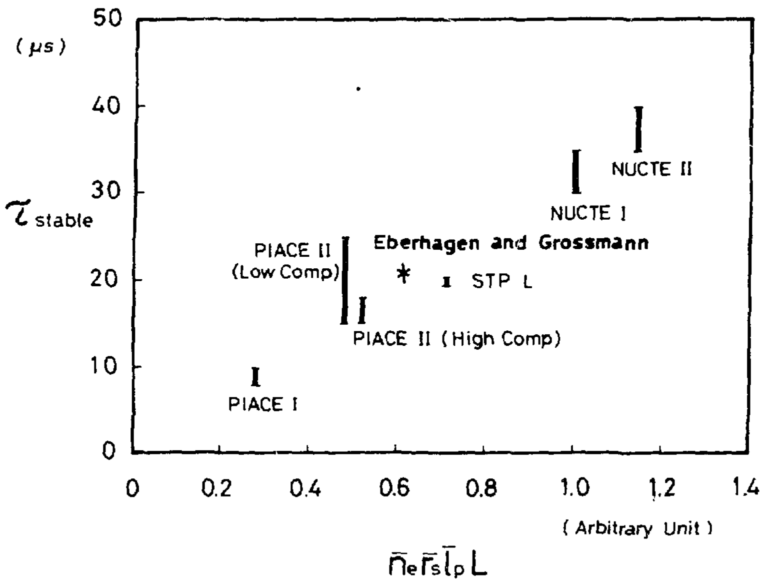

Fig. 1 Scaling of FRC Plasmas

References

1. A.G.Es'kov et al., Proc. 7th IAEA Conf. on Plasma Physics and Controlled Nuclear Fusion Research, Innsbruck (1978) CN-37/U-4-1
2. J.P.Freidberg and L.D.Pearlstein, Phys. Fluids, 21 (1978) 1207
3. D.C.Barnes and C.E.Seyler, Proc. US-Japan Joint Symposium on Compact Torus and Energetic Particle Injection, Princeton,(1979) p.110
4. Hamasaki et al., Proc. International Conf. on Plasma Physics, Nagoya, 1 (1980) 176
5. W.T.Armstrong et al., Proc. US-Japan Joint Workshop on Compact Toroids, Osaka, (1981) p.11
6. L.C.Steinhauer, Phys.Fluids, 24 (1981) 328
7. K.S.Thomas, Phys. Rev. Lett.,23 (1969) 746
8. C.A.Ekdahl et al., Phys. Fluids 23 (1980) 1832
9. Y.Nogi et al., Ref.5 p.29
10. Y.Aso et al., Ref.5 p.21
11. S.Ohi et al., Ref.5 p.11
12. A.Eberhagen and W.Grossmann, Z.Physik, 248 (1971) 130

RECONNECTION STUDIES IN A LOW-COMPRESSION THETA PINCH

E. Sevillano, F.L. Ribe, and H. Meuth
Aerospace and Energetics Research Program
University of Washington
Seattle, Washington 98195

Introduction

Compact Toroids (CT) are produced in the High Beta Q Machine (HBQM) with lifetimes that depend on the time the separatrix closes on axis. At low filling pressures when this closure occurs during the first 5 μsec of the discharge, the excluded-flux radius is nearly constant for 30-40 μsec. At higher pressures when reconnection occurs after approximately 10 μsec the excluded flux decays exponentially in 25-35 μsec. In the latter case an open field line configuration persists longer and end-loss is more important. The discharge can operate reproducibly in either regime.

Experiment

The HBQM has been described elsewhere;[1] however, a few modifications have been made. For the sequence of experiments reported here the 2-meter central section of the 3-meter coil is used in order to achieve higher confining fields. In this configuration the risetime of the main field is 400 ns when plasma is present and the L/R decay time is ~40 μs. The preionization is a ringing theta discharge with a frequency of 330 kHz. Bias fields B_b from -390 G to -510 G are used. The filling pressure is p_o = 5 mTorr for early CT formation and p_o = 10 mTorr for later formation. A CAMAC based computerized data acquisition system is also available. The discharge coil is very close to the discharge tube and therefore passive mirrors cannot be used. Reconnection without mirrors will be reported here.

The diagnostics include a single chord He-Ne (λ = 6328Å) quadrature interferometer for density measures, axial arrays of internal and external magnetic field probes and a one-turn loop around the discharge tube measuring the total flux ϕ. The external probes are positioned at z = -70, -60, 0, 60, 70 cm, where z = 0 is the center of the theta pinch coil. They are used with the ϕ loop to give the excluded flux radius $r_{\Delta\phi}$ defined from

$$B_o \pi r_{\Delta\phi}^2 = \int_0^{r_\ell} (B_o - B(r)) 2\pi r dr,$$

where r_ℓ is the loop radius and B_o the external field. It is easily shown that if the pressure on open field lines is neglected, $r_{\Delta\phi}$ measures the separatrix radius r_s. (Pressure on open field lines can be taken into account to estimate the error in $r_{\Delta\phi}$.[2]) The internal probes are enclosed in a 1 cm O.D. quartz sheath that reaches 30 cm into the theta pinch coil. The 3 internal probes used can be moved axially and the whole assembly can be positioned at various radii.

Results

Earlier experiments in bias flux trapping in the 3m machine with large initial bias (-1.5 kG) have been reported.[3,4] In those experiments only open field line configurations were observed. The main field did not rise to a sufficiently high value to force the separatrix close to the axis and produce reconnection. This behavior was also predicted by two-dimensional MHD codes.[5,6]

In order to get unaided reconnection the bias level was reduced and the main compression field increased by using a shorter coil. It was expected that these changes would induce early reconnection; however, it was not observed. Radial scans of the internal magnetic field showed a large fraction (40%) of the flux being trapped even at the end of the coil. The preionization voltage was subsequently lowered by a factor of 0.6 and reconnection was then observed.

Formation of a CT is indicated by several diagnostics. The internal magnetic field on axis near the end of the coil should change sign as the separatrix moves axially across the probe position. Figure 1 shows this field at 2 different axial positions, z = 70 cm and z = 100 cm (edge of coil) for p_0 = 5 and 10 mTorr. The feature at t = 0 is noise pickup by the probe when the main discharge is triggered.

The main difference between the two pressures used is the time of separatrix closure on axis. In the case of 5 mTorr, the change of sign occurs early in the discharge for the z = 100 cm position. This is an indication of reconnection at the end of the coil. The later change of sign at z = 70 cm indicates an axially contracting CT; this observation has been confirmed by measurements at z = 90 cm. For 10 mTorr at z = 100 cm separatrix closure on axis occurs after approximately 10 μsec and is later observed at the 70 cm position. An open field line configuration persists for about twice as long as in the 5 mTorr discharges; this delay changes the characteristics of the excluded flux as will be discussed below.

Figure 2 shows the excluded flux radius $r_{\Delta\phi}$ at z = 0 and 60 cm for the two filling pressures used. The 10 mTorr signal shows an exponential decay, similar to that of an ordinary theta pinch. The radius $r_{\Delta\phi}$ is essentially the same at the two axial positions. In the 5 mTorr case at z = 0, $r_{\Delta\phi}$ remains nearly constant for approximately 38 μsec, dropping rapidly after this time. It is not yet known what causes this sudden decrease. A possible cause is the m = 2 rotational instability observed in other experiments. At z = 60 cm $r_{\Delta\phi}$ decreases rapidly after ~5 μsec. This observation is also consistent with axial contraction. Some axial asymmetry in the excluded flux radius has been observed but only two discharges show an FRC leaving the coil axially. The axial contraction is not very strong in our case as evidenced by the lack of a large increase in $r_{\Delta\phi}$ at the center. Having less drastic axial motion might explain why the FRC has little tendency to escape axially.

Figure 3 shows internal magnetic field profiles as functions of radius taken at z = 70 cm. Four different times are displayed for each pressure, the magnetic axis position (radius of zero magnetic field) at 25.6 μsec is different for the two; radial motion is slower for the 10 mTorr fill. At 5 μsec only a small percentage (6%) of the initial flux is left for the 5 mTorr case; presumably most of it has been swept toward the central plane by the axial contraction. For 10 mTorr 50% of the initial flux is still present at this time. No negative field is observed at any radial position for 5 mTorr at 20 μsec whereas 10 mTorr still retains some.

When making the radial scans it was observed that as the probe was removed to the outside (less in contact with the plasma) the excluded flux signal lasted for longer times, up to 50 μsec. It appears that the probe is affecting the lifetime of the configuration. This has been observed by other groups.[7,8] Axial density measures also show signals of axial contraction but so far have not given indications of rotation. More analysis of these data is required.

Conclusions

Field reversed configurations with open or closed field lines are created reliably depending on the filling pressure, bias field, and preionization.

Compact toroids with lifetimes of 30-40 μsec are observed. It is not known yet whether the $m = 2$ instability is responsible for their termination. The internal magnetic-field probe affects the lifetime of the compact toroids and their time of formation. However, excluded-flux data without the probe are similar to those with it.

Acknowledgments

We wish to thank G. Harper, E. Hedin, and C. Greenfield for assistance in carrying out the present experiments.

This work was supported by the U.S. Department of Energy.

References

(1) S.O. Knox, et al., Conference Record-IEEE International Conference on Plasma Science, Madison, WI (1980), Paper IA5.
(2) M. Tuszewski, Los Alamos Report LA-8512-MS (1980).
(3) S.O. Knox, et al., Proceedings of the Third Symposium on the Physics and Technology of Compact Toroids (1980).
(4) S.O. Knox, et al., Reversed-Field Flux Trapping in a Low-Compression Theta Pinch. Submitted to Phys. Fluids.
(5) R.D. Milroy, private communication (1980).
(6) Z.A. Pietrzyk, private communication (1980).
(7) W.T. Armstrong, private communication (1980).
(8) S. Ohi, et al., Proceedings of the Third Symposium on the Physics and Technology of Compact Toroids (1980).

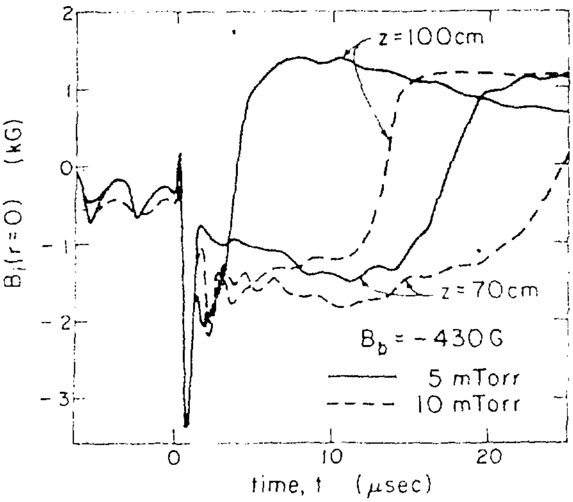

Figure 1. Internal magnetic field on axis at two axial positions. Time t=0 is the initiation of the main discharge.

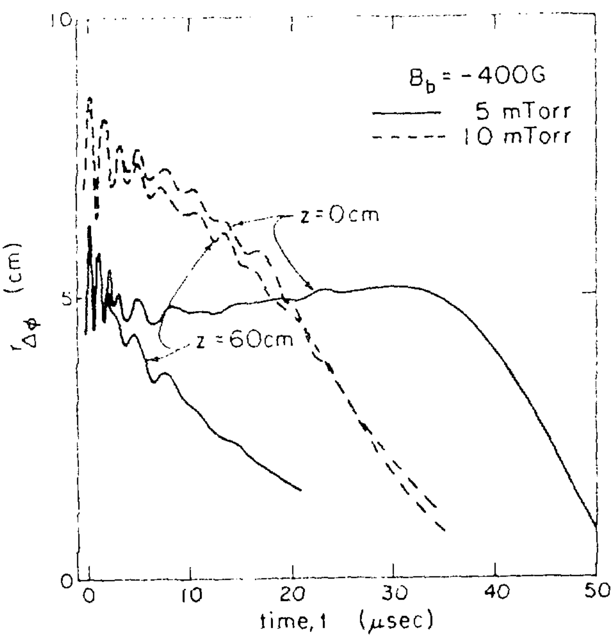

Figure 2. Excluded flux radius at two axial positions.

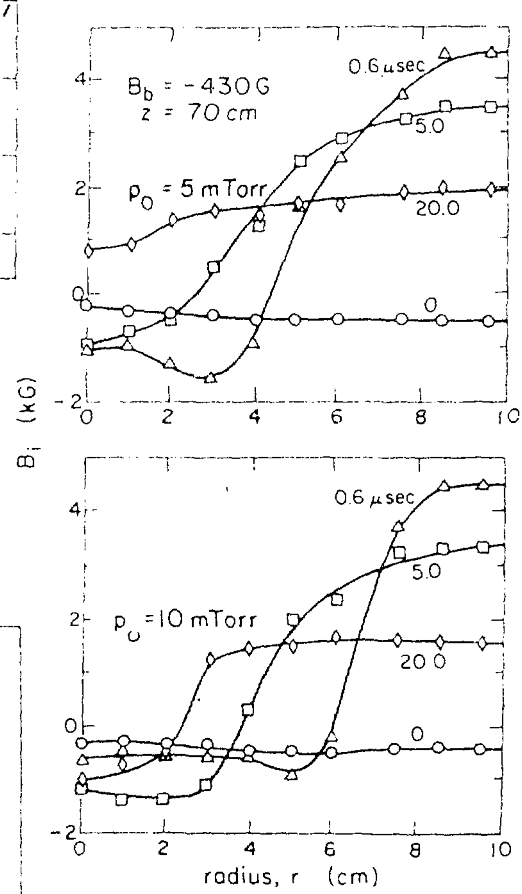

Figure 3. Internal magnetic field profiles at different times during the discharge. The position of the probe is z=70 cm. (z=0 is the center of the coil).

III. SPHEROMAK - THEORY

Analytic Model of the Radiation-Dominated Decay of a Compact Toroid*

Steven P. Auerbach
Lawrence Livermore National Laboratory, University of California
Livermore, California 94550

The coaxial-gun, compact-torus experiments at LLNL and LASNL are believed to be radiation-dominated,[1,2] in the sense that most or all of the input energy is lost by impurity radiation. This paper presents a simple analytic model of the radiation-dominated decay of a compact torus, and demonstrates that several striking features of the experiment (finite lifetime, linear current decay, insensitivity of the lifetime to density or stored magnetic energy) may also be explained by the hypothesis that impurity radiation dominates the energy loss. The model incorporates the essential features of the more elaborate 1 1/2-D simulations of Shumaker et al.,[3] yet is simple enough to be solved exactly. Based on the analytic results, a simple criterion is given for the maximum tolerable impurity density.

The model assumes that power flow in the compact torus decay is dominated by the following processes: magnetic energy is transferred to the electrons by ohmic heating; the electrons then lose their energy by radiation. Other loss channels, such as electron-ion equilibration, electron cross-field heat conduction and ion cross-field heat conduction are assumed to be negligible. Given the observed temperatures and densities, neglecting these other loss channels is readily shown to be justified. The power flow equations are then

$$\frac{dW_B}{dt} = - P_{OH} \tag{1}$$

$$\frac{dW_{T,e}}{dt} = P_{OH} - P_{RAD} \tag{2}$$

where W_B is the magnetic energy, $W_{T,e}$ the electron thermal energy, P_{OH} the ohmic heating power, and P_{RAD} is the radiated power. Model expressions for W_B, P_{OH} and P_{RAD} will be discussed next.

The plasma is in MHD equilibrium inside the flux conserver. The equilibrium will be modeled by the spherical force-free Spheromak equilibrium of Morikawa,[4] and Rosenbluth and Bussac.[5] Essentially identical results would be obtained if the force-free cylindrical equilibria of Bondeson et al.[6] were used. For the Spheromak equilibrium, the magnetic energy is $W_B = bI^2R$ where b = constant, I = total toroidal current, R = separatrix radius. For this equilibrium, the current is parallel to the magnetic field. Thus, using the Spitzer parallel resistivity,

$$P_{OH} = \int \eta_{\parallel} J^2 d^3x = \bar{\eta}_{\parallel} \int J^2 d^3x \tag{3}$$

*Work performed under the auspices of the U.S. DOE by the Lawrence Livermore National Laboratory under contract number W-7405-ENG-48.

where $\bar{\eta}_{\parallel}$ is an average parallel resistance. For the Spheromak equilibrium, P_{OH} is then $P_{OH} = aI^2/(RT^{3/2})$ where a = constant, T = electron temperature. If I is measured in amperes, R in cm, T in eV, then the constants are a = .6, b = 1.8 x 10^{-9}.

The radiated power will be modeled by a power law fit to the coronal equilibrium radiation calculations of D. E. Post et al.[7] Thus, the radiated power is taken to be $P_{RAD} = cn_e n_I VT^k$ where c and k are constants, n_e and n_I are the electron and impurity densities, respectively, and V is the plasma volume. As an example, for oxygen radiation in the range $5 < T < 20$ eV, a decent fit to the coronal equilibrium calculations is $c = 4.2 \times 10^{-28}$, $k = 1.92$ (if P_{RAD} is measured in watts, V in cm^3, and T in eV). For carbon, the appropriate values are $c = 7 \times 10^{-28}$, $k = 2.55$ for $3 < T < 10$ eV. Similar parameterizations are also reasonable above the radiation barriers. For example, for oxygen in the temperature range $30 < T < 100$ eV, $c = 4.5 \times 10^{-21}$, $k = -3.8$ provides a reasonable fit. However, for these higher temperatures the neglect of cross-field ion heat transport may not be correct, so these temperature ranges will not be discussed further.

To derive soluble equations, three further assumptions will be made: (1) the separatrix radius R is constant. This is indeed approximately true for the decay of plasma in a flux conserver, for which R $\sim$ flux conserver radius, (2) n_e, n_I are constant during the discharge. This is certainly true classically, since the particle loss rate is of order β times the field decay rate ($\beta = 8\pi P/B^2$), and (3) $P_{OH} = P_{RAD}$. This is reasonable because, in a low beta plasma, the electron heat capacity is so small that the electron energy sources and sinks must very closely balance. All of these assumptions agree well with the results of numerical simulations.

As a result of these assumptions, Eqs. (1) and (2) become, respectively

$$bR \frac{dI^2}{dt} = - \frac{aI^2}{RT^{3/2}} \tag{4}$$

$$\frac{aI^2}{RT^{3/2}} = cn_e n_I VT^k \tag{5}$$

Equation (5), the electron power balance equation, determines the electron temperature:

$$T^{3/2} = \left(\frac{aI^2}{cRVn_e n_I}\right)^{\alpha} \tag{6}$$

where $\alpha = 3/(3 + 2k)$. Combining Eqs. (4) and (6) and solving the resulting equation, the result is

$$I(t) = I(0) \left(1 - \frac{t}{t_E}\right)^{1/2\alpha} \tag{7}$$

where the "extinction time" t_E is

$$t_E = \frac{\left(I(0)\right)^{2\alpha}}{\gamma} \qquad (8)$$

$$\gamma = \frac{a\alpha}{bR^2}\left(\frac{cn_e n_I RV}{a}\right)^{\alpha}$$

The magnetic field components will also obey an equation like Eq. (7) because, for fixed R, the fields are proportional to the current I. Equations (7) and (8) have the following consequences:

A.) Finite lifetime--Obviously, the currents and fields are extinguished in a finite time t_E.

B.) Lifetime scaling--Since $W_B = bI^2R$, the extinction time scales as

$$t_E \sim \frac{\left(W_B\right)^{\alpha}\ (R)^{2-5\alpha}}{(n_e n_I)^{\alpha}} \qquad (9)$$

For oxygen, $\alpha = .44$, and so t_E is only weakly sensitive to the magnetic energy, the impurity level or the radius ($2 - 5\,\alpha = -.19$).

C.) Essentially linear current decay--For oxygen, $1/2\alpha = 1.14$, so

$$I(t) = I(0)\left(1 - \frac{t}{t_E}\right)^{1.14}$$

which is almost indistinguishable from linear decay.

These results are in good qualitative agreement with the experiments which indeed exhibit finite lifetimes, apparently linear current decay, and insensitivity to W_B. The impurity levels in the experiment are not known; thus detailed comparisons with the theory are difficult.

The analytic results are in good quantitative agreement with a 1 1/2-D simulation performed by Shumaker et al.[3] The parameters of this simulation are $R \sim 38$ cm, the average electron density was $\sim .6 \times 10^{15}$ cm^{-3}, the oxygen impurity density was $n_I \approx 10^{13}$ cm^{-3}, and the poloidal field at the geometric center of the plasma ($r = z = 0$) was $B_c = 3.1$ kG. For the spheromak equilibrium, $B_c = 1.398$ IR (if B_c is measured in Gauss, I in amperes). Using this relation Eqs. (12) and (14) become, for oxygen impurity radiation

$$T = .70\left(\frac{B_c^{\,2}}{4.28 \times 10^{-28} n_e n_I R^2}\right)^{.293} \text{ eV} \qquad (10)$$

$$t_E = 3.9 \times 10^{-9}\ \frac{\left(B_c\right)^{.88}(R)^{1.12}}{(4.28 \times 10^{-28} n_e n_I)^{.44}} \text{ sec.} \qquad (11)$$

(B_c measured in Gauss)

For the parameters of the simulation, this gives $T = 6.9$ eV, $t_E = 180$ μsec. The simulation finds $T = 6.1$ eV at the 0 point, after the electron temperature equilibrates, i.e., after T adjusts so that $P_{RAD} = P_{OH}$. The analytical and simulation results for T are in reasonable agreement. In the simulation, the current does decay roughly linearly, but it does not decay to zero at 180 μsec. This is probably because the power law fit overestimates P_{RAD} at these low temperatures ($T \sim 3.5$ eV at 180 μsec.). However, the current decay time at $t = 20$ μsec, when the electrons are first equilibrated is

$$\frac{I}{\dot{I}} = \begin{cases} 200 \ \mu\text{sec, simulation} \\ 2\alpha t_E = 160 \ \mu\text{sec, theory} \end{cases}$$

The overall agreement between theory and simulation appears to be good.

The results of this analysis demonstrate that several features of the coaxial-gun CT experiments at LLNL and LASNL, viz., finite lifetime, linear decay, and insensitivity to magnetic stored energy and to density, may be simply explained by impurity radiation. This analysis thus gives support to the hope that the performance of these devices will improve if the impurity level is decreased sufficiently. With this in mind, it is useful to derive a criterion for the tolerable impurity density. Clearly, the plasma will burn through the peak of the oxygen radiation curve at ~ 20 eV if the equilibrated electron temperature is greater than 20 eV, i.e., if the temperature derived from Eq. (10) exceeds 20 eV. This requires

$$n_e n_{oxygen} < 2.6 \times 10^{22} \frac{B_c^2}{R^2} \tag{12}$$

(where B_c is the field at the geometric center $r = z = 0$, measured in Gauss, R is the separatrix radius in cm, and n is measured in cm^{-3}). As an example for $n_e = 2 \times 10^{14}$ cm^{-3}, $B_c = 5$ kG, $R = 40$ cm, which is typical of the low density higher current Beta-II experiments, burn through requires $n_I < 2 \times 10^{12}$ cm^{-3}; i.e., less than 1% oxygen is required. Burning through the carbon peak at ~ 10 eV requires $n_e n_{carbon} < 3.6 \times 10^{22} B^2/R^2$. Caramana and Perkins have derived a similar criterion.[8]

REFERENCES

1. W. C. Turner et al., Beta-II Compact Torus Experiment, these proceedings.
2. H. W. Hoida et al., Impurity Observations in Coaxial-Source Generated Spheromaks, these proceedings.
3. D. E. Shumaker, J. K. Boyd, B. McNamara, W. C. Turner, Lawrence Livermore National Laboratory report UCRL-85579, October 1981.
4. G. K. Morikawa, Phys. Fluids 12, 1648 (1969).
5. M. N. Rosenbluth and M. N. Bussac, Nucl. Fusion 19, 489 (1979).
6. A. Bondeson et al., Phys. Fluids 24, 1682 (1981).
7. D. E. Post et al., Princeton Plasma Physics Laboratory report PPPL-1352, July 1977.
8. E. J. Caramana and F. W. Perkins, Princeton Plasma Physics Laboratory report PPPL-1626, January 1980.

0202u/2561n

A Theory of the Relaxation of Finite Beta Toroidal Plasmas*

John Brandenburg
Lawrence Livermore National Laboratory
University of California, P.O. Box 5511
Livermore, CA 94550

In a previous paper (Brandenburg[1]) and elsewhere om these proceedings a model of the relaxation of a toroidal plasma without toroidal field is proposed wherein the plasma relaxes in the presence of plasma on open field lines. This model is called the "Sonic Bath" model.

In this paper a summary of the generalization of the Sonic Bath Model to include toroidal fields is presented. The principal results being that the closed field line magnetic field relaxes with the constraint of two flux invariants, A,B and the ψ^2 invariant seen in the absence of toroidal field. As in previous studies a near perfectly conducting, adiabatic plasma relaxes in a rigid, perfectly conducting chamber. The plasma, containing both poloidal and toroidal magnetic fields relaxes from an unstable intermediate equilibrium through saturated shear-Alfven turbulence that couples to compressional magnetic-sonic waves. The compressional waves leave the closed field lines and deposit their energy in a bath of plasma that is assumed to exist for a few sound transit times on the open field lines. Alternatively, the bath of plasma could be in the limiter "scrape off region" of a Reversed Field Pinch (RFP).

Small energy changes and flux losses and weak turbulence are assumed for this model.

Assuming a saturation scaling similar to that given by Drake et al.[2] will hold and that the plasma Beta, β, will be insensitive to energy, and using a simple model for the coupling of the shear-Alfven turbulence to magneto-sonic waves, we obtain an approximately fractional energy loss during the relaxation. That is, the energy of the magnetic field of the intermediate state is relaxed to the final state magnetic energy by a coefficient that is itself independent of energy. This is the simplest energy scaling and also one that fits results of experiments.

$$W_f = \varepsilon W_i \, , \quad \frac{\partial \varepsilon}{\partial H} = 0 \tag{1.1}$$

where W_i and W_f are the magnetic energies of the intermediate and final equilibrium.

Assuming near perfect conductivity, non-compressional turbulence, and the axisymmetry of the intermediate state, plus the assmption of Taylor[3] that resistivity will destroy all but one global MHD invariant of each type, we obtain the Lagrange multiplier minimization problem for the magnetic energy:

* Work performed under the auspices of the U.S. Department of Energy by the Lawrence Livermore National Laboratory under contract number W-7405-ENG-48.

$$\delta W + \lambda\, \delta I + \mu\, \delta K = 0 \tag{1.2}$$

with the invariants:

$$I = \int \psi^2 \, d\tau \tag{1.3}$$

which we will call the "Laminativity", because it leads to a flux surface that is "Laminar" in analogy to hydrodynamics. This invariant was first suggested by Leaf Turner[4] for turbulence in near-perfectly conducting, incompressible fluids.

We also have the invariant used by Taylor:

$$K = \int A \cdot B \; dx^3 \tag{1.4}$$

Whereas Taylor's invariant can be understood as being the topological property of "Flux Linking" of the magnetic field, the Laminativity may be understood as another topological property of the magnetic field that must be conserved as it relaxes (with preservation of volume). This topological property is the ordered nesting of the flux surfaces to which magnetic field lines are bound at finite Beta. (See figures.) Since it is only in the presence of finite pressure gradients that each flux surface can be labeled and oriented, it is natural that this invariant leads to finite Beta equilibria.

By using the condition that $d\psi$ vanish on a conducting wall, we obtain the equation for the relaxed field. We can integrate this equation by parts and with a vanishing surface term on the separatrix and obtain:

$$W_f = \lambda\, I + \mu\, K \tag{1.5}$$

as the magnetic energy on closed field lines in the relaxed state. Therefore, the relaxation takes the closed field line system to final state where the energy in the relaxed magnetic field is just a linear combination of the two invariants.

Assuming only small energy changes of both invariants can be verified by considering the relaxation as a linear transformation between two states in two independent variables, σ and ζ. Since energy total is conserved by the process the variables are independent of energy H.

$$\frac{\partial \sigma}{\partial H} = 0 \,, \quad \frac{\partial K}{\partial H} = 0 \tag{1.6}$$

where we also must have:

$$\frac{\partial \varepsilon}{\partial I} = \frac{\partial \varepsilon}{\partial K} = 0 \qquad (1.7)$$

because I and K are the invariants of the process. We can always write:

$$W_i = \lambda_0 I + \mu_0 K \qquad (1.8)$$

and then:

$$W_f = (\lambda_0 + \delta\sigma)I + (\mu_0 + \delta\zeta)K . \qquad (1.9)$$

Using our fractional energy loss for this process we then find:

$$\frac{\partial^2 W_f}{\partial I \partial H} = \varepsilon \frac{\partial^2 W_i}{\partial I \partial H} . \qquad (1.10)$$

However, we also have:

$$\frac{\partial^2 W_f}{\partial I \partial H} = \frac{\partial^2 W_i}{\partial I \partial H} = \frac{\partial \lambda_0}{\partial H} \qquad (1.11)$$

so that the quantities must be zero. From which it can be shown that both I and K must scale quadratically with the flux as do W_i and W_f.

We then have for the relaxed magnetic field equation:

$$\nabla \cdot \frac{\nabla\psi}{r^2} = - 2\lambda\psi - 2\mu \frac{\psi}{r} \qquad (1.12)$$

This is just the Grad-Shafronov equation for $P = a\psi^2$ and $rB_0 = \beta\psi$.

The solution to Grad-Shafronov equation for our relaxed magnetic field has been worked out generally (Weitzner[5]) and consists of Coulomb wave functions. In most compact torus experiments Beta is very low so that w can find a pressure-density profile (assuming uniform temperature) as a perturbation on a Taylor state:

$$P = \alpha \left[r J_1(r) \right]^2 \qquad (1.13)$$

This results in a characteristically peaked density profile for the compact torus.

To simplify stability analysis and also to apply the theory to the large aspect ratio RFP we go to the limit of a cylindrical stabilized-pinch.

In this limit of infinite aspect ratio the Laminativity becomes:

$$I = \int A_z^2 \, dx^3 . \tag{1.14}$$

The Sonic Bath Model then yields the field equations:

$$J_z = \lambda A_z + \mu B_z , \tag{1.15}$$

$$J_\theta = \mu B_\theta .$$

This set of equations was first derived by Montgomery and Turner[6]. Using a two-dimensional model of turbulent cascades in incompressible, near perfectly conducting fluids they were able to show that $A \cdot B$ and A_z^2 would be preferentially conserved. These equations lead to a modified Bessel function model with finite Beta, field reversing equilibria. However, field reversal now occurs at a pinch parameter θ that is enhanced over the Taylor value:

$$\theta = 1.2 \sqrt{1 + \beta_0} \tag{1.17}$$

where β_0 is the central Beta of the pinch. Using the Suydam criterion for stability it is found that the core will be unstable because of insufficient shear. Thus, one is led to a compound equilibrium with what is "Laminar" in the outer regions but has a force-free, non-laminar core that may be turbulent. Such models as a Suydam turbulent core have been porposed elsewhere on the basis of transport considerations[7]. The central Beta of this compound model is limited by flattening of the pressure profile to approximately .05.

I would like to thank Steve Auerbach, Leaf Turner, and George Goldenbaum for their suggestions and discussions. I would also like to thank Richard F. Post for his encouragement of this research.

REFERENCES

1. Brandenburg, J. E., APS Bull., 26, 27, 905 (1981).

2. Drake, J. F., N. T. Gladd, C. S. Liu, and C. L. Chang, Phys. Rev. Lett., 39, 460 (1977).

3. Taylor, J. B., "Relaxation of Toroidal Plasma and Generation of Reverse Magnetic Fields," Phys. Rev. Lett., 33, 19, 1139 (1974).

4. Turner, L., LANL, unpublished.

5. Weitzner, H., H. L. Berk, and J. Hammer, UCRL-85338, submitted to Phys. Fluids.

6. Montgomery, D., and L. Turner, APS Bull., 26,27, 1026 (1981).

7. Bodin, H. A. B. and Newton, A. A., Nuc. Fusion, 20, 10, 1255 (1980).

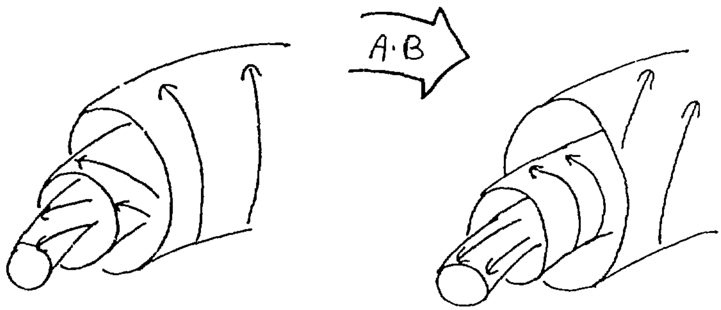
A·B

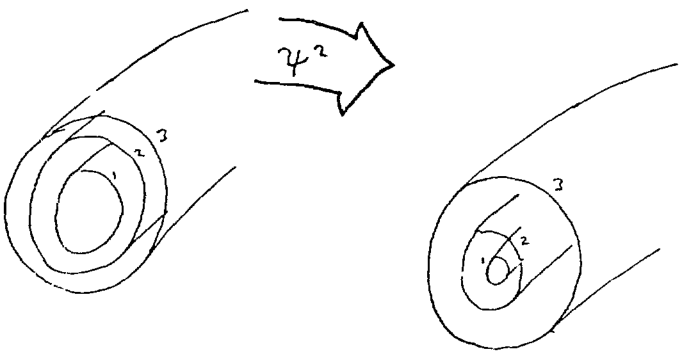
ψ²
3
2
1
3
2
1

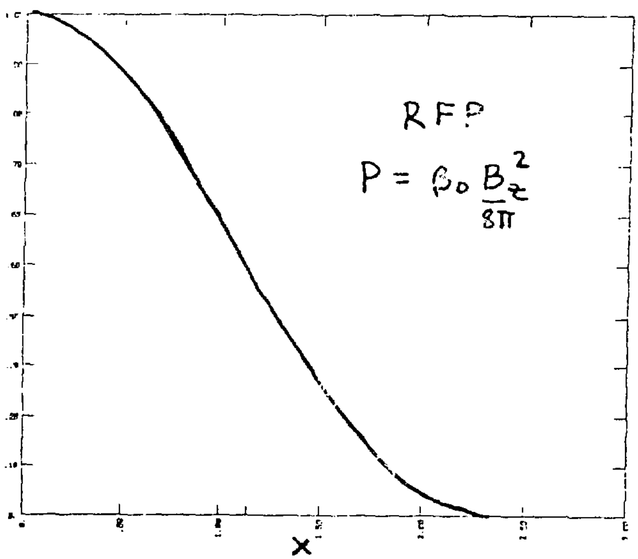
RFP
P = β₀ B_z²/8π
x

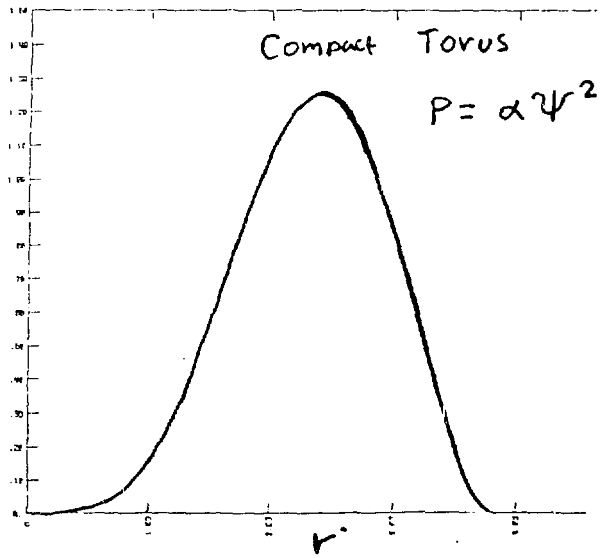
Compact Torus
P = αΨ²
r

Compressible MHD Fluctuations

Eliezer Hameiri
Courant Institute of Mathematical Sciences
New York University, New York, New York 10012

Harvey A. Rose
Los Alamos National Laboratory
University of California, Los Alamos, New Mexico 87545

Introduction

The typical compact torus plasma, being confined by toroidal and poloidal magnetic fields of comparable magnitude and without the strong and externally maintained toroidal field of the tokamak configuration, is expected to exhibit large fluctuations in the equilibrium state quantities. Such fluctuations in fact are the underlying mechanism for self reversal of the magnetic field in the toroidal pinch, the phenomenon which gave rise to the concept of the compact torus itself. Fluctuations could be a source for enhanced transport and, indeed, have proven to be of enormous consequence in the case of two dimensional gas dynamics because of the long time tails of correlation functions (decaying as $1/t^{d/2}$) which are inconsistent with a hydrodynamic description of transport.

In this paper we study a model of fluctuating magnetohydrodynamic plasma near thermal equilibrium. Such a model exists in the literature[1] and is based on adding small "noise" terms into the usual equations which are then linearized. In contrast, our approach does not involve extra terms and is fully non-linear. The two models agree in the limit of small fluctuations. Students of Kraichman's absolute equilibrium approach to turbulent relaxation[2] will recognize our model as following a similar line but, even in that context, the treatment of compressible plasmas is new and unexpected.

The Model

We treat a plasma described by the ideal MHD equations and, for simplicity, occupying a 3-dimensional cube of length 2π with periodic boundary conditions. In order to facilitate a statistical treatment, it is necessary to discretize the equations and replace them by a large, but finite, number of particle-like equations. Because of the truncation involved, not all representations of plasma variables are equivalent. We use variables common in shock theory, thus guaranteeing conservation of mass, momentum, energy and magnetic fluxes even under truncation. The equations are

$$\rho_t + \operatorname{div} \underset{\sim}{m} = 0, \qquad \underset{\sim}{B}_t + \operatorname{curl}\, (\underset{\sim}{B} \times \underset{\sim}{m}/\rho) = 0$$

$$\underset{\sim}{m}_t + \operatorname{div}\, (\underset{\sim}{m}\underset{\sim}{m}/\rho - \underset{\sim}{B}\underset{\sim}{B}) + \operatorname{grad}\, (p + \underset{\sim}{B}^2/2) = 0 \tag{1}$$

$$\varepsilon_t + \operatorname{div} \rho^{-1}[\underset{\sim}{m}(\varepsilon + p + B^2/2) - \underset{\sim}{m}\cdot\underset{\sim}{B}\underset{\sim}{B}] = 0$$

where $\underset{\sim}{m}$ is the momentum, replacing $\rho \underset{\sim}{v}$, and ε is the total energy density. We use the equation of state for polytropic gases

$$p = (\gamma-1)(\varepsilon - \frac{1}{2}\underset{\sim}{B}^2 - \frac{1}{2}\underset{\sim}{m}^2/\rho) \tag{2}$$

with γ the adiabatic constant. Eq. (2) replaces the usual equation of state $p = (\gamma-1)\sigma\rho^{\gamma}\exp(cs)$, with some constants c,σ and with s the specific entropy. The most common way of discretizing system (1) is by expanding every variable in Fourier series and truncating the high wave numbers. Athough we will not pursue this approach here, we show how the use of the conservation law variables implies the existence of a Liouville theorem for this truncated system. This easy proof should replace other proofs for other models, usually given on a case by case basis. Every conservation law equation is of the form $dv/dt + \text{div}\, \underset{\sim}{f}(v,w) = 0$, where w indicates all variables other than v. It reduces to

$$\frac{dv^{\underset{\sim}{\kappa}}}{dt} + i\underset{\sim}{\kappa}\cdot\underset{\sim}{f}^{\underset{\sim}{\kappa}}(v,w) = 0 \text{ , where } v(x,t) = \sum_{\underset{\sim}{\kappa}} v^{\underset{\sim}{\kappa}}(t)\, e^{i\underset{\sim}{\kappa}\cdot\underset{\sim}{x}} . \tag{3}$$

Evaluate $\partial f^k/\partial v^k$, with k being, say, the x component of $\underset{\sim}{\kappa}$. This derivative equals

$$\frac{d}{d\lambda} f^k(v+\lambda e^{ikx},w)\Big|_{\lambda=0} = (2\pi)^{-1}\frac{d}{d\lambda}\int_0^{2\pi} e^{-ikx} f(v+\lambda e^{ikx},w)dx\Big|_{\lambda=0} .$$

which equals $(\partial f/\partial v)^o$. We have

$$\sum_{s=1}^{3} \frac{\partial \dot{v}^{\underset{\sim}{\kappa}}_s}{\partial v^{\underset{\sim}{\kappa}}_s} + i\underset{\sim}{\kappa}\cdot\left(\frac{\partial \underset{\sim}{f}}{\partial v}\right)^o = 0 , \tag{4}$$

and when the sum is extended over $\underset{\sim}{\kappa}$ and $-\underset{\sim}{\kappa}$, the last term in (4) cancels and the flow in the phase space of Fourier coefficients is incompressible.

Difference Equations

We replace system (1) by its finite-difference approximation over an equally spaced grid of length $\Delta = 2\pi/N$, with N some odd integer, $N = 2K+1$. The variables are now the $8N^3$ time-dependent grid values of the original plasma variables, for which we have a system of ordinary differential equations in time. This approach corresponds to the numerical "method of lines"[3]. To approximate a spatial derivatine, we use any centered difference approximation. Thus, if D is the approximation to d/dx, we have

$$(Df)_j = \sum_{\ell=-L}^{L} a_\ell f_{j+\ell} , \qquad a_\ell = -a_{-\ell} \tag{5}$$

where j denotes any component of the lattice point $\underset{\sim}{j}$. A frequently used numerical approximation has $L = 1$, $a_1 = -a_{-1} = 1/(2\Delta)$. Each equation has the form

$$\frac{d}{dt} v_{\underset{\sim}{j}} + \sum_{s=1}^{3} (D_s \underset{\sim}{f}_s)_{\underset{\sim}{j}} = 0 . \tag{6}$$

Since all points on the lattice were treated equally, it is clear that the approximation for an integral is $\int v(\underset{\sim}{x})d\underset{\sim}{x} \sim (2\pi/N)^3 \sum v_{\underset{\sim}{j}}$, and the conservation form (6) guarantees that $(d/dt)\sum v_{\underset{\sim}{j}} = 0$ for all 8 quantities. Also, since the second term of (6) does not involve values at the site $\underset{\sim}{j}$, we have the Liouville theorem

$$\sum_{\underset{\sim}{j}} \partial\dot{v}_{\underset{\sim}{j}}/\partial v_{\underset{\sim}{j}} = 0 . \tag{7}$$

An additional constant of the motion of the discrete system corresponds to the magnetic helicity and can be defined most easily by introducing the useful lattice-Fourier representation for lattice-valued functions. We define $v^{\underset{\sim}{\kappa}}$ such that for all $\underset{\sim}{j}$

$$v_{\underset{\sim}{j}} = \sum_{\underset{\sim}{\kappa}} v^{\underset{\sim}{\kappa}} \exp\,(i\Delta\underset{\sim}{\kappa}\cdot\underset{\sim}{j})\ ,\ -K \leq \kappa_s \leq K\ ,\ s = 1,2,3\ . \tag{8}$$

Notice that the lattice functions $\exp\,(i\Delta\underset{\sim}{\kappa}\cdot\underset{\sim}{j})$ are the periodic eigenfunctions of the numerical gradient operator, with eigenvalues

$$\underset{\sim}{\lambda}^{\kappa}_{s} = 2i \sum_{\ell=1}^{L} a_\ell \sin\,(\Delta\underset{\sim}{\kappa}_s \ell). \tag{9}$$

We now expand the magnetic field $\underset{\sim}{B}_{\underset{\sim}{j}}$ in Fourier series and define

$$\underset{\sim}{A}^{\underset{\sim}{\kappa}} = \underset{\sim}{\lambda}^{\underset{\sim}{\kappa}} \times \underset{\sim}{B}^{\underset{\sim}{\kappa}} / |\underset{\sim}{\lambda}^{\underset{\sim}{\kappa}}|^2\ (\underset{\sim}{\kappa} \neq 0)\ ,\ \underset{\sim}{A}^{o} = 0\ . \tag{10}$$

It can be shown that the helicity $\Sigma \underset{\sim}{A}^{\underset{\sim}{\kappa}}\cdot\underset{\sim}{B}^{-\underset{\sim}{\kappa}}$ corresponding to $\Sigma \underset{\sim}{A}_{\underset{\sim}{j}}\cdot\underset{\sim}{B}_{\underset{\sim}{j}}$ is a constant of the motion. Employing the previous results we use the Gibbs distribution functions to describe plasma fluctuations (assuming zero total momentum and magnetic fluxes)

$$P(\varepsilon,\rho,\underset{\sim}{m},\underset{\sim}{B}) = Z^{-1} \exp - \left(\frac{2\pi}{N}\right)^3 \sum_{\underset{\sim}{j}} \left(\alpha\varepsilon_{\underset{\sim}{j}} + \beta\rho_{\underset{\sim}{j}} + \delta \underset{\sim}{A}_{\underset{\sim}{j}}\cdot\underset{\sim}{B}_{\underset{\sim}{j}}\right) \tag{11}$$

where Z is a normalizing factor and α,β,δ are constants to be found by imposing known expected values for total mass, energy and helicity. In physical plasma flows $\rho \geq 0$ and $S \geq \sigma = \text{const.}$, where $p = (\gamma-1)S\rho^{\gamma}$. We impose these restrictions on the domain of voliality of (11), and for convenience substitute $\varepsilon = \frac{1}{2}\underset{\sim}{B}^2 + \frac{1}{2}\underset{\sim}{m}^2/\rho + S\rho^{\gamma}$, thus obtaining

$$P(S,\rho,\underset{\sim}{m},\underset{\sim}{B}) = Z^{-1} \left(\prod_{\underset{\sim}{j}} \rho^{\gamma}_{\underset{\sim}{j}}\right) \exp - \left(\frac{2\pi}{N}\right)^3 \sum_{\underset{\sim}{j}} \left[\alpha\left(\frac{1}{2}\underset{\sim}{B}^2_{\underset{\sim}{j}} + \frac{1}{2}\underset{\sim}{m}_{\underset{\sim}{j}}^2/\rho_{\underset{\sim}{j}} + S_{\underset{\sim}{j}}\rho_{\underset{\sim}{j}}^{\gamma}\right) + \right.$$

$$\left. + \beta\rho_{\underset{\sim}{j}} + \delta\underset{\sim}{A}_{\underset{\sim}{j}}\cdot\underset{\sim}{B}_{\underset{\sim}{j}}\right],\qquad \rho_{\underset{\sim}{j}} \geq 0,\ S_{\underset{\sim}{j}} \geq \sigma,\ \underset{\sim}{\lambda}^{\underset{\sim}{\kappa}}\cdot\underset{\sim}{B}^{\underset{\sim}{\kappa}} = 0. \tag{12}$$

The measure of integration is the product of $dSd\rho d\underset{\sim}{m}d\underset{\sim}{B}$ for each grid point $\underset{\sim}{j}$.

Magnetic Fluctuations

The magnetic part of (12) decouples from all other variables and, in terms of the Fourier coefficients, can be written as

$$P(\underset{\sim}{B}) = Z^{-1} \exp - (2\pi)^3 \sum_{\kappa} \left(\frac{1}{2}\alpha|\underset{\sim}{B}^{\underset{\sim}{\kappa}}|^2 + \delta\underset{\sim}{A}^{\underset{\sim}{\kappa}}\cdot\underset{\sim}{B}^{-\underset{\sim}{\kappa}}\right). \tag{13}$$

This is the same expression as in incompressible plasma and differs from familiar results[4] in that $\underset{\sim}{\lambda}^{\underset{\sim}{\kappa}}$ replaces $i\underset{\sim}{\kappa}$ in the definition of $\underset{\sim}{A}^{\underset{\sim}{\kappa}}$. We get

$$\left\langle\frac{1}{2}|\underset{\sim}{B}^{\underset{\sim}{\kappa}}|^2\right\rangle = \frac{1}{(2\pi)^3\alpha\ D(\underset{\sim}{\kappa})}\ ,\ \text{where } D(\underset{\sim}{\kappa}) = 1 - \left(\frac{2\delta}{\alpha|\underset{\sim}{\lambda}^{\underset{\sim}{\kappa}}|}\right)^2 . \tag{14}$$

Note that normalizability of the distribution function requires $\alpha > 0$, $D(\underset{\sim}{\kappa}) \geq 0$. The last condition implies that $|\delta|/\alpha$ should be small enough to accommodate the longest wave length (smallest $|\underset{\sim}{\kappa}|$) for which $|\underset{\sim}{\lambda}^{\underset{\sim}{\kappa}}| \to 0$ as $N\to\infty$. Indeed, $\underset{\sim}{\lambda}^{\underset{\sim}{\kappa}} \sim i\underset{\sim}{\kappa}$ for $|\underset{\sim}{\kappa}|/K \ll 1$, which can be obtained from (9) after observing that the operator D commonly gives the exact derivative for the function $f \equiv x$, i.e., $(Df)_j = 1$ for $f_j \equiv j\Delta$. It is interesting to note that we can obtain exactly the familiar result by defining the operator D such that $\lambda^{\kappa}_{\sim} \equiv i\kappa$. A change of representation from Fourier coefficients to lattice functions will yield the a_{ℓ} in (5), with L=K.

While for long wave lengths, predictions by the finite-difference and Fourier methods agree, they can be very different for short wave lengths. Indeed, the sinusoidal behaviour of $\lambda^{\kappa}_{\sim}$ implies that it peaks at some finite $|\kappa|$ and becomes small again near K. This discrepancy may be due to the fact that a wave requires at least 4 grid points for a reasonable approximation, so only prediction for $|\kappa| < K/2$ can be trusted.

Fluid-Dynamical Fluctuation

Integrating out $\underset{\sim}{m}$ and S in (12), we get

$$P(\rho) = Z^{-1} \rho^{3/2} \exp - (\alpha'\sigma\rho^{\gamma} + \beta'\rho) \ , \ 0 \leq \rho < \infty \tag{15}$$

at each grid point, and fluctuation at different grid points are uncorrelated. $\alpha' = (2\pi/N)^3\alpha$, $\beta' = (2\pi/N)^3\beta$. The limit of small fluctuations can be found by taking $\alpha' \to \infty$, $\beta' \to -\infty$, such that α'/β' is constant. In this case the distribution function (15) is concentrated at $\rho = \rho_0$, where

$$\rho_0 = \left(\frac{-\beta}{\gamma\sigma\alpha}\right)^{1/(\gamma-1)} . \tag{16}$$

In this limit one can use Laplace's asymptotic method to evaluate moments of (15). We find

$$\langle(\delta p)^2\rangle \equiv \langle(p - \langle p\rangle)^2\rangle = \gamma(\gamma-1)\sigma\rho_0^{\gamma}/\alpha' + O(1/\alpha'^2) . \tag{17}$$

To leading order in α',$(\gamma-1)\sigma\rho_0^{\gamma}$ is the expected value of the pressure, and, recalling that the speed of sound c is given by $c^2 = \gamma p/\rho$, we have to leading order $\langle(\delta p)^2\rangle = (N/2\pi)^3 \langle\rho c^2\rangle/\alpha$. This result is identical to Landau's result in the linear approximation[1]

$$\langle\delta p(\underset{\sim}{x}_1)\ \delta p(\underset{\sim}{x}_2)\rangle = \rho c^2 T\delta(\underset{\sim}{x}_2 - \underset{\sim}{x}_1) \tag{18}$$

after we identify α with the inverse temperature T. Thus, one may view our treatment as the non-linear extension to Landau's method.

Acknowledgement

One of the authors (E.H.) has done the bulk of his work while visiting the CTR-6 group at the Los Alamos National Laboratory, and he would like to thank Dr. R. Gerwin for his kind hospitality. This work was carried out under Air Force Contract No. AFOSR-81-0020 and the U.S. Department of Energy Contract Nos. DE-AC02-ER03077 and W-7405-ENG-36.

References

1. L.D. Landau and E.M. Lifschitz, Fluid Mechanics (Pergamon, London, 1959), Ch. 17.
2. D. Montgomery, L. Turner and G. Vahala, Phys. Fluids 21, 757 (1978).
3. J.M. Hyman, NYU Report COO-3077-139 (1976).
4. U. Frisch, A. Pouquet, J. Leorat and A. Mazure, J. Fluid Mech. 68, 769 (1975).

CURRENT DRIVE, HEATING AND FUELING BY COMPACT TORUS INJECTION*

James H. Hammer and Charles W. Hartman
Lawrence Livermore National Laboratory, University of California
Livermore, California 94550

We consider here the possibility of injecting small compact-torus (CT) plasma rings into magnetic fusion devices. This discussion concentrates on a proposed new method for efficient current drive in Tokamaks and other toroidal devices in which the magnetic flux in the CT acts to excite the current. In addition to this aspect, CTs may be selectively loaded with matter or energetic particles, or may be accelerated to high kinetic energy[1] (0.1 - 1 MeV/ion) to provide fuel or auxiliary heating for low-density fusion devices including tandem mirrors. The potential exists for high-Q (~100) Tokamak operation as well as penetration to distances well beyond those available by neutral beams or fuel particles.

We examine current drive by noting that the plasma current in a Tokamak provides a twist, or net helicity to the magnetic field lines. Current drive mechanisms resupply the magnetic helicity, $K = \int \vec{A}\cdot\vec{B}\, dV$, which would decay on the L/R time scale (L = inductance, R = plasma resistance) in the absence of a drive.

For simplicity we assume that the plasma is surrounded by a conducting shell which preserves toroidal flux. In this case K is an approximate, additive constant of the motion for times short compared to the L/R time, i.e., *K is preserved even in the presence of MHD or tearing-type activity.* If another helicity-containing entity, i.e., a CT, is inserted inside the conducting shell and merged with the Tokamak plasma on a rapid time scale, then we have the possibility of a current drive--helicity has been added.

From the point of view of J. B. Taylor's minimum energy theory,[2] the merging process is automatic: the plasma relaxes to the state of minimum magnetic energy consistent with the conservation of K and toroidal flux. If the Tokamak is axisymmetric before the CT is added, then it again approaches axisymmetry but with a larger circulating current. A possible drawback of this approach is that the relaxation may be sufficiently turbulent to cause unacceptable energy losses. In the following we develop a detailed picture of the merging without making any strong turbulence assumptions.

The first consideration is the availability of helicity containing CTs. Coaxial plasma gun experiments at LLNL[3] and elsewhere[4,5] have successfully produced CTs containing $\gtrsim$50% of the helicity injected at the gun breech. The final state of these toroids is close to that predicted by the Taylor theory.

Secondly, we must be able to move the CT from the region of formation into the Tokamak, i.e., across the equilibrium magnetic field. To see how

*Work performed under the auspices of the U.S. DOE by the Lawrence Livermore National Laboratory under contract number W-7405-ENG-48.

this is possible, consider a CT in a conducting channel, e.g., a rectangular wave guide, where the axis of the CT and the confining field are perpendicular to the direction along the channel, $\vec{x}$ (see Fig. 1). If the cross section and the magnetic flux frozen into the channel are independent of x, then the CT is neutrally stable to motion in the $\vec{x}$ direction (this is fairly obvious on the grounds of translational invariance, but can be verified from the ideal MHD energy principle). The CT may then be accelerated along the channel by establishing a field gradient. This technique allows us to transport the CT from the formation region into the Tokamak.

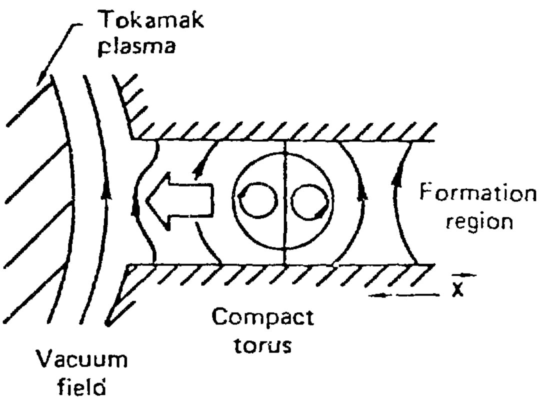

Fig. 1. Injection of a CT across the ambient magnetic field.

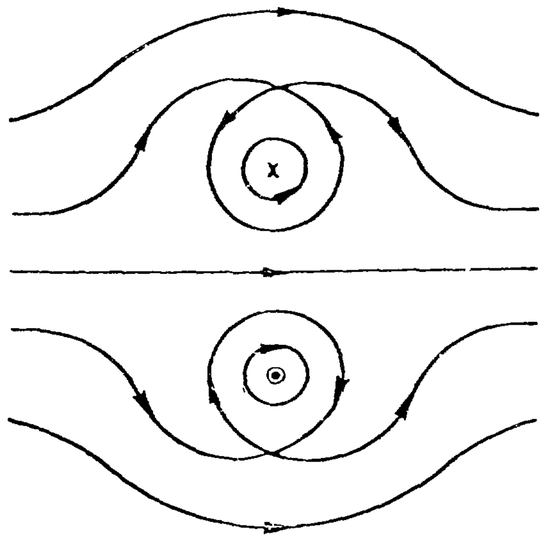

Fig. 2. A CT configuration following a 180° tilt in an applied field.

An experimentally confirmed feature of CTs is the tendency to tilt 180° in an applied field[3,4] (see Fig. 2). Once tilting occurs, field line reconnection rapidly annihilates the CT. During the propagation phase, tilt stability must be insured by placing the conducting channel walls close enough to the plasma ring to force an oblate shaped CT.[6] After arriving at the Tokamak, however, tilting and annihilation work to our advantage. The poloidal field of the ring reconnects with the predominantly toroidal field of the Tokamak (see Fig. 2 again). The toroidal flux contained by the CT is approximately poloidal with respect to the Tokamak and is spilled out of the ring by the reconnection process. If the CT has penetrated to the magnetic axis, this represents a direct refluxing or EMF at the magnetic axis (the most crucial point for current drive). If the CT releases its flux at an outer surface , the flux pulse must diffuse inward just as the EMF from a transformer must penetrate to the magnetic axis by current diffusion (for a large enough flux pulse, a resistive kink mode may be driven that moves the added flux to the magnetic axis more rapidly[7]).

Solution of the flux diffusion problem gives roughly the same answer as a straightforward application of the Taylor theory: the poloidal flux is increased by a fraction of the order of $K_{ring}/K_{Tokamak}$. Balancing the rate of injection of CTs with the resistive decay rate of the Tokamak to achieve steady state allows the calculation of the thermonuclear $Q = P_{fusion}/P_{current\ drive}$.

Given an efficiency of ring production, $\mathscr{E}$, and neglecting the kinetic energy of the ring we can estimate the Q (assuming 15 keV temperature and no bootstrap current):

$$Q = 7.5 \times 10^{-10} \frac{\beta_p^2 \, \varepsilon^4 \, B_T^2 \, R^2 \, \mathscr{E} \, J_0\left(\frac{\lambda_{01} \, r_0}{r_p}\right)\left(\frac{r_{ring}}{R}\right)}{q^3 \, Z_{eff}} \tag{1}$$

where r_{ring} is the ring radius, R is the major radius, β_p is the poloidal β, ε the inverse aspect ratio and q the safety factor. Taking some typical reactor parameters: $\beta_p = 2$, $\varepsilon = 1/3$, $q = 2$, $Z_{eff} = 1.3$, $R = 600$ cm, $B_T = 5 \times 10^4$ G; and taking $\mathscr{E} = 0.5$, $J_0 (\lambda_{01} \, r_0/r_p) = 0.5$ gives:

$$Q \cong 800 \, (r_{ring}/R) \tag{2}$$

so large rings are advantageous. Taking $r_{ring}/R = 0.1$ gives a Q of 80.

As a final remark, note that CT reactors may have easier accessibility than Tokamaks (injection along the symmetry axis is possible in principle) allowing for larger rings and higher Q's.

REFERENCES

1. C. W. Hartman, in preparation.
2. J. B. Taylor, Phys. Rev. Lett. 33, 1139 (1974).
3. W. C. Turner, et al., Proc. of Third Symposium on Physics and Technology of Compact Toroids, Los Alamos, New Mexico, Dec. 2-4, 1980, p. 113; Lawrence Livermore National Laboratory, Livermore, CA, Rept. UCRL-85122 (1980).
4. T. R. Jarboe, et al., Phys. Rev. Lett. 45, 1264 (1980).
5. K. Watanabe, et al., Proc. of the U.S./Japan Workshop on Compact Toroids, Feb. 17-19, 1981, Osaka Univ., Osaka, Japan.
6. M. N. Rosenbluth and M. N. Bussac, Nucl. Fusion, 19 (1979) 489.
7. R. White, et al., in Plasma Physics and Controlled Nucl. Fusion Res., 1, IAEA, 1974.

0203u/2565n

A NEW TYPE OF COLLECTIVE ACCELERATOR

Charles W. Hartman and James H. Hammer
Lawrence Livermore National Laboratory, University of California
Livermore, CA 94550

ABSTRACT

We describe here a collective accelerator based on magnetically confined plasma rings. Typical rings which have been produced and which have 10 kJ magnetic energy and 0.1 to 10 coulombs of nuclei are predicted to be accelerated magnetically to 10 MJ or higher in acceleration lengths of 100 m if the final power delivered to the ring is 10^{12} W. Applications are discussed of current drive in Tokamak fusion reactors, fueling and heating magnetic fusion reactors, transuranic element synthesis, and, for focused rings, a high energy density driver for inertial confinement fusion.

This paper describes a new type of collective accelerator and discusses possible applications. The accelerator is based on plasma rings, confined magnetically in a nearly force-free field configuration consisting of a dipole-like poloidal field with an entrapped toroidal field. The rings, which are considered to be accelerated magnetically, have very high magnetic moment per unit of mass (10^8 greater than superconducting pellets) and, on the other hand, may have a coulomb or more of total ion charge--greatly in excess of previous electrostatic, collective accelerators.

Considering rings which have been produced experimentally, we anticipate acceleration over reasonable lengths up to kinetic energies in the 10 MJ range, and for low ion mass rings up to 1 to 10 MeV kinetic energy per nucleon. Among possible applications we discuss here are current drive, fueling, and heating of a conventional Tokamak or other fusion reactor, transuranic element synthesis, and, for focused rings, a high energy, high energy density drive for inertial confinement systems.

Magnetically confined plasma rings have been studied for some time as possible controlled thermonuclear fusion devices. Ring formation was first demonstrated at low energy by Alfven and co-workers in the 1950's.[1] More recently, plasma gun experiments,[2,3] shown in Fig. 1, have produced rings having typically 10 kJ magnetic energy, 10 to 20 cm major radius, 10^{19} to 10^{20} total number of ions, and a 10 eV plasma having a $\beta = p/(B^2/2\mu o)$ of order 0.01. Two important aspects for the considerations here are that the lifetime of the rings is adequately long for acceleration, typically 100 μs or so, and that the rings are highly resilient, undergoing large departures from symmetry with only minor changes in lifetime.[2]

In consequence of the resiliency of the rings we assume that an accelerating force can be applied which is comparable to the force,[4] $F_{eq} \approx U_{magnetic}/R$, necessary to maintain radial equilibrium. Letting

$F_{acc} = \kappa F_{eq} = M_{ring} \ddot{Z}$, and assuming the ring remains unchanged in size, field strength, and number of particles during acceleration, quantities of interest are,

$$\frac{U_{kinetic}}{U_{magnetic}} = G = \frac{\kappa L}{R} \quad , \quad \tau_{acceleration} = \frac{(2G)^{1/2}}{\kappa\Omega} \quad , \quad V_{ring} = (2G)^{1/2}\,\Omega R \quad ,$$

$$P_{ring} = F_{acc}\,V_{ring} = (2G)^{1/2}\,\Omega\,U_{magnetic} \quad ,$$

and

$$E_{nucleon} = \frac{G\,U_{magnetic}}{Q}\,eV \quad .$$

Here L is the accelerator length, $Q = eM_{ring}/m_p$, and

$$\Omega = \left(\frac{U_{magnetic}}{M}\right)^{1/2} \frac{1}{R}$$

is the Alfven wave transit frequency of the ring. The basic dynamical equations, of course, describe the plasma as a magnetized fluid which, because of charge neutrality, constrains the ions to move with the highly magnetized electron component of the plasma. Of various scaling laws which may be formulated from the above, if high $U_{kinetic}$ or $U_{nucleon}$ is desired, a limiting quantity for a given accelerator length is the power which can be delivered to the ring. In terms of P_{ring} the scaling becomes,

$$U_k \propto Q^{1/3}\,P_{ring}^{2/3}\,L^{2/3} \quad , \quad \tau_{acc} \propto \frac{Q^{1/3}\,L^{2/3}}{P^{1/3}}$$

$$E_{nucleon} \propto \frac{P_{ring}^{2/3}\,L^{2/3}}{Q^{2/3}}$$

and

$$\frac{\kappa\, U_{magnetic}}{R} \propto \frac{Q^{1/2}\, P_{ring}^{2/3}}{L^{1/3}} \quad .$$

Setting $P_{ring} = 10^{12}$ W, the above quantities vs accelerator length L are shown in Fig. 2. The range of $M_{ring} = (Q/e)\, m_p$ corresponds to rings which have been produced recently with $m_{ions}/m_p = 1 - 10$. However, further significant variations in this parameter appear quite possible. Note also in Fig. 2 that $\kappa\, U_{magnetic}/R$ falls in the range of rings which have been produced provided $\kappa \simeq 0.01 - 1$. For all parameters shown, $\tau_{acc} < 100$ μs--less than the observed lifetime.

Several embodiments of the ring accelerator are possible, we consider two in this note. First, since the basic field structure of the ring is dipolar, a traveling magnetic mirror field exerts a force $F_{acc} = -\mu\, \nabla B_{external}$ in the usual manner. Stability of the ring is important, particularly against a 180^0 tilting of the ring. One method of stabilizing against tilt is to spin the ring at near Alfven speed.[5] A second method of acceleration is to extend the coaxial gun electrodes and accelerate the ring by toroidal field injected by capacitor banks fed through insulating breaks in the outer electrode (Fig. 3). This configuration, a "super gun" or coaxial rail gun, appears in preliminary estimates to avoid the tilt instability.

Having accelerated the ring to large $U_{kinetic}/U_{magnetic}$, a potentially useful aspect is that it can be focused to a small size by arranging to direct radially inward a force on the order of F_{acc}. A simple possibility is to pass the ring into an appropriately shaped conducting funnel. As viewed by the ring, the funnel appears as a compressing liner where scaling laws and numerical calculations[6] indicate that the ring compression (even if tilted) should be self-similar, i.e., radial focusing is accompanied by axial contraction. A detailed study of the focusing limits has not yet been made, however rough estimates suggest radius/axial compression ratios of 10 to 100 may be possible. Roughly, the focal distance is $L_{focus} \approx (2G)^{1/2} R$ for an inward force of $2F_{eq}$, where R is the initial ring radius and $G >> 1$.

Next, we consider applications of accelerated rings, progressing from low to high kinetic energy. The first application is in employing the ring magnetic field as a "flux-pump"-like drive to maintain a Tokamak reactor current in steady state. This application is discussed in another paper of this Symposium [7] along with the possibility of injecting fuel, such as tritium, or injecting energetic ions. Rings formed with predominantly high energy electrons (0.1 to 1 MeV) may provide a means of forming hot electron mirror cells without high frequency ECR heating.

At high kinetic energy (10 MJ or so) and with focusing, it appears possible to concentrate very high power density, short pulses of ion bombardment for purposes of driving an inertial fusion pellet. Consider for example a ring having $R_0 \approx 10$ cm, $N = 6 \times 10^{18}$ ions, $U_{magnetic} = 10$ KJ ($B \approx 10$ KG) accelerated to $U_{kinetic} = 10$ MJ. During compression in the focusing funnel, $U_{magnetic} \propto 1/R$ (magnetic flux ψ = constant on the short time scales) and, if the conventional MHD stability limit $\beta_{max} \approx 0.1$ holds and is limited by enhanced electron thermal conduction rather than plasma loss, focusing to $R_f = 0.2$ cm increases $U_{magnetic}$ to 500 kJ << $U_{kinetic}$ (U_{plasma} is small) and increases $B \propto 1/R^2$ to 25 MG. Since the compression is self-similar, the ring length is reduced to $L \approx 0.2$ cm. The ring velocity depends on the mass, however taking $V_{ring} \simeq 10^8$ cm/s, the focused ring could potentially deliver 10 MJ to a 0.1 cm^2 target in 2 ns. The ion current density at this level is 5×10^9 A/cm.^{2}

If, instead of maximizing the total kinetic energy of the ring, high energy per nucleon is desired, a low mass ring is required. From Fig. 2 for $10 < L < 100$ m and $Q = 0.1$, proton kinetic energies in the range 1 to 10 MeV are predicted. For purposes of creating transuranic nuclei, several percent of mass 100 to 200 amu nuclei could be added which would be accelerated along with the ring to the same kinetic energy per nucleon as the protons.

In summary, we have considered a new type of collective accelerator which potentially can bridge the many orders of magnitude gap between conventional particle accelerators and accelerated solid pellets. At high power input with reasonable accelerator lengths, presently achievable plasma rings that are accelerated and focused may provide access to particle fluxes and pulsed power levels not here-to-for available under controlled laboratory conditions.

3864r/ls

REFERENCES

1. H. Alfven, L. Lindberg, and P. Mitlid, J. Nucl. Energy 1, 116 (1960).
2. T. R. Jarboe et al., Phys. Rev. Lett. 45, 1264 (1980).
3. W. C. Turner, et al., Proc. 3'd Symposium on Physics and Technology of Compact Toroids, Los Alamos Scientific Laboratory, Dec. 1980, LA-8700-C, p. 113.
4. V. D. Shafranov, "Plasma Equilibrium in a Magnetic Field," Reviews of Plasma Physics, Vol. 2, p. 103.
5. S. I. Itoh and K. Itoh, Spinning Plasma Ring and Tilting Instability, HIFT 36, Jan. 1981.
6. E. Hameiri, W. Grossman, "Two Dimensional Compression of General Compact Tori," Proc. of the US-Japan Joint Symposiusm on Compact Toruses and Energetic Particle Injection, Princeton, Dec. 1979, p. 118.
7. J. H. Hammer, C. W. Hartman, "Current Drive, Heating and Fueling by Compact Torus Injection Proc., 4th Symposium on Physics and Technology Compact Toroids, Lawrence Livermore National Laboratory, Oct. 1981

FIGURE CAPTIONS

Fig. 1. The Beta II plasma gun experiment[3] shown schematically. The initial field is established, D_2 gas if puffed in, and the gun is fired. Plasma with embedded acceleration gun-field emerges from the gun stretching the initial field into the flux conserver. Reconnection of the field produces an isolated trapped ring.

Fig. 2. Ring kinetic energy U_k, energy per nucleon $E_n = U_k/Q$, and ring magnetic energy divided by radius $\kappa U_m/R$ vs accelerator length L for several values of Q. Here the maximum power delivered to the ring is held constant at $P_{ring} = 10^{12}$ W, and $Q = eM_{ring}/m_p$. The quantities κ and P_{ring} are defined in the text.

Fig. 3. An extended gun accelerator. Here a ring is produced as described in Fig. 1 and accelerated by B_θ field injected behind the ring by successively firing accelerator banks 1, 2, etc.

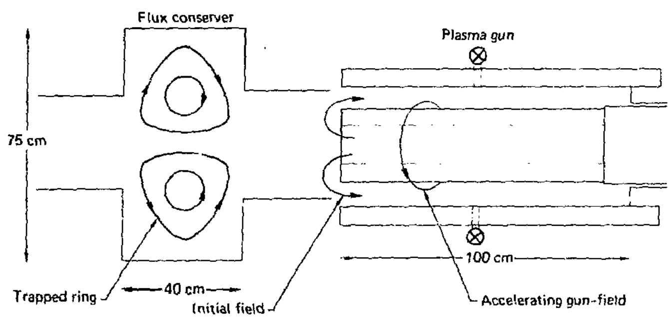
Flux conserver
Plasma gun
75 cm
100 cm
Trapped ring
40 cm
Initial field
Accelerating gun-field

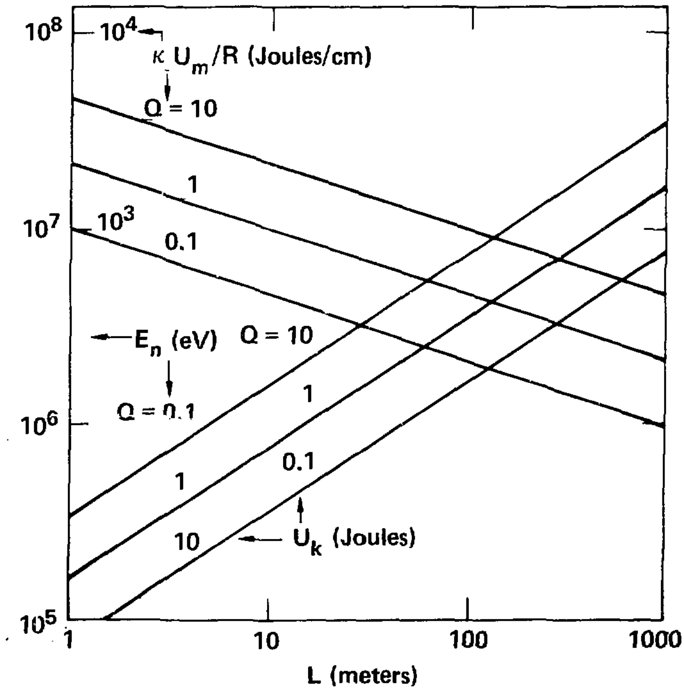
10^8
10^4
κ U_m/R (Joules/cm)
Q = 10
1
10^7
10^3
0.1
E_n (eV)
Q = 10
Q = 0.1
1
10^6
1
0.1
10
U_k (Joules)
10^5
1
10
100
1000
L (meters)

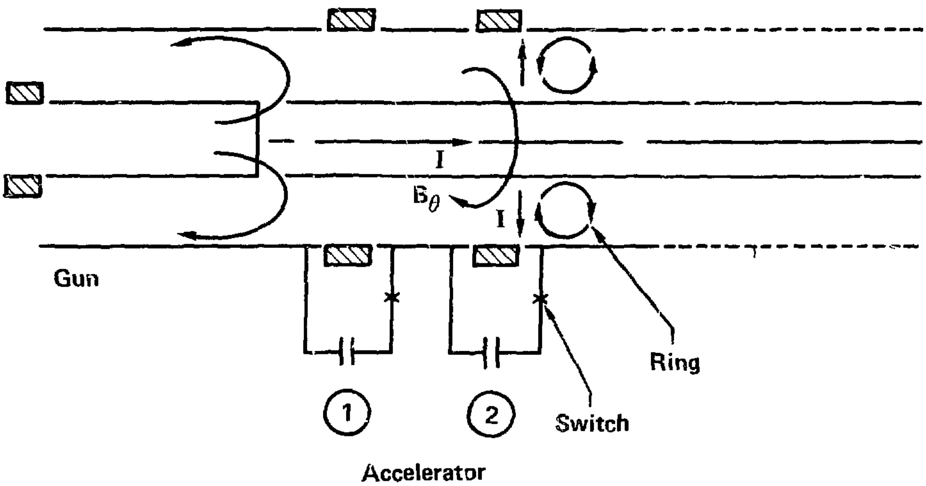
I
B_θ
I
Gun
Ring
1
2
Switch
Accelerator

MHD Simulation and the Implication in Reactor Concept of Merging Spheromaks

M. Katsurai and K. Katayama

Dept. of Electronic Engr. University of Tokyo
Bunkyo-ku, Tokyo 113, Japan.

T. Sato

Institute for Fusion Theory, Hiroshima University
Hiroshima 730, Japan

ABSTRACT----Application of merging process to enlarge a spheromak plasma in a reactor chamber is studied. The possibility of the poloidal flux enhancement is investigated using MHD computor simulations.

1. Introduction

Successful productions of spheromak configuration have been experimentally demonstrated by making use of a coaxial-gun or a toroidal flux-core[1]. They have motivated us to carry out reactor studies with the expectation that advantages in configurational simplicity of spheromak plasmas enable us to come up with more practical reactor systems than those based upon other conventional confinement schemes.

It should be noticed, however, that in the spheromak plasma the major portion of magnetic field is produced by the plasma current and the magnetic energy stored in plasma is as large in amount as the thermal energy of plasma devided by the average beta value $<\beta>$. This energy should be supplied into plasma at the initial start-up phase within a time scale of the energy confinement time . Therefore, the technological problems associated with the large power handling system of a spheromak reactor seem to be the greatest concern contrasting with the huge superconducting magnet system of tokamak reactors. The reasonable design of spheromak reactor should be provided with practical power suppling systems, and in this connection, possibilities of applying merging effects of spheromak plasmas are discussed following the previous studies[2,3].

2. Reactor configurations

Generally, the application of merging effect is conceivable not only for spheromak plasmas but also for other sorts of toroidal plasmas so far classified as compact toruses such as the reversed field mirror (RFM) and the reversed field theta pinches. Examples of common reactor configuration utilizing the merging effect of compact toruses are shown in Fig.1, where G is a generator and D is a divertor. The fundamental operational principle is shown in Fig.2 where multi-stage injectors with repetitive operation are installed to feed sufficient numbers of compact toruses in a reaction chamber. The utilization of such start-up scheme may allow us to use generators of a moderate size with a practical rating power. Steady state operation is foreseeable by the use of repetitive injections of compact toruses which supply the same amount of magnetic fluxes lost from the main plasma by the resistive diffusion during each cycle.

In the concept above mentioned, it is postulated that the merging could augment both toroidal and poloidal fluxes. Otherwise, we could not figure out such a simple scenario for the production of a reactor grade spheromak plasma without using alternative current driving methods such as NBI and RF drivings. It is discussed in the following section whether the flux enhancement is actually expected.

3. The MHD simulation and the flux conditions

Fig.3 shows the merging processes calculated by the 2-D MHD simulation code[4], where two similar spheromak plasmas are initially produced separately by the toroidal flux-cores, and then they are driven into the center region by decreasing the vertical field there.

The flux conditions are obtained as follows. In Fig.4 which shows the merging process, the plasmas along two closed contours in poloidal and toroidal directions, C_{pe} and C_{to}, behave like short-circuiting conductors. Therefore, the total amounts of fluxes interlinking with these loops should be conserved.

$$\Phi_{t3} = \Phi_{t1} + \Phi_{t2} \quad \text{---} (1), \qquad \Phi_{p3} = \max(\Phi_{p1}, \Phi_{p2}) \quad \text{---} (2)$$

These conditions are consistent with the results of the MHD simulation, and particularly, the maintenance of initial poloidal flux is easily confirmed in Fig.3. Eq.(2) discourages us from employing the merging effect to enlarge the poloidal flux of spheromak plasmas.

4. The application of Taylor's theory

The conservation of the helicity(K) introduced by Taylor[5] is written as

$$\frac{d}{dt}K = \int_V \frac{\partial}{\partial t}(\mathbf{A}\cdot\mathbf{B})\,dv + \int_S (\mathbf{A}\cdot\mathbf{B})(\mathbf{n}\cdot\mathbf{v})\,dS = -2\int_V \eta\,\mathbf{j}\cdot\mathbf{B}\,dv \qquad (3)$$

for a moving surface S on which $\mathbf{B}\cdot\mathbf{n}=0$ and $\mathbf{j}=0$ (fig.4(a)). Various anomalous effects may occur during merging process unless the merging is made quasi-statically stable by the control of external magnetic field. Along with the Taylor's theory for the force-free plasmas, relaxation of energy is much faster than that of the helicity during anomalous transformation of plasma configuration, and the total helicity inside the surface S is to be conserved.

$$K_3 = K_2 + K_1 \qquad (4)$$

Spheromak plasmas are not entirely surrounded by a conducting wall, and the plasmas along C_{pe} and C_{to} do not necessarily behave like perfect conductors during anomalous phases of the merging . So that, Eqs.(1) and (2) are no longer necessary conditions. It is hoped that some artificial geometrical constraints for the plasma boundary can allow the poloidal flux to be enhanced unlike the result of the MHD simulation.

Based upon the simplified model for the spheromak equilibrium condition in the uniform vertical field $B_\perp$[2], the following relations are obtained.

$$\Phi_t \sim aRB_\perp \quad , \quad \Phi_p \sim R^2 B_\perp \qquad (5)$$

$$K \sim aR^3 B_\perp^2 \sim \Phi_t \Phi_p \qquad (6)$$

where R is the major radius, a is the minor radius, and the term containing [ln(8R/a)-1] is assumed to be a constant. Special selections of geometrical relation between R and a can increase Φ_t and Φ_p when K is increased by mergings. Two cases are suggested here;

1) Constant aspect ratio: R/a=const.

$$\Delta\Phi_p/\Phi_p \sim \Delta\Phi_t/\Phi_t \sim 0.5\,\Delta K/K \qquad (7)$$

2) Constant inner-bore of plasma: R-a=const.

$$\Delta\Phi_p/\Phi_p \sim (2a/R+3a)\,\Delta K/K, \quad \Delta\Phi_t/\Phi_t \sim (R+a/R+3a)\,\Delta K/K \qquad (8)$$

Another expectation can be made of the possibility of automatic adjustment of the aspect ratio through the mechanism investigated by Lindberg[6]. Equation(5) leads to a relation $R/a \sim \Phi_p/\Phi_t$. As mergings go on, R/a becomes smaller according to Eqs.(1) and (2) untill R/a approaches unity where the screw type instability may begin due to the current concentration along the center axis which is supposed to enhance the poloidal flux in increasing the aspect ratio. This speculation needs future experimental investigation because the MHD simulation will not be capable of handling such problem.

5. Concluding remarks

The simple merging process based upon the MHD theory does not lead to the enhancement of poloidal flux, therefore, its application to reactor concept requests auxiliary current driving installations when the enlargement of plasma is considered. However, there is every reason to expect that some helicity conserving processes may enhance poloidal flux during merging.

References
[1] M.Yamada, Phys. Rev. Let., 46, 3, 188 (1981)
[2] M Katsurai and M.Yamada, Princeton PPPL-1614 (1980)
[3] M.Katsurai, Proc. (US-JAPAN) Workshop on CT., Osaka, p.161 (1981)
[4] T.Sato, J. Geophys. Res., 84, 7177 (1979)
[5] J.B.Taylor, IAEA-CN-33/PD-I 161 (1975)
[6] L.Lindberg and C.Jacobsen, J. Astrophys, 133, 1043 (1961)

Fig.1

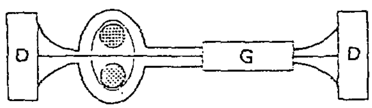

Merging type compact torus reactors using mirror field

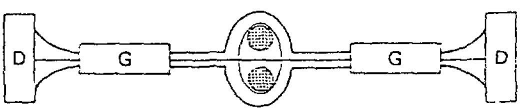

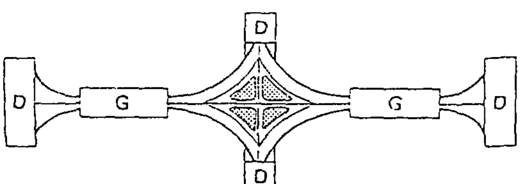

Merging type compact torus reactors using cusp field

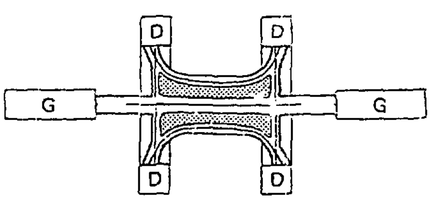

Fig.2

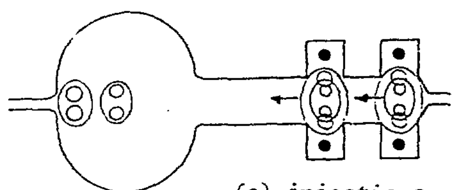

(a) injections

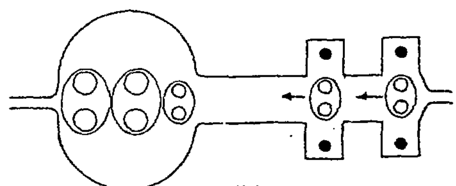

(b) enlargement

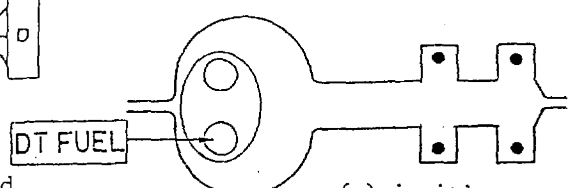

(c) ignition

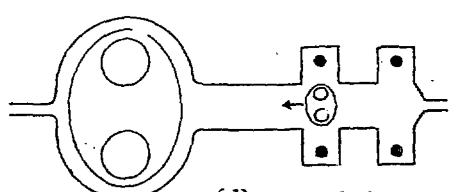

(d) sustaining

Fig.3 Poloidal flux Toroidal flux

t=69.92

$\Phi_{p1}=0.197$
$\Phi_{p2}=0.078$
$\Phi_{t1}=0.110$
$\Phi_{t2}=0.036$

t=72.11

t=74.31

t=76.50

$\Phi_{p3}=0.192$ $(\sim\Phi_{p1})$
$\Phi_{t3}=0.141$ $(\Phi_{t1}+\Phi_{t2})$

t=78.69

t=80.89 (Alfvén time)

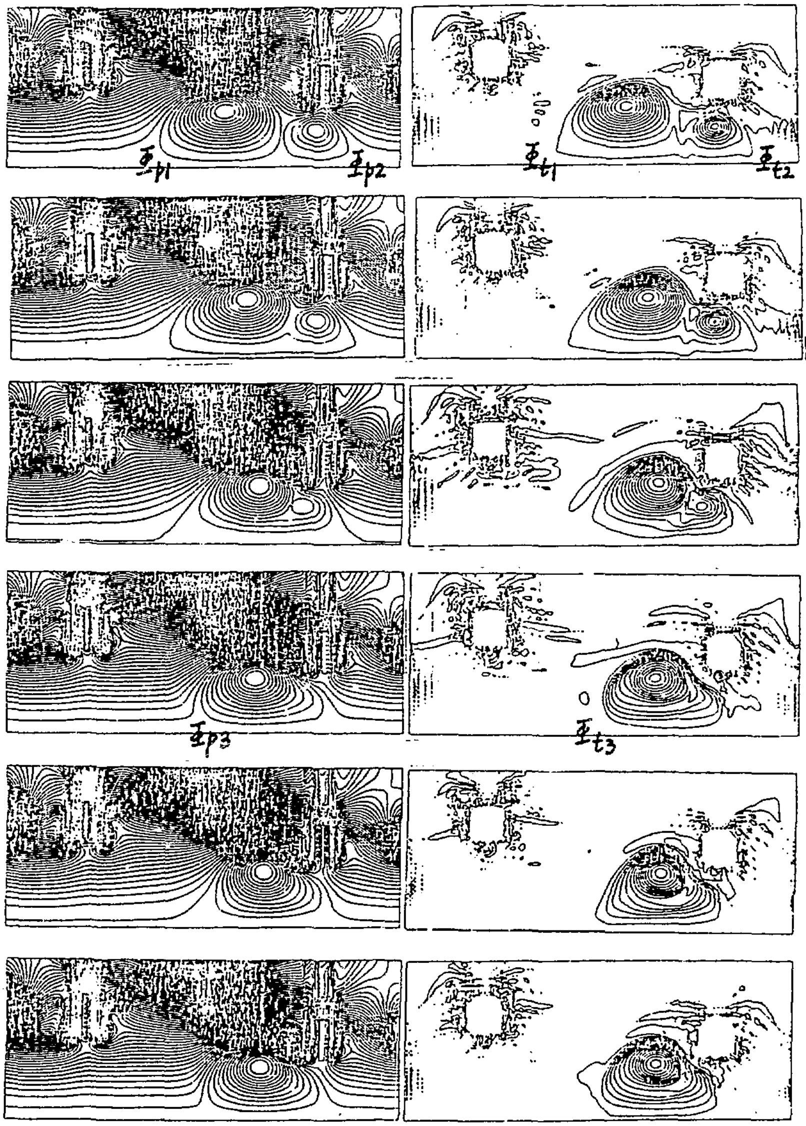

Fig.4 (a) (b) (c)

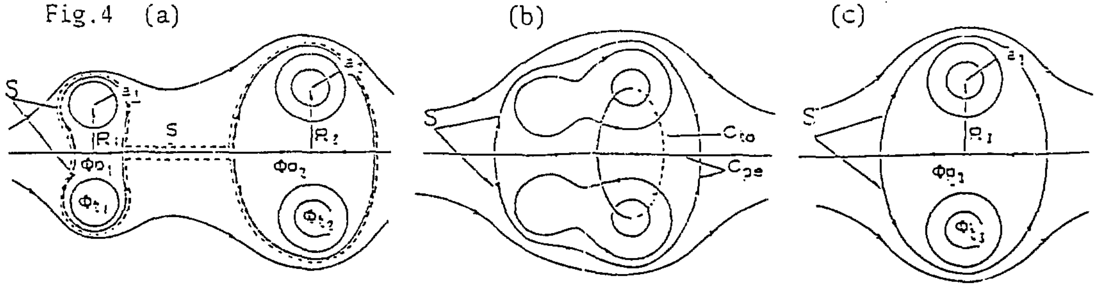

RESISTIVE MHD STABILITY CALCULATIONS OF
FORCE-FREE SPHEROMAK CONFIGURATIONS*

A.I. Shestakov and N.J. O'Neill
National MFE Computer Center
Lawrence Livermore National Laboratory
Livermore, California 94550

The linear resistive stability code RIPPLE VI is used to study a family of SPHEROMAK equilibria. The code solves a linearized model of the resistive incompressible MHD equations[1]:

$$\frac{\partial \vec{B}_1}{\partial t} = -\frac{1}{S} \nabla \times (\eta \nabla \times \vec{B}_1) + \nabla \times (\vec{v}_1 \times \vec{B}_0) \quad , \tag{1}$$

$$-\frac{\partial}{\partial t} (\nabla^2 \vec{v}_1) = \nabla \times \nabla \times \left((\vec{B}_0 \cdot \nabla) \vec{B}_1 + (\vec{B}_1 \cdot \nabla) \vec{B}_0 \right) \quad , \tag{2}$$

where $\vec{v}_1$, $\vec{B}_1$, $\vec{B}_0$ and η respectively denote the perturbed velocity, magnetic fields, equilibrium fields and zero order resistivity. Time is normalized to the Alfvén time and S is the magnetic Reynolds number. Cylindrical coordinates are used. The equilibria, $\vec{B}_0 = \vec{B}_0(r,z)$, while the perturbations vary as $f_1(r,z,t)\exp(in\theta)$. In this paper we consider only $n = 1$.

The domain of interest consists of a rectangle: $0 \leq r \leq R_w$, $-Z_{max} \leq z \leq Z_{max}$.[2] The perturbations satisfy symmetric boundary conditions along $r = 0$ and conducting wall boundary conditions along the other sides.

The plasma torus is surrounded by a vacuum. In this region we solve a different set of equations:

$$\frac{\partial \vec{B}_1}{\partial t} = \frac{Y_\eta}{S} \nabla^2 \vec{B}_1 \quad , \quad Y_\eta = \text{const.}, \quad \frac{Y_\eta}{S} > 1 \quad , \tag{3}$$

$$\nabla \times \nabla \times \frac{\partial \vec{v}_1}{\partial t} = -\nu \nabla \times \nabla \times \vec{v}_1 \quad , \nu = \text{const.} > 0 \quad , \tag{4}$$

Equation (3) models the vacuum property, $\nabla \times \vec{B}_1 = 0$, while Equation (4) dampens the velocity fields.

Although the model does not have any beta limitations, the equilibria under consideration are all force-free. The resistivity profile, η, is inversely proportional to the toroidal equilibrium current. We neglect

*Work performed under the auspices of the U.S. Department of Energy by the Lawrence Livermore National Laboratory under contract number W-7405-ENG-48.

effects of resistivity gradients and truncate η at some large value near the plasma limiter. Beyond the limiter, η is replaced by the plateau value Y_η. Both the resistivity cut-off and Y_η are chosen large enough so that further increases do not affect the results.

We study a collection of five SPHEROMAK equilibria[3] categorized by the following parameters:

NAME	RMAX	ZMAX	CHARAC DIST. a	FIELD STRENGTH-B	ZPL/ RPL	τ_H
E1	60cm.	50cm.	36.7cm.	49.3kG	1.85	.0483µsecs.
E2	60	50	35.8	57.1	1.33	.0407
E3	60	50	34.0	65.0	1.11	.0339
E4	60	40	34.8	69.6	.93	.0325
E5	60	30	34.0	76.7	.78	.0287

where ZPL and RPL respectively measure the height and width of the poloidal cross section of the plasma torus. The profiles range from prolate (E1) to oblate (E5). The equilibrium toroidal field function, $rB_{\theta 0}$, varies linearly with ψ_0, the equilibrium flux function. Although the fields above are considerably higher than those found in present experiments, the results here are meaningful after a proper renormalization. The characteristic time, $\tau_H = a\sqrt{4\pi\rho_0}/B$ where we estimate the particle density $n \approx 10^{14}$ cm^{-3}. Figure 1 displays contours of the flux function and poloidal current of E1 and E5.

The results show that all five equilibria are unstable. Figure 2 plots normalized growth rate p ($= \omega\tau_H$) vs. equilibrium vs. S. For $S > 4.10^4$, the results are independent of S. Figure 3 displays the perturbed poloidal velocity at $\theta = 0$, $\pi/2$, for the equilibria E1 and E5. These structures are taken from runs with $S = 10^5$ but are representative of results at high S. At $\theta = 0$ the dominant mode is a non-rigid shift in all the cases studied. Along $\theta = \pi/2$, the displacement varies between a vertical motion and a tilt depending on the equilibrium profile. The ratio of v_1^R / $v_1^I \approx 2$ means that the shift is dominant. The large growth rates ($p \approx .5$) illustrate that the configurations are very unstable to n = 1 modes. We expect similar results for n > 1.

We have performed a stability study of a family of SPHEROMAK configurations. The configurations were found to be unstable. They possessed large growth rates, a global mode structure and an independence of S signifying ideal modes driven by magnetic energy. Similar results were obtained by other workers using time independent ideal models[3,4]. However, we do not find any of the equilibria to be more stable and do not notice that the dominant instability changes from a tilt for prolate shapes to a shift for oblate cross-sections.

References

1. A. I. Shestakov, J. Killeen, and D. D. Schnack, "A Numerical Model for Non-Axisymmetric MHD Instabilities," submitted to J. Comp. Phys., also available as Lawrence Livermore National Laboratory report UCRL-86493, July 1981.
2. J. A. Dibiase and J. Killeen, J. Comp. Phys. 24, 2 (1977), 158.
3. C. Bernard, private communication, 1981.
4. S. C. Jardin, et al., Nuclear Fusion 21, 9 (1981), 1203.

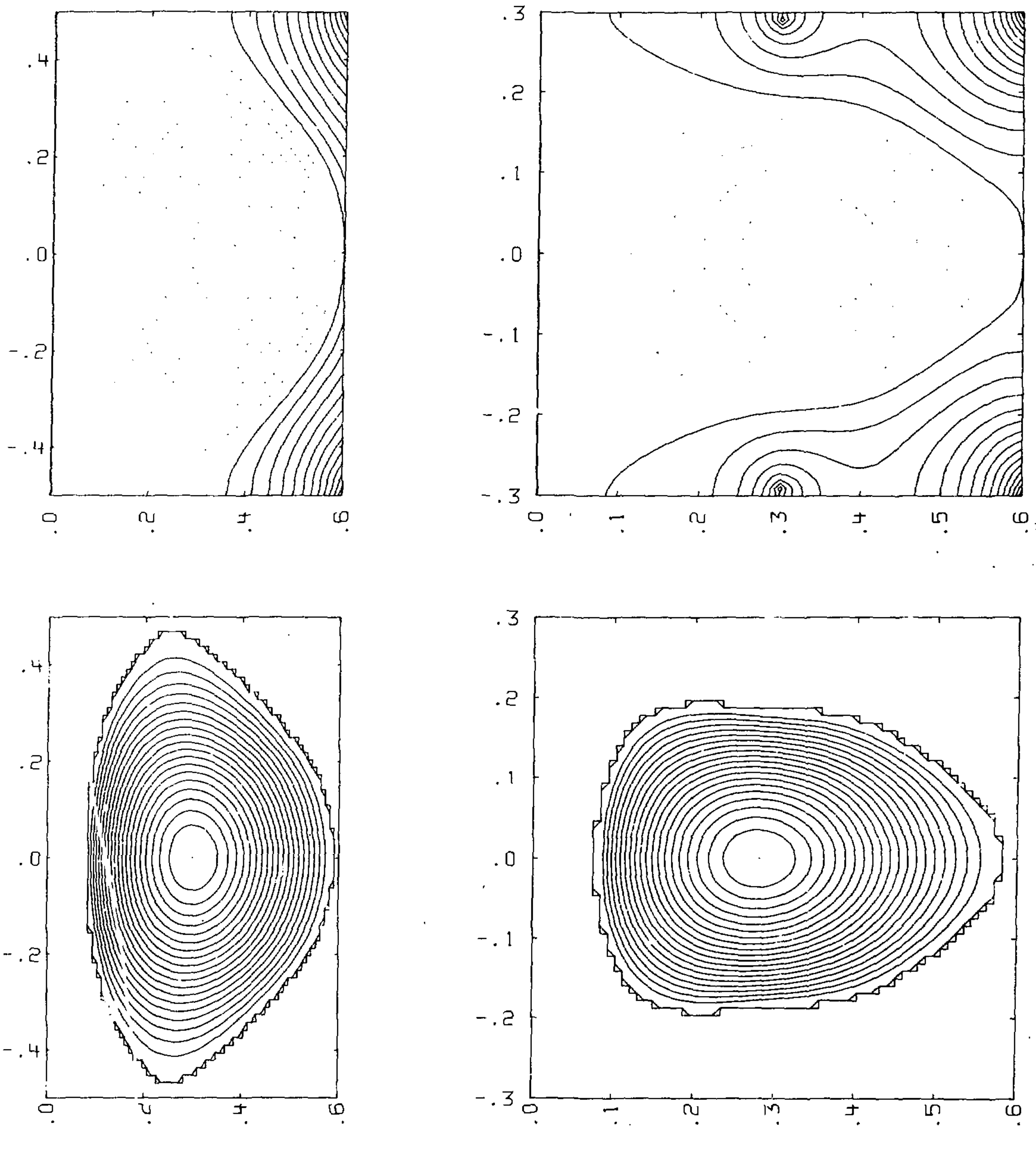

FIGURE 1. Equilibrium flux and toroidal current contours for E1 and E5 equilibria.

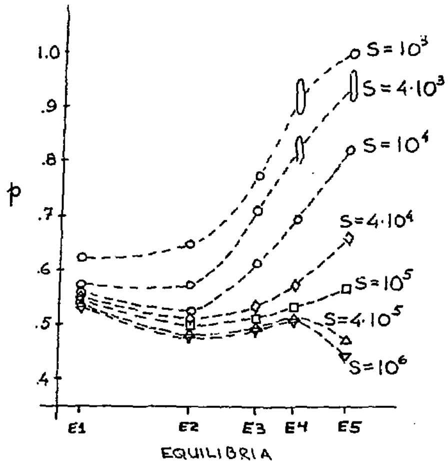

FIGURE 2. Normalized growth rate p ($=\omega\tau_H$) vs. equilibria vs. Reynolds numbers.

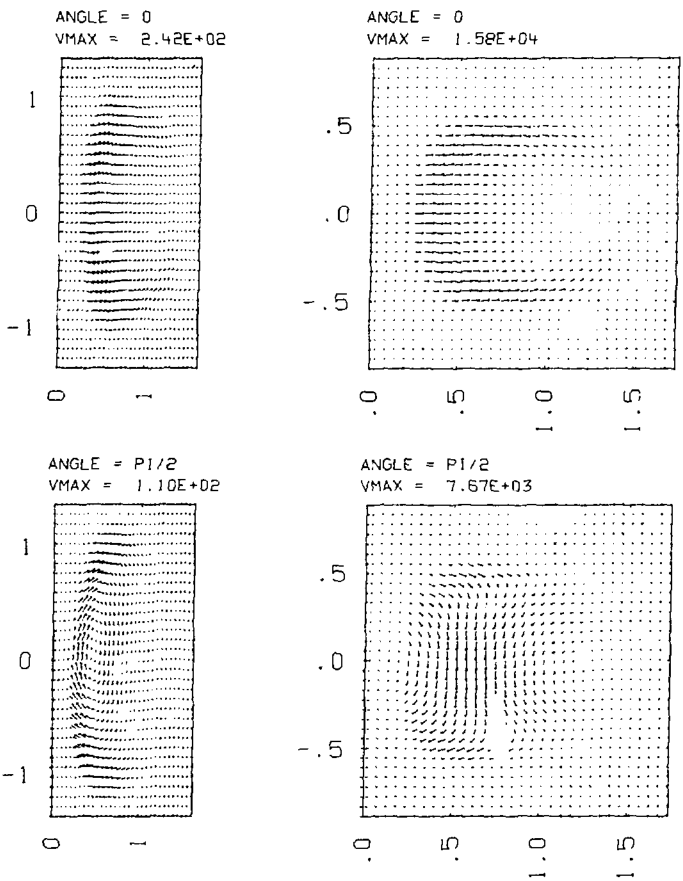

FIGURE 3. Perturbed poloidal velocities at θ = 0 and $\pi/2$ for the E1 and E5 equilibria.

NUMERICAL SIMULATION OF A BEAM HEATED COMPACT TORUS*

D. E. Shumaker, B. McNamara, W. C. Turner

Lawrence Livermore National Laboratory
University of California
Livermore, CA 94550

The transport code, FRT,(1) was used to study the evolution of a beam heated compact torus. This code is a coupled 1-D transport and 2-D equilibrium calculation. The plasma and magnetic fields are assumed to be axisymmetric.

The transport calculation consists of the simultaneous solution of four transport equations for ion density, electron entropy, ion entropy, and toroidal magnetic flux. The physical processes included in this calculation are classical transport, Joule heating of electrons, collisional transfer of energy from ion to electrons, and heating of ions by neutral beams.

An anomalous electron energy loss is included in some of the calculations presented here. A loss rate is included in the electron entropy equation which is inversely proportional to a given electron energy confinement time, τ_e. The confinement time, τ_e, is determined from a given value of $n\tau_e$.

The calculations presented here are done to determine to what extent a compact torus can be heated by a neutral beam. The target plasma is assumed to have been injected into a flux conserver such as in the Beta II experiment at LLNL.(2) The transport code models the subsequent changes in the plasma and magnetic fields. The beam power used in these calculations was 4 M watts at an energy of 12 keV. Three target plasmas are used in these calculations. The parameters of these equilibria are given in Table I. All three equilibria have the same central ion density of 9.8×10^{13} cm^{-3} and a central q (magnetic stability factor) of 0.72. Equilibrium A has the lowest current and magnetic fields, and equilibrium C has the highest current and magnetic field. These equilibria are similar to those obtained in the Beta II experiment.

The final state attained is limited by either the transport loss of energy or a β limit. The behavior of each of these target plasmas is studied assuming completely classical transport, in which case ion thermal conduction is the dominate transport process, and assuming a constant prescribed anomalous electron energy loss $n\tau_e = 10^{10}$ cm^{-3} sec. This anomalous loss is about two orders of magnitude worse than empirical scaling in a tokamak of the same minor radius.(3) It was chosen as a rough lower bound of interest since compact torus scaling is unknown at present.

*Work performed under the auspices of the U.S.D.O.E. by Lawrence Livermore National Laboratory under contract W-7405-ENG-48.

These three equilibria used are stable to the tilting node.[4] A study of the effect of pressure on the stability is given in ref (5). The critical beta, β_c, will most likely be in the range, .2 to .4. For the calculations presented here β_c will be defined as the ratio of central plasma pressure to the magnetic pressure at the outer edge of the plasma, and will be assumed to be .4, which is an optimistic value.

The three equilibria were each run with and without the anomalous electron energy loss. Fig. 1 is a plot of the central ion temperature vs. time. Fig. 2 is a plot of β_c vs. time. Without the anomalous electron energy loss the β_c reaches the value of .4 at 70 μsec for equilibrium A, 300 μsec for equilibrium B, and 800 μsec for equilibrium C. The ion temperature at these times are 0.25 keV for equilibrium A, 0.90 keV for equilibrium B, and 2.05 keV for equilibrium C. Fig. 3 is a plot of the central electron temperature vs. time.

With the anomalous electron energy loss the β at a given time is reduced. The β_c = .4 is reached at a later time, for equilibrium A at 70 μsec, for equilibrium B 400 μsec, and for equilibrium C about 1300 μsec. For these calculations $n\tau_e$ has been set to 10^{10} cm^{-3} sec. All of the calculations presented here have reached the β limit before they reached a steady state limited by diffusion. Equilibrium C came close to reaching steady state, of course the β limit used here of .4 is somewhat arbitrary, if it were .5 then this run would have reached steady state. Fig. 4 is a plot of the central ion temperature vs. β for these runs.

In summary, we found that if electron energy confinement time exceeds $n\tau_e = 10^{10}$ cm^{-3} sec in present plasma gun generated compact torus experiments, then it is feasible to examine MHD β stability limits with a technologically reasonable amount of neutral beam injection power. In particular we have found that 4 Mwatt of neutral beam power injection into compact tori already produced with the Beta II plasma gun will result in beta values greater than 0.4 in less than a millisecond. This value of beta is near an optimistic value for the stability limit.

Acknowledgment:

The equilibria used in these calculations were generated by a code written by J. K. Boyd.

References:

1. D. E. Shumaker, J. K. Boyd, S. P. Auerbach, and B. McNamara. "Numerical Simulation of Transport in a Field-Reversed Mirror Plasma" to be published in JCP, UCRL 86566.

2. W. C. Turner, G. C. Goldenbaum, E. H. A. Grannaman, C. W. Hartman, D. S. Prono, J. Taska, and A. C. Smith, Jr. "Formulation of Compact Toroidal Plasmas by Magnetized Coaxial Plasma Gun Injected into an Oblate Flux Conserver," Proc. of Third Symposium on the Physics and Technology of Compact Toroids, Los Alamos, NM, LA-8700-C (1980).

3. "Status of Tokamak Research" DOE/ER-0034, UC-20, Oct. 1979, pg. 2-46.

4. H. E. Dalhed "Critical Bias Field for Tilting Stability in the Beta II Experiment," Proc. of Third Symposium on the Physics and Technology of Compact Toroids, Los Alamos, LA-8700-C (1980).

5. H. E. Dalhed "Beta Limitations in Spheromak and FRM Configurations" Annual Controlled Fusion Theory Conference, Austin, TX, April 1981.

TABLE I

Equilibrium	A	B	C
toroidal current (t = 0)	150 kA	290 kA	430 kA
B_{Tor}(0-point)			
(t = 0)	2850 G	5430 G	7970 G
(t = 500 μsec)	1200 G	4240 G	6840 G
B_{Pol}(r = 0, z = 0)			
(t = 0)	-3200 G	-6060 G	-8910 G
(t = 500 μsec)	-2400 G	-5390 G	-8070 G
B_{Pol}(r = r_{wall}, z = 0)			
(t = 0)	1410 G	2823 G	4220 G
(t = 500 μsec)	2400 G	3500 G	4850 G
poloidal flux			
(t = 0)	3140 kG cm^2	6280 kG cm^2	9420 kG cm^2
toroidal flux			
(t = 0)	1330 kG cm^2	2660 kG cm^2	4000 kG cm^2

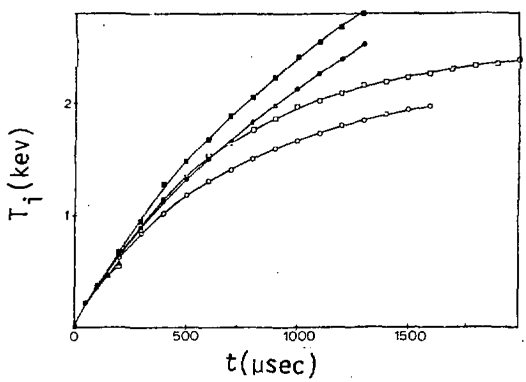

Fig. 1 Central ion temperature vs. time

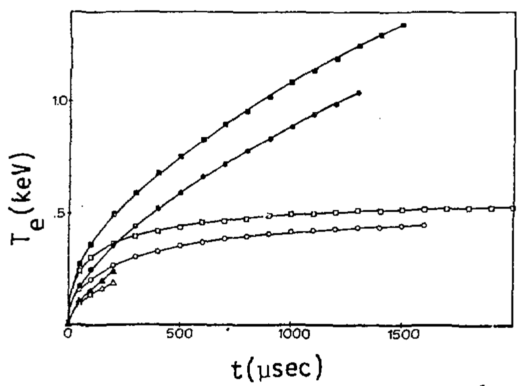

Fig. 2 Central electron temperature vs. time

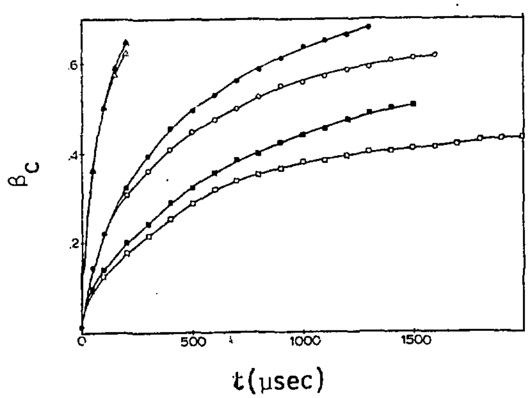

Fig. 3 β_c vs. time

▲ Equilibrium A classical transport
△ Equilibrium A $n\,\tau_e = 10^{10}$
● Equilibrium B classical transport
○ Equilibrium B $n\,\tau_e = 10^{10}$
■ Equilibrium C classical transport
□ Equilibrium C $n\,\tau_e = 10^{10}$

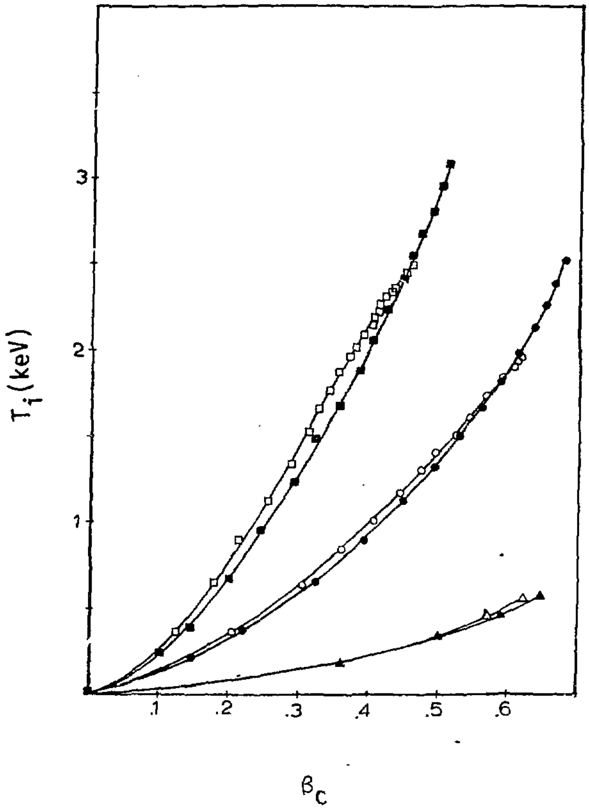

Fig. 4 Central ion temperature vs β_c

Numerical Simulation of the Energy Balance in the Proto S-1C Spheromak

by

Y. C. Sun, S. C. Jardin, D. Heifetz, M. Yamada, and D. E. Post

Plasma Physics Laboratory, Princeton University,
Princeton, N.J. 08544

The numerical simulations of the spheromak formation process performed previously[1,2] predicted peak temperature of the center of plasma much higher than those experimentally measured.[3,4] It is the purpose of this research to find out the possible sources of this discrepancy. We considered the radiation losses of carbon and oxygen. We are now investigating the effect of energy loss due to ionization and charge exchange of background neutral atoms.

The governing equations of the formation process are:

$$\frac{\partial}{\partial t} \vec{m} + \nabla\cdot\left(\frac{1}{\rho} \vec{m}\vec{m}\right) + \nabla p = \vec{J} \times \vec{B} ,$$

$$\frac{3}{2} \frac{\partial}{\partial t} p + \nabla\cdot\left(\vec{q} + \frac{5}{2} \frac{p}{\rho} \vec{m}\right) = \vec{J}\cdot\vec{E} + Se ,$$

$$\frac{\partial}{\partial t} \rho + \nabla\cdot\vec{m} = \nabla \cdot \frac{\vec{B}\vec{B}}{B^2} D_{\parallel} \eta \nabla\rho + Sp ,$$

$$\frac{\partial}{\partial t} \vec{B} = - \nabla \times \vec{E} ,$$

$$\vec{J} = \frac{1}{\mu_o} \nabla \times \vec{B}$$

and

$$T = \frac{Mi}{2\rho k} p .$$

Here $\vec{m} = \rho\vec{v}$ is the momentum density and $\vec{q}$ is the heat flux vector. In an axisymmetric device with symmetry angle ϕ, $\vec{B}$ can be expressed in terms of poloidal flux ψ and toroidal function g,

$$\vec{B} = \nabla\phi \times \nabla\psi + g\nabla\phi .$$

In addition to these equations, we have circuit equations to couple the inductance due to change of current in the poloidal and toroidal coils to the plasma.

Impurity radiation losses are computed using coronal equilibrium atomic physics method by Tarter.[5] BALDUR[6] subroutines provide us the loss term in our energy equation.

The neutrals are treated by Monte Carlo method with a pseudo collision algorithm.[7,8] Test particles with a weight $\omega = 1$ are born in the spheromak. Each particle is followed through a sequence of collisions. At each location where a collision occurs, the charge exchange probability μ is computed and the particle weight ω is reduced by μ to account for attenuation by ionization. A new velocity is then chosen from a 3-D Maxwellian distribution at the local ion temperature and the particle is followed until its next collision or until its weight becomes neglibible. We record the charge exchange rate, ionization rate, change exchange energy and ionization energy at each location. All these terms are included in our continuity equation and energy equation as the source (loss) terms S_e and S_p.

With Proto S-1C spheromak parameters, we made a formation run without impurity and neutral. The initial density and temperature were 4×10^{14} cm^{-3} and 5 ev respectively. In about 50 μsec, a spheromak plasma was formed. The time evolution of poloidal flux and toroidal field are shown in Fig. 1. The temperature history along a radius through the center of the device is shown in Fig. 2. At the end of formation, the peak temperature is about 56 ev and the density is about 6×10^{14} cm^{-3}.

The same run was then made with 2.5% carbon and 2.5% oxygen. Figure 3 shows the temperature history. After the spheromak plasma is formed, the temperature is only 3 ev. Due to increased pinching effect of this low temperature discharge, the central plasma density piles up to more than 4×10^{15} cm^{-3} which does not agree with the experimental observations.[4]

Another run was made with neutral effect. We started with 2000 test particles at T = 5 ev and $n_o = 10^{14}$ cm^{-3}. The neutral effect was switched on at t = 36 μsec. After about 20 μsec, the temperature profile dropped by 10% comparing with the case which has no neutral effect as shown in Fig. 4.

ACKNOWLEDGMENT

This work was supported by DoE Contract No. DE-AC02-CHO-3073.

REFERENCE

1. S. C. JARDIN and W. PARK, Phys. Fluid 24, 679 (1981).
2. Y. S. SUN and S.C. JARDIN, Bull. Am. Phys. Soc. 25, 1023 (1980).
3. M. YAMADA, et al, Phys. Rev. Lett. 46, 188 (1981).
4. A. JANOS, et al, Paper B2 of this proceedings.
5. B. TARTER, "Radiation Losses From Impurity Ions." UCRL-78119, LLL.
6. D. E. POST et. al., PPPL TM-298 (1977).
7. M. H. HUGHES and D. E. POST JPC 29, 43 (1978).
8. D. HEIFETZ, D. E. POST, and S. C. JARDIN (submitted to JPC) (1981).

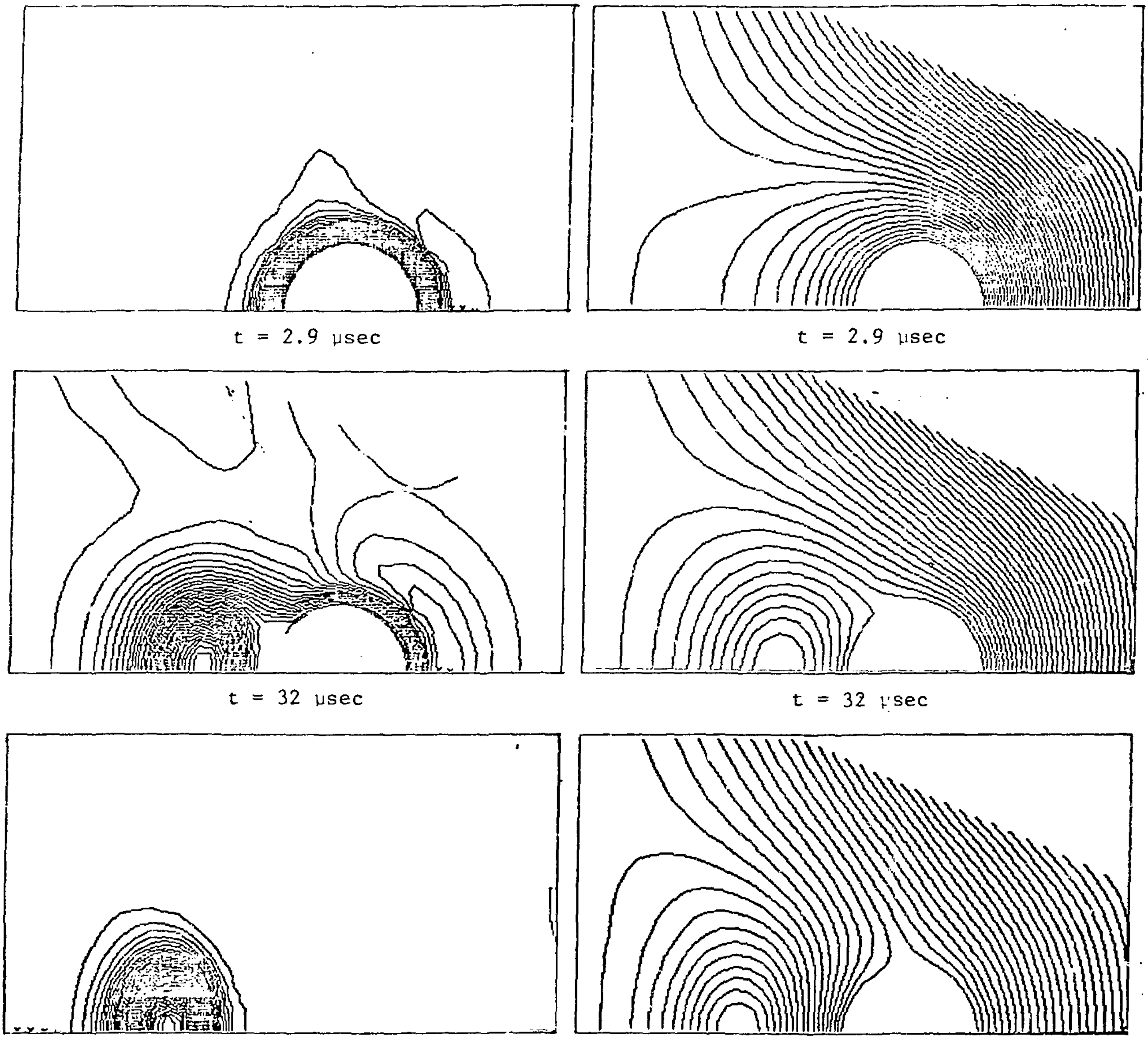

t = 2.9 μsec | t = 2.9 μsec

t = 32 μsec | t = 32 μsec

t = 55 μsec | t = 55 μsec

Toroidal g Function | Poloidal Flux

Fig. 1. Evolution of toroidal g function and poloidal flux during formation

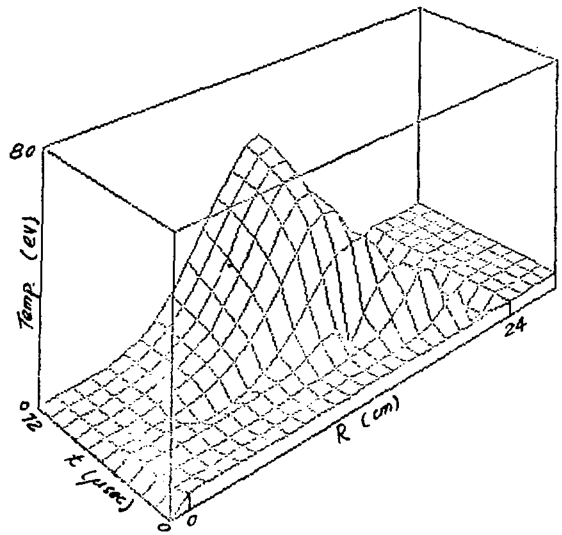

Fig. 2. Temperature history without impurity and neutral effect.

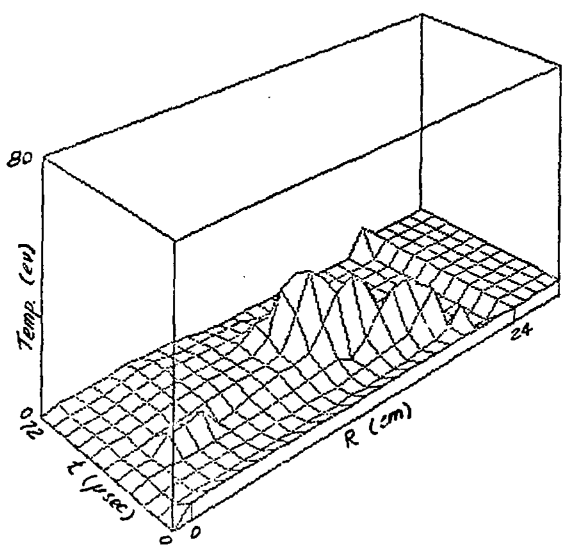

Fig 3. Temperature history with impurity effect.

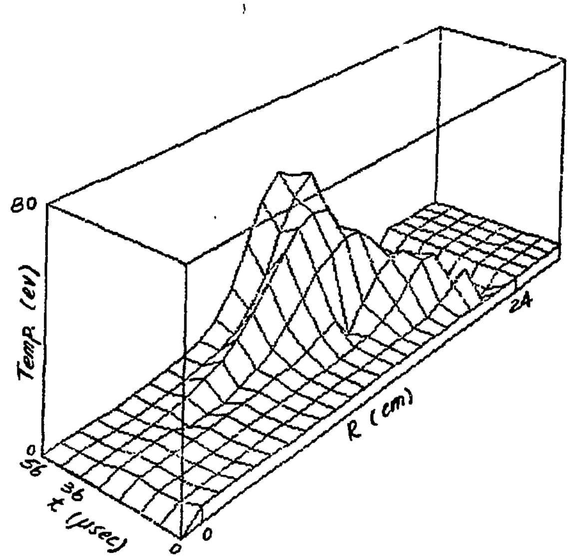

Fig. 4. Temperature history with neutral effect.

Formation and Merging of Spheromaks and Formation of FRC

Tetsuya Sato, Shusuke Otsuka and Koichiro Araki

Institute for Fusion Theory, Hiroshima University, Hiroshima 730, Japan

We present three different 2-D MHD simulations of spheromaks and the field reversal configuration, namely, 1) formation of the Princeton spheromak, 2) merging of two spheromaks and 3) formation of the field reversal configuration.

In the first part we wish to emphasize that the spheromak size is largely dependent upon the formation speed. Fig.1 shows three spheromaks formed for three different formation speeds. The left panel shows the case where τ_f/τ_A (τ_f:formation time, τ_A: Alfven transit time)= 4.35. The middle and right panels correspond to the cases for τ_f/τ_A=21.7 and 68.6, respectively. It is clearly shown that the spheromak size is controlled by the formation speed.

Secondly, we show an example of merging of two spheromaks in Fig. 2. We have found that the toroidal flux is doubled but the poloidal flux remains the same before and after the merging. Attempts to merge two spheromaks with different sizes are made to find that it is difficult to enhance the poloidal flux by merging, rather the poloidal flux tends to decrease.

Finally, we show a simulation run of the reversed field theta pinch in Fig. 3. In this simulation, we have adopted an artificial resistivity model; the resistivity is assumed to be larger near the side boundaries (z=0 and 1.5m) and the top boundary (r=1m). The left three panels show the time evolution of the poloidal flux and the right panel shows the radial distribution of the force at about a time corresponding to the middle panel on the left.

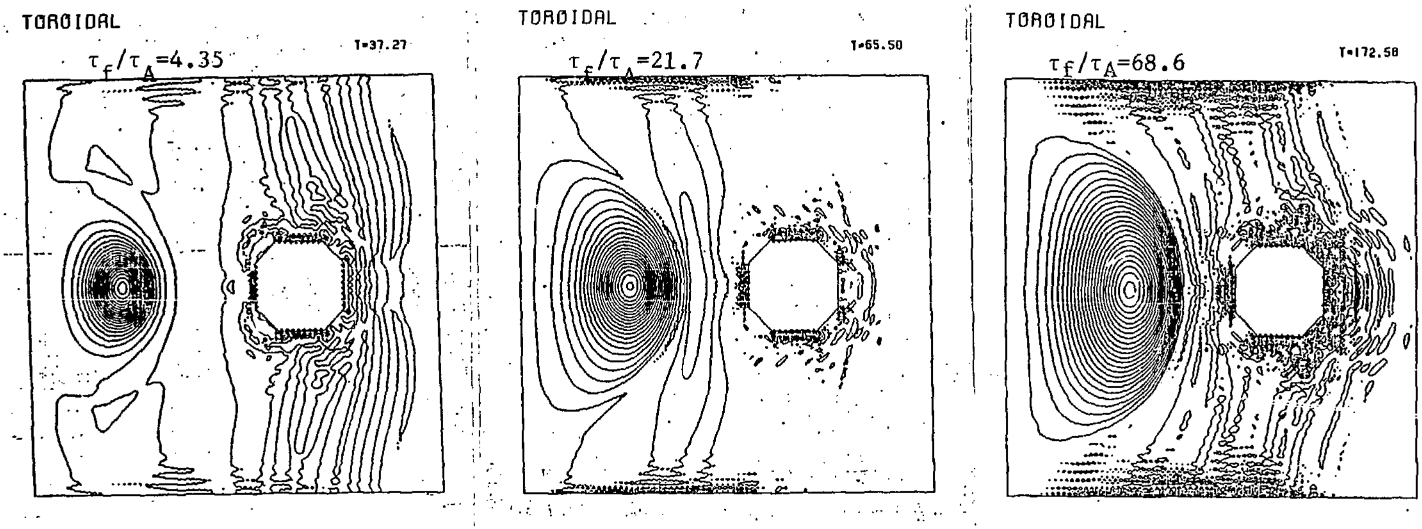

Fig.1 Controll of the spheromak size by the formation speed.

Initial Poloidal Field

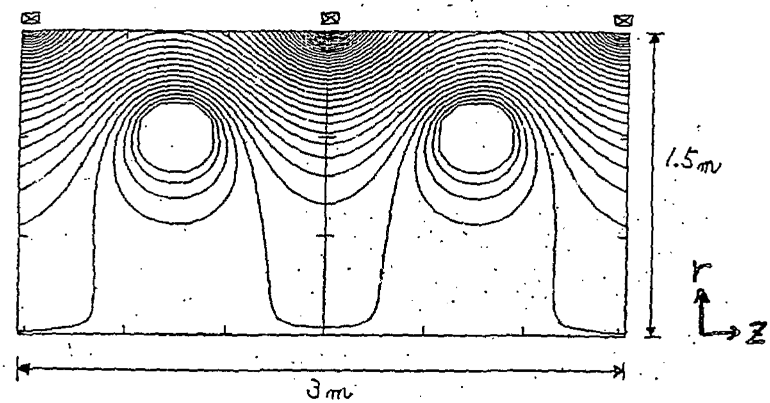

Toroidal

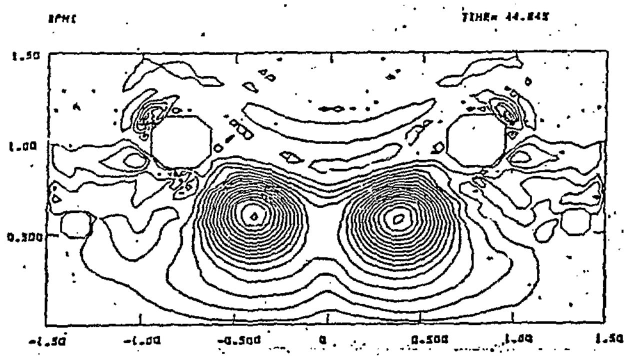

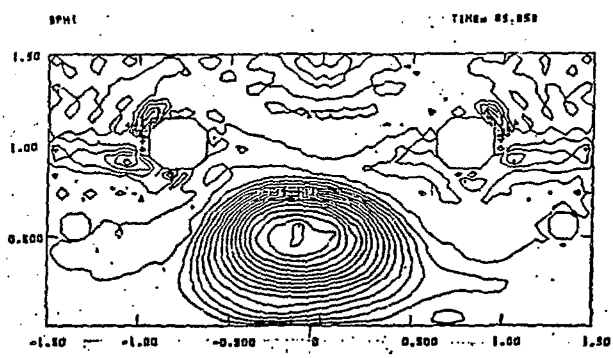

Fig.2

Merging of two spheromaks

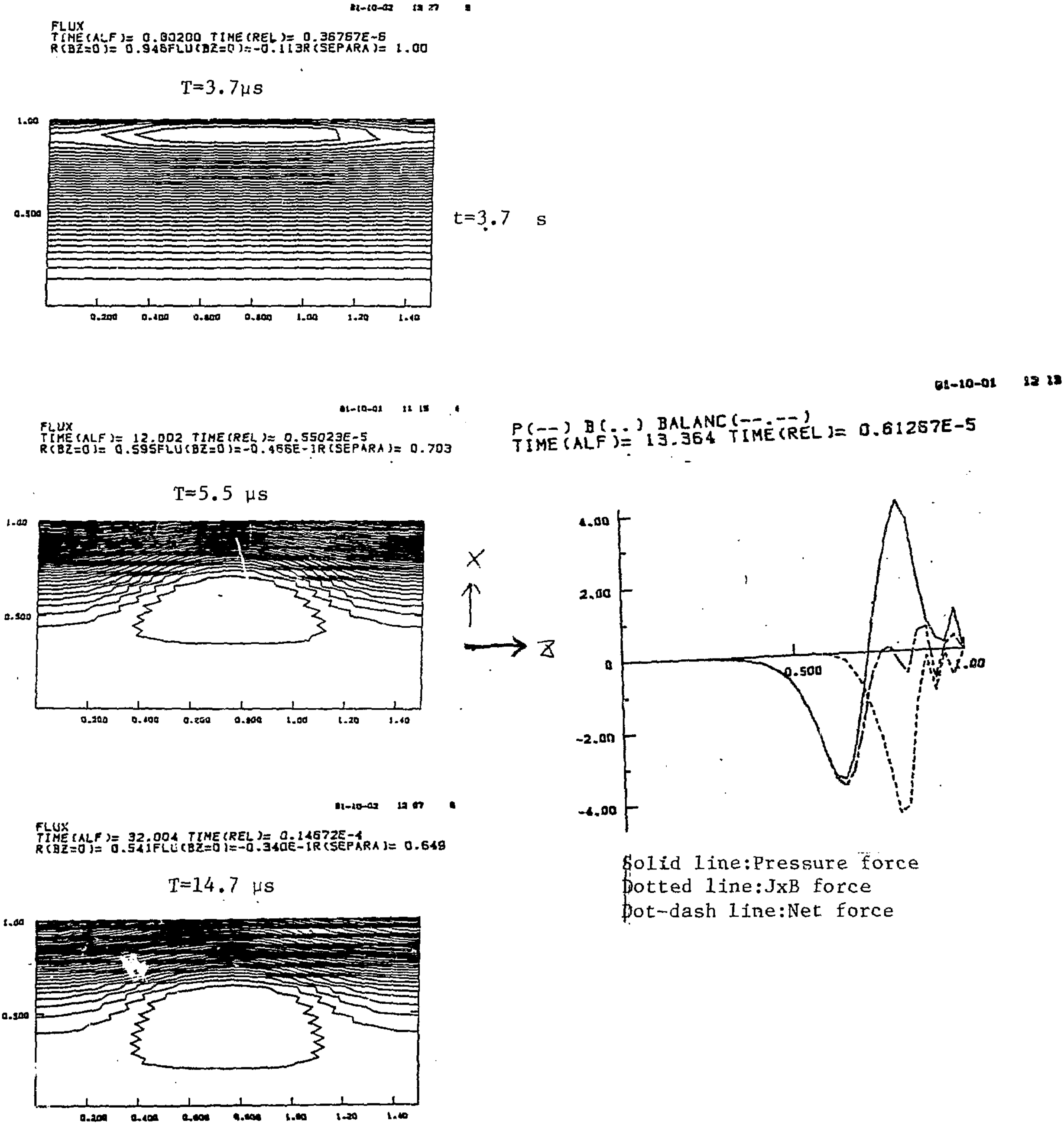

Fig. 3 Formation of FRC

4

IV. SPHEROMAK - EXPERIMENT

PLASMA IMPURITY CONTROL STUDIES IN CTX

Cris W. Barnes, I. Henins, H. W. Hoida, T. R. Jarboe, R. K. Linford,
J. Marshall, A. R. Sherwood, and M. Tuszewski
Los Alamos National Laboratory
Los Alamos, New Mexico 87545

I. INTRODUCTION

In the CTX experiment spheromak-type compact toroids (CTs) are produced by a magnetized coaxial gun and trapped in a metal flux conserver. In the past, these CTs have exhibited magnetic field and density lifetimes of about 250 to 350 μs and electron temperatures of about 10 eV.[1] In recent experiments, after hydrogen discharge cleaning the gun and flux conserver surfaces, the lifetimes have been extended to 550 μs. This improvement in lifetime, together with spectroscopic and bolometric measurements,[2] are consistent with the interpretation that the CT plasma losses are impurity dominated and that discharge cleaning is reducing the impurities. Details of these measurements are described below as well as successful experiments which led to a more open flux conserver.

II. DESCRIPTION OF THE CTX EXPERIMENT

The present configuration of the CTX experiment is shown in Fig. 1. The plasma gun parameters are: inside electrode diameter = 20 cm; outside electrode diameter = 30 cm; electrode length = 112 cm; puffed gas load from six valves = 6 cm^3-atm; capacitor bank = 74 μF at 45 kV; gun bias field = 1 kG; poloidal field flux = 0.02 Wb; maximum current = 1 MA. The present base pressure in the 8,000 ℓ volume vacuum tank is $\sim 5 \times 10^{-8}$ torr. In order to allow diagnostic access, the copper flux conserver has a 7.5-cm wide slot at its periphery bridged by twelve copper bars. See Fig. 1. The spheromaks generated have peak fields on axis of ~ 6 kG and total energies of ~ 6 kJ.

There are two stainless steel glow discharge electrodes as shown in Fig. 1. One is a 2.5-cm wide ring placed inside the entrance tunnel just in front of the plasma gun, and the other is a flat annular ring placed on the axis of the vacuum tank 40 cm behind the flux conserver. To minimize contamination of the plasma by probes, we now use only one three-axis magnetic probe on the axis of the flux conserver. This is adequate for stability and flux lifetime observations. Quartz UV spectroscopy and double-pass single beam interferometry are carried out along a diameter in the midplane of the flux conserver.

III. IMPURITY SOURCES AND METHOD OF REDUCTION

An important source of the CTX plasma impurities is from the contaminant layers, mostly carbon and oxygen, on the interior surfaces of the gun and the flux conserver. In addition, there may be metallic impurities generated from the stainless steel gun electrodes and the copper flux conserver.

The magnitude of metallic impurity radiation can be varied by changing operating conditions of the magnetized gun.[2] In The CTX gun at relatively low poloidal field flux (0.011 W) FeII line radiation is sharply (> 3 to 10 times) increased by reducing the delay between the gas fill and gun firing from 300 to 150 μs. At high gas loads (> 7 atm-cm^3) this effect is reduced, and the plasma density is increased. When the gun is operated at higher poloidal field flux (0.018 W) the FeII radiation is generally reduced. In addition, increasing the delay increases the plasma density and reduces the lifetime, while at these fluxes the high-Z radiation does not consistently vary with delay. We presently operate with a gas load of 6 cm^3-atm, a delay of 175 μs, and a poloidal field flux of 0.018 W. These values have been determined by optimizing the plasma lifetime, magnetic field strengths, and impurity line radiation.

A reduction of carbon and oxygen surface contamination has been attempted by glow discharge cleaning in a flowing hydrogen atmosphere at approximately 15 mtorr pressure. Our decision to use this procedure is based on cleaning experience of large tokamaks at other laboratories.[3] Typical glow discharge currents are 10^{-5}A/cm^2 of cathode (vacuum tank) surface with approximately 300 volts dc applied to the electrodes. Because the glow discharge does not penetrate very far into the 5-cm wide annular space between the gun electrodes, we are using simultaneously low energy (3.0 kJ at 1.5 kV) coaxial gun discharges at a 5-second repetition rate to aid in cleaning of the gun electrodes.

IV. RESULTS OF DISCHARGE CLEANING

After about 100 hours of discharge cleaning, as described above, there has been an almost complete elimination of CIII radiation, an increase in the duration of the OIV radiation emission and an increase of about 50% in the spheromak configuration lifetime.

The levels of the CIII radiation before and after discharge cleaning are shown in Fig. 2(A), which allows us to conclude that the carbon impurity situation has been greatly improved. Figure 2(B) shows the change in the history of the OIV radiation. The duration of the OIV radiation increases, which indicates that the plasma now is hot enough to triply ionize oxygen for a longer time and, therefore, it may not be cooling as rapidly as before. However, there is probably still too much oxygen in the plasma. Carbon surface impurities are more easily removed by discharge cleaning than oxygen[3] and more discharge cleaning may also solve the oxygen problem. The increased plasma lifetime is shown in Figs. 3(A) and 3(B) where both the density and the magnetic fields show a substantial increase in lifetime (~ 50%). Figure 4 shows a strong correlation between the increased OIV duration and the increase in the magnetic field lifetime. All of the above results are consistent with the interpretation that plasma losses are dominated by impurities and that discharge cleaning is reducing the impurities.

V. OPEN FLUX CONSERVER RESULTS

Experiments were conducted to establish the effect of a peripheral open slot on the behavior of the spheromak trapped in the flux conserver. A completely open slot caused the toroid to tip sideways with its return flux outside the flux conserver. Slot widths of 2.5 cm to 7.5 cm were tried, both with and without pulsed guide fields ranging from 50 G to 5 kG applied just outside the slot, with no success in trapping of the CT. The fields were excluded from within flux conserver by the skin depth of the copper. Four bridging straps gave well-behaved spheromaks with a 2.5-cm slot. We now are using twelve bridges with a 7.5-cm slot. The bridges are moveable to accommodate various diagnostics or heating apparatus.

REFERENCES

1. I. Henins, H. W. Hoida, T. R. Jarboe, R. K. Linford, J. Marshall, K. F. McKenna, D. A. Platts, and A. R. Sherwood, "Physical Properties of Compact Toroids Generated by a Coaxial Source," Proceedings Third Symposium on Physics and Technology of Compact Toroids, Los Alamos, NM (December 2-4, 1980), p. 101.

2. H. W. Hoida, et al., "Properties of Spheromaks Generated by a Magnetized Coaxial Source," Proceedings Fourth Symposium on the Physics and Technology of Compact Toroids, Livermore, CA (October 27-29, 1981).

3. H. F. Dylla, "A Review of the Wall Problem and Conditioning Techniques for Tokamaks," J. Nucl. Mater, 93/94 (1980), p. 61.

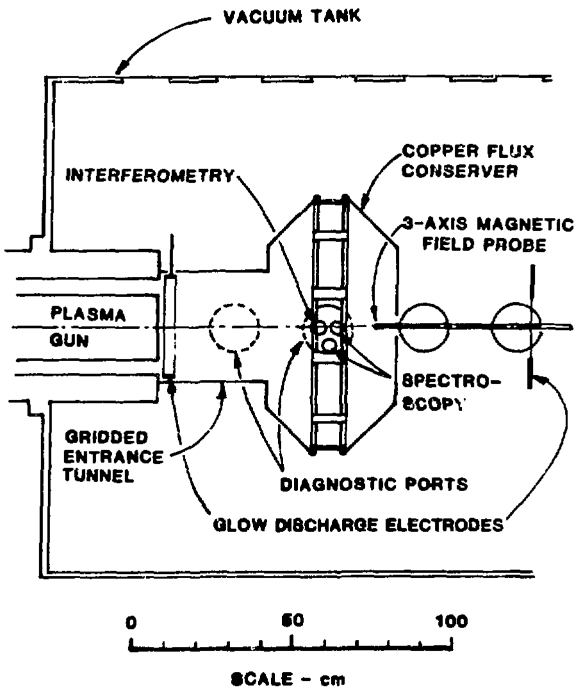

Fig. 1. Diagram of the CTX experiment.

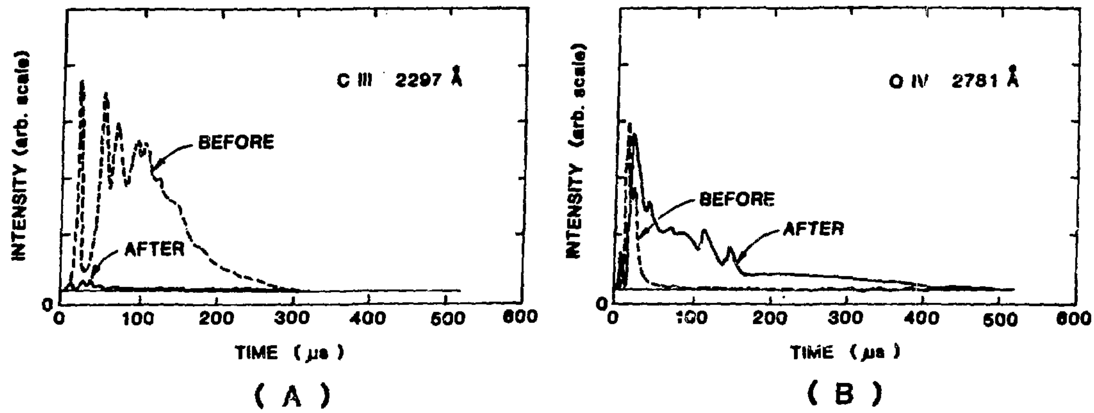

Fig. 2. Typical time resolved relative intensities of the CIII and OIV spectral lines before and after discharge cleaning.

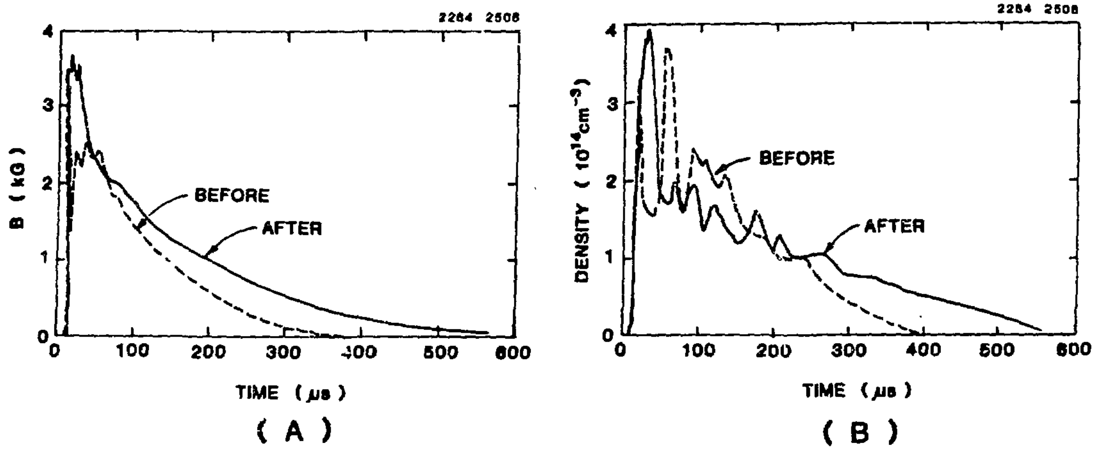

Fig. 3. Poloidal magnetic fields on the axis, 7 cm from flux conserver wall, and average densities on the flux conserver diameter before and after discharge cleaning.

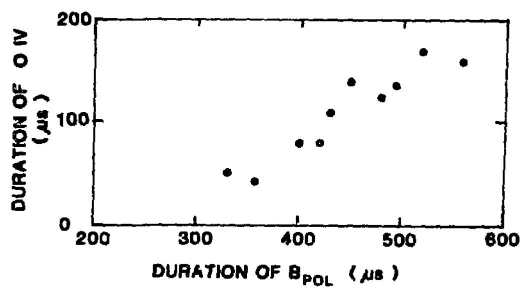

Fig. 4. Shot-to-shot correlation of the duration of the OIV radiation and poloidal magnetic field. The OIV duration is measured as the time it takes to decrease to 10% of its peak value. The magnetic field duration is the time it takes to decrease to zero.

Metallic Liner, Electrode Material and Stabilization Coil Studies in the PS-1 Experiment

H. Bruhns†, C. Chin-Fatt, Y. P. Chong, A. W. DeSilva, G. C. Goldenbaum
H. R. Griem, G. W. Hart, R. A. Hess and R. Shaw

Laboratory for Plasma and Fusion Energy Studies
University of Maryland
College Park, Maryland 20742

When the Paramagnetic Spheromak experiment was first designed[1] the reversal fields were fast rising ($\tau_{1/4} \simeq 1.5\ \mu$sec) in order to obtain a large amount of nonadiabatic compressional heating as well as to close the flux surfaces inside the plasma as rapidly as possible. In order to allow the fast rising applied field to penetrate into the plasma it was necessary to use a dielectric vacuum chamber wall. Early time electron temperatures of 50 eV and ion temperatures of 200 eV were obtained. These temperatures dropped rapidly as did the fields. In an effort to reduce metal impurities from the elkonite (W-Cu) electrodes carbon electrodes were substituted, resulting in little, if any, improvement in late time performance. The magnetic surfaces produced by these fast rising fields were very prolate, extending into the electrode region, and were also thought to be susceptible to a gross tilting instability[2] associated with the prolate shape.

In order to make the plasma more oblate, widely separated mirror coils were used[3,4] to provide axial compression as well as some slight radial compression. Without the large radial compression the temperatures dropped. In addition it was found that a combined tilting and shift occurred if the separatrix was more than approximately a centimeter inside the glass vacuum chamber wall. In order to prevent large excursions of the separatrix from the wall it was necessary to increase the reversal field quarter period to 7 μsec, thereby further reducing the nonadiabatic heating. Thomson scattering measurements show that the late time electron temperature is about 8 eV suggesting that low z impurity radiation is limiting the temperature.

In an effort to reduce low z impurities the carbon electrodes were replaced by the elkonite electrodes. With the electrode change the CIII 2297Å intensity decreased by a factor of two. No change was seen in the ion temperature as measured by Doppler broadening. (No electron temperature measurements were made for this situation.)

Further reduction, by a factor of three, was made in the CIII intensity by lining the glass walls with thin (50 μ) stainless steel. The L/R time for azimuthal currents is 5 μsec so the effective field risetime is slightly increased from its vacuum value of 7 μsec. An additional reduction of a factor of ten in the CIII intensity was made by RF discharge cleaning. This was done continuously between shots with a hydrogen base pressure of 0.1 mTorr. Because of the reduced line intensity the Doppler broadening measurements were ambiguous. Again no electron temperature measurements were possible in this case.

Although the liner was inserted primarily to reduce low z impurity levels, electrical effects were also noted. At the time the I_z discharge is initiated only the bias magnetic field is present. In order to enhance the axial compression the bias field is produced by anti-mirror coils. In the first approximation the current density follows the bias magnetic field lines from the electrodes to regions near the symmetry axis in the mid-plane. After field reversal, without the liner, a substantial amount of current still flows from the electrodes through the center of the torus. This effect is illustrated in the plot of the current density vectors shown in Fig. 1-a. In the figure we have drawn solid lines around the current paths closed in the plasma and the current passing through the electrode-endplate structure. Approximately 30% of the maximum current passes through the center of the torus. With the liner inserted we show in Fig. 1-b that only 10% of the maximum current passes through the center of the torus. The total current remains about the same suggesting that the remainder of the externally circulating current passes through the liner.

In addition to this effect the liner appears to have an effect on gross stability. For conditions which without the liner a combined tilt and radial shift are seen we find no tilt with the liner. Only a randomly oriented shift toward the walls is observed.

Jardin[5] has recently suggested the use of external passive coils to stabilize both the tilt and shift motions. These coils, called Figure 8 coils, are two sets of two orthogonal coils at each end of the spheromak. The coils are constructed so that there is no net flux in the coils from the axisymmetric fields, but when a tilt or shift occurs current is generated in the coils producing a restoring force. We have tested this concept using a modified version of the Figure 8 coils as shown in Fig. 2. Depending on the location of the wires the coil can be optimized for stabilizing a shift. Since with our present experimental arrangement only a shift is seen the effectiveness of the stabilizing coils against the shift is increased by extending the wires to the midplane. The stabilizing coils were found to be most effective with the wires placed on the inside of the vacuum chamber and liner. In Fig. 3a we plot radial profiles of the poloidal (B_z) field at successive 2.5 μsec time intervals without the stabilizing coils inserted. We see the symmetry axis (peak field) drift to the chamber wall as time progresses. In Fig. 3b we show the same plot with the stabilizing coils inserted and all other conditions the same. The most obvious difference is that the shift has stopped and the plasma current decays resistively on a timescale characteristic of a 5 eV (z=1) plasma.

Acknowledgements

This work was supported by the U.S. Department of Energy. H. Bruhns was partially supported by the Humboldt Foundation.

References

1. G. C. Goldenbaum, H. J. Irby, Y. P. Chong and G. W. Hart, Phys. Rev. Letts. 44 (1980) 393.

2. M. N. Rosenbluth and M. N. Bussac, Nucl. Fusion 19 (1979) 489.

3. Z. G. An et al, Proc. of the Eighth International Conference on Plasma Physics and Controlled Nuclear Fusion Research, Brussels (1980) IAEA-CN-38-R-3-2.

4. H. Bruhns. Y. P. Chong. G. C. Goldenbaum, G. W. Hart and R. A Hess, Proceedings of the Third Symposium on the Physics and Technology of Compact Toroids in The Magnetic Fusion Energy Program, Los Alamos (1980), LA-8700-C, 97.

5. Private communication (from H. P. Furth and M. Yamada).

†Permanent address: Institut fur Angewandte Physik, Univ. Heidelberg.

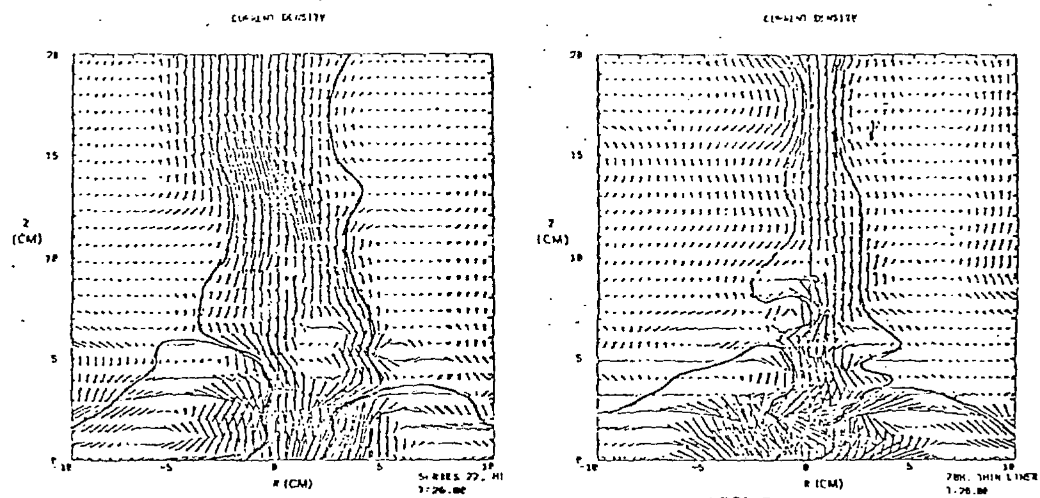

30% PENETRATES

10% PENETRATES

Fig. 1. Current density vectors derived from magnetic probe measurements.
a) left - Without liner 30% of the maximum current observed passes through the torus.
b) right - With liner only 10% of the maximum current observed passes through the torus.

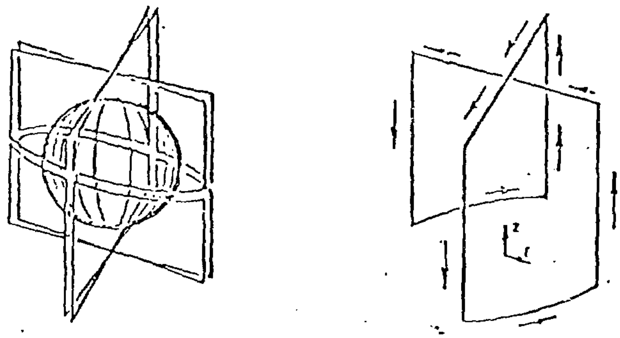

Fig. 2. On the left four stabilization coils are shown placed around a spherical shaped plasma with a vertical symmetry axis. A single coil is shown on the right.

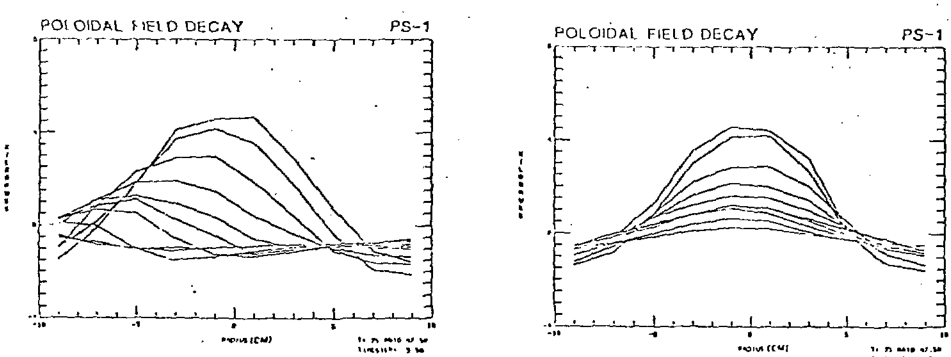

Fig. 3. Radial profiles of the poloidal magnetic field at 2.5 μsec intervals.
a) left - Profiles with the stainless steel liner but without stabilization coils.
b) right - Profiles with both liner and coils.

PROPERTIES OF SPHEROMAKS GENERATED BY A MAGNETIZED COAXIAL SOURCE

H. W. Hoida, J. Lipson, I. Henins, T. R. Jarboe, R. K. Linford,
J. Marshall, D. A. Platts, A. R. Sherwood, and M. Tuszewski
Los Alamos National Laboratory
Los Alamos, New Mexico 87545

In the CTX facility at Los Alamos spheromak-type compact toroids are generated by a magnetized coaxial source (a magnetized Marshall gun), as shown in Fig. 1. These spheromaks are trapped and studied in a metal flux conserver not shown in the figure. The plasma and magnetic field properties are measured using magnetic probes, Thomson scattering, interferometry, bolometry, and quartz UV spectroscopy. The electron density and temperature of the separated, trapped compact toroid are typically found to be $n_e \sim 2\text{-}4 \times 10^{14} cm^{-3}$ and $T_e \sim 10$ eV. Magnetic probes measuring all three orthogonal components of magnetic field along the axis of symmetry show that magnetic reconnection, leading to separation of the compact toroid from the coaxial source, is completed by about 40 μs. Typical lifetimes of the magnetic field configuration, about 250 μs, are consistent with classical resistive decay.

A major concern with these observations is the low electron temperatures. In an attempt to achieve higher temperatures, a "snipper coil" was installed at the reconnection region. Faster reconnection reduces the time for electron heat conduction along magnetic field lines connected to the coaxial source. Use of the snipper coil reduced the time required for reconnection to about 12 μs, but no increase in either electron temperature or plasma lifetime was observed.

Investigation of radiation losses was undertaken in parallel with the "snipper coil" experiments. Spectroscopic data indicated that Fe, Cr, Ni from the stainless steel electrodes, Cu from the copper flux conserver and C and O were present. The Fe, Ni, Cr and Cu levels were substantially reduced by altering the operating parameters of the coaxial sources. Increasing the delay between the puff gas filling and initiation of the discharge from 150 μs to 300 μs reduced the metallic impurity level by an order of magnitude (Fig. 2). The CIII radiation was not visibly affected. The OIV radiation was substantially increased (Fig. 3) suggesting that a hotter plasma resulted from the decrease in metallic impurities. The total radiation was not greatly affected and the short lifetime of the OIV radiation at the longer delay is indicative of the rapid cool-down of the plasma. An interpretation is that the oxygen barrier (peak at ~ 22 eV) has been reached and that oxygen and carbon are replacing the metallic impurities as the principal radiators. Attempts to reduce the oxygen and carbon impurities are being instigated in CTX, and current results are reported in a companion paper.

A single pyro-electric detector was employed to measure the spectrally integrated radiated power fom the plasma. The detector viewed the plasma across a diameter of the flux conserver just off the axial midplane. The radiation was collimated such that the viewing cone was approximately 20 cm wide at the opposite side of the flux conserver. Provision was made for the insertion of a LiF window in front of the detector. The data were reduced using the model of a uniform isotropically radiating plasma.

Figure 4 represents data taken during a sequence of nine discharges where the interval between shots was approximately three minutes. A reduction of radiation with shot number is observed. This may be attributable to a clean-up of the gun and/or flux conserver surfaces. The magnetic energy at 50 μs is calculated from on-axis probe data using a force-free equilibrium model. It is apparent that most of the energy data lie above the calculated available magnetic energy. Several interpretations are possible. If radiation is equally localized in the field of view for late and early shots, then all the data of Fig. 4 should be dropped by at least a factor of five to be consistent with the calculated magnetic field energy. This would imply that for late shots some magnetic energy is lost via other transport processes. It is also certainly possible that radiation is preferentially enhanced in the field of view for early shots (increased quantities of impurities) as might naturally occur for increased edge cooling. It is difficult to believe, however, that this effect would account for a factor of five in the data. Finally, the pyro-electric detector may be providing us with a spurious signal.

We did endeavor to eliminate other sources of energy incident on the detector by interposing a LiF window. It was found that the peak power was reduced by a factor of ten, whereas the integrated power from 50 to 150 μs was reduced only by a factor of three. A possible interpretation of this phenomenon is that the plasma, by virtue of its higher temperature at early times, initially radiates a greater fraction of its energy below the ultraviolet cutoff of LiF (~ 0.104 μm). Unfortunately it is not possible to conclude definitively that the observed signal is attributable solely to radiation. However, if the signal is primarily radiation, the peak power corresponds to approximately 10-50% oxygen (time independent coronal model).

The ambiguity with respect to spatial profiles inherent in a single detector measurement will be reduced using an array of detectors. The remaining uncertainties with respect to detector performance seem to be very difficult to resolve.

CONCLUSIONS

In gun-generated spheromaks impurity contamination plays an important role in determining the energy loss. Metallic impurities can be reduced by an appropriate change of source parameters. The reduction of the level of metal impurities results in a spectrum showing a preponderance of oxygen and carbon lines and OIV radiation is observed to increase indicating a warmer plasma. However, the plasma lifetime is not changed. Discharge cleaning techniques appear to be necessary. It is still possible that electron heat conduction during the reconnection process will be found to be important once the impurities are reduced.

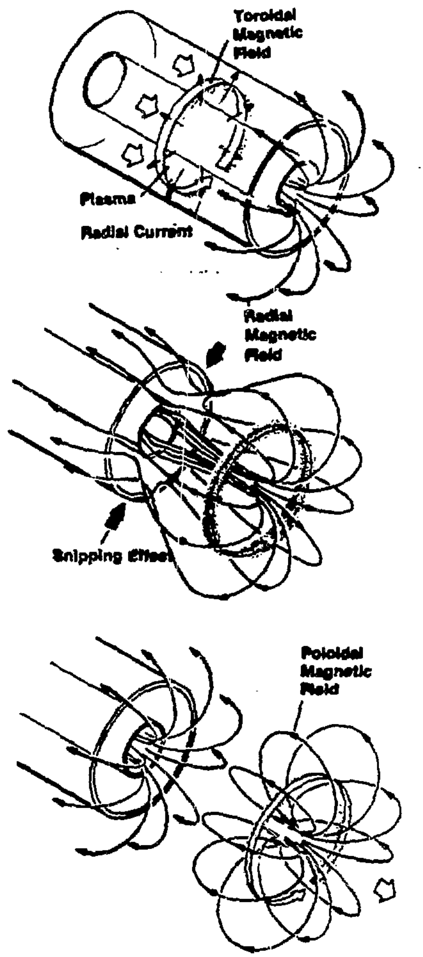

Fig. 1. Formation of coaxial source generated spheromaks.

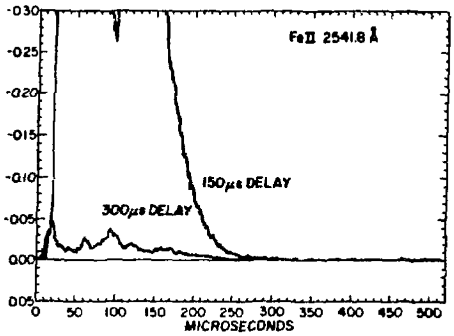

Fig. 2. FeII intensity time histories at 150 μs delay and 300 μs delay.

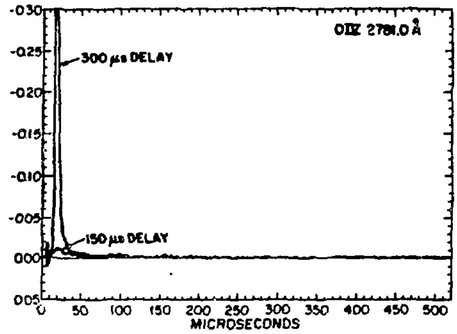

Fig. 3. OIV intensity time histories at 150 μs delay and 300 μs delay.

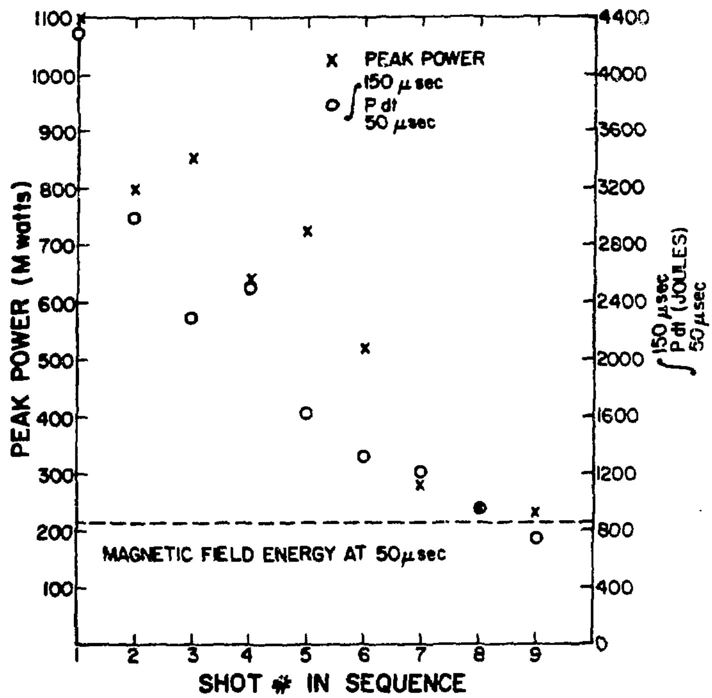

Fig. 4. Peak radiated power and power integrated from 50 μs (~ reconnection time) to 150 μs (~ termination time) as a function of shot number in sequence.

Spheromak Experiments in Proto S-1C*

A. Janos, S. Cowley, H. Hsuan, S. Paul, C. Skinner,
F. Wysocki, and M. Yamada

Princeton University, Plasma Physics Laboratory
Princeton, New Jersey 08544

I. Introduction

The Proto S-1C device (Fig. 1) was constructed to extend the earlier experimental investigation [1-3] of the S-1 spheromak formation scheme proposed by PPPL. In this device a spheromak with major radius R = 12 cm and minor radius a = 6-8 cm has been generated in a slow time scale ($\tau_{Alfven} << \tau_{form} \approx 40\mu sec$). Toroidal plasma current obtained to date is 60 kA. Measured electron temperature and density are 10-20 eV and 2-8 x 10^{14} cm^{-3}, respectively. The spheromak configuration lasts as long as 100 μsec (duration after poloidal field reversal near the reconnection point).

The Proto S-1C flux core (and therefore, spheromak plasma) shown in Fig. 2 is twice as large (R_{core} = 30 cm, a_{core} = 6 cm) as that of the Proto S-1A device, but one third as large as that of S-1 in which first plasma is expected in 1983. The specific purposes for building Proto S-1C were: 1) Study MHD behavior of a larger spheromak plasma; 2) Verify predicted scaling of plasma parameters with device size, and 3) Preliminary examination of plasma confinement properties of the spheromak by reducing impurity content and working plasma densities in order to surpass the radiation barrier.

II. Description of the Proto S-1C Device

The Proto S-1C vacuum vessel is made of 1/4" stainless steel, with a surface area of approximately 8.6 x 10^4 cm^2 and a volume of roughly 1.9 x 10^6 cm^3. The pumping system includes a 1500 ℓ/sec turbomolecular pump. A base pressure of 2 x 10^{-7} torr N_2 equivalent is attainable with the flux core inside. Two flux cores have been used. One employs a 5 mil stainless steel liner while the later one a 4 mil Inconel liner. Liners were fabricated by hydroforming half toruses and welding them together at the midplane. Neither flux core has a conducting aluminum shell as will S-1. Both have toroidal field coil cancellation loops (unlike Proto S-1A) to minimize the poloidal field component generated by the toroidal field magnet. Both cores have three symmetrically located electrical feedthroughs (120° toroidal separation, in midplane) which double as mechanical supports.

The toroidal (TF) and poloidal (PF) field coils in the flux core are both energized by capacitor banks: toroidal field bank energy is 72 kJ, PF bank energy is 24 kJ. Both systems are under-damped and are crowbarred after spheromak formation. One-quarter cycle time for the current pulses (which characterizes the formation time scale τ_{form}) is ≈ 40μ sec for the TF and PF. Toroidal field flux generated in the coil is 0.02 volt-sec while the stored PF flux is 0.1 volt-sec. The equilibrium field, provided in part by the steady-state (EF) mirror-like coils outside the vacuum vessel, has a strength of $\lesssim$ 2 kG. The equilibrium field is determined by both the EF coils and the PF coils inside the flux core, and is therefore a function of time during the formation process and depends on how the PF coil current is programmed. This has important consequences to spheromak tilting and shifting, as will be discussed below. By adjusting the crowbar time of the PF current, the equilibrium field index can be controlled.

III. Experimental Results

Spheromak configurations with < 100μsec lifetimes have been obtained, with H_2 (3-20 mtorr) and He (3-20 mtorr) gases. Plasma currents have generated toroidal and poloidal magnetic fields of 1.7 kG and 2.2 kG, respectively (Fig. 3). These were measured with arrays of magnetic field pickup loops used to map the two-dimensional evolution of the spheromak configuration (Fig. 4). The maximum plasma currents obtained to date are about 60 kA in the toroidal direction and over 100 kA in the poloidal direction. Figure 3 shows a toroidal field induction into the plasma starting between 0 and 10μsec. Poloidal field is simultaneously induced. The magnetic axis (zero crossing of the poloidal field) moves inward until the spheromak plasma reaches equilibrium around 40μsec. This position is maintained until the current decays and the equilibrium moves inward. The toroidal field between 40 and 80μsec is that expected for poloidal currents encircling the magnetic axis.

Plasma temperature and density have been measured with double Langmuir probes, calibrated by CO_2 interferometry, and found to be $T_e \lesssim 20$ eV and 5×10^{14} cm^{-3}, respectively, in the fully formed spheromak configuration. This translates into a beta value $\beta_o = P_o/(B_o^2/2\mu_o)$ of 10%.

Plasma MHD stability to tilting and shifting modes has been measured. Proto S-1C spheromak plasmas were observed to tilt, when the index of the equilibrium field was negative or slightly positive, but not reproducibly as in Proto S-1A. This difference in behavior is probably due to Proto S-1A's smaller size. Perturbing fields are therefore relatively larger and the plasma may be "kicked" unstable in the same sense during each discharge.

The general good stability in present discharges, evidenced by $\tau_{discharge} \lesssim \tau_{resistive}$, may be due to: 1) line-tying around the core such that the spheromak plasma is not completely "pinched-off" from the flux core. Experimental data supports this phenomenon. 2) Image currents induced in the core liner and/or toroidal field coil after crowbar may aid stability. 3) Possible plasma rotation may act as a gyroscopic stabilizing mechanism. There is preliminary evidence for such a toroidal rotation.

Visible spectroscopic measurements have been made to estimate the electron temperature, and to access the impurity content and utility of various vacuum system conditioning techniques. Measurements were primarily made in He discharges. Emission from the following lines was observed: OII-OIII, CII-CIV. Nitrogen, Iron, Nickel, and Titanium radiation (from earlier gettering) was also observed. Emission from OIV or CV could not be identified. Electron temperatures were deduced from spectroscopic line intensity ratios by comparison with a time-dependent coronal model (Fig. 5). This type of model is necessary since the plasma duration and particle confinement time is insufficient for the plasma to reach a steady-state. The coronal model is a reasonable approximation--especially for the higher ionization stages. The model utilized a step function temperature and computed the ionization balance as a function of elapsed time. Measured intensities were corrected for energy of the transition levels, the transition probability, and statistical weight in order to estimate the relative population in each ionization stage. A temperature range from 7 eV - 15 eV was consistent with the data, with corresponding confinement times ranging from 50 μsec to 2 μsec. This temperature was confirmed by a double Langmuir [3] probe.

Oxygen and carbon impurity concentrations were estimated by intentional introduction of known quantities of the same. Results indicated concentrations of between 2 and 10% without discharge cleaning or gettering. More precise estimates were not possible as it is difficult to correct the data for the effect of changes in temperature due to the addition of impurities. Other observations include: 1) Relative oxygen concentration is reduced by a factor of 2 to 4 by Ti-gettering the vacuum vessel prior to discharges. 2) Removing magnetic probes inserted into the plasma decreased the carbon content by a factor of 2 to 4. 3) The oxygen and carbon impurity levels relative to the electron density did not markedly change at different fill pressures. Also, CIII and CIV intensities were observed to increase at lower Helium fill pressures when a preionization electrode was employed.

The successful formation of spheromak plasmas in the Proto S-1A and the larger Proto S-1C device can be used to infer parameter scaling with size. Plasma (device) size has certain implications for the temperature and density operating regimes, based on β_o^* limits for MHD stability and streaming parameter limits for microinstablities, once a plasma current is chosen. For a plasma (device) of twice the linear dimensions, the lower density limit for a given beta limit is halved. Temperature depends on the plasma current (the ohmic power available) and the impurity concentrations. A larger device is compatible with slower formation time scales and lower density (see above). If the ratio of impurity to electron density stays roughly constant, then the impurity line radiation power decreases as n_e^2, allowing higher temperatures.

Thus, by reducing the filling pressure of working gas and by controlling further impurity influx, we expect the electron temperature of the spheromak to surpass the radiation barrier and reach 100 eV. In this operation regime a more detailed investigation of the MHD stability relevant to a fusion device and of the confinement features of the spheromak configuration will be carried out.

Figure Captions

Fig. 1. Proto S-1C Vacuum Vessel.

Fig. 2. Proto S-1C Flux Core.

Fig. 3. Toroidal and Poloidal magnetic fields as a function of time in the midplane.

Fig. 4. Time evolution of poloidal flux $\Psi = 2\pi \int_o^R R\, B_z dr$ and Toroidal flux $g = 2\pi R B_T$.

Fig. 5. Time-dependent coronal model fitted to experimental results a) example of T_e and n_e input to code; b,c) oxygen, carbon ionization balance as a function of time; d,e) power radiated by oxygen, carbon as a function of temperature; f) power balance as a function of temperature.

[1] Formation of the Spheromak Plasma by a Slow Induction Scheme, M. Yamada, H.P. Furth, W. Heidbrink, A. Janos, S. Jardin, M. Okabayashi, E. Salberta, J. Sinnis, and F. Wysocki, in Proceedings of the Third Symposium on the Physics and Technology of Compact Toroids in the Magnetic Fusion Energy Program, Los Alamos Scientific Laboratory, Los Alamos, New Mexico, December 1980, pp. 124-129, LA-8700-C.
[2] Quasistatic Formation of the Spheromak Plasma Configuration, M. Yamada, H.P. Furth, W. Hsu, A. Janos, S. Jardin, M. Okabayashi, J. Sinnis, T.H. Stix, K. Yamazaki, Phys. Rev. Lett. 46 (3) 1981, p. 188.
[3] Investigation of the Quasi-static Spheromak Formation in the Proto S-1 Experiments, M. Yamada and A. Janos, in Proceedings of U.S.-Japan Workshop on Compact Toroid, Welding Research Institute, Osaka University, Japan, (1981) US-J FRC-003.

Fig. 1

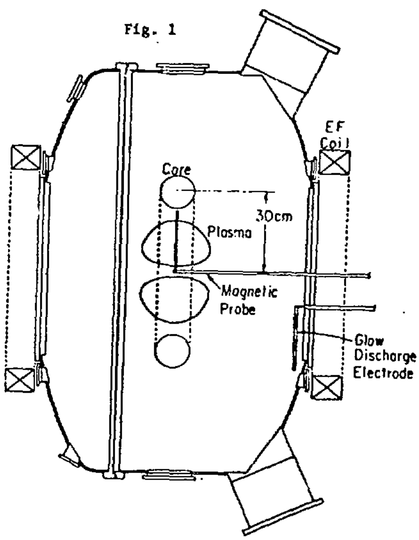

Fig. 2

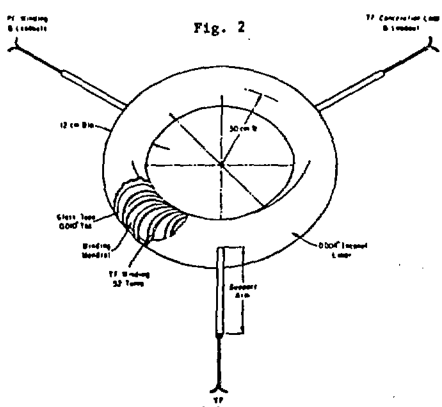

Fig. 3

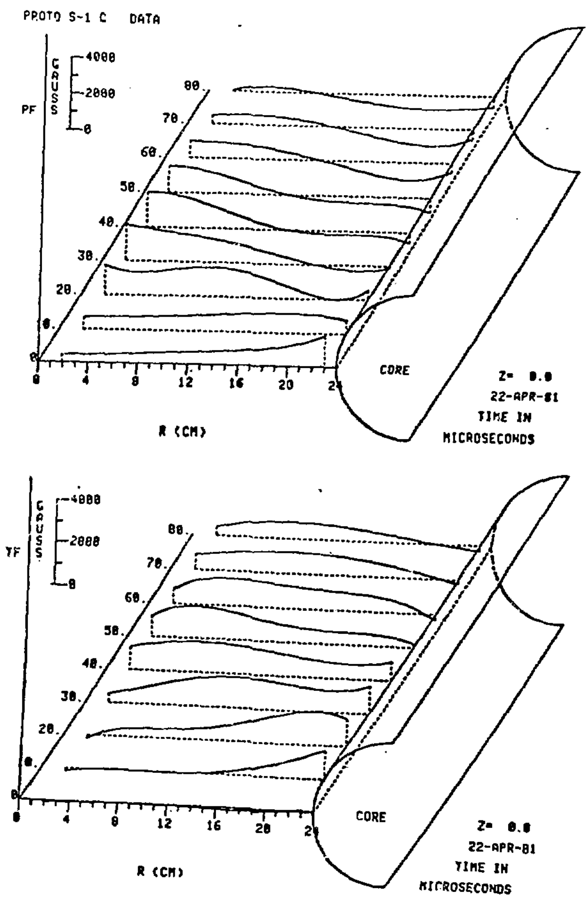

Fig. 4

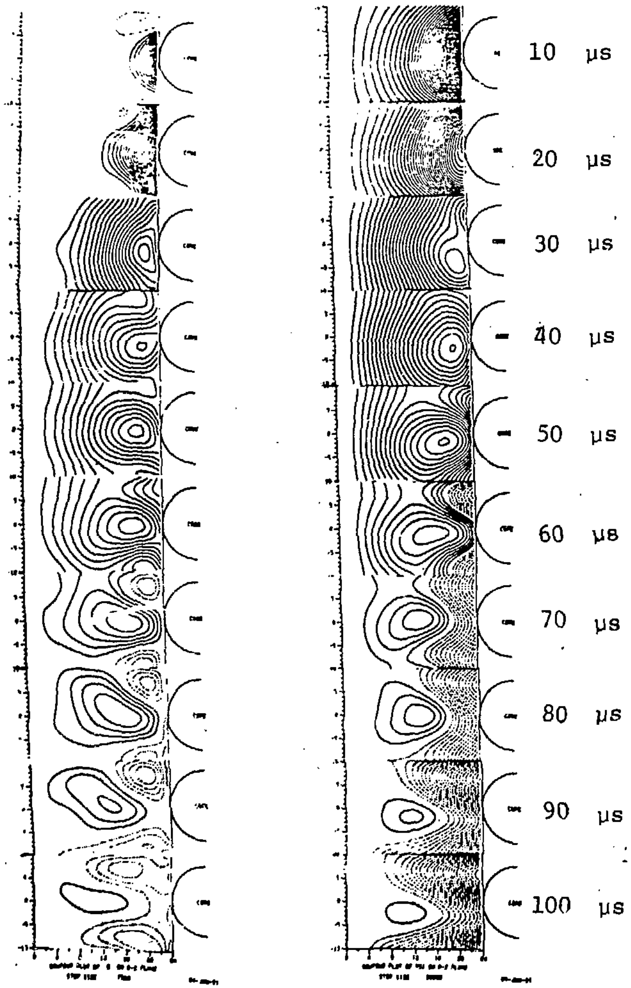
10 µs
20 µs
30 µs
40 µs
50 µs
60 µs
70 µs
80 µs
90 µs
100 µs

Fig. 5

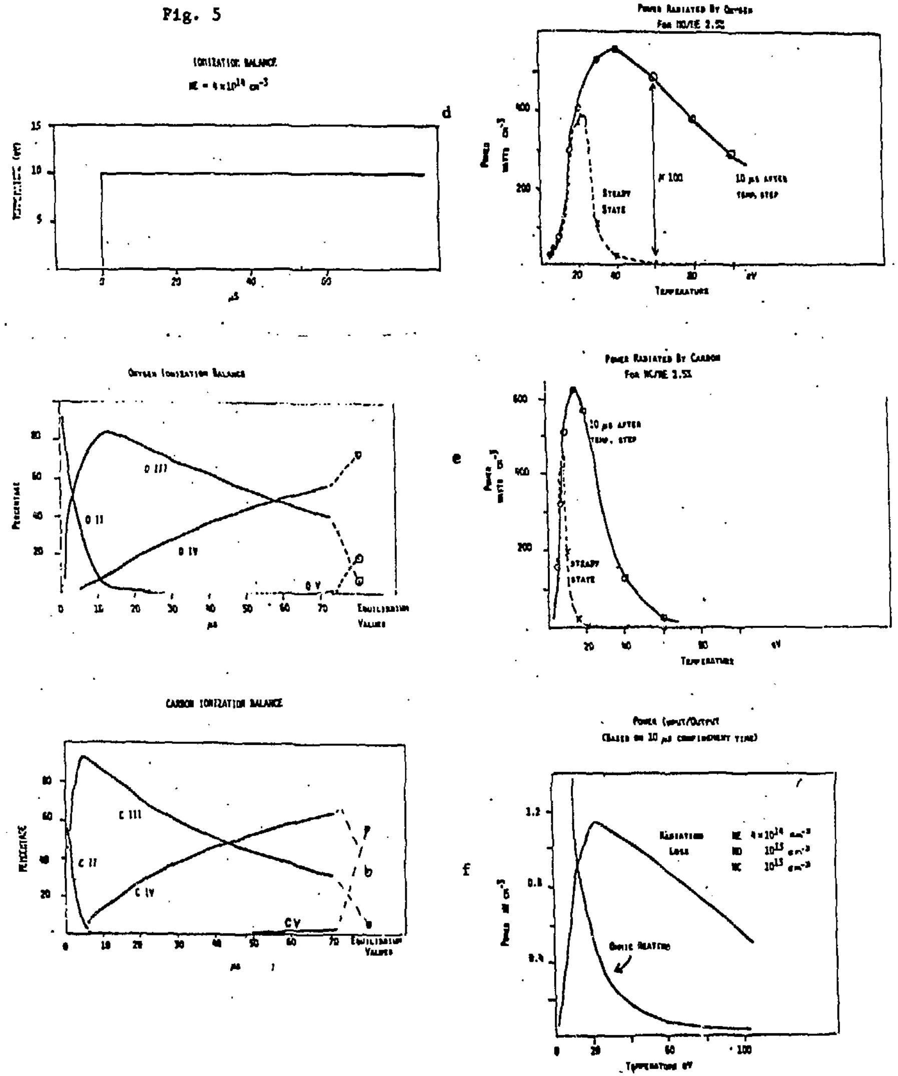
a
b
c
d
e
f
IONIZATION BALANCE
OXYGEN IONIZATION BALANCE
O II
O III
O IV
O V
CARBON IONIZATION BALANCE
C II
C III
C IV
C V
PERCENTAGE
µs
EQUILIBRIUM VALUES
POWER RADIATED BY OXYGEN
POWER RADIATED BY CARBON
STEADY STATE
10 µs AFTER TEMP. STEP
TEMPERATURE
POWER INPUT/OUTPUT
OHMIC HEATING
TEMPERATURE eV

CREATION OF A SPHEROMAK BY A CONICAL θ-PINCH

K. Kawai and Z.A. Pietrzyk
Aerospace & Energetics Reseach Program
University of Washington
Seattle, Washington 98195

A conical θ-pinch has been used to create a "spheromak" configuration in a plasma. The reversed field is obtained by trapping magnetic field produced during the first 1/2 cycle of an oscillating discharge. The plasmoids created are ejected from the coil liner due to an axial magnetic force and translate into a glass tube surrounded by an aluminum flux conserver (see Fig. 1). It has been observed, as previously reported,[1] that this configuration has an imbedded toroidal component of magnetic field. Figure 2 shows the $B_z(r)$ component of magnetic field measured in various positions along the axis outside of the discharge coil. Figure 3 shows the toroidal component of the field. It appears likely that this field configuration is close to a minimum energy state as proposed by Taylor.[2] The plasmoids are stable against tilting for 15-20 μs in about 80% of the cases. The mechanism which creates the toroidal field is not very clear. The Hall effect, proposed previously,[3] should not be very strong in the present configuration. It is possible that an end shorting effect[4] is responsible for initial creation of the toroidal field. Its final value is most likely obtained by "Taylor relaxation" to the minimum energy state. The mechanism of creation of the toroidal field and subsequent relaxation is currently under study. The conical discharge is 7% efficient as measured by the change in terminal input energy with and without plasma. An absence of CV emission lines from the plasma suggests that the temperature is below 60 eV, implying rapid loss of energy from the plasma, either by radiation (impurities) or heat transfer. Both energy losses would give approximately the observed decay time, if the plasma has an initial temperature of 50 eV, and heat transfer is perpendicular to measured β.

This work was supported by the U.S. Department of Energy Magnetic Fusion Divison.

References

1) D.R. Wells, Phys. Fluids 9, 1010 (1966).

2) J.B. Taylor, Phys. Rev. Lett. 33, 1139 (1974).

3) W.H. Bostick and D.R. Wells, Phys. Fluids 6, 1325 (1963).

4) J.P. Freidberg and L.D. Pearlstein, Phys. Fluids 21, 1207 (1978).

COMPACT TOROID FORMATION BY A CONICAL THETA PINCH COIL

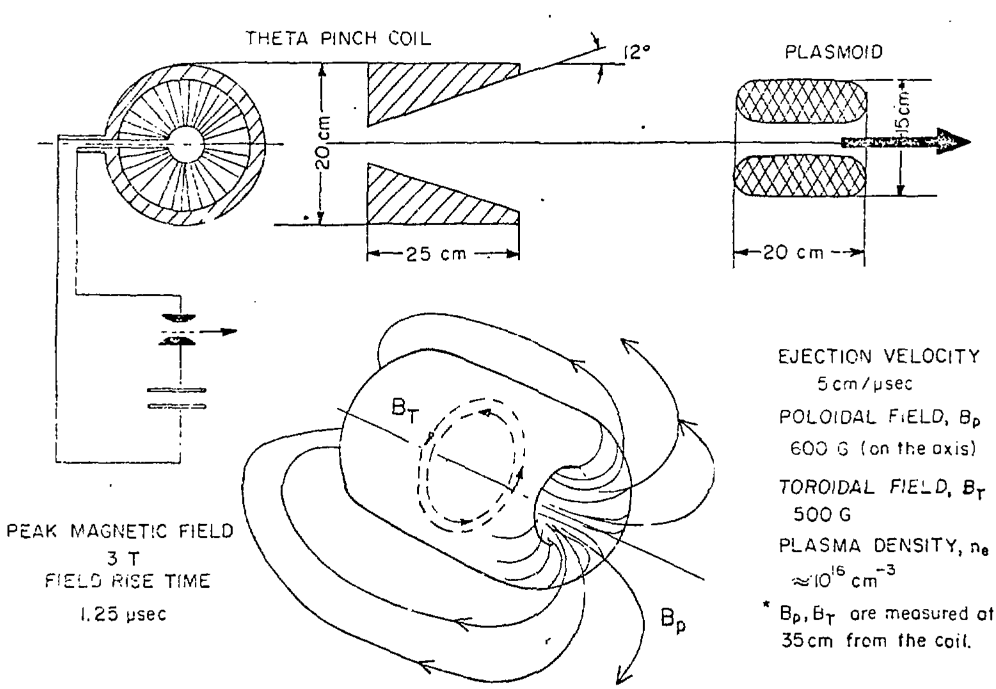

Figure 1.

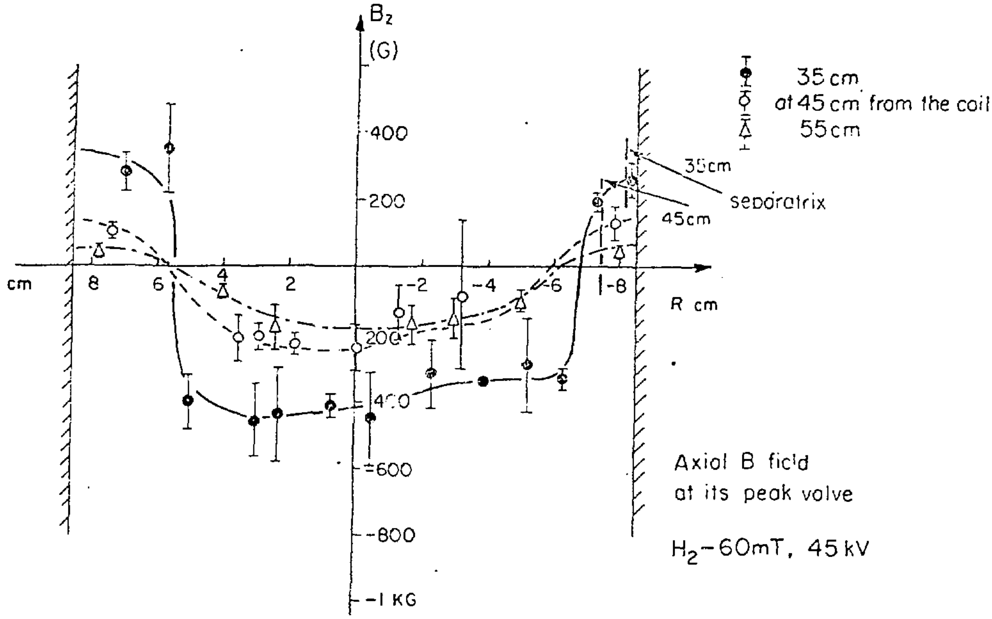

Figure 2.

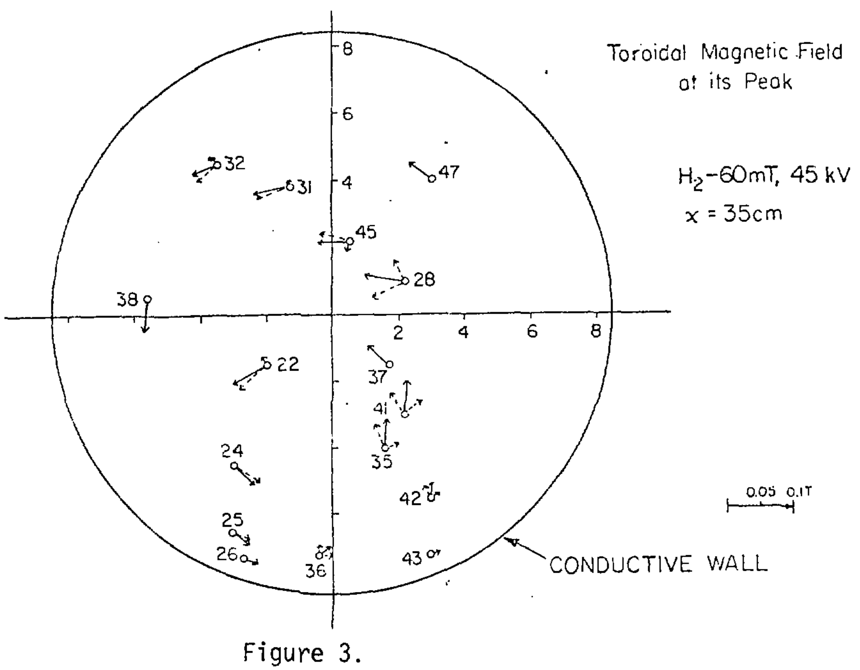

Figure 3.

RF HEATING PLANS FOR CTX

S. O. Knox and B. L. Wright
Los Alamos National Laboratory
Los Alamos, New Mexico 87545

Even with present efforts to reduce impurity levels in the CTX experiment, electron thermal conduction and residual impurity radiation may still cause substantial cooling of the plasma toroid by the time it has formed inside the flux conserver. Auxiliary heating of the stable structure is needed. If an energy of several hundred joules is to be supplied over a hundred-microsecond time scale, several megawatts of power are required. Such levels can be achieved from pulsed rf sources at frequencies in the ion-cyclotron range and below (0.1-10 MHz). Encouraged by the successes reported from other experiments in this regime[1], we are undertaking the development of an rf heating system for CTX.

There are several features that distinguish the heating problem in a compact torus from the conventional tokamak setting. The magnetic field near the wall is essentially poloidal rather than toroidal, the field changes direction rapidly over a comparatively short scale length ($B_{pol} \sim B_{tor}$), and the small aspect ratio implies that field curvature cannot be neglected. These three features bear on the largely theoretical issue of mode structure but do not detract from the possibility of successful rf heating *via* plasma resonances. The fact that the magnetic field in a compact torus is determined entirely by plasma currents may give rise to rf penetration characteristics that change considerably during a shot and exhibit significant shot-to-shot variations. Thus we must look for heating methods that do not depend on precise resonant conditions. Finally, it should be noted that, at present plasma temperatures, the absorption of rf power will be collision-dominated. However, as temperatures are raised, a collisionless absorption mechanism will be required.

To maintain azimuthal and midplane symmetry while coupling to the poloidal field at the wall, we are considering the use of an antenna strap that encircles the toroidal equator. The general arrangement for our present "roof-top" flux conserver is sketched in Fig. 1. Antenna insulation and electrostatic shielding will be utilized.

If we take, for example, a peak poloidal field on the symmetry axis of 5.0 kG (toroidal field of 3.3 kG at the magnetic axis) and a uniform density of 2.5×10^{14} cm^{-3} we have at the magnetic axis:

$$\Omega_{ci}/2\pi = 2.6 \text{ MHz.}$$
$$\text{Alfven speed} = 3.3 \times 10^{7} \text{ cm/s.}$$

With a major radius of around 20 cm, one can therefore expect the appearance of toroidal shear Alfven modes beginning at roughly 260 kHz. The other polarization of interest in this regime is the fast magnetosonic mode. To estimate the lowest resonant frequency for this wave we note that its phase velocity is largely isotropic. One can therefore view the flux conserver as a cavity resonator with a uniform dielectric constant of $(c/V_A)^2_{ave}$. For a single azimuthal strap antenna (cf. Fig. 1), the lowest coupled resonance is the TE_{011} mode. The rf magnetic field of this mode is topologically identical to the dc poloidal field of a compact torus. In a cylinder with radius and length both 40 cm, the above estimate of V_A gives 650 kHz for the lowest fast magnetosonic resonance.

To reinforce these estimates we plot in Fig. 2 the radial wavenumber, k_r, that one would expect at the midplane if the dispersion relation of an infinite uniform plasma applied locally. The wave vector normal to the direction of propagation is assumed to be constant with a half-wavelength equal to the length of the flux conserver (40 cm), and to be parallel to the magnetic field at the wall. A Bessel-function model is used for the field profile. At 300 kHz the figure shows accessibility to a shear Alfven resonance whereas the fast magnetosonic wave is cut off near the wall because of the rising magnetic field. At 700 kHz the Alfven resonance is broader and the fast wave propagates with a wavenumber near 0.08 cm^{-1} which is appropriate for the first radial eigenmode.

Because both the magnitude and the direction of the dc magnetic field change over the scale of a wavelength, one expects some coupling between the uniform-field modes discussed above. A proper theory must incorporate finite geometry from the beginning. We are aware of current theoretical efforts by C. Kieras and J. Tataronis[2] on MHD resonances in spheromak geometries and by T. Cayton and R. Lewis[3] on ion kinetic effects in a screw-pinch column. For our own part, we are developing a slab model to compute coefficients of *transmission, reflection and conversion between shear Alfven and fast* magnetosonic waves when the direction of the dc magnetic field varies significantly over a short distance.

For present CTX plasma parameters ($n_e \sim 2 \times 10^{14}$ cm−3, $T_e \sim T_i \sim 10$ eV), collisional processes can be expected to dominate the absorption of rf energy. Employing the fundamental fast (compressional) magnetosonic wave, the amplitude of the rf field within the plasma can be greatly increased at resonance, and heating due to viscosity is very effective. There is, however, a limit on the effectiveness of such absorption as the plasma temperature increases. A transition to a different absorption mechanism that does not degrade with temperature can be made by selecting the parallel wave number of the fast wave such that a mode conversion[4] to the "kinetic Alfven" wave[5] occurs. Here, coupling between the fast wave mode and the continuous wave modes would lead to energy deposition at the Alfven critical layer where $\omega = k_{\parallel}V_A$ is satisfied. This mode conversion process has received theoretical attention,[6,7] as have various linear and nonlinear absorption mechanisms[8] associated with the converted wave. Depending upon the strength of the absorption mechanism, energy may be deposited in a narrow region at the critical layer (strong absorption), or high-Q cavity eigenmodes can occur (weak absorption) which result in desirable high antenna loading resistances and energy deposition primarily at the plasma core.

Ion cyclotron heating experiments at other laboratories indicate that antenna coupling does not depend strongly on rf power. It is thus possible to study plasma response with low-power experiments. To this end, we will use a 100 W source for exploratory work from 0.01 to 100 MHz. By examining both antenna loading and the signals on magnetic pickup probes, we expect to determine empirically the most favorable modes for heating CTX.

At the low frequencies of immediate interest, it is possible to use ringing capacitor discharges to generate very high rf power levels for tens of microseconds. Selecting a capacitor (C = 0.1 μF, 75 kV) with a Q of 50 at 700 kHz, taking L_{ant} = 0.4 μH, and employing the pulsed power techniques illustrated in Fig. 3, one can expect a V-I product at the antenna of $\sim 1 \times 10^9$ with an "unloaded" 1/e time of 40 μs. We will use this basic circuit in our initial investigations.

In anticipation of the utility of ion-cyclotron heating and a more sustained rf pulse, we are conducting a parallel development of an rf circuit based on high-power triodes. As the schematic diagram in Fig. 4 illustrates, we are considering a push-pull Colpitts oscillator in which the antenna serves as the tank circuit inductance. This device will operate at a few MW in the 1 to 10 MHz range that is inaccessible to the ringing capacitor approach.

REFERENCES

1. D. Hwang, et al., Bull. Am. Phys. Soc. 26, 1045 (1981).

2. C. Kieras and J. Tataronis, Univ. of Wisconsin Report TSL-81-6 (1981).

3. T. E. Cayton and H. R. Lewis, Phys. Fluids 23, 109 (1980).

4. T. H. Stix, Third Symposium on Plasma Heating in Toroidal Devices, Varenna, Italy (1976), p. 156.

5. L. Chen and A. Hasegawa, Phys. Fluids 17, 1399 (1974).

6. C. F. F. Karney, F. W. Perkins, and Y.-C. Sun, Phys. Rev. Lett. 42, 1621 (1979).

7. T. H. Stix, Second International Grenoble-Varenna Symposium on Heating in Toroidal Devices, Como, Italy (1980).

8. A. Hasegawa and L. Chen, Phys. Fluids 19, 1924 (1976).

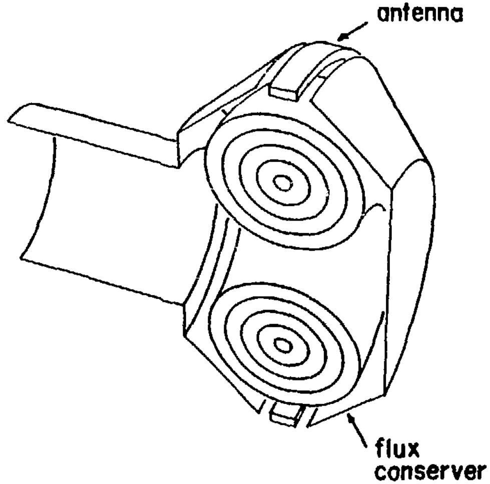

Fig. 1. Cutaway view of flux conserver showing antenna location.

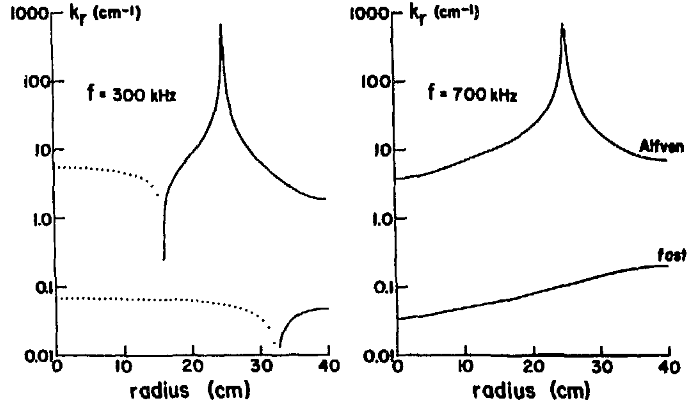

Fig. 2. Radial wavenumber vs. radius at 300 and 700 kHz (solid = real, dashed = imaginary).

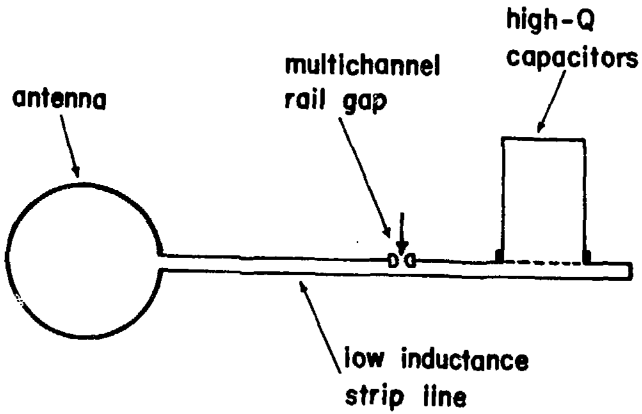

Fig. 3. Schematic of ringing capacitor technique.

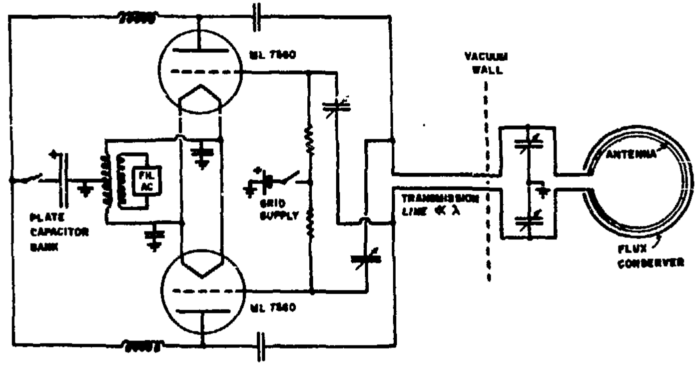

Fig. 4. Schematic of high-power oscillator.

MHD STABILITY STUDIES IN THE PROTO S-1 A/B DEVICE

C. Munson, A. Janos, M. Newhouse, E. Salberta,
F. Wysocki, and M. Yamada

Plasma Physics Laboratory, Princeton University
Princeton, New Jersey 08544

ABSTRACT

An experimental study of the gross MHD stability properties of Spheromak plasmas in the Proto S-1 A/B device is presented. Utilizing the previously demonstrated "S-1 slow formation" technique, plasmas have been produced which exhibit the predicted tilting instability in a regime of slightly negative field index $[n_i \equiv -(r/B_v) \cdot (\partial B_v/\partial r)]$. A relatively simple passive coil system suggested by numerical stability studies has proven to be effective in stabilizing the observed tilting mode.

Introduction

The "S-1 slow formation" technique first proposed in 1979[1] and demonstrated at PPPL in 1980[2,3] with the Proto S-1 A/B device has been used to study the gross MHD stability properties of the Spheromak plasma configuration. The viability of the Spheromak concept as a possible fusion reactor design depends on the ability to control the gross MHD instabilities which are theoretically predicted[4,5,6] and experimentally observed.[7,8,9] The most basic of these instabilities being the tilting, shifting, and vertical modes. The behavior of these modes is predicted to depend upon the magnetic field index, $n_i \equiv -(r/B_v) \cdot (\partial B_v/\partial r)$, as shown in Table I.

TABLE I

Index	n < 0	0 < n < 1	1 < n
Tilt	Unstable	Slightly Unstable	Stable
Shift	Stable	Slightly Unstable	Unstable
Vertical	Unstable	Stable	Stable

Since early theoretical work[4] indicated the presence of gross instabilities in the Spheromak and the stabilizing effect of a close fitting conducting shell, computer studies of numerically generated equilibrium solutions have been performed.[6] These studies give the parametric dependence of plasma instabilities on the plasma shape and the position of the conducting shell. The current patterns calculated to act in stabilizing the tilting and shifting modes led to the suggestion of a relatively simple coil configuration for this purpose,[10] the "Fig. 8" coil. Jardin and Christensen indicate that a set of four passive conducting coils, each with the Fig. 8 topology, will stabilize a Spheromak to the rigid body toroidal mode number n = 1 tilting and shifting modes.

Apparatus

The Proto S-1 A/B device[2,3] consists of a cylindrical stainless steel vacuum vessel (24 inch diameter, 30 inch length, and 3/8 inch wall thickness), with eight pancake coils just outside each end plate providing the required equilibrium magnetic field (~1.2 Gauss/Amp, $n_i \simeq 0.05$). Either of two interchangeable flux cores may be mounted at the midplane. Both of these flux cores (see Fig. 1) contain a 3 turn poloidal field coil and a 40 turn toroidal field coil with associated current feed in legs, have a major radius $R_c = 15$ cm, minor radius $r_c = 3$ cm, and are covered by a 3 mil stainless steel liner. The currents to the core are provided by capacitor banks. Vacuum base pressures of $\sim 6 \times 10^{-7}$ Torr have been obtained using oil diffusion pumps.

Magnetic field information is provided by a probe array composed of five sets of orthogonal coils (B_r, B_θ, B_z) spaced 2 cm apart radially. This probe may be rotated toroidally and translated axially, providing access to the entire Spheromak region. Signals from the probe are intergrated and digitized at a rate of 1 MHz. This information is then stored for later use. Plasma reproducability is generally very good ($\lesssim$ 5% deviation), therefore multi-shot scans along z may be performed at a number of toroidal angles to give a detailed global time evolution of the magnetic field configuration.

Experimental Results

By adjusting the currents in the flux core and the value of the equilibrium magnetic field, it is possible to produce a spheromak plasma in Proto S-1 A/B which is stable to both the tilting and shifting modes for the lifetime of the plasma (~20 μsec). The apparent stability is present even though this configuration is in the range $0 < n_i < 1$ which should be slightly ($\gamma << 1/\tau_{alf}$) unstable to both modes. Possible explanations of this anomalous stability are "line-tying" to the flux core, i.e., some fraction of the poloidal current continues to flow around the core, and eddy currents flowing in the liner and crow-barred toroidal field winding.

If core current parameters are adjusted to allow the index to become slightly negative, a tilting instability occurs. The tilting is very reproducable, apparently due to the magnetic perturbation of the current leads to the core, and proceeds on an axis defined by these leads. By producing contour plots of the toroidal field in the plasma, it is possible to measure the growth rate, γ, of the tilting mode. Measured values of $2.2\ \mu\text{sec} \lesssim \gamma^{-1} \lesssim 3.6\ \mu\text{sec}$ have been obtained for various plasma conditions.

Simple Fig. 8 coils were constructed from 3/16 inch copper rod and mounted with the inner edge 6 cm from the midplane of the core as shown in Fig. 2. Figure 3 shows on the right the time behaviour of the toroidal field of a particular tilting mode ($\gamma^{-1} \simeq 3.6$ μsec). On the left is the same mode after the addition of the Fig. 8 coils. It is apparent that the coils have had a stabilizing effect on the tilting. Although at later times there is still an instability present, similar field information in the plane 90° from that shown indicates a higher order mode which the Fig. 8 coils should not affect.

Conclusion

The gross MHD behavior of Spheromak plasmas in the Proto S-1 A/B device has been studied, and the tilting instability as well as stable behavior has been demonstrated. Passive stabilization coils of a Fig. 8 configuration have proven to have a stabilizing effect on the tilting mode.

REFERENCES

1. H. P. Furth, in Proceedings of the U.S.-Japan Joint Symposium on Compact Toruses and Energetic Particle Injection, 1979, Princeton Plasma Laboratory, p. 1.
   M. Okabayashi et al., ibid p. 166.
   M. Yamada et al., ibid p. 171.
2. M. Yamada, H. P. Furth, W. Hsu, A. Janos, S. Jardin, M. Okabayashi, J. Sinnis, T. H. Stix and K. Yamazaki, Phys. Rev. Lett. 46 (1981) 188.
3. M. Yamada et al. in Third Symposium on Physics and Technology of Compact Toroids in the Magnetic Fusion Energy Program, Los Alamos Scientific Lab, p. 124.
4. M. N. Rosenbluth and M. N. Bussac, Nuclear Fusion 19 (1979) 489.
5. M. Okabayashi and A. M. M. Todd, Nuclear Fusion 20 (1980) 571.
6. S. C. Jardin, M. S. Chance, R. L. Dewar, R. C. Grimm, D. A. Monticello, Nuclear Fusion 21 (1981) 1203.
7. T. R. Jarboe, I. Henins, H. W. Hoida, J. Marshall, A. R. Sherwood, in Proceedings of the U.S.-Japan Joint Symposium on Compact Toruses and Energetic Particle Injection, 1979, Princeton Plasma Physics Laboratory p. 53.
8. H. Bruhns, C. Chin-Fatt, Y. P. Chong, G. C. Goldenbaum, H. R. Griem, G. Hart, R. Hess and A. Desilva, presented at 23rd APS/DPP Meeting in New York, NY, October 12-16, 1981.
9. F. Wysocki, E. Salberta, A. Janos, and M. Yamada, presented at 23rd APS/DPP Meeting in New York, NY, October 12-16, 1981.
10. S. C. Jardin and U. Christensen, Stabilizing Windings for the Tilting and Shifting Modes in an Inductively Formed Spheromak, PPPL-1814, August, 1981.

#81X0076

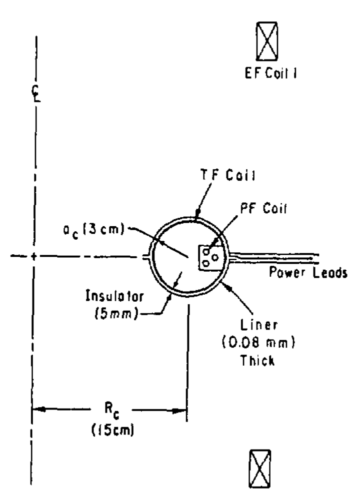

Fig. 1
Flux Core

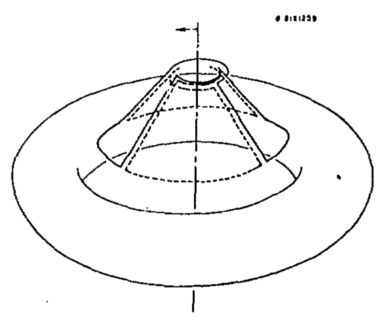

INSTALLATION OF THE "FICURE 8" UMBRELLA COILS

Fig. 3

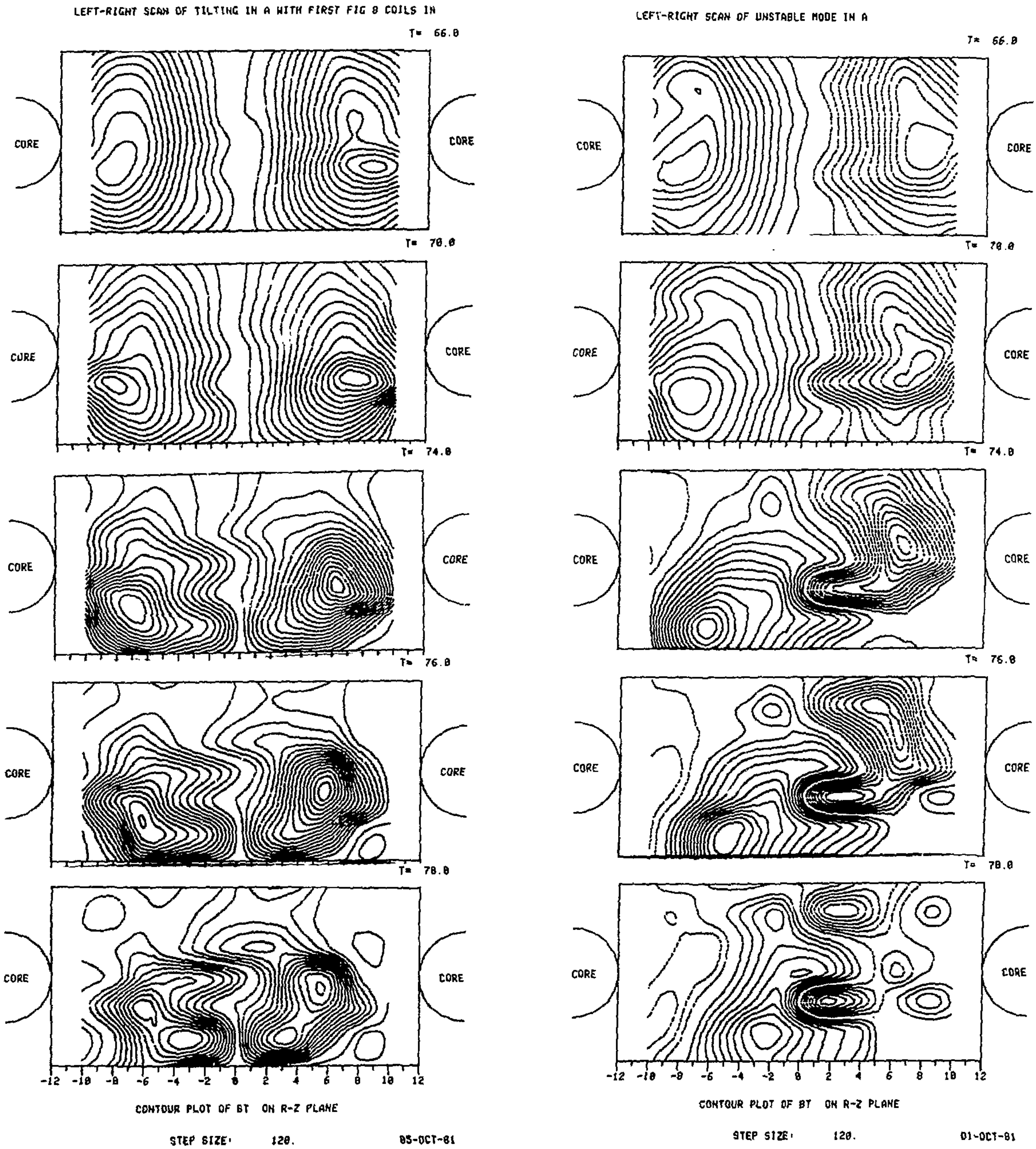

Fig. 3

Work supported by U.S. DOE contract no. DE-AC02-76-CHO-3073

A New Approach to Controlling Impurity Contamination of a Plasma-gun-produced Compact Torus*

R. F. Post and W. C. Turner
Lawrence Livermore National Laboratory
University of California, P.O. Box 5511
Livermore, CA 94550

I. Introduction

The presence of impurity ions, notably carbon and oxygen, has been determined to be a major factor limiting the lifetime of field-reversed plasma entities produced by coaxial plasma guns such as the Beta II gun at LLNL.[1] Similar problems are encountered in other toroidal plasmas, e.g. those in tokamaks. However, the solution employed there, discharge cleaning, followed by initiation of the plasma at low density (where impurity radiation losses are exceeded by ohmic heating rates) is not applicable here. This note discusses a proposed means for drastically reducing the level of impurities. (These are believed to be evolved from the gun electrode surfaces as a result of thermal shock associated with UV emission from the gun plasma) The idea: Take advantage of the UV pulse preferentially to release hydrogen from the electrode surfaces. These surfaces are to be coated with a few-micron-thick layer of titanium, outgassed by preheating and subsequently loaded with hydrogen.

Upon initiation of the gun discharge, by puffing in pure hydrogen gas in an annular region midway between the muzzle and the insulator at the rear of the gun, the following sequence of events is predicted to occur:

1. The intense UV flash from the discharge will be absorbed on the gun electrode surfaces adjacent to the region of the discharge.

2. The rapid rise in surface temperature caused by the UV flash will desorb a dense layer of hydrogen gas from the electrode surfaces, augmenting the initial gas pulse, and providing a continuing source of hydrogen for the discharge as it is magnetically propelled toward the muzzle.

Experiments with the existing Beta II gun, and with similar guns at Los Alamos[2] have shown that an additional source of contaminants - metal sputtered from the electrodes - appears only when the discharge is run in a "gas-starved" condition. The method proposed here, where the discharge current always terminates on a dense surface layer of hydrogen (thereby limiting sheath drops), should insure that sputtered metal impurities will remain at the negligible concentration levels characteristic of present gun operation in other than gas-starved conditions. In addition to employing metal hydride electrode surfaces it would be desirable to use ultra-high vacuum techniques to reduce the background pressure of impurity contaminants to the 10^{-10} to 10^{-9} Torr range, so that the time for formation of impurity monolayers is long compared to the interval between plasma shots.

* Work performed under the auspices of the U.S. Department of Energy by the Lawrence Livermore National Laboratory under contract number W-7405-ENG-48.

II. Theoretical estimates of critical parameters

The critical parameters for the proposed system are as follows:

- o Heat pulse at gun electrode surfaces (principally from UV emitted by discharge).
- o Transient temperature rise of electrode surfaces caused by heat pulse.
- o Limits on concentration levels of hydrogen or deuterium in thin titanium coatings.
- o Rates of internal transport and surface desorption of hydrogen/deuterium for pulse-heated titanium.

Some theoretical estimates of these above parameters will be given below.

A. Surface heat inputs in a "clean" gun

In the Beta II gun approximately 10 torr-liters of hydrogen gas are ionized in approximately 5 microseconds. The accompanying UV pulse emitted can be estimated by taking the difference between the energy required per ion-electron pair ($\sim$32 eV) and the energy required to ionize hydrogen atoms:

- o UV $\approx (32 - \chi_i) \approx$ 20 eV/atom.
- o 10 torr-liters = 6×10^{20} atoms $H_0(D_0)$
- o UV energy $\approx (6 \times 10^{20}) \times (20) \times 1.6 \times 10^{-19} \approx$ 2000 Joules
- o <UV power > $\approx$ 400 MW ($\sim$4 percent of gun input power)
- o At estimated 10^3 cm^2 illuminated area, $Q_{UV} \approx 0.4$ MW/cm^2

Compared to the UV heat pulse, other surface heat inputs (ion bombardment of the cathode, electron collection, etc.) are estimated to be small (of order 10% of <UV power > or less).

B. Transient temperature rise of surface

From classical theory: For a surface receiving a heat flux F beginning at t = 0, the surface temperature rise in time t is

$$\Delta T(0,t) = \frac{2Ft^{1/2}}{(\pi \rho K C_p)^{1/2}} \qquad (1)$$

where ρ, K and C_p are the density, heat conductivity and heat capacity of the material, respectively. Table I gives the above parameters and the surface temperature rise (in 1 microsecond) for various metals, normalized to a rate F = 1 MWatt/cm^2.

The thermal "skin depth" to which the heat pulse penetrates (ΔT = 1/e times the surface ΔT) in time t is given by the expression

$$\delta_T = 2 \left[\frac{Kt}{\rho C_p}\right]^{1/2} . \qquad (2)$$

For solid Ti, from Table I, by interpolation to 0.4 MW/cm^2 one finds $\Delta T \approx 660^0$ C. However the thermal skin depth in Ti in 10^{-6} sec. is approximately 6 microns. Thus for Ti coatings a few microns thick ΔT will be influenced even at early times by the substrate on which the coating is formed. With a copper substrate for example, ΔT would tend to be reduced, relative to that for solid Ti, as is evident from Table I.

C. Concentration levels of hydrogen in titanium

As is well known, titanium is capable of adsorbing large amounts of hydrogen. Starting from a hydrogen-free state, heating to 200-400^0 C (to accelerate diffusion rates) and exposing the titanium surface to hydrogen at adequate pressure will cause titanium to load to high levels (up to a limit of nearly TiH_2, if desired). Values of the solubility levels (at 1 atm) vs temperature are listed in Table II.[3]

Following cooldown (in the presence of a hydrogen atmosphere) titanium retains hydrogen with negligible evolution in vacuo at room temperature (desorption rates are discussed in a later section).

D. Rates of internal transport and surface desorption of hydrogen/deuterium for pulse-heated titanium

The thermally-induced release of hydrogen/deuterium from a loaded titanium layer is determined by two rate processes, both highly temperature dependent: Thermally-activated surface desorption involves the surface recombination of hydrogen/deuterium atoms that have migrated to the surface; the rate at which desorbed atoms are replaced from below depends on the rate of this migration across a concentration gradient.

The rates of surface desorption may be estimated, by detailed balancing arguments, using existing data for the equilibrium density of hydrogen above a heated titanium surface.[4] In equilibrium (incident and emergent fluxes balancing) we have

$$S = \left(\frac{1}{4} n\bar{v} \right) (\sigma) \; (2) \; , \tag{3}$$

where S is the emergent flux (of H/D atoms) and σ is the sticking coefficient. For D:Ti concentrations of order 1:1, $\sigma \approx 10^{-2}$ to 10^{-3}.[5] In practical units this equation becomes:

$$S = 3.5 \times 10^{22} \left[\frac{\sigma \, P(\text{torr})}{(T^0 \, K)^{1/2}} \right] \text{atoms cm}^{-2} \text{ sec}^{-1} \tag{4}$$

Also from the literature we have for the equilibrium pressure[6]

$$P = 2 \times 10^{12} \exp \left[\frac{-1.97 \times 10^4}{T^0 \, K} \right] \text{Torr} \tag{5}$$

for D:Ti ≈ 1.0.

Our objective is to achieve a number of desorbed atoms

$$Q = S A \tau = 1 - 10 \text{ Torr-liters } (7 - 70 \times 10^{19} \text{ atoms H/D}). \qquad (6)$$

With $A = 10^3$ cm^2 and $\tau \approx 5$ µsec., this implies $S \approx 10^{22}$ to 10^{23} atoms H/D cm^{-2} sec^{-1}. Inserting this value in Eq. (4), and using Eq. (5) to solve for T yields 600^0 C $\lesssim T \lesssim 850^0$ C, depending on the value of σ assumed. This is in the range of transient surface temperature rise due to UV emission that was estimated in B above. At the same time, owing to the exponential dependence of P, the pre-pulse value of S is down by 6 orders of magnitude at $T = 300^0$ C, for example, and becomes negligibly small at room temperature. As a consequence, it would be possible to pre-heat the titanium surface (thus inhibiting its contamination by impurities) for a reasonable period of time prior to the actual gun pulse, without thereby leading to an excessive loss of hydrogen from the loaded surface. This should allow some control over the amount of H/D actually desorbed.

It remains to show that hydrogen/deuterium can diffuse to the surface rapidly enough to maintain the surface density. Again, because of the exponential dependence of these rates on temperature, and because of the steepness of the concentration gradients that result from pulse heating and from surface desorption, transport rates appear to be more than adequate. We have, for the diffusion process:

$$D = D_0 \exp[-U_0/kT], \qquad (7)$$

i.e. thermally-activated diffusion. Although modified by phase change considerations, rough values for D_0 and U_0 for Ti at elevated temperatures are[3]: $D_0 \approx 2 \times 10^{-2}$ cm^2 sec^{-1} and $U_0 \approx 0.50$ eV. This gives a value of $D \approx 3 \times 10^{-5}$ cm^2 sec^{-1} at 600^0 C. The diffusion flux to the surface is given by

$$q = D\left(\frac{\Delta C}{\Delta x}\right) \quad cm^{-2}\ sec^{-1} \qquad (8)$$

where $[\Delta C/\Delta x]$ is the concentration gradient.

The concentration gradient will be determined by:

a) The degree of loading of the titanium; at a relative loading $c = 1$, $C \approx 6 \times 10^{22}$ atoms H/D cm^{-3}.

b) The depth and degree of depletion near the surface.

Here, the number of atoms to be desorbed from area $A = 10^3$ cm^2 is between 1 and 10 torr liters ≈ 7 to 70×10^{19} in 5 µsec, i.e. 1.4 to 14×10^{19} per microsecond, implying at $c = 1$ a depletion layer thickness of order 0.23 to 2.3×10^{-6} cm. With these values the available diffusion flux would be of order $q \approx 3 \times 10^{-5} \times [6 \times 10^{22}/(0.23 \text{ to } 2.3 \times 10^{-6})] \approx .8$ to 8×10^{24} cm^{-2} sec^{-1}, i.e. the limiting values of qA would lie in the range of .8 to 8×10^{21} atoms in 1 µsec. These numbers being large compared to the number to be desorbed, the rates of diffusion of atoms to the surface should be adequate, at the elevated temperatures attained, to sustain the surface desorption rates.

Parenthetically it should be noted that any impurity atoms within the metal lattice will diffuse at rates that are orders of magnitude slower than those for hydrogen, thus will contribute negligibly to the density.

Finally, returning to the question of ΔT, it can be seen from the discussion that by adjustment of the Ti layer thickness, its degree of loading, and its substrate material it should be possible to arrive at a self-consistent set of design parameters that will satisfy the quantitative requirements of the technique we have proposed.

Table I

ΔT at 10^{-6} sec; $F = 10^6$ W/cm^2

Metal	K	ρ	C_p	ΔT °C
Cu	3.6	9.0	0.4	310
Pd	0.75	12.2	0.23	780
Nb	0.53	8.4	0.25	1070
Ti	0.22	4.5	0.47	1650
Zr	0.23	6.4	0.28	1760
(304SS	0.16	8.0	0.46	1470)

K, J cm^{-1} sec^{-1} °C^{-1}; ρ gm cm^{-3}; C_p, J gm^{-1} °C^{-1}.

Table II

T°C	S cm^3/gm (STP)	c	C atoms/cm^3
0	410	1.8	9.9 X 10^{22}
200	400	1.7	9.6
400	380	1.6	9.2
600	320	1.4	7.7
800	140	0.6	3.4

References

1. W. C. Turner, G. C. Goldenbaum, E. H. A. Granneman, D. S. Prono, C. W. Hartman, J. Taska, "Beta II Compact Torus Experiment, Plasma Equilibrium and Power Balance," this Proceedings.
2. H. Hoida, I. Henins, T. Jarboe, J. Lipson, J. Marshall, D. Platts, A. Sherwood, "Impurity Observations in Coaxial-Source Generated Spheromaks," this Proceedings.
3. J. Völkl and G. Alefeld in Diffusion in Solids, A. S. Nomick and J. J. Burton, editors, Academic Press, NY (1975).
4. M. E. Malinowski, J. of Nucl. Materials, 85, 86, 957 (1979).
4. M. E. Malinowski (private communication).
5. Metal Hydrides, W. M. Mueller, J. P. Bleckedge, and E. C. Libowitz, ed. Academic Press, NY (1968).

BETA II COMPACT TORUS EXPERIMENT PLASMA EQUILIBRIUM AND POWER BALANCE*

W. C. Turner, G. C. Goldenbaum,† E. H. A. Granneman,††
D. S. Prono, C. W. Hartman, J. Taska
Lawrence Livermore National Laboratory, University of California
Livermore, CA 94550

In this paper we follow up some of our earlier work that showed the compact torus (CT) plasma equilibrium produced by a magnetized coaxial plasma gun is nearly force free and that impurity radiation plays a dominant role in determining the decay time of plasma currents in present generation experiments.(1,2)

Figure 1 shows a schematic of the magnetized coaxial gun injecting into a metallic flux conserver (1 mm thick copper). Not shown in Fig. 1 are modifications to the vacuum system that allowed glow discharge cleaning of the gun electrode and flux conserver surfaces. A stainless steel ring anode with major (minor) diameter 25 (2.5) cm could be inserted in the annular gap between the flux conserver and gun and removed during plasma shots. Glow discharges were run at 40 microns of argon or deuterium with 2.67 Torr-liters/s gas throughput. The discharge current and voltage were typically 1 A and 300 V (argon) 400 V (deuterium). After discharge cleaning for several hours the system was pumped down to 10^{-6} Torr base vacuum and further reduced to 10^{-7} Torr with LN cyropanels and Ti gettering on vacuum chamber walls away from the gun and flux conserver.

Since the plasma equilibrium is nearly force-free only a single parameter is needed to describe it. In Fig. 2 we have chosen this parameter to be the CT poloidal flux ψ_{pol} measured by magnetic probes. ψ_{pol} is plotted vs the square root of the product of plasma gun inner electrode flux (= ψ_{gun}) and the volt-seconds input to the gun discharge (= $\int_0^\infty V\,dt$). The magnetic helicity input to the plasma gun during formation is related to this product by

$$K_{in} = 2\,\psi_{gun} \int_0^\infty V\,dt \quad .$$

Two straight lines are drawn in Fig. 2 for constant ratios of $K_p/K_{in} = 0.5$, 1.0 where K_p is the plasma helicity. Two sets of data are presented in Fig. 2

*Work performed by LLNL for USDOE under contract W-7405-ENG-48.
†On leave from University of Maryland, College Park, Maryland.
††Present address: FOM Institute, Amsterdam, The Netherlands.

according to whether ψ_{gun} or $\int V\,dt$ is variable while the other parameter is held fixed. As long as $\int V\,dt$ is not too low or ψ_{gun} too high, the data (Fig. 2) fall close to the line $K_p/K_{in} = 0.5$ independently of which input variable is fixed. The overall electrical efficiency is reduced from 0.5 by another factor equal to how far the initial plasma state is driven from the Taylor minimum energy state[3] before relaxation takes place. Experimentally, the electrical efficiency equals about 0.15 away from the cutoffs at too low $\int_0^\infty V\,dt$ or too high ψ_{gun}.

Plasma impurity radiation has been measured with a calibrated, magnetically shielded pyroelectric detector that is collimated to view a chord through the midplane of the flux conserver. The total power radiated is inferred from this measurement by assuming that the plasma radiates isotropically and uniformly. The total energy radiated is obtained by integrating the radiated power forward in time from an instant when a compact toroidal plasma has been formed (usually about 40 μs after firing the plasma gun). In Fig. 3 we compare the radiated energy (W_{rad}) to the plasma magnetic energy (W_B) for four conditions; (1) with magnetic probe arrays inserted in the plasma, (2) with probe arrays retracted from the plasma, Ti gettering and cold LN liners, (3) same as (2) but after 14 hours glow discharge cleaning with argon, and (4) same as (3) but after 96 hours of glow discharge cleaning with argon and 8 hours with deuterium. It is apparent from Fig. 3 that a large fraction, always greater than 50% and statistically consistent with 100%, of the magnetic energy is being radiated. VUV spectroscopy has identified the major impurity contaminants to be carbon and oxygen. In Fig. 4 we have plotted the magnetic field lifetime τ_B, defined as the 1/e decay time of plasma magnetic fields, as function of W_B for the same data as in Fig. 3. A clear trend of increasing lifetime emerges from Fig. 4. With probes inserted $\langle\tau_B\rangle$ = 95 μs, with probes retracted $\langle\tau_B\rangle$ = 115 μs and after discharge cleaning $\langle\tau_B\rangle$ = 140 μs. After about 14 hours of discharge cleaning with argon the improvement in τ_B saturated and further improvement was not noted by switching briefly to deuterium. Improvement of lifetime with discharge cleaning is encouraging. However, the saturation of improvement in lifetime and the large amounts of energy radiated even for the longest lifetime shots point to the necessity of developing more effective techniques of reducing impurity contamination.

In order to gain some understanding of the source of plasma generated by the gun discharge we studied the scaling of CT density with variation of experimental parameters. Data for three of these scaling studies is shown in Fig. 5 where chord averaged electron density is plotted as a function of (a) plenum gas fill in Torr-liters of D_2, (b) gas valve pre-trigger time before discharging the gun capacitor bank, and (c) the electrical energy input to the gun terminals during the gun discharge. If all of the CT plasma density was derived from deuterium gas filling the plenum chambers then a linear dependence of $\langle n_e \rangle$ vs Torr-liters of D_2 that extrapolates to zero density at zero gas fill would be expected. In fact what we see is a rather weak linear dependence superimposed on a constant density $\langle n_e \rangle \approx 2 \rightarrow 3 \times 10^{14}$ cm^{-3} that is independent of the plenum gas fill. For comparison purposes a line is drawn on Fig. 5(a) labeled "100% gas utilization." This is the density that would be obtained if all the gas originally in the plenum chambers wound up as ionized plasma filling the flux conserver with volume average density equal to the chord average.

The lowest gas fill in Fig. 5(a) was 1.25 Torr-liters D_2 ($= 8.8 \times 10^{19}$ D atoms). Below this gas fill the gas does not reliably break down when the capacitor bank is triggered. The data in Fig. 5(a) was taken with the gas valve fired at a fixed 300 μs interval before discharging the capacitor bank. From direct measurements, the gas valve seat opens 50 μs after it is triggered. We have not measured the gas distribution in the gun barrel but rough estimates indicate the valve has completely emptied by the time the bank is fired and gas extends a distance roughly $\pm$ 40 cm from the valve.

In Fig. 5(b) the chord averaged electron density is plotted as the gas valve trigger time is varied from 400 to 150 μs preceding discharging the capacitor bank. Again the plasma density is relatively insensitive to this parameter variation. For gas valve pre-trigger times less than 150 μs the gas in the gun does not break down when the bank is fired.

Finally, in Fig. 5(c) the chord averaged electron density is plotted as a function of electrical energy input to the gun discharge. The gas fill was fixed at 7.25 Torr-liters D_2 and the gas valve pre-trigger time was 300 μs. From Fig. 5(c) we see that $\langle n_e \rangle$ depends approximately linearly on the discharge energy.

The picture that emerges from Fig. 5 is that the D_2 gas puffed in through the gas valve plenum is important for initiating the discharge between gun electrodes but that a substantial fraction of the CT plasma density is derived from material that is desorbed from the gun electrode surfaces during the discharge. It seems likely that the carbon and oxygen impurities observed in the plasma result from desorption of hydrocarbons and oxides on the gun electrode surfaces.

We have written a 0-D rate equation code to model the plasma response to impurity contamination[5]. The results of the code calculations are that if the carbon or oxygen impurity fraction exceeds a critical level ($\sim$ few per cent for carbon), the plasma does not burn through the low Te radiation barrier and the plasma parameters are clamped at values near $Z_{eff} \simeq 2.5$, Te $\simeq$ 10 eV and $\tau_B \simeq 150\ \mu s$. This calculation, which used classical Spitzer resistivity, roughly fits the observed experimental lifetime and values of Te deduced by the absence of radiation from He-like ionization states.

The improvement of plasma lifetime with discharge cleaning is encouraging, but more needs to be done. Some attention has recently been given to the possible benefits of improving the vacuum conditions and using metal hydride liners for the gun electrode surfaces[6].

REFERENCES

1. W. C. Turner, G. C. Goldenbaum, E. H. A. Granneman, C. W. Hartman, D. S. Prono, J. Taska, A. C. Smith, Jr., Proc. 3rd Symposium on Physics and Technology of Compact Toroids, Los Alamos, New Mexico, LA-8700-C, pg. 113. Dec. 2-4, 1980.
2. E. H. A. Granneman, G. C. Goldenbaum, J. H. Hammer, C. W. Hartman, D. S. Prono, J. Taska, W. C. Turner, Proc. of 10th European Conf. on Cont. Fusion and Plasma Physics, Moscow, USSR. Sept. 14-19, 1981.
3. J. B. Taylor, Phys. Rev. Lett., 33, 1139 (1974).
4. W. C. Turner, H. E. Dalhed, G. C. Goldenbaum, E. H. A. Granneman, J. H. Hammer, C. W. Hartman, D. S. Prono, J. Taska, "Investigation of the Magnetic Structure and the Decay of a Plasma Gun Generated Compact Torus," report in preparation.
5. G. C. Goldenbaum, E. H. A. Granneman, C. W. Hartman, D. S. Prono, J. Taska, W. C. Turner, "Experimental Observations and Model Calculations of Impurity Radiation in a Plasma Gun Compact Torus Experiment", report in preparation.
6. R. F. Post and W. C. Turner, "A New Approach to Controlling Impurity Contamination of a Plasma-Gun-Produced Compact Torus," this proceedings.

EXPERIMENTAL CONFIGURATION

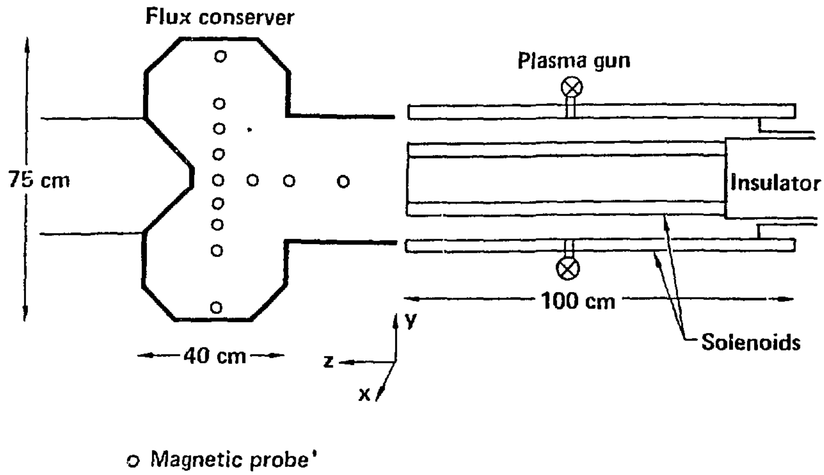

Figure 1.

POLOIDAL FLUX SCALING

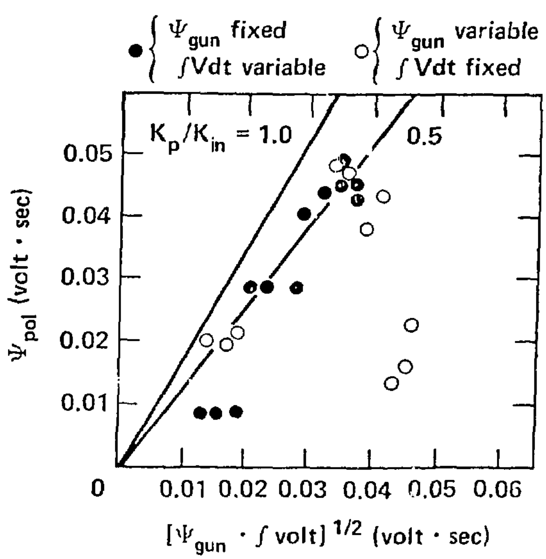

Figure 2.

MAGNETIC ENERGY VERSUS RADIATED ENERGY

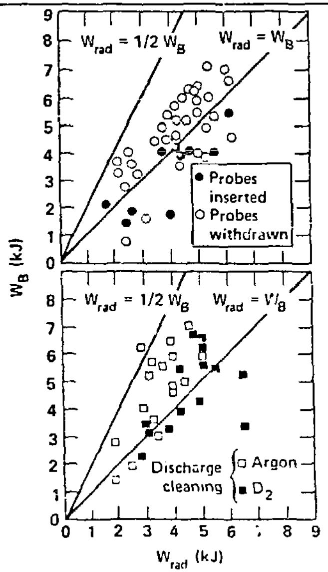

Figure 3.

MAGNETIC FIELD LIFETIME VERSUS MAGNETIC ENERGY

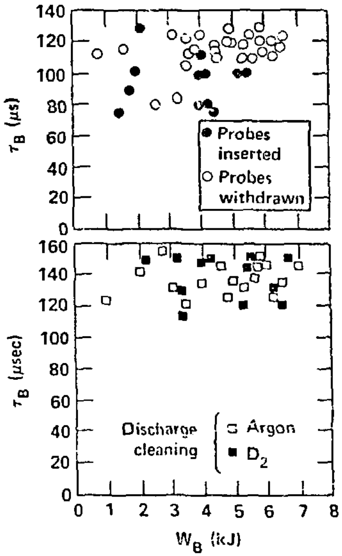

Figure 4.

VARIATION OF PLASMA DENSITY WITH EXPERIMENTAL PARAMETERS

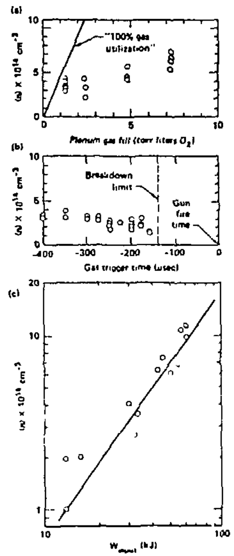

Figure 5.

Experiments on CT Plasma Merging in the CTCC-1

K. Watanabe, K. Ikegami, M. Nishikawa
A. Ozaki, N. Satomi and T. Uyama

Course of Electromagnetic Energy Engineering
Faculty of Engineering, Osaka University
2-1, Yamada-Oka, Suita, Osaka 565, Japan

Abstract

A compact toroid (CT) plasma merging experiment has been tried preliminarily in the CTCC-1 experiment as a method for further-heating of CT, on producing two CT plasmas in the flux conserver successively. Two CT plasmas were observed really to merge with each other in the flux conserver. In the merging process, it is found that the field reconnection of surface magnetic field lines of CT is completed until 30μs after the second CT injection, but magnetic field lines around the center of CT merge slowly, taking about 100μs. Experimental results indicate that merging of CT results in doubled addition of toroidal fluxes and no-addition of poloidal fluxes.

1. Introduction

The gun-produced plasma toroid is introduced into a flux conserver and stably confined in it without any MHD instability. Electron temperature has been observed to be about 60eV in the gun-production phase, nevertheless it decreased rapidly to less than 10eV during the bouncing and embedding phase of plasma in the flux conserver.[1] These experimental results suggested that further heating is necessary to get a long-lived CT plasma trapped in the flux conserver.

In our laboratory, a CT plasma merging experiment has been tried preliminarily in the CTCC-1 experiment for the further-heating of CT. In the experiment, two CT plasmas were produced successively. The first CT plasma was produced as a target-CT in the flux conserver and then the second toroid was injected into the identical flux conserver occupied by the first one. A CT plasma merging experiment is expected hopeful for obtaining a high temperature CT plasma, since secondary-injected CT plasma is probably trapped by the target CT plasma before the former should hit at the opposite wall of the flux conserver. In this report, we present a preliminary study of two CT plasmas merging, in which we found that the merging proceeds rather slowly and gently, compared with the single CT plasma formation. However, we have not yet obtained any experimental result that shows effective plasma heating due to the CT merging. We will make experiments in a high vacuum under 1×10^{-8} Torr, with cryo-material surfaces near furture.

2. Experimental Apparatus

The CTCC-1 is able to produce two CT plasmas successively at an interval using a single gun energized with two capacitor banks each of $C=34\mu F$ charged to 40kV, which are triggered independently with each other (see Fig.1). This successive production of CT plasma make it possible to study a merging process experiment of two CTs in the flux conserver.

The CT plasma is injected into the oblate flux conserver of 1.5mm thick, 0.75m diameter, 0.4m height, drum-type copper vessel having an entrance region of 0.3m diameter and 0.32m length stainless steel cylinder. Others are given elsewhere in more details.[2,3]

3. Experimental Results

In CT plasma merging experiment, two CT plasmas were injected into the flux conserver successively in the manner described above. We can freely select the timing, τ_m, of the second plasma injection after formation of the first target CT plasma in the flux conserver. Results presented here have been obtained in the operation of $\tau_m=80\mu s$.

To study the merging process we have measured magnetic fields at various position by magnetic probes. There is a little shot-to-shot variation of magnetic field signals measured at each position. Figures 2 and 3 show signals measured shot by shot at egiht posotions along the Z-axis of R=19.5cm near the magnetic axis(R=25cm). Fig.2 shows the time development of toroidal field, B_t, at each posistion and Fig.3a and Fig.3b show the axial and radial component of poloidal field, B_p, respectively. Here, Z denotes the distance from the gun muzzle and T is the time after the initiation of first CT production. As shown in Fig.2, B_t increases rapidly just after the second plasma toroid enter the confinement region. This rapid increase of B_t at each position indicates the addition of toroidal magnetic flux of the second injected plasma. After the rapid increase, these signals decrease with rather larger decrement than that of signals in the case of a single confined CT. On the other hand, B_p decreases to zero or negative rapidly in the range up to Z=62cm as shown in Fig.3.

We are reasonably to consider this rapid decrease as being due to appearance of neutral X-point between two CT facing with each other. Such a neutral point appears to travel in the axial direction away from the entrance and to return back to stop around Z=42cm. Signals observed at both Z=42cm and Z=47cm recover gradually during about 100μs. This fact indicates that the magnetic field reconnection takes place slowly without any violent turbulence. According to these and additional probe data, we make patterns of poloidal magnetic field at various times, although they can not be drawn completely from the limited probe data as shown in Fig.4. The field pattern appears to proceed as each CT opens the previously closed poloidal field lines of it and field lines of the oppositely facing CTs reconnect each other at the position of around Z=42cm, becoming a single CT configuration in about 100μs after the injection of second CT plasma.

4. Conclusion

The experiment has been carried out to confirm whether the CT plasma merging is really obtained or not. Experimental results show rather smooth progressing of the merging process.

The magnetic field lines contained in the surface region of each CT complete the field reconnection in the early stage until 30μs after the second injection, becoming one closed field configuration. On the other hand, the magnetic field lines in the center region of each CT make the field reconnection slowly, taking about 100μs.

It is then concluded that two CT plasmas are really merged in rather slow progressing and result in a CT toroid with doubled toroidal and not-doubled poloidal magnetic fluxes. The transfer from toroidal flux to poloidal flux proceed too slow to get the fundamental mode equilibrium state within plasma life time.

References

1) A. R. Sherwood et al., Proc. US-Japan Workshop on Compact Toroid, Osaka Japan, (1981) pp47-55.
2) K. Watanabe et al., ibid. pp66-75.
3) K. Watanabe et al., J. Phys. Soc. Japan, 50(1981) 1823.

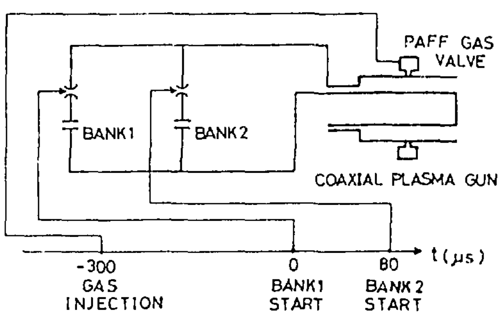

Fig. 1 Gun discharge circuit for the CT plasma merging experiment.

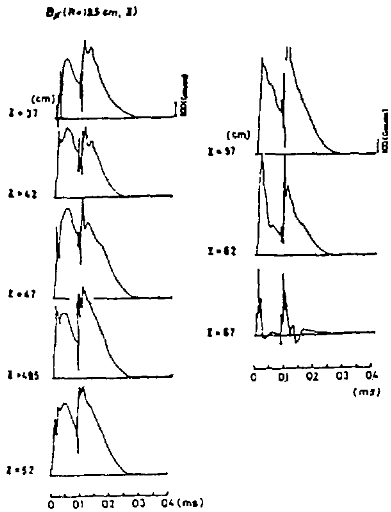

Fig. 2 Toroidal magnetic field obtained at eight positions on the parallel line (with the Z-axis) of R = 19.5 cm during CT plasma merging process.

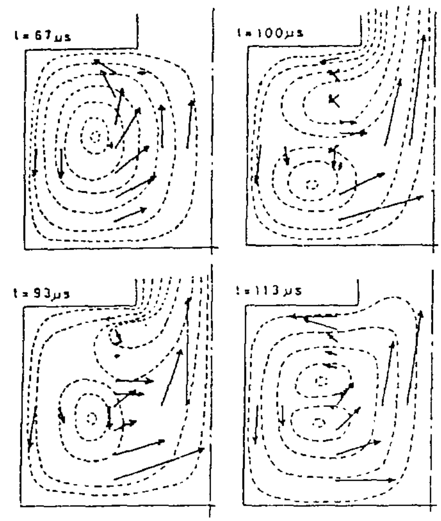

Fig. 4 Poloidal magnetic field pattern drawn from the data of magnetic field measurements in the R-Z plane.

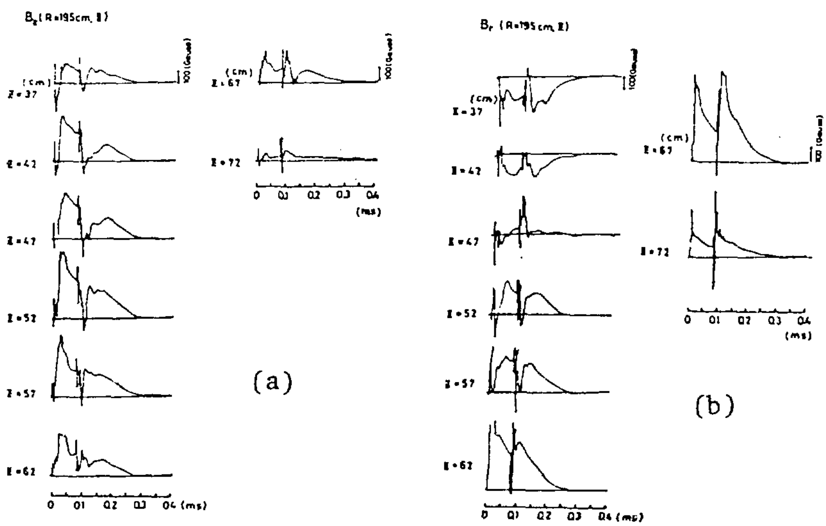

Fig. 3 Poloidal magnetic field B_p obtained at eight positions on the parallel line (with the Z-axis) of R = 19.5 cm during CT plasma merging process; (a) is Z-component of B_p and (b) is R-component of B_p.

V. GENERAL

Traveling Mirror Adiabatic Compressor

P. M. Bellan, Caltech

I Review of the concept

By injecting a double-hump current pulse [Fig. 1(a)] into a macroscopic electronic delay line, a traveling magnetic mirror, i.e. a double-humped magnetic field, is made to propagate in wave-like fashion along the delay line. The actual delay line consists of solenoid coils connected to external capacitors as shown in Figs. 1(a) and (b). The direction of propagation is along the symmetry axis and the propagation velocity is determined by both the solenoid geometry and the external capacitance. This traveling magnetic mirror is used to carry a reversed field particle ring or compact torus in its trough (for a reversed field theta pinch a single humped propagating B field could be used instead of a mirror field because the axial pinching self-force of this plasma provides axial confinement).

By gradually changing the radius r, intercoil spacing Δ, turns number m and/or capacitance C, of successive coils in the solenoid delay line [as shown in Fig. 1(b)], the sectional delay time of successive delay line sections is made to be a slowly increasing function of axial position. Consequently, the propagation velocity becomes a slowly decreasing function of axial position. From WKB theory, this causes the propagating magnetic mirror (or, for theta pinches, single hump) to *steepen* - - i.e., its intensity increases and its axial extent decreases in a manner wherein the total magnetic energy remains constant (not counting particle diamagnetism). Thus, this scheme provides adiabatic compression. The adiabatic compression is extremely efficient because, unlike conventional adiabatic compression, *the volume occupied by the magnetic field shrinks along with the particle volume* so no magnetic energy is wasted filling up unused volume.

The precise functional dependence of the WKB steepening on the coil parameters is derived in Refs. 1 and 2 where it is shown that the magnetic field scales as $B \sim \frac{m^{1/2}C^{1/4}}{\Delta^{3/4}r^{1/2}}$ and the characteristic mirror length λ scales as $\lambda \sim \frac{\Delta^{3/2}}{mr\,C^{1/2}}$ so that the magnetic energy W_B, which is proportional to $B^2r^2\lambda$, stays constant (not counting particle diamagnetism). The analysis of Refs. 1 and 2 and, hence these scalings, is based on the assumptions that (i) $\lambda >> r$, Δ and (ii) the coils are so closely spaced that each coil links more flux from adjacent coils than from itself (i.e. the coils act as a solenoid). Thus, to achieve an increasing field intensity having decreasing volume, all that is required is to gradually increase the quantity $m^{1/2}C^{1/4}/\Delta^{3/4}r^{1/2}$ for successive coils in the solenoid delay line while ensuring that the $\lambda >> r$, Δ assumption always holds.

II Table top experiments

A series of small table top models have been constructed which demonstrate that these scalings are correct. A new, somewhat larger system, now being constructed, will be used to compress a low beta ring of ~15 keV electrons. The main design parameters of this device are listed below:

characteristic compression time	2 μsec
magnetic energy	2 J

	large end	small end
confining field diameter	22 cm	4.4 cm
" " length	110 cm	22 cm
coil turns	2	2
impedance	4.2 Ohms	0.8 Ohms
capacitors	0.1 μF	0.5 μF
voltage	2 kV	0.9 kV
B	100 G	1100 G

Bench tests of this device show that the magnetic compression works very well (witin about 10% of the design). The power supply for this device is a triple pulse line having a design very similar to the compressor itself. It is expected that the rest of the experiment (electron gun, vacuum system, magnetic probes) will be constructed by early 1982.

[1] P. M. Bellan, Phys. Rev. Lett. 43,858(1979).

[2] P. M. Bellan, to be published in October, 1981 Phys. Fluids.

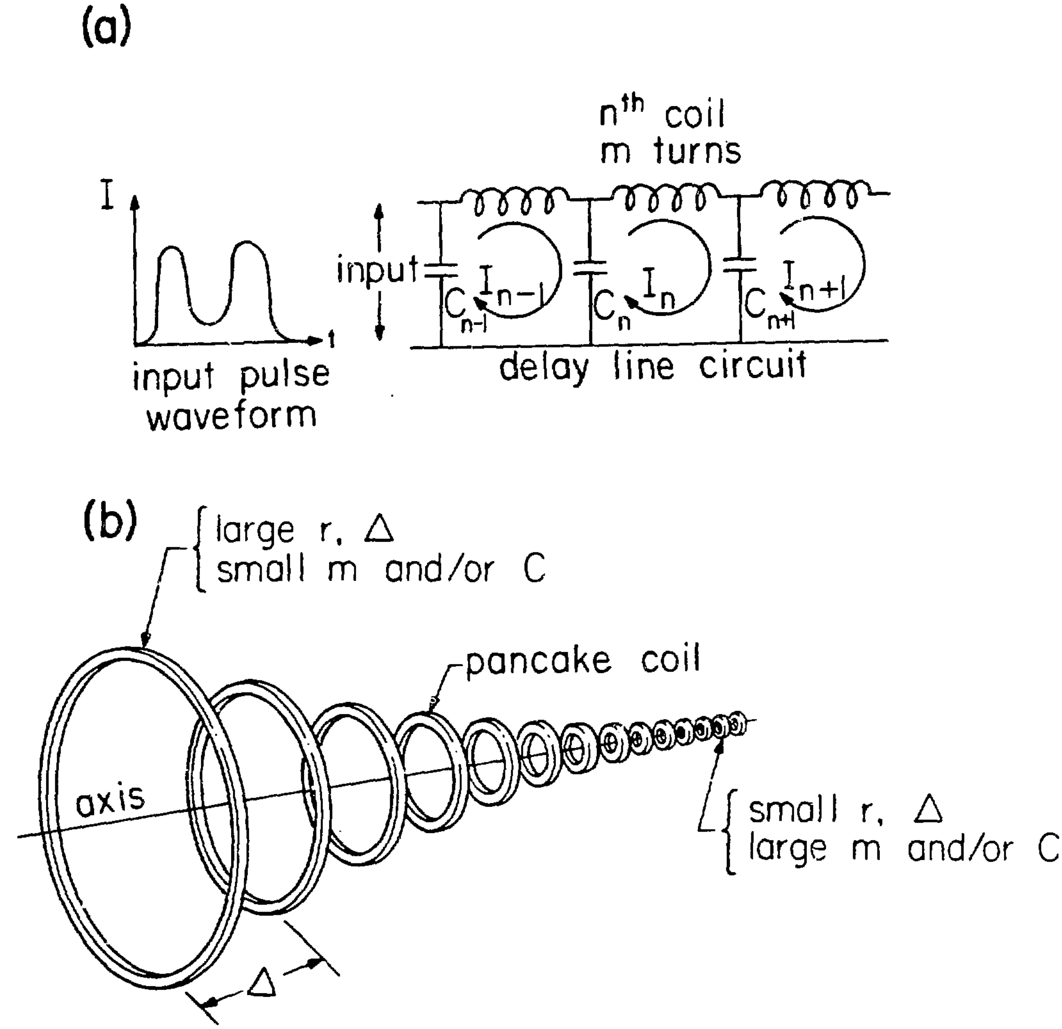

Fig. 1 (a)Input pulse and circuit; (b) coil geometry.

ANALYTIC FIELD REVERSED MIRROR EQUILIBRIUM WITH AN ELECTRIC FIELD*

J. K. Boyd
Lawrence Livermore National Laboratory, University of California
Livermore, CA 94550

Analytic, axisymmetric 1D equilibria have been derived to study self consistent electric and magnetic fields in a field reversed mirror. It is assumed such a configuration is sustained by high energy neutral beams, and as a consequence the ion Larmor radius is comparable to the plasma minor radius. The ions are then described by a distribution function and the electrons are treated as an inertialess fluid. The electron model is taken as a starting point from previous work.[1] The complete model consists of four equations.

$$n_e = \sum_j n_j z_j \tag{1}$$

$$J_r = 0 \tag{2}$$

$$\frac{\partial}{\partial r}\left(\frac{1}{r}\frac{\partial\psi}{\partial r}\right) = -\frac{4\pi}{c} J_\theta \tag{3}$$

$$\begin{aligned} 0 = {} & -e\left(\vec{E} + \frac{1}{c}\vec{V}_e \times \vec{B}\right) - \frac{1}{n_e}\nabla n_e T_e \\ & + \frac{m_e \nu_{ei}}{n_e} \sum_j n_j z_j^2 \left(\vec{V}_j - \vec{V}_e\right) . \end{aligned} \tag{4}$$

Equation (1) is quasineutrality, where n_e is the electron density, n_j is the jth ion species density and z_j is the charge state. Equation (2) is the r component of Ampere's law and is a result of allowing only a poloidal magnetic field, $B = \nabla\psi \times \nabla\Theta$. J_r is the radial current. Equation (3) is the theta component of Ampere's law. It is solved for the magnetic field using a current which is the difference between the theta velocity moment of the ion distribution function and the density times the electron fluid velocity in the theta direction. Because electrons are able to cancel the current due to a single ion species it is necessary to include several species with different theta velocities. The drag term in (4) allows Coulomb friction between ions and electrons to cause the electrons to have a theta velocity intermediate between slow and fast ion velocities. The result is a net Ohkawa[2] current, J_θ^{ok}, in the theta direction.

$$\begin{aligned} J_\theta^{ok} &= e\sum_j n_j V_{j\theta} z_j \left(1 - \frac{z_j}{\langle z\rangle}\right) \\ \langle z\rangle &= \sum_j n_j z_j^2 \left(\sum_k n_k z_k\right)^{-1} . \end{aligned} \tag{5}$$

*Work supported by U.S. DOE contract #W-7405-ENG-48.

The electric field in steady state is $-\partial\phi/\partial r$, where ϕ is the potential. Phi is obtained from the r component of (4), which must be solved simultaneously with (3). In general the current, which is the source of ψ, depends on ϕ. Successful decoupling of (3) and (4) is obtained by using an f_j from previous work of Post.[3]

$$f_j = c_j\,\delta(H - H_{oj})\,\delta(P_\theta - p_{oj}) \quad . \tag{6}$$

The results of this model yield a potential which requires integration of products of modified Bessel functions. To avoid this complication an alternate distribution has been implemented.

$$f_j = C_j\,\delta(p_z)\,\delta(H - H_{oj})\left(P_\theta + \frac{ez_j\psi_c}{c}\right) \quad . \tag{7}$$

The individual species current arising from (7) depend on ϕ, however, the sum over species only depends on r. Using (7) expressions for ψ and ϕ have been obtained for two models. First for $V_{re} = 0$ and $J_\theta = J_\theta^{ok}$,

$$\psi = -2\left(\frac{S_6\psi_o}{\psi_o + \psi_c}\right)^{1/2} r^2 - \frac{S_6}{\psi_o + \psi_c}\, r^4 \tag{8}$$

$$\phi = \frac{S_4\psi}{\psi + \psi_c} + \frac{1}{e}\,T_e \tag{9}$$

$$S_4 = e^{-1}\sum_j n_{oj}H_{oj}z_j\left(\sum_j n_{oj}z_j^2\right)^{-1}$$

$$S_6 = .5\,\tau\sum_j n_{oj}H_{oj}\left(1 - \frac{z_j}{\langle z\rangle}\right)$$

where S_4, S_6, ψ_o, ψ_c are constants and ϕ and T_e are only functions of ψ. Second for $J_\theta = J_\theta^{ok} - B_zV_{re}/\eta c$,

$$\psi_< = -\frac{8S_6}{\psi_o + \psi_c}\left(\frac{r^3}{3\alpha} - \frac{r^2}{2\alpha^2} + \left[\frac{-re^{\alpha r}}{\alpha} - \frac{1}{\alpha^2}\left(e^{\alpha r} - 1\right)\right]\left(\frac{1}{\alpha^2} - \frac{r_o}{\alpha}\right)e^{\alpha r_o}\right) \tag{10}$$

$$\psi_> = \psi_o - \frac{8S_6}{\psi_o + \psi_c}\left(\frac{r_o^3 - r^3}{3\alpha} + \frac{r_o^2 - r^2}{2\alpha^2}\right.$$

$$\left. - \left(\frac{1}{\alpha^3} + \frac{r_o}{\alpha^2}\right)\left[re^{\alpha(r-r_o)} - r_o + \frac{1}{\alpha}\left(1 - e^{\alpha(r-r_o)}\right)\right]\right) \tag{11}$$

$$\phi = e^{-1} T_e + S_4 + \frac{2S_6}{e\pi S_1} + \frac{K}{\psi + \psi_c} + \frac{\psi_o + \psi_c}{\psi + \psi_c} \frac{B_z^2}{e8\pi S_1}$$

$$+ \frac{S_{sum}}{\psi + \psi_c}\left(\mathscr{H}(r - r_o) \int_{r_o}^{r} (\psi_> + \psi_c)^2 \, dr - \mathscr{H}(r - r_o) \int_0^{r_o} (\psi_< + \psi_c)^2 dr \right.$$

$$\left. - (1 - \mathscr{H}(r - r_o)) \int_0^r (\psi_< + \psi_c)^2 dr\right) \tag{12}$$

$$S_{sum} = \frac{\eta e}{\psi_o + \psi_c} \left(\sum_j n_{oj} z_j^2\right)^{-1} \sum_k n_{ok} z_k^2 \sum_\ell n_{o\ell} z_\ell (V_{r\ell} - V_{rk})$$

$$S_1 = \sum_j n_{oj} z_j$$

$$\eta = \frac{m_e \nu_{ei}}{n_e e^2} \langle z \rangle$$

where K, T_e, r_o are constants and $\alpha = 4\pi V_o/\eta c^2$. <(>) refers to below (above) the field null. The radial electron velocity V_{re} is assumed to be a step function, $V_{re} = V_o$ for $B_z > 0$ and $V_{re} = -V_o$ for $B_z < 0$. Figure 1 shows ψ, B_z, E_r, $e\phi$ for two cases. In case I, V_o = 10 cm/sec and in case II, V_o = 1000 cm/sec. Parameters common to both cases are $n_1 = 10^{13}$ cm^{-3}, $n_2 = 5 \times 10^{11}$ cm^{-3}, $z_1 = 1$, $z_2 = 2$, H_{01} = 3 keV, H_{02} = .5 keV, $\langle z \rangle$ = 1.09, Te = .1 keV. The magnitude of B_z increases as V_{re} increases and the electric field is larger near r = 0 and the separatrix.

REFERENCES

1. D. E. Baldwin, M. E. Rensink, Comments Plasma Phys. Vol. 4, No. 2, p. 55 (1978).
2. T. Ohkawa, Nuclear Fusion 10, 185 (1970).
3. R. F. Post, Fourth International Conference on Driven Magnetic Fusion Reactors, Erice, Italy, Sept. 18-26 (1978).

FIGURES

1. a. Flux, ψ (gauss-cm^2) versus r for case I and II.
   b. Magnetic field, B_z (gauss) versus r for case I and II.
   c. Radial electric field, E_r (volts cm^{-1}) versus r for case I and II
   d. Potential, $e\phi$ (keV) versus r for case I and II.

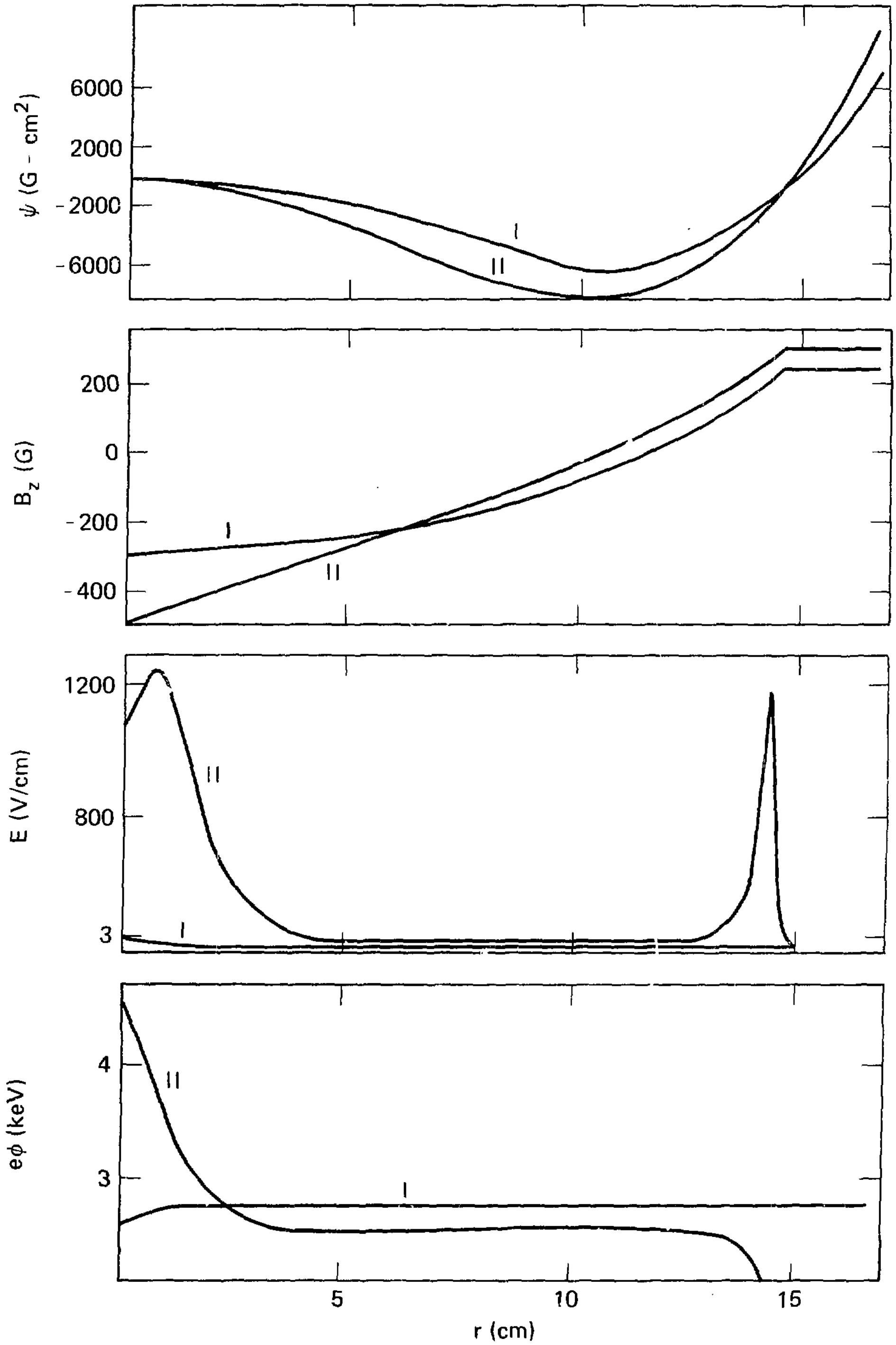

6000
2000
-2000
-6000
ψ (G - cm²)
I
II
200
0
-200
-400
B_z (G)
I
II
1200
800
3
E (V/cm)
II
I
4
3
eφ (keV)
II
I
5
10
15
r (cm)

PRESENT STATUS OF REB RING STUDIES AT INSTITUTE OF PLASMA PHYSICS, NAGOYA UNIVERSITY

M. Hasegawa, A. Mohri, K. Narihara, Y. Tomita and T. Tsuzuki

Experiment on REB rings has recently been focussed on search for new methods of ring formation so as to raise the applicability of REB ring to fusion. Formation methods should be chosen to the purpose. For radial adiabatic compression, rings of large major radius have to be formed initially. When we think of micro-toroids which confine very high density ($10^{17\sim19}$ / cm^3), the external magnetic field necessary for holding the rings would be too high to be realized. However, this idea would become feasible if we can form a intense ring inside a conducting chamber;that is, flux-conserver, since we no longer need the external field. Several methods of ring formation have been checked experimentally to see their practical feasibility. Those are

* use of flux-conserver,
* use of self-poloidal field,
* use of beam launcher.

The experiment was carried in small devices.

RING FORMATION IN FLUX-CONSERVER

Figure 1 shows the experimental setup. A REB is injected into a plasma filled box in which a half-cusp field is generated with a pulse field coil. The REB particles get azimuthal momenta due to the axial change of the magnetic vector potential. Then,a REB ring is formed and introduced into a flux-conserver which has the inner space 18 cm in dia. and 9 cm in depth.

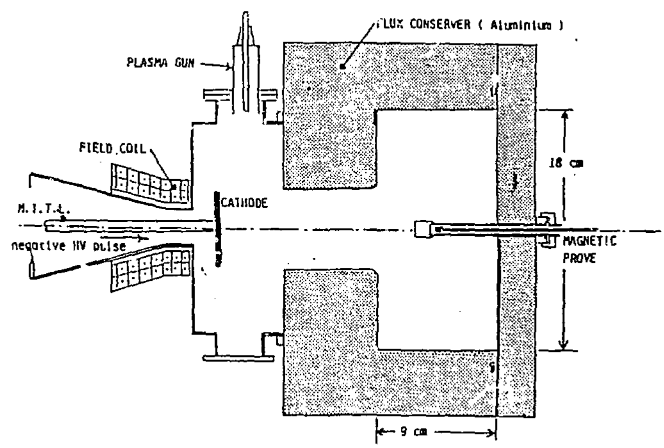

Fig.1 SPAC-UHD-1

REB rings were formed in the flux-conserver. Characteristics of the rings much depended on the operation condition. The lifetime was fairly long compared with the data of plasma-vortex injection at LASL, LLL and Osaka, probably owing to the presence of high energy electrons as the current carriers. Figure 2 shows a typical case, where a REB of 0.5 MeV, 60 kA and 80 ns was injected and the external field components were B_r= 530 G and B_z= 900 G at the radial edge of the cathode. The decay time of the poloidal field on the axis was nearly 700 μs. The estimated toroidal current was nearly 16 kA at the peak.

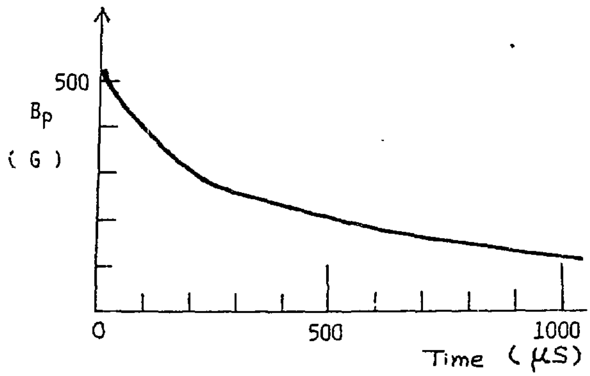

Fig.2 B_p at the center of the axis.

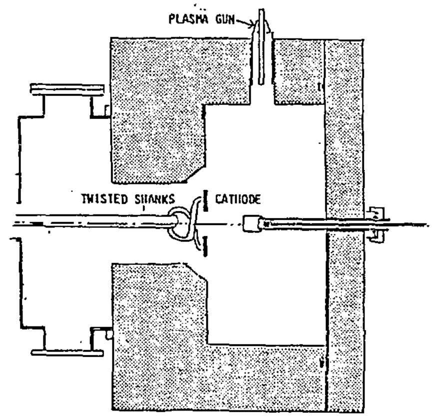

Fig.3 Use of Twisted shanks to generate a self-field.

The other injection method tried was the use of twisted shanks for producing a self-poloidal field as shown in Fig.3. No external field was used in this case. Rings could be formed in the flux-conserver. The attained ring current reached 100 kA where the life, however, was 15 μs.

This experiment shows that REB rings can be formed inside the conducting flux conserver. That suggests there is a possibility to have very strong micro=rings in the similar way, though we have to improve the method so as to fit the operation at much higher power.

RING FORMATION IN A MIRROR MACHINE WITH TOROIDAL FIELD

A small mirror machine with a centre conductor for producing an azimuthal or toroidal field was made to check several formation methods. Cathodes used for REB injection are depicted in Fig.4. A cathode generating a self-poloidal field (Fig.4-a) was set coaxial to the mirror so that the self-field was reverse to the mirror field. Then, a large axial change in the vector potential appears in front of the cathode surface. Thus, we can form a ring by injection of REB into a plasma. The mirror machine has the axial length of 90 cm and the inner wall diameter of 26 cm. The current obtained with this type of cathode reached 70 kA where the lifetime was 20 μs.

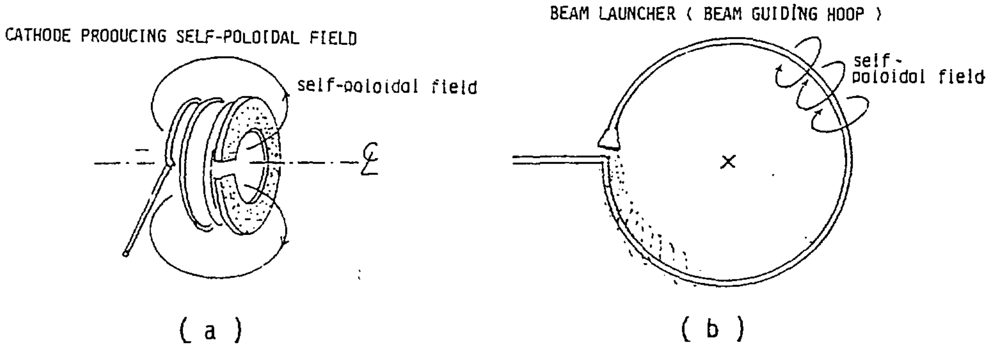

Fig.4 Cathodes examined in the mirror machine.

The other examined method was the use of ' Beam Launcher ' having a shape of sigle circular hoop. The one end of the hoop is connected with the MITL and a disk cathode is attached to the other end. The feeding current to the cathode produces a poloidal field around the hoop. The field synthesized with the external mirror field (i.e. vertical field) becomes to have a stagnation circle, on the inner side of which there appears a steep radial decrease of the field. When the REB ejected from the cathode launches on this weak field region, its orbital major radius can be held to be sufficiently large even in the case of strong vertical field. Then, stacking of the injected REB becomes easy and thus formed intense ring is sustained in an equilibrium position by the strong vertical field,when the hoop current has already faded away. Figure 5 shows an experimatal result, where the REB (0.5 MeV, 30 kA, 80 ns) was injected with the method mentioned above. The peak ring current reached 140 kA. The lifetime was, however, short, probably due to the field error. X-ray measurement showed that energies of the beam electrons of the ring were less than 100 keV. Also, the forming condition of ring became wider than in the case of the normal tangential injection.

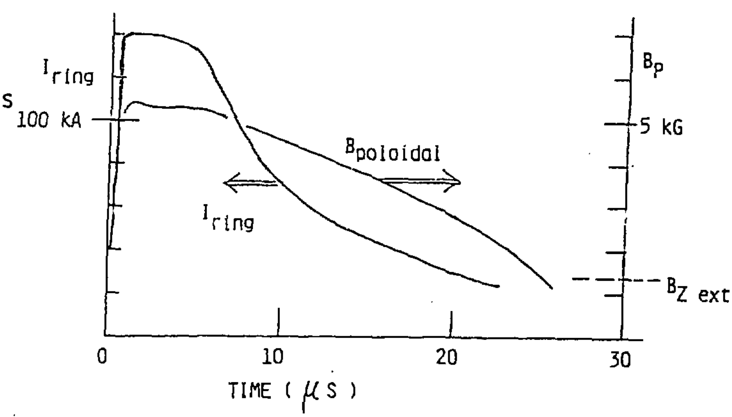

Fig.5 Wave forms of the ring current I_{ring} and the poloidal field on the axis $B_{poloidal}$.

The ' Beam Launcher ' method is now being tested in SPAC-VI to have a ring of larger major radius, which is necessary as an initial condition for strong major-radial adiabatic compression.

CONSTRUCTION OF SPAC-VI-DR

A new experimental device named ' SPAC-VI-DR ' is now under construction, aiming at

* Simultaneous formation of two rings, one of which is a high current REB ring and the other is a high energetic electron ring or ion beam ring.
* Compression of both the rings.
* Conveyance of the rings along the axis by making the axial gradient of the external field
* Merging of the rings at the midplane of the device.

A centre conductor is installed to stabilize the tilting instability during the conveyance of rings and to generate a toroidal field. The possible radial compression ratio is more than 2.0 and the conveying distance is 1.2 m. Figure 6 shows the cross sectional view of the device.

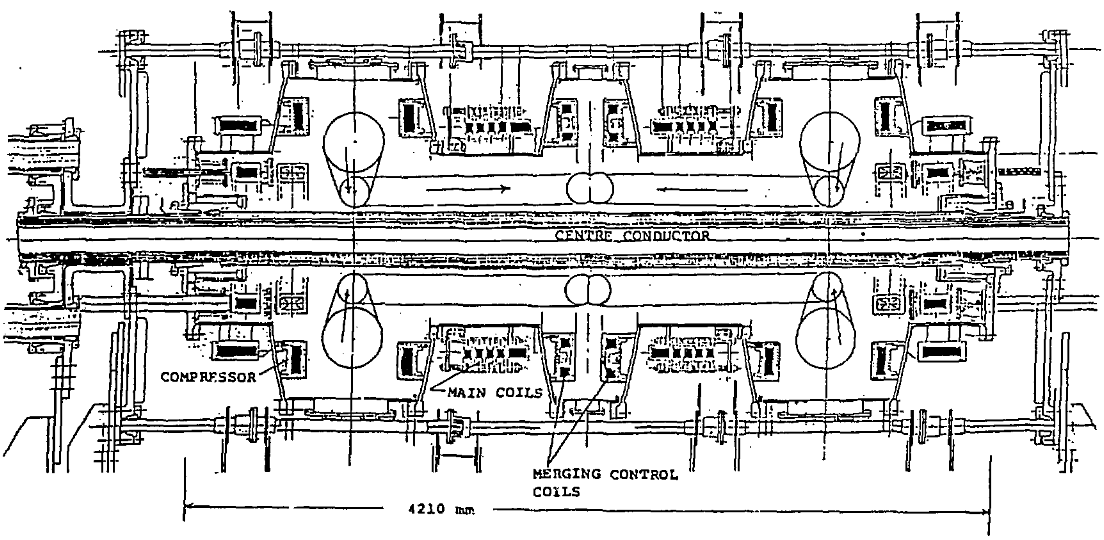

Fig.6 SPAC - VI - DR

ANOMALOUS DIFFUSION IN TOROIDAL PLASMA

N. A. Krall
Jaycor
San Diego, CA 92138

INTRODUCTION

This review, which is merely one man's view of the present state of anomalous diffusion theory, will be broken up into the following segments:

I. BASIS AND FORMALISM FOR ANOMALOUS DIFFUSION THEORY
   - A. Quasilinear Theories
   - B. Fluid Theories

II. LOWER-HYBRID WAVE RESULTS
   - A. Properties of Lower-Hybrid Waves
   - B. Application to Reversed Field Theta Pinch
   - C. Application to High Beta Q-Machine

III. ANOMALOUS DIFFUSION IN TOROIDAL SYSTEMS
   - A. Resistive Interchange, $\eta\beta$-II
   - B. Dissipative Trapped Electron Tokamak Transport, I
   - C. Dissipative Trapped Electron Tokamak Transport, II

IV. BEYOND QUASILINEAR THEORY
   - A. Resonance Broadening
   - B. Renormalized Turbulence Theories
   - C. Global/Generic Analyses

V. NEW DIRECTIONS

In attempting to review anomalous diffusion theory, it is necessary to begin with quasilinear theories, for two reasons. Firstly, they form the basis of the original applications of turbulence theory to experiments and, therefore, have been most closely tied to the experiments and verified by comparisons with both experiments and with particle simulations. And, secondly, in analyzing the work that is presently being done in dozens of different papers and laboratories, it is clear that quasilinear theory and extensions of the quasilinear approach form the bulk of the work currently being done. The original approaches to anomalous diffusion theory were based on the fact that two time scales are appropriate. The first is the time scale for stability, $\tau_S \sim \gamma^{-1}$, the second is the time scale for diffusion, $\tau_D \sim k^2a^2\gamma^{-1}$, where γ is the growth rate for the instabilities which cause the diffusion, and a is the typical plasma size. Since the wavelengths of plasma modes are typically shorter than the plasma size, the diffusion time scale is substantially longer than the time scale for stability. This then led to the idea of developing stability theories localized in space and time and using the local properties to predict diffusion. In writing down the diffusion time scale, I have used one of the original estimates of diffusion due to its stabilities, namely, $D \sim \gamma/k^2$. This result was written down by many authors,[1,2] including Kadomtsev, et al., and was based on the idea that due to ExB drifts a particle will diffuse or drift one wavelength in approximately one growth time. Taking that drifting distance as the excursion, the diffusion is proportional to $D \sim \Delta x^2/\tau \sim \gamma/k^2$. This estimate when first written down seems a bit crude, because it does not involve the level of fluctuations due to the wave, for example, which must clearly be important in determining the amount of diffusion. Nonetheless, as we will see, this provides a surprisingly good estimate of diffusion, even though in practice we seldom use the raw formula. It correctly places great emphasis on a thorough knowledge of linear stability properties.

I. BASIS AND FORMALISM FOR ANOMALOUS DIFFUSION THEORY

The basis for anomalous diffusion theory is the Vlasov equation[3]

$$\left[\frac{\partial}{\partial t} + v\cdot\nabla + F\cdot\nabla_v\right] f = 0 \begin{cases} f = f_o(r,v,t) + \delta f(r,v,t); \text{ waves} \\ n, nV\ldots = \int dv\ (1,v,\ldots)f; \text{ fluid} \end{cases} \tag{1}$$

$$\text{Waves:}\quad L\delta f = 0,\ \nabla\cdot\delta E = 4\pi\sum_\alpha q_\alpha \int dv\ \delta f_\alpha;\ \chi(\omega,k)\ \delta E = 0 \tag{2}$$

$$\text{Quasilinear:}\quad L_o f_o(t) = -\ \delta F\cdot\nabla_v \delta f\quad . \tag{3}$$

As indicated, the distribution function of particles can either be broken up into two parts, a slowly varying background distribution which describes the bulk of the plasma and a rapidly varying part, presumably small, which represents the development of plasma waves, or alternately, the distribution function can be integrated with various moments of velocity to provide fluid equations. The two can be combined to provide quasilinear fluid theories and these are in fact the basis for applying kinetic theory to anomalous diffusion.

Equations (2) and (3) show the procedure which is generally followed, namely, the Vlasov equation is analyzed and combined with Poisson's equation to provide a calculation of plasma waves, which, as indicated in Eq. (2), basically requires a calculation of the plasma susceptibility. As Eq. (3) indicates, the eigenfunction for the plasma waves, δf, as well as the related force due to the waves, δF, are used in the quasilinear equation to provide the quasilinear response. Having the wave properties well in hand, one then integrates the Vlasov equation to obtain fluid equations which can describe the evolution of plasma on the diffusion time scale, and Eqs. (4), (5), and (6) indicate the time development of the momentum and the temperature in terms of the waves and instabilities of the plasma which are in general calculated in terms of the fluctuation level, ϵ_K, and the plasma susceptibility, χ.[4]

$$\frac{\partial N_jV_{jy}}{\partial t} + \frac{\partial NV_{jy}V_{jx}}{\partial x} = \frac{e_j}{m_j}\left(N_jE_y - \frac{N_jV_{jx}B_z}{c}\right)$$

$$+ \frac{e_j}{m_j} < \delta N_j \delta E_y > \tag{4}$$

$$\frac{3}{2}\left(\frac{\partial T_j}{\partial t} + \frac{\partial T_jV_{jx}}{\partial x}\right) - \frac{1}{2} T_j \frac{\partial V_{jx}}{\partial x}$$

$$= \frac{e_j}{N_j} <\delta\vec{E}\cdot[\delta(N_j\vec{V}_j) - \vec{V}_j\delta N_j]> \tag{5}$$

$$\vec{R}_j^{AN} = e_j<\delta N_j\delta\vec{E}> = \sum_n \int d\vec{k}\ 2\vec{k}\ \epsilon_{\vec{k}}(x,t)\ \mathrm{Im}\chi_j(\vec{k},\omega+i\gamma) \tag{6}$$

In analyzing and using the wave properties to produce the diffusion properties of the system there are in fact four key elements which have evolved over the years.

1. A realistic calculation of the susceptibility, $\chi(k,\omega+i\gamma)$,
2. A rigorous calculation of the nonlinear behavior of the susceptibility,
3. A realistic estimate of the fluctuation level, and
4. A systems type approach.

Item 4 has been a key element in the development of anomalous diffusion theory. As has been demonstrated over the years, in a typical plasma situation the susceptibility is a strong function of space and time. This is because plasma waves and instabilities depend strongly on beta, shear, gradient lengths, electron to ion temperature ratios, and so on, and each of these quantities varies dramatically in space. The most common situation is that if the calculation is done accurately and the stability regions in space and time determined from fluid equations describing the entire coupled system, scaling laws will develop (e.g., for the plasma confinement time or the time for penetration of magnetic fields) which in general do not reflect directly the linear properties of <u>any</u> single instability. The first "failure" of the quasilinear approach to anomalous resistivity came when it was observed that a number of shock wave experiments did not follow the scaling time for plasma implosion and magnetic field penetration predicted by the instabilities which were assumed to be dominant.[5] The first major success of anomalous resistivity theory came when it was demonstrated that if these very same instabilities were applied locally, that is, fluid equations were integrated with anomalous properties varying in space and time just as the instability properties varied in space and time, then the plasma implosion and magnetic field penetration agreed extremely well with experiment over a wide range of ionization level, magnetic field strength, density, and magnetic field pulse time.[6] The transition from failure to success required no new knowledge, merely more careful computation of the <u>system</u>.

II. LOWER-HYBRID WAVE RESULTS

Because the intent of this review is to demonstrate the present state of anomalous transport theory, I will not dwell on the many, many examples of application of these theories in the past,[4] but will describe only an application which is also used in describing reversed field theta pinches. That example is the application of lower-hybrid-drift waves to anomalous transport.

A. Properties of Lower-Hybrid Waves

Lower-hybrid waves became popular in theta pinch analysis because that instability was fluid-like in many of its applications, did not depend crucially on electron to ion temperature ratios, and, as the scale lengths for plasma density and temperature changed, evolved from one mode to another. In order to apply the lower-hybrid instability (note this instability is being used simply as an example - all relevant modes must be treated in the same way), one calculates the properties of this mode, including scale size as indicated in Eqs. (7), (8), and (9) where the scale sizes are defined in Figure 1.[7]

Lower Hybrid - Strong Drift Limit [$L_n < a_i$]:

$$\omega_o \simeq \gamma \simeq \omega_H \equiv \left(\omega_{ce}\omega_{ci}\right)^{\frac{1}{2}} \left(1 + \omega_{ce}{}^2/\omega_{pe}{}^2\right)^{\frac{1}{2}} \tag{7}$$

Lower Hybrid - Weak Drift [$(m_i/m_e)^{\frac{1}{4}}\, a_i > L_n > a_i$]:

$$\omega_o \simeq \omega_H(a_i/L_n) \quad , \quad \gamma \simeq \omega_o(a_i/L_n) \tag{8}$$

Drift Cyclotron:

$$\left[\left(\frac{m_i}{m_e}\right)^{\frac{1}{2}} a_i > L_n > \left(\frac{m_i}{m_e}\right)^{\frac{1}{4}} a_i\right]$$

$$\omega_o \simeq \ell\omega_{ci} \simeq kV_D$$

$$\gamma \simeq \omega_o \left(\frac{m_e}{m_i}\right)^{\frac{1}{4}} \tag{9}$$

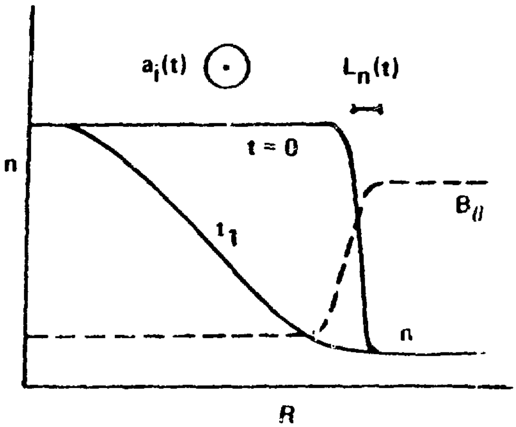

Figure 1.

Next, the property of the mode with various temperature gradients is calculated,

Instability Condition (Low β, General Distribution):

$$1 > b_e > \frac{T_e}{2T_i} \frac{\eta_{Ti}}{1 - \frac{1}{2}\eta_{Ti}} \left(1 + \frac{\omega_{ce}^2}{\omega_{pe}^2}\right)^{-1} \qquad (10)$$

$$b_e^{\frac{1}{2}} > \frac{T_e}{T_i\sqrt{2\pi}} \frac{(1 - \frac{1}{2}\eta_{Te})}{(1 - \frac{1}{2}\eta_{Ti})(1 + T_e/T_i + b_e\omega_{ce}^2/\omega_{pe}^2)} > 1 \qquad (11)$$

where beta is the ratio of temperature to density gradients and b is the product of wavenumber times electron gyroradius. Another important parameter for lower-hybrid modes is shear, and Figures 2 and 3 show the range of stability as a function of shear for the case of cold electrons as in Figure 2, or warm electrons as in Figure 3. Some analytic results can be obtained for some ranges of shear parameters,

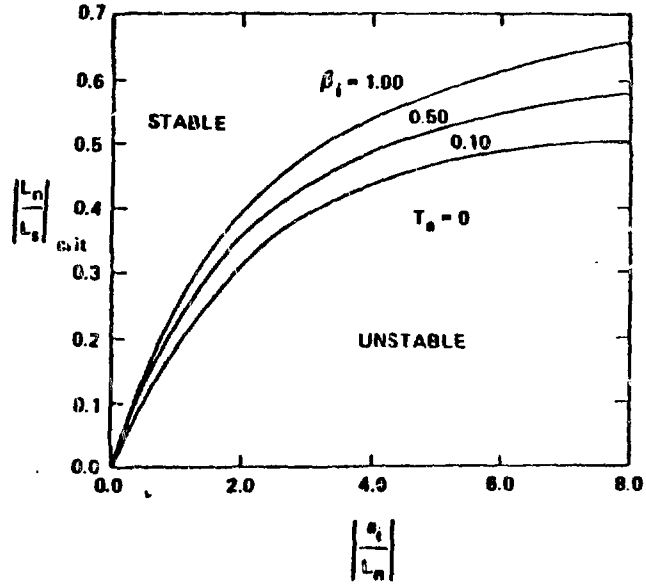

Figure 2.

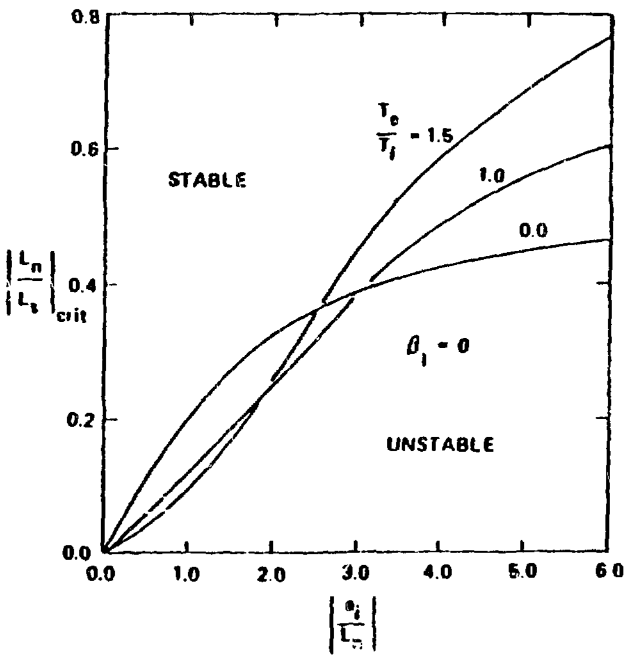

Figure 3.

Weak Drift, Low β, Stable if:

$$\frac{L_s}{L_n} < \frac{4L_n}{a_i}\left(1 + \frac{\omega_{ce}^2}{\omega_{pe}^2}\right)^{\frac{1}{2}} \quad \text{if} \quad \frac{T_e}{T_i} << 1 + \omega_{ce}^2/\omega_{pe}^2 \tag{12}$$

$$\frac{L_s}{L_n} < \frac{L_n}{a_i} \; \frac{(1 + T_e/T_i)^2}{T_e/T_i} \quad \text{if} \quad \frac{T_e}{T_i} >> 1 + \omega_{ce}^2/\omega_{pe}^2 \quad . \tag{13}$$

Finally, the plasma beta is critical in determining stability properties of this mode and Figures 4 and 5 indicate this effect. The actual result is given by the solid lines in Figures 4 and 5. The dotted line is to show a common mistake in calculating the beta effects. The finite value of plasma beta alters the drift orbits in the electrostatic dispersion relation and this affects the stability. However, another effect of beta is to introduce magnetic fluctuations. If the electrostatic calculations are kept while ignoring the magnetic fluctuations, the answer in general is wrong and that is shown by the comparison between dotted and solid lines in Figures 4 and 5. The reason this mistake is generally made is because it is quite a bit simpler to calculate the finite beta effects on electrostatic modes and simply overlook the electromagnetic effects.

By no means is this detailed calculation of lower-hybrid stability effects gilding the lily. If the proper variation of stability with local parameters is not included, it can be demonstrated in theta pinch applications that the anomalous diffusion predictions are far from being in agreement with the experimental results; however, with all of this detail it is possible to reproduce the experiments quite accurately. I do not mean to imply that anomalous diffusion is always a big effect. Figures 6 and 7 give a comparison of the development of a reversed field pinch on a one millisecond time scale with ZT-1 parameters as opposed to ZT-40 parameters. Since the instability depends on the density scale length, the larger machine has a much longer time scale for evolution in response to this mode. Over one millisecond the predicted changes are almost negligible in ZT-40 while they are quite substantial in ZT-1.

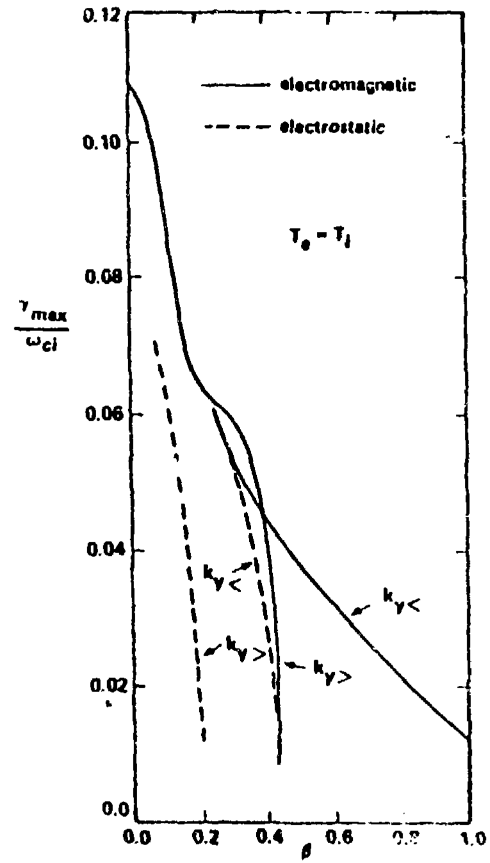

Figure 4.

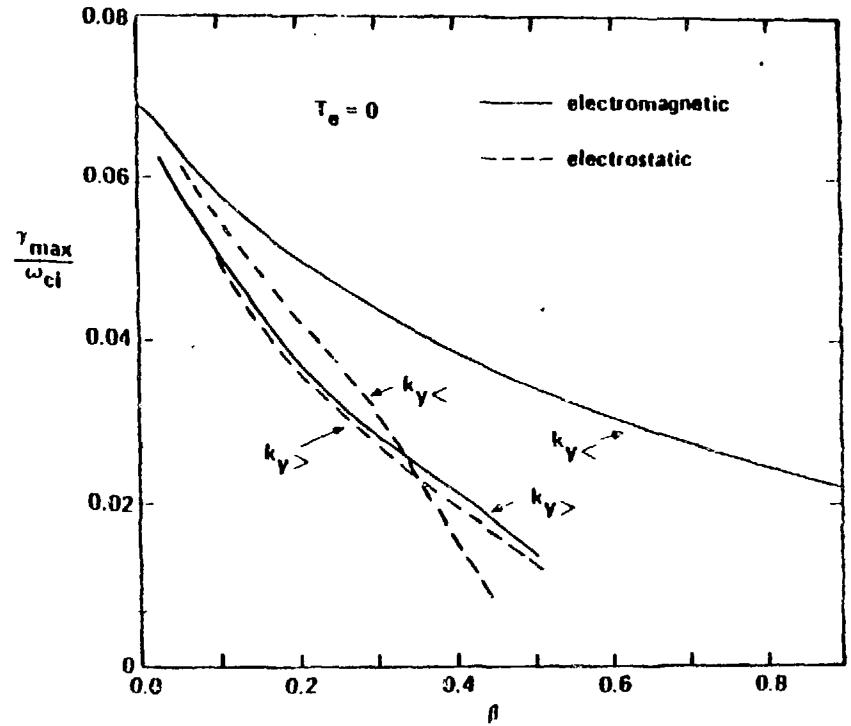

Figure 5.

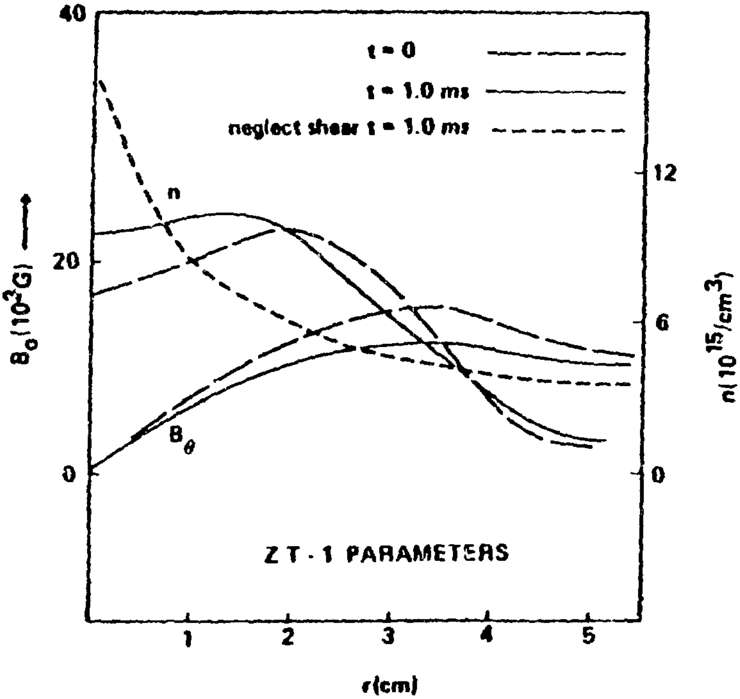

Figure 6.

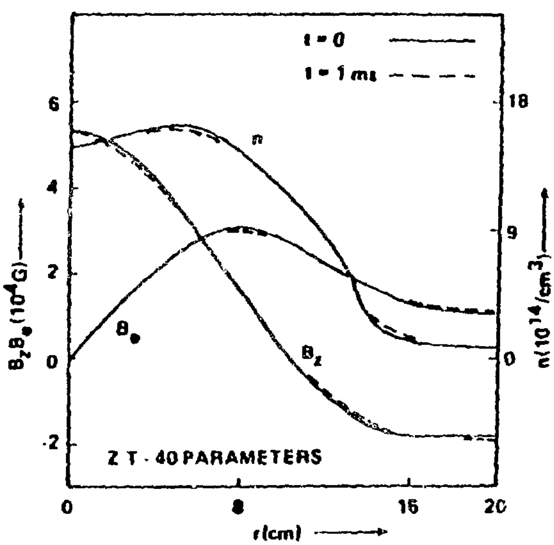

Figure 7.

Now, before I go on to more current work, it is fair to ask how seriously one should take the predictions of this theory. The fact that everyone seems to be using the same theory is by no means justification for it. I would like, therefore, to show at least one example (of many) of the detailed agreement between this model and experiment. Figure 8 shows the profiles of density as a function of time and radius in an implosion heating experiment.[8,9] The theory[10] used a hybrid code which integrated the fluid equations described above and included several instabilities in detail, also as described above. The experiment measured the density as a function of time over a number of radial slices. It is possible to interpret these experimental and theoretical profiles in very convincing ways in terms of an initial density peak due to reflected particles, a peak due to the magnetic pulse imploding, a peak due to reflected particles having passed through the axis and reencountering the plasma sheath, and a peak due to the magnetic piston bouncing in the center and being reflected toward the wall. The agreement between theory and experiment is more than simply good, particularly if you keep in mind that the theory was not adjusted at either space points or time points. Once the model was set up, it was simply run and the results are as shown.

This stability behavior was developed for a specific geometry and parameter range. By no means does this sort of behavior say that lower-hybrid turbulence is going to explain any arbitrary experiment. In fact, the simulations shown in Figures 7 and 8 were developed using a number of instabilities, included over the years as we increased our understanding of what the stability mechanisms appropriate to that experiment were. This theory is a device-specific theory and requires detailed analysis of the stability properties in every case.

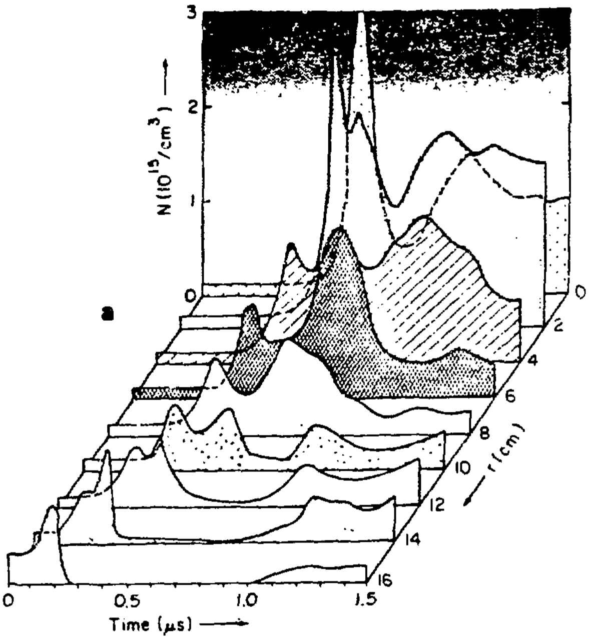

HYBRID CODE

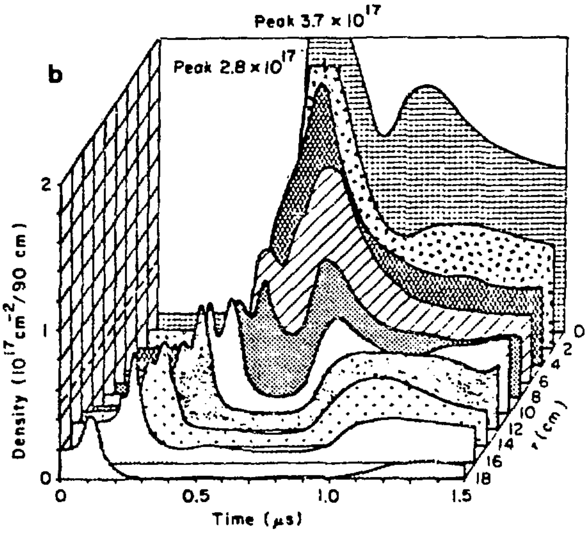

EXPERIMENT

Figure 8.

B. Application to Reversed Field Theta Pinch

I would now like to describe an application of this model, due to Linford and Hamasaki,[11] to the Reversed Field Theta Pinch. The geometry is shown in Figure 9. The model was born one-dimensional, but a reversed field theta pinch after the reconnection phase is not at all one-dimensional. This was taken into account in various ways. For one thing, pressure balance in the axial direction was included as one of the constraints on the one-dimensional code. A second constraint was that flux lines which, as shown in Figure 9, are closed, will require different one-dimensional points to have related same properties, e.g., temperature. This constraint was imposed upon the code. Thirdly, the transport across closed field lines and the transport along open field lines is quite different. In the code the closed field lines were assumed to have classical and anomalous transport across the magnetic field while the open field lines were assumed to have classical transport parallel to the magnetic field. A large number of cases were run and various effects examined. The effect of various models for the boundary, the effect of axial contraction, the effect of either connecting field lines when they should be connecting or omitting that effect were all examined and it was concluded that each of these physically realistic effects also made a difference in the results predicted by the model. Rather than dwell in detail on all of these effects which have been discussed elsewhere,[12] I will simply present the results of the Linford and Hamasaki analysis.

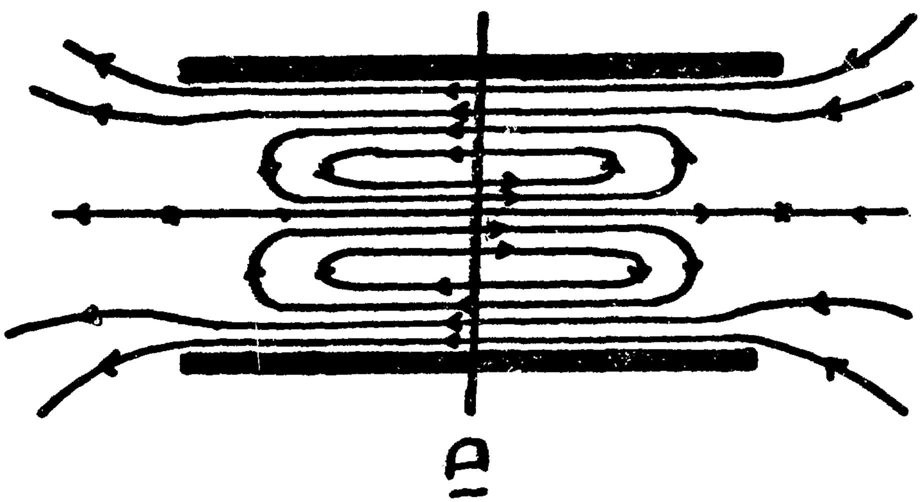

Figure 9.

Figure 10 shows theoretical prediction for the confinement time of a system assumed to have a fixed value of R, where R is the distance from the center of the cylinder to the maximum of plasma density. In the runs shown in Figure 10, the ion temperature was taken in various cases to range over a factor of eight, and for each ion temperature the magnetic field was allowed to vary also over a factor of about eight. The results are plotted showing the confinement time as a function of $1/\rho_i$, ρ_i = the ion gyroradius. The confinement time is predicted to be roughly inversely proportional to the ion gyroradius. Figure 11 shows the result of a number of code runs in which the ion temperature and the magnetic field were kept constant and the radius, R, which again is the location of the point of maximum density, was allowed to vary about over a factor of two. Figure 11 shows that the confinement time varies approximately with the square of this plasma radius. Figures 12a and 12b show the results of a number of reversed field theta pinch experiments plotted as a function of different parameters.[13,14] These experiments include substantial differences in input energy to the plasma. If you look up the details of the experiment you can find a corresponding range of other experimental parameters. Figure 12a shows that if the confinement time is plotted in terms of one over the ion gyroradius, there is quite a spread. Figure 12b on the other hand shows that if the confinement time is plotted as a function of R^2/ρ, a very orderly straight line is obtained in agreement with the predictions of Hamasaki.

When the theory was developed, the confinement time of the plasma in fact had not been measured. What was measured was the time required for the plasma to begin to rotate with a speed which then terminated the plasma confinement. Subsequently, the plasma confinement was also measured and it turned out to be very comparable to the spinup time. So this was a case where the theory in fact was developed before the appropriate measurement had been made. When the plasma density and its decay with time was directly measured and found also to agree with the results shown in Figure 12b, one was forced to conclude that the lower-hybrid based anomalous transport theory was indeed describing at least the density decay in the FRX, if not the spinup process itself. I would like to emphasize that although the results for the implosion heating experiment shown in Figure 8 are ancient history, the results of Linford and Hamasaki are quite recent and in quite a different geometry from IHX. This demonstrates that the success of the IHX modeling was by no means restricted either to that particular experiment or to that particular state of knowledge of turbulence theory.

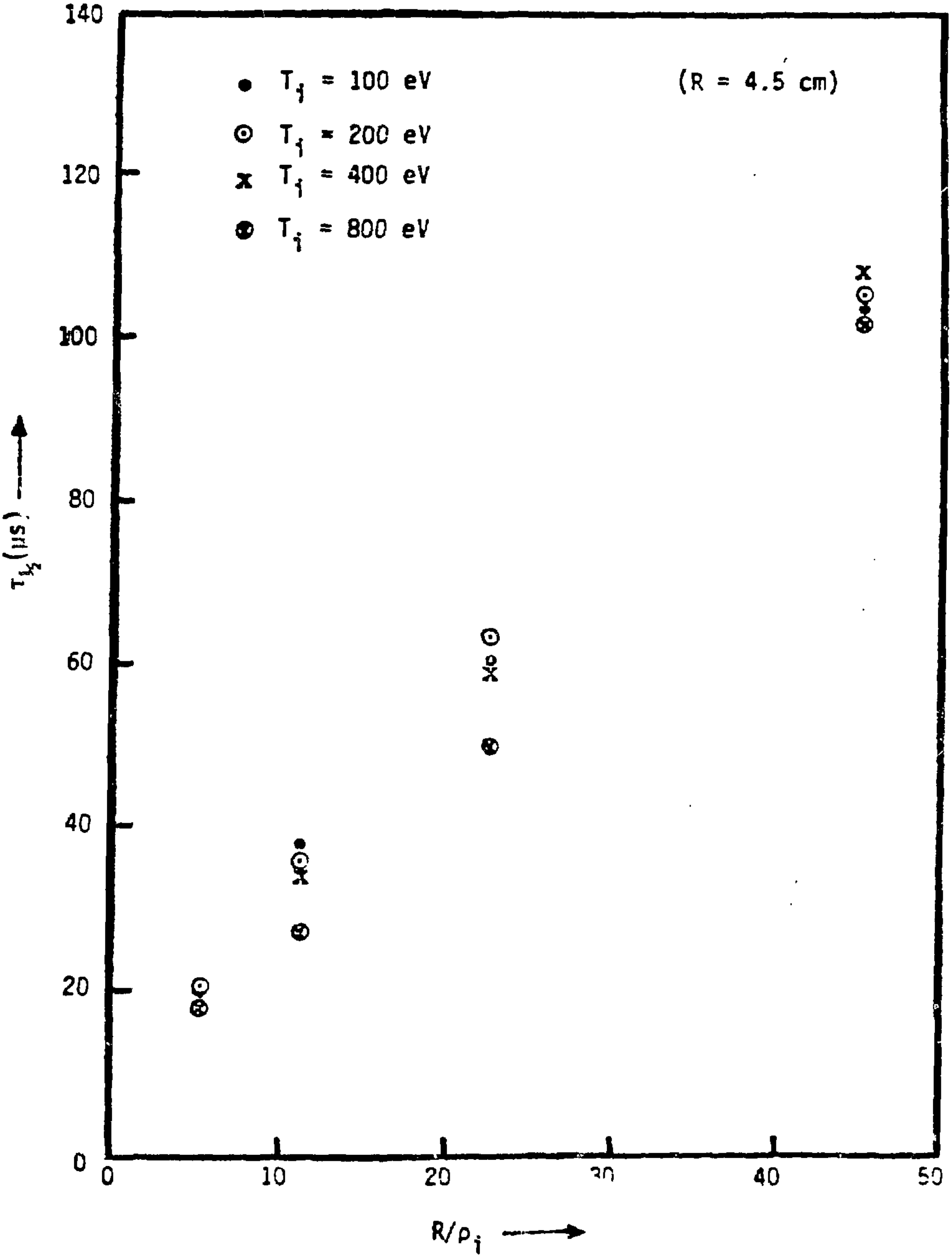
140
120
100
80
60
40
20
0
0
10
20
30
40
50
$\tau_{1/2}(\mu s)$
R/ρ_i
T_i = 100 eV
T_i = 200 eV
T_i = 400 eV
T_i = 800 eV
(R = 4.5 cm)

Figure 10.

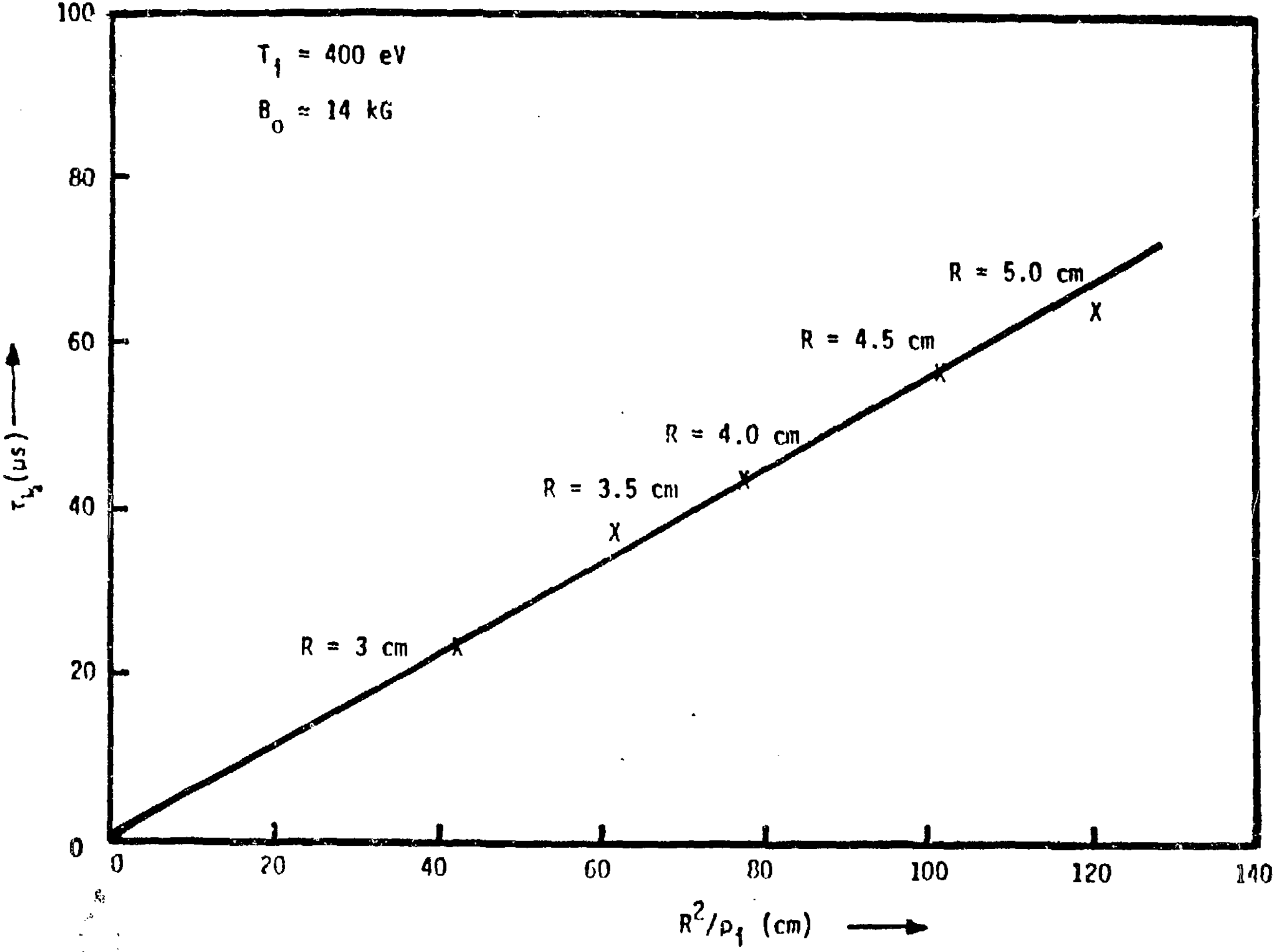

T_i = 400 eV
B_o ≈ 14 kG
R = 3 cm
R = 3.5 cm
R = 4.0 cm
R = 4.5 cm
R = 5.0 cm
$\tau_{\frac{1}{2}}(\mu s)$
R^2/ρ_i (cm)
0
20
40
60
80
100
120
140

Figure 11.

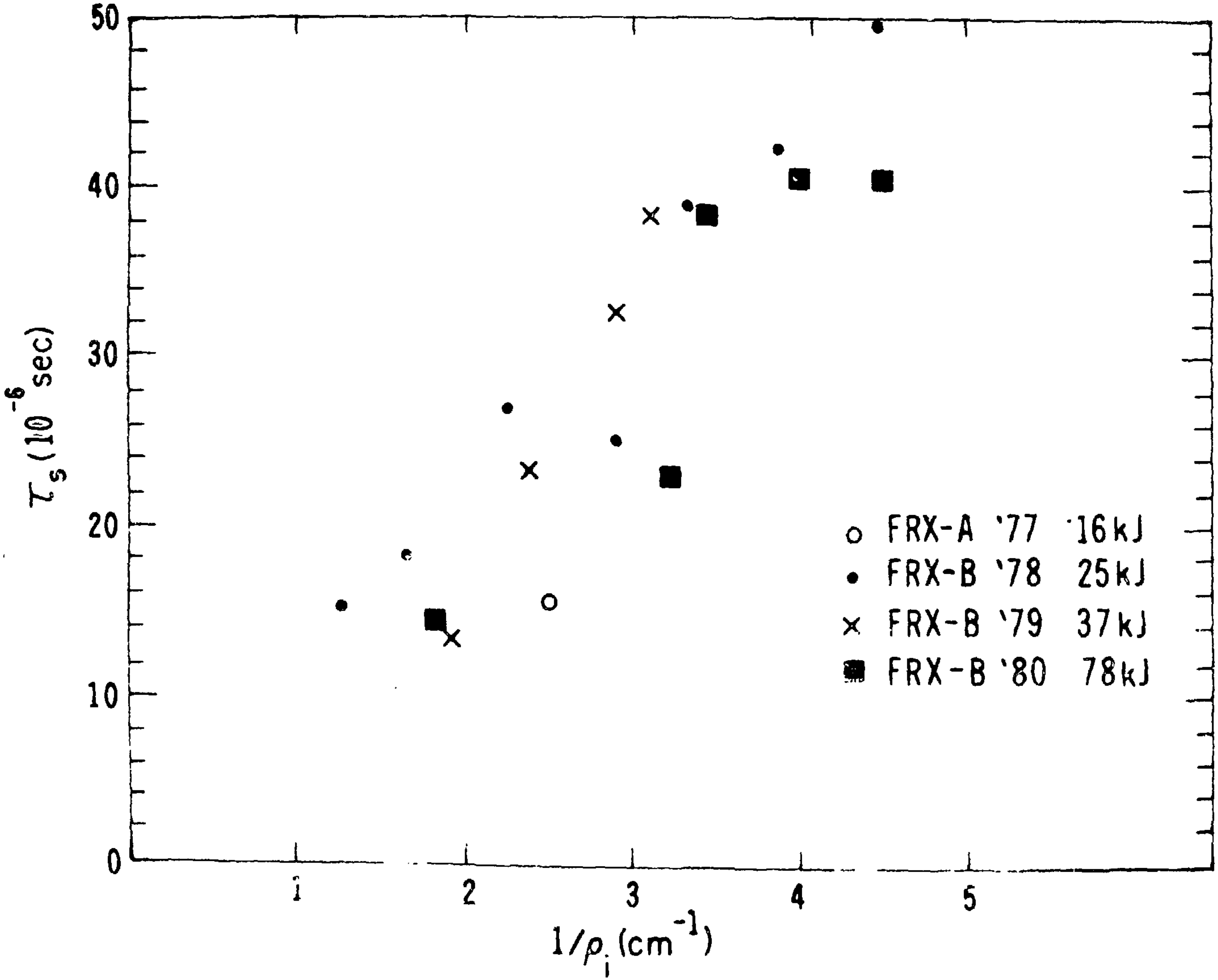

50
40
30
20
10
0
1
2
3
4
5
τ_s (10^{-6} sec)
$1/\rho_i$ (cm^{-1})
○ FRX-A '77 16kJ
• FRX-B '78 25kJ
× FRX-B '79 37kJ
■ FRX-B '80 78kJ

Figure 12a.

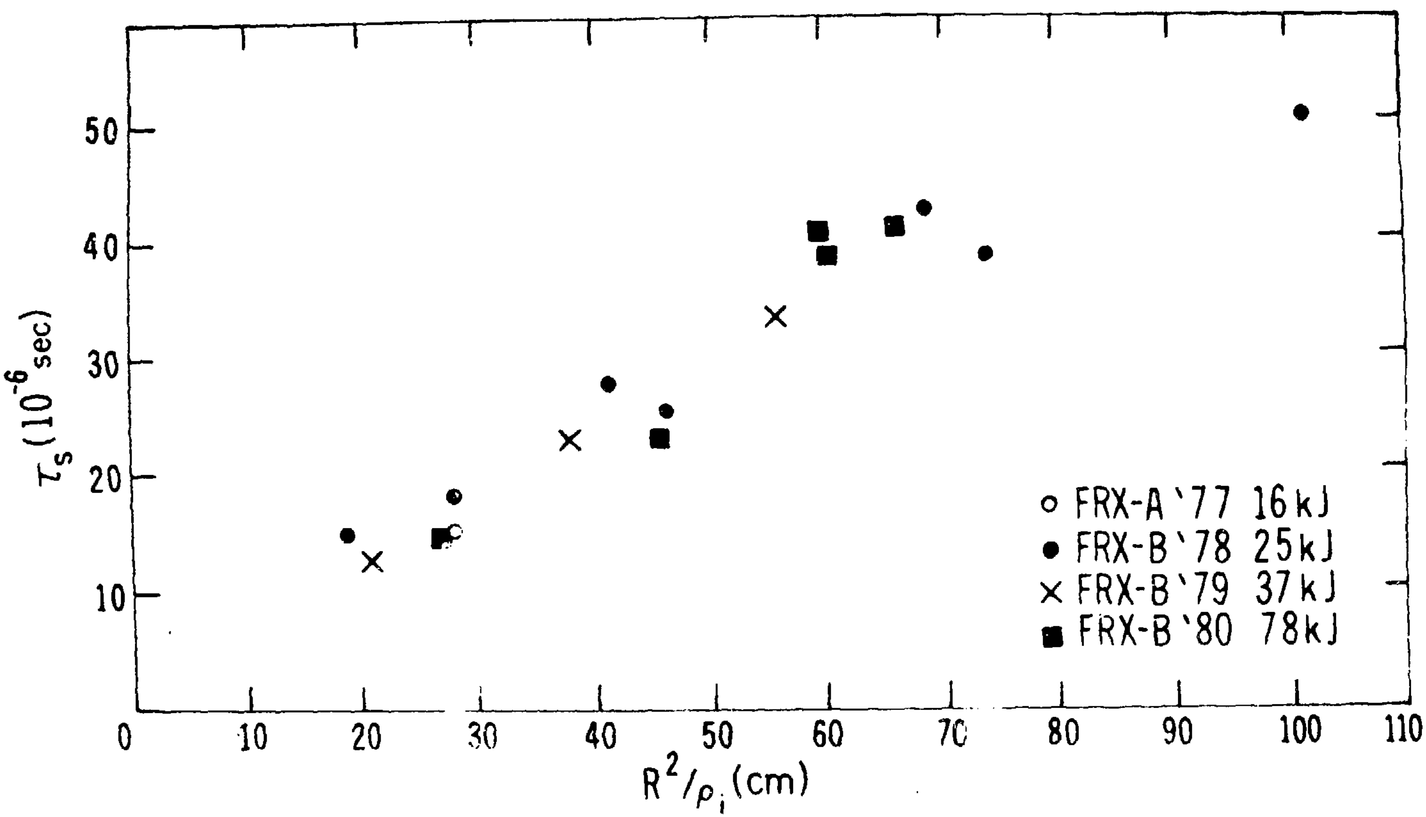

τ_s (10^{-6}sec)
50
40
30
20
10
0
10
20
30
40
50
60
70
80
90
100
110
R^2/ρ_i (cm)
FRX-A '77 16 kJ
FRX-B '78 25 kJ
FRX-B '79 37 kJ
FRX-B '80 78 kJ

Figure 12b.

C. Application to High Beta Q-Machine

The next example is even more recent, based on a preprint kindly given to me by Fred Ribe. This work describes an experiment of Knox, Meuth, Ribe, and Sevillano on the High Beta Q-Machine at the University of Washington.[15] This experiment is a theta pinch in which an original bias field is applied and a magnetic field of opposite sign is imposed at the surface. This produces a reversed field configuration, although the time scale of the experiment may not permit field reconnection. The experiment is 300 cm long with a 10 cm bore.

The experimental results are that within 1 μs half to three quarters of the magnetic bias flux is trapped. The trapped flux then decays in about 1 μs to a plateau value in which about 25 percent of the flux is trapped and then subsequently decays on a comparable time scale, until the flux is released. Probes are used to measure the magnetic field as a function of time and analytic calculations are then used to deduce the resistivity as a function of time. Figure 13 is an experimental result in which the internal flux is plotted as a function of time for three different values of field pressure. Notice that the characteristic decay times are several microseconds. A little bit of analytic work shows that the magnetic profiles can be described in this sort of experiment as a Bessel function

$$B = B_0 \exp(-t/\tau) \qquad r < r_0$$

$$B = [B_1 J_0(\alpha r) - B_2 Y_0(\alpha r)] \exp(-t/\tau) \qquad r > r_0$$

where $r_0 \simeq 4$ cm and $\alpha = (4\pi/\eta c^2 \tau)^{\frac{1}{2}}$ is the inverse diffusion length. By comparing the magnetic profiles with the profiles predicted by the theory, the resistivity can be deduced from the magnetic shape. Magnetic shapes are shown in Figure 14. These are experimental values and in the various curves the magnetic profile at 0.3, .5, 1, 2, and 6 microseconds is shown. The values between 1 and 2 microseconds are values which are used by the researchers in deducing the resistivity. They conclude that the experimental value of the resistivity is of order 1.3×10^{-4} ohm-m, while, using the measured values of temperature $T_e \simeq 30$ eV, they conclude that the classical resistivity is of order 8×10^{-6} ohm-m. Clearly the experimental value of resistivity is substantially greater than predicted classically; therefore, other loss mechanisms are required. One possible loss

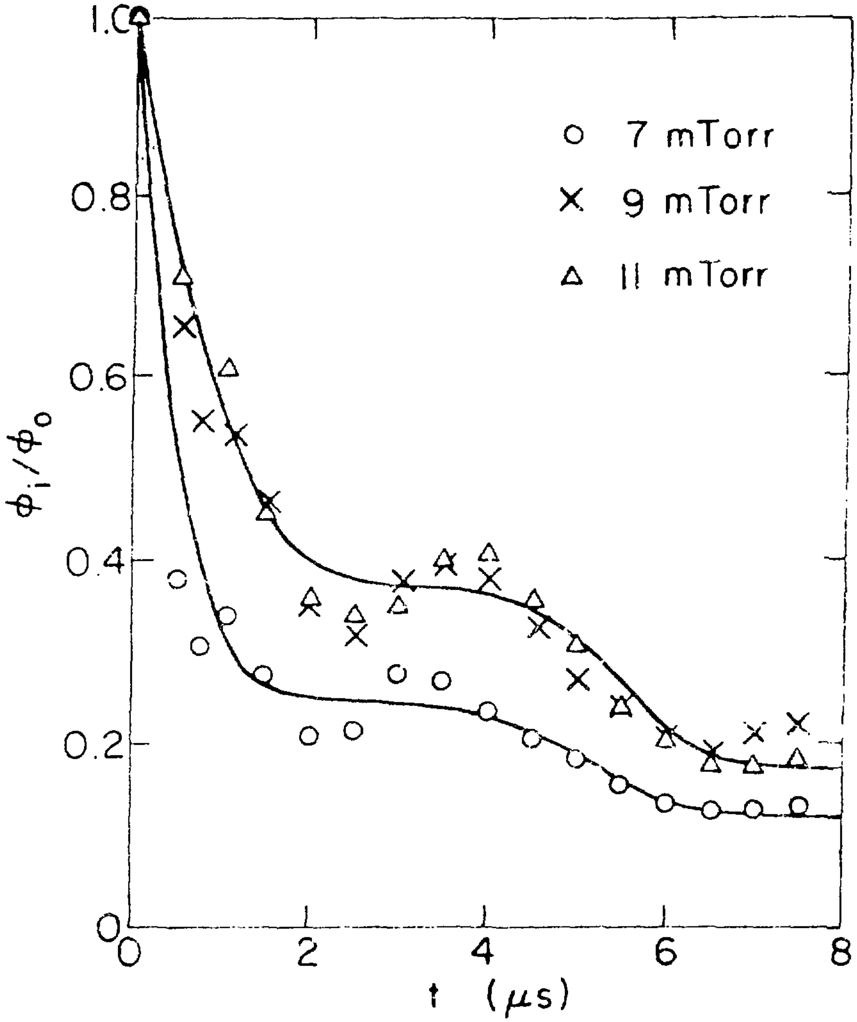

Figure 13.

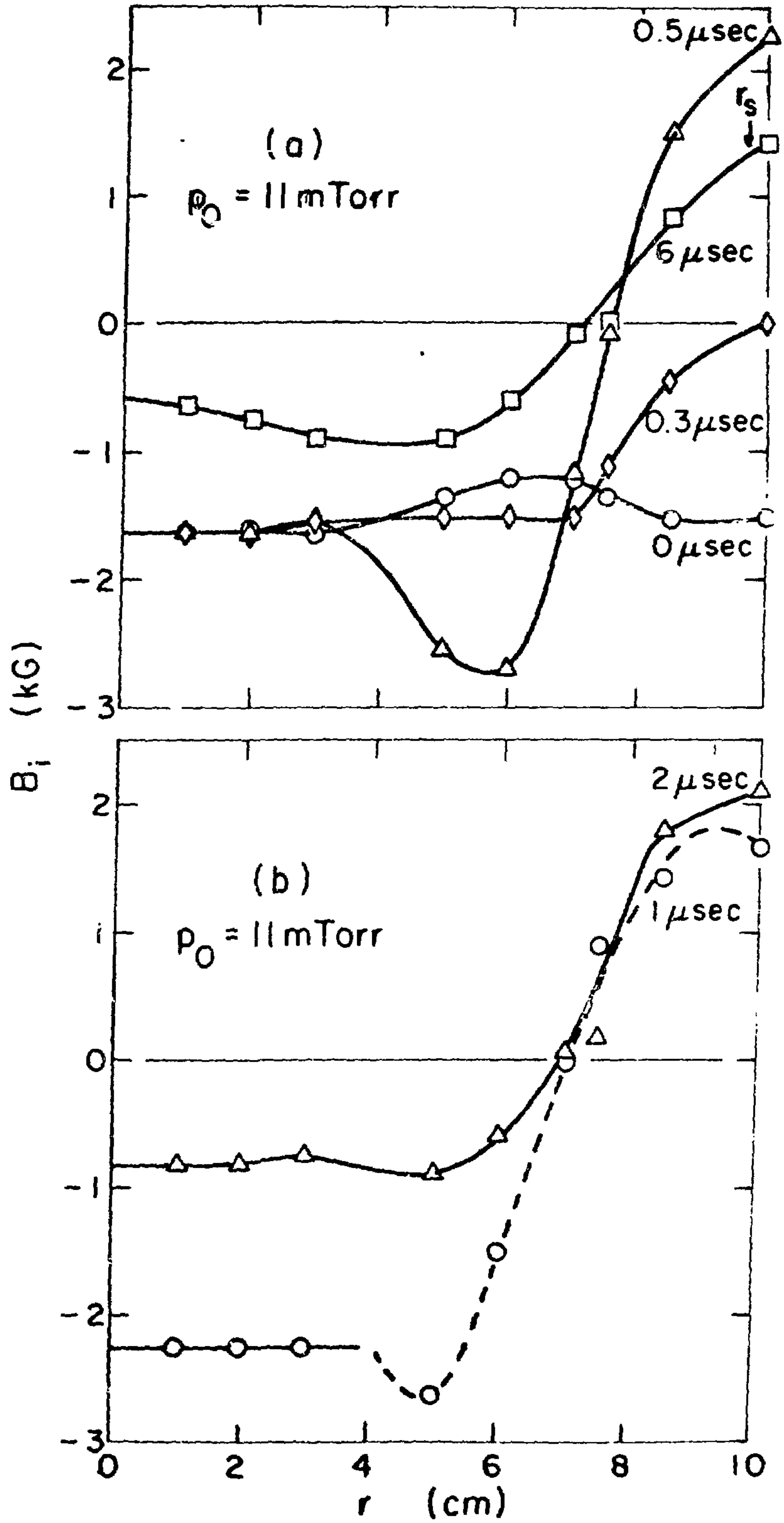
0.5 μsec
2
r_s
(a)
1
p_0 = 11 mTorr
6 μsec
0
0.3 μsec
-1
0 μsec
-2
-3
B_i (kG)
2 μsec
(b)
1 μsec
p_0 = 11 mTorr
0
2
4
6
8
10
r (cm)

Figure 14.

mechanism is end loss. An analysis of the classical predictions for end loss gives an end loss time $\tau_E \simeq 14$ μs. Another source of energy loss is radiation due to impurities. Oxygen V and Oxygen VI are expected to be the dominant impurities in the system and this is confirmed spectroscopically. They observe that the radiation time for temperature loss is given by $\tau_{RAD} \simeq 22$ μs. So having deduced that the experiment is not dominated by classical resistivity, the experimenters did not simply turn to anomalies, but first calculated the other processes that seemed plausible. They concluded that those processes would operate on time scales which were substantially longer than found in the experiment. Therefore, they turned to anomalous resistivity calculations previously published by Davidson and Gladd[16] which they felt would apply to the experiment. In order to perform the application, it was required to make some modifications in the parameter range of the theory, which was based on lower-hybrid-drift waves, and having made these modifications they concluded that the resistivity due to lower-hybrid waves should be of order $\eta \simeq 0.95 \times 10^{-4}$ ohm-m. In making that estimate a fluctuation level had to be used. The fluctuation level was taken to be that given by Liewer and Davidson[17] which was based on an energetic bound to the allowed level. The agreement is good: certainly the calculation of Davidson and Gladd is a space averaged calculation, while the magnetic properties certainly vary strongly across the layer, in fact going through a null point. The Davidson and Gladd calculations are presumably applicable only away from the null point. Nonetheless, the agreement leads the experimentalists to conclude that the observed resistivity is quite consistent with the lower-hybrid predictions. Since Gladd and others have done further work on this problem, I would like to comment that there is a nagging problem with this analysis, which is, that the lower-hybrid waves are apparently relatively localized away from the magnetic null point. A similar effect has been observed in particle simulations performed very recently. In trying to connect these two regions of lower-hybrid instability with a central region in which there is apparently no instability we have to do something creative. What we should do in fact is do a little further research on the topic. Nonetheless, the agreement found by Knox, et al., certainly motivates this further research.

III. ANOMALOUS DIFFUSION IN TOROIDAL SYSTEMS

I now would like to turn to some anomalous transport work, done recently for toroidal systems, that is not based on lower-hybrid modes.

A. Resistive Interchange, $\eta\beta$-II

As a first example, I describe a calculation due to Manheimer[18] which calculates the effect of resistive interchange modes on Reversed Field Pinches. This recent paper was motivated by the results of $\eta\beta$-II.[19] The work is based on quasilinear theory and starts with the magnetic geometry

$$\vec{B} = B_o\left[\hat{z} + \frac{x}{L_S}\hat{y}\right] \tag{14}$$

and uses that geometry to analyze resistive interchange modes. These modes are well known to be unstable and from the linear theory of these modes, perturbed values of velocity magnetic field and growth rates are predicted.

$$\tilde{v}_x = \frac{ik\ell^2}{x}\tilde{v}_y = -\frac{\eta c^2}{4\pi(\partial B_y/\partial x)\ell^2}\tilde{B}_y$$

$$= \tilde{V}_o \exp -\frac{1}{2}\left(\frac{x}{\ell}\right)^2 \quad ,$$

$$\tilde{B}_x = -ik\frac{4\pi\tilde{V}_o}{\eta c^2}\frac{\partial B_y}{\partial x}\ell^3\left(\frac{\pi}{2}\right)^{\frac{1}{2}}\operatorname{erf}\left(\frac{x}{\sqrt{2}\ell}\right) \quad ,$$

$$\ell = \left(\eta c^2\right)^{1/3} k^{-1/3}\left(\frac{\partial B_y}{\partial x}\right)^{-2/3}\left(-g\frac{\partial\rho}{\partial x}\rho\right)^{1/6} \quad ,$$

$$\gamma = \left\{-g\frac{\partial\rho}{\partial x}k\left(\frac{\partial B_y}{\partial x}\right)^{-1}\right\}^{2/3}\left(\frac{\eta c^2}{\rho}\right)^{1/3} \quad . \tag{15}$$

The theory now assumes that the resistive interchange mode develops according to linear theory until a steady state is reached in which the fluctuating values of magnetic field, velocity, scale size, and so on are given by the linear values. This is, therefore, a quasilinear calculation. Ohms law

$$E_z = \frac{(\tilde{V}_y B_x{}^* - \tilde{V}_x B_y{}^*)}{c} + \text{c.c.} + \eta J \tag{16}$$

now requires that the resistive interchange mode will give rise to an electric field parallel to the toroidal magnetic field. This electric field can be used to predict the diffusion of the magnetic field and therefore the decay of the reversed field pinch geometry.

$$\frac{\partial B_y}{\partial t} - \frac{\partial}{\partial x}\frac{\eta c^2}{4\pi}\frac{\partial B_y}{\partial x} = -\frac{\partial}{\partial x}(\tilde{V}_x\tilde{B}_y{}^* - \tilde{V}_y\tilde{B}_x{}^*) + \text{c.c.}$$

$$= 2\frac{\partial}{\partial x}\sum_i \frac{4\pi}{\eta c^2}\left|\tilde{V}_{oi}\right|^2 \left\{\ell_i{}^2 \exp\left[-\left(\frac{x - x_i}{\ell_i}\right)^2\right] + \left(\frac{\pi}{2}\right)^{\frac{1}{2}}\ell_i(x - x_i)\ \text{erf}\left(\frac{x - x_i}{\sqrt{2}\,\ell}\right) \cdot \exp\left[-\frac{1}{2}\left(\frac{x - x_i}{\ell_i}\right)^2\right]\right\}\frac{\partial B_y}{\partial x} \tag{17}$$

A second prediction can be made and that is the energy transport which depends on $\vec{J}\cdot\vec{E}$ given by the quasilinear theory. To produce quantitative results from Eq. (16) and Eq. (17), it is required to develop a saturation model for the instabilities to deduce the value of fluctuations in magnetic field and so on in steady state. As a possible mechanism, Manheimer suggests that as the perturbed velocities increase they eventually will reach a value comparable to the sound speed. When this happens, it is plausible that the interchange energy will then compress the plasma rather than produce plasma waves, and this assumption is used to deduce the saturated value. The saturated value can then be used to produce a diffusion coefficient which is proportional to the cube root of the resistivity

$$\tilde{V}_0/k\ell v_s \approx \left(24\sqrt{3}\ \ell^2/r^2\right)^{\frac{1}{4}} \quad , \tag{18}$$

$$D \approx \tfrac{1}{2}(4\pi/\eta c^2)\ \alpha^2 k^2 \ell^4\ T/M \quad . \tag{19}$$

With this value for the diffusion coefficient, based on the given saturation mechanism, both the level of magnetic fluctuations observed in $\eta\beta$-II and the decay time observed in $\eta\beta$-II is found to be in agreement with this quasilinear prediction based on the resistive interchange mode. It would be interesting to compare this theory with the results that are recently obtained by ZT-40 now that ZT-40 has achieved a quiescent phase similar to that of $\eta\beta$-II.

B. Dissipative Trapped Electron Tokamak Transport, I

In discussing the anomalous transport in toroidal systems, it would be a major oversight not to at least mention the situation in tokamak. For one thing, the tokamak is much more thoroughly explored. For a second thing, there is a general conception that anomalous transport theory has been very ineffective in describing tokamak development and, thirdly, there may be some similarities down the road between the behavior of spheromak and experience in tokamak.

Many of you are probably familiar with the major review on transport in tokamak, published by Paul Rutherford in Nuclear Fusion,[20] so I would like to discuss, instead, two possibly less well known calculations on the same line. The first one is by Horton, et al.,[21] and is an example of an attempt to explain heat loss in transport in tokamak by trapped electron instabilities. Horton uses standard techniques for the drift wave trapped electron mode to estimate the particle flux beyond the q = 1 surface, as well as the spectral distribution of fluctuation.

$$\Gamma_{d\omega} = \frac{nc\,T_e}{eB} \sum \left(\frac{e\phi}{T_e}\right)^2 k_y\ (\Delta \mathrm{Im}\ G^0 + \eta_e\ \mathrm{Im}\ G^1) \quad ,$$

$$\Delta = 1 - \omega_k/\omega_* \quad , \quad \eta \sim d\ell n\ T/d\ell n\ n$$

$$\Delta G^0 + \eta G^1 = 1 - \frac{\tilde{n}_k\ T_e}{n_0 e \phi_k} \tag{20}$$

These fluxes and distributions are obtained in terms of the linear properties of the mode and the level of fluctuations; therefore this calculation is also a quasilinear type calculation. Because of the inhomogeneity of the plasma density and temperature, there is a level of free energy in the plasma.

The turbulent energies that appear in Eq. (20) are taken to be a constant fraction of the free energy available to the modes in all regions where the plasma is in fact unstable. With this assumption, the flux and the spectrum are compared with experiment for a wide variety of experimental cases. Figure 15 shows the ratio of the observed flux to the flux predicted by drift wave theory as a function of radius in the tokamak. The comparison is only made outside the $q = 1$ surface because of the assumption that MHD effects will dominate inside that surface. A large number of cases are described in the two graphs of Figure 15: one set from the TFR tokamak, and the other from Ormak. In the case of TFR, the observed flux is roughly half of the anomalous transport theory flux over a wide range of radius and experimental conditions. For Ormak, the observed flux is about one third of the theoretically predicted flux, also over a wide range of experimental conditions.

In Figure 16 a comparison is shown between the spectrum of density fluctuations observed in the ATC tokamak indicated by the bars and the linear growth rate as a function of wavenumber indicated by the solid line. These researchers were pleased that there was some correspondence between observed spectra and theoretically predicted unstable spectra, and also encouraged by the fact that the observed to predicted flux was a constant ratio over such a wide range of conditions. But the proportionality constant between theory and experiment changed substantially from device to device. Moreover, there was no clear theoretical way to choose this constant. The correlation between theory and experiment appear significant, but to obtain a really predictive aspect of this theory something else is clearly required.

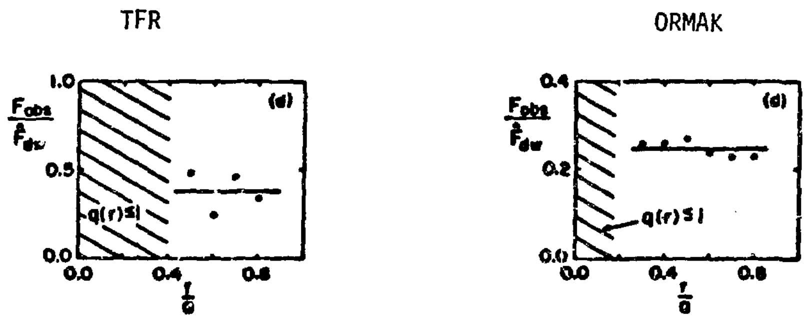

Figure 15.

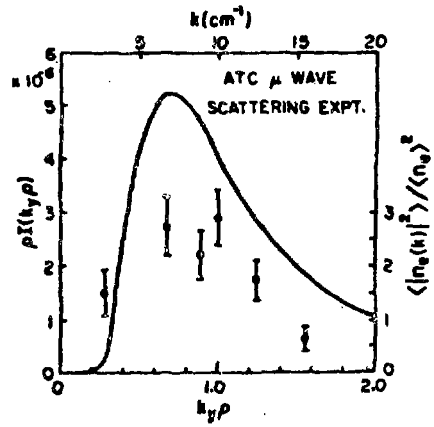

Figure 16.

C. Dissipative Trapped Electron Tokamak Transport, II

Next, I describe a modeling due to Cotsaftis, et al.,[22] in which again the dissipative trapped electron mode is a primary input to anomalous resistivity but which recognizes that in fact there is a layered effect in the tokamak, e.g., considers the tokamak as a highly structured system. Inside the $q = 1$ surface, the transport is expected to be due to MHD effects, so Cotsaftis uses the transport due to sawtooth oscillations to dominate inside the $q = 1$ surface. In an annulus toward the middle of the plasma a substantial fraction of the particles are trapped and the trapped electron modes are assumed to be the dominant transport mechanism. In the outer fringes of the plasma the temperature is low, the plasma is substantially more collisional than in the center, and the assumption is that resistive modes and such will probably dominate. In the model, the assumption is that the transport in the outer layers of the plasma is in fact due to a current driven thermal instability which had been worked out by Cotsaftis to explain current penetration in TFR. The same general structure of this instability that was used to explain current penetration is used in calculating the resistivity in the outer layers of the plasma. This instability naturally disappears as the plasma temperature rises going inward into the device. The actual form of the transport taken is shown in Eq. (21).

$$K^{CT1} \sim \frac{1}{n_e T_e} \quad ; \quad K^{TED} \sim \left(\frac{r}{R}\right)^{3/2} \frac{T_e^{\;3.5}}{n}$$

$$K^{SR} \sim \left(\frac{r_o}{R}\right)^2 \frac{BV}{nT} \quad , \quad q < q_o \tag{21}$$

Note this calculation is particularly interesting in the context of the present talk because we stress the importance of taking local stability conditions and using these conditions in global transport models in order to obtain a realistic description of the experiment, and in the model described here there has been an attempt to separate the plasma into regions of various physics behavior and to input into the model the anomalous transport mechanisms into those regions.

These transport effects were incorporated into a one-dimensional transport model of the same sort described earlier in the talk, but in this case of course with tokamak-type geometry. Predictions for electron temperature, density, and so on as a function of radius and time were made for various values of plasma current and various time behaviors of plasma current. Comparison was made with the results from the TFR tokamak.

In fact, Cotsaftis conceived this problem originally because of a specific effect that was observed in the TFR. This effect was that at relatively low input energy, which was the most usual case, the current increased rapidly with time, the electron temperature increased rapidly with time, and both formed a plateau which lasted for several hundred milliseconds. The electron temperature, that is, rose monotonically and then plateaued. In a relatively fewer number of cases there was substantially greater input energy to the TFR and the plasma became substantially more collisionless, the electron temperatures becoming substantially higher. In this case, although the current again rose quickly to a plateau, the electron temperature rose to quite a large value and then declined to its plateau. The electron temperature, therefore, overshot its equilibrium value and decayed back to an equilibrium type value which it maintained for several hundred milliseconds. This behavior is shown in Figures 17a and 17b. The idea was that since there was a change in TFR behavior between the low input energy and the high input energy cases, that there was probably a physical effect that was onsetting between those two cases and that a most plausible physical effect was the appearance of trapped electron modes in the more collisionless case shown in Figure 17b.

An estimate of linear stability theory did show that the lower temperature cases of 17a were not expected to be unstable to the trapped electron mode while the parameters of 17b were unstable to this mode. The calculation was carried out integrating the fluid equations numerically and the results are shown in Figures 18 through 21. Figure 18 shows, indicated by the solid lines, that the model does in fact give the overshoot of electron temperature with time as found in the experiment. The ion temperature in contrast does not show this overshoot and increases monotonically to its plateau value. For comparison, the dotted lines show neoclassical predictions. The electron temperature, as is well known, is much smaller in the experiment than would be predicted by neoclassical theory. Figure 18 shows, however, that the ion temperature also is smaller by a factor of about 1.5 than predicted classically. This is because, as you will recall from the early part of this talk, the transport effects as they evolved from the Vlasov equation are present for all species and depend

(a)

(b)

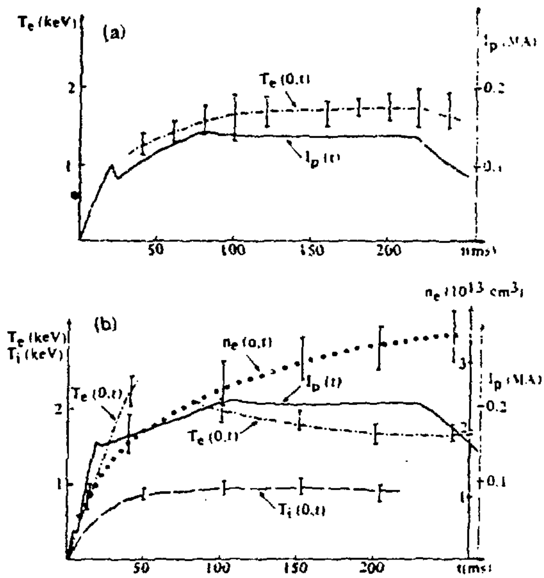

Figure 17.

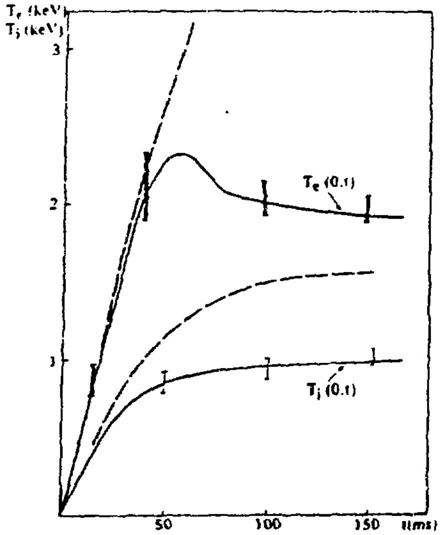

Figure 18.

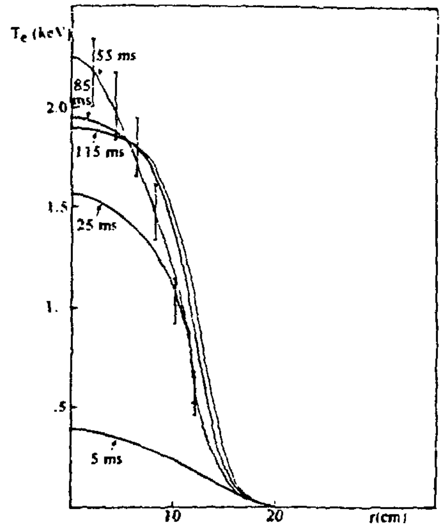

Figure 19.

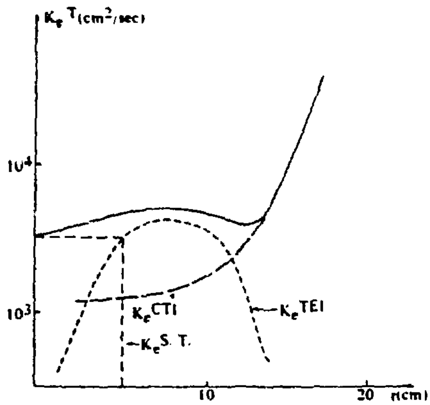

Figure 20.

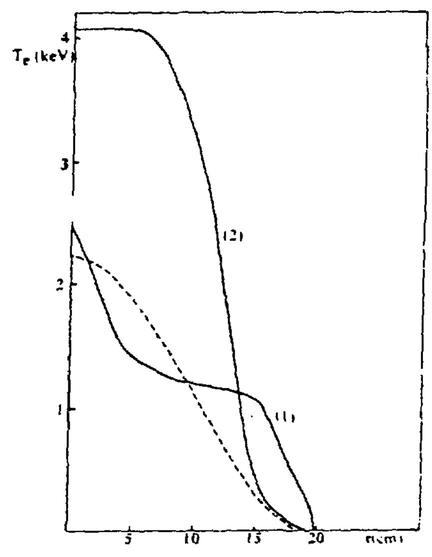

Figure 21.

on the density and electric field fluctuations which are determined by the plasma dielectric; there will be a relation between the transport anomalies of various species. So, we were not surprised to find this change in ion temperature from neoclassical predictions, since anomalous transport theory in fact gives a well defined relation between the electron and ion anomalous conductivity

$$K_{ion}^{TE} \simeq \frac{3}{7}\left(\frac{d\ell n\ T_e}{d\ell n\ n_e}\right) K_e^{TE} \quad . \tag{22}$$

At the time there was a general feeling that ions were neoclassical, probably because ion transport was classically substantially greater than electron transport, and therefore the anomaly (which was a given fraction of the electron anomaly) was masked by neoclassical effects. We predicted, however, that as the temperature increased and the plasma became more collisionless, then the anomalous ion transport would eventually emerge and be noticeable as it was in pinch experiments. Figure 19 shows the temperature profiles as a function of time predicted by the model, starting at 5 milliseconds, rising to a maximum at 55 milliseconds and then decreasing to a plateau at about 85 milliseconds. The experimental values were shown by the bars at 55 milliseconds but similar agreement is obtained throughout the run, at least in those times at which the experiment measures the profiles. A common problem with tokamak modeling has been that the trapped electron transport, while giving reasonable results for confinement time, in many cases fails in predicting the profiles. This is described in some detail in Rutherford's article.[20] In the present calculation, the inclusion of the current thermal instability near the cool plasma boundary has a fairly substantial effect in giving profiles that are smooth and agree with experiment. This is shown also in Figure 21 in which a calculation with trapped electron modes only was carried out giving again reasonable central temperatures but very unrealistic profiles. We note again that the current thermal instability was originally invoked to explain another discrepancy between theory and experiment, namely, profiles and penetration times during the current formation stage of tokamak.

Figure 20 shows the interplay between MHD, trapped electron, and current thermal instabilities as a function of radius, each doing their part in the region in which they are naturally excited. The calculation was also done using various forms of empirical thermal conductivity. The empirical transport simply does not reproduce the electron temperature as a function of radius and time, although it is not too difficult to write down an empirical number which in the present range of experiments would give the central value of the electron temperature; after all, that's where empirical models come from. So, in concluding this tokamak section, I would say that the tokamak modeling has not been as bad as it is sometimes made out to be. In fact, I think that tokamak modeling was very much on the right track. A problem with tokamak was ironically that there was such a wide range of experimental results that there was a constant temptation to abandon this very painstaking, tedious modeling with anomalous effects and simply retreat to things that we knew very well, namely, the measurements. This tendency to replace the model by empirical results proved to be an overwhelming temptation and in the last few years empirical scalings have dominated the planning process for tokamak. In fact at this stage, Cotsaftis and many other tokamak modelers simply were forced out of the game and should not be blamed for the present situation, in which some of the so-called theoretical predictions (which were in fact really only empirical projections) have proved not to hold for the more advanced examples of tokamak.

IV. BEYOND QUASILINEAR THEORY

In the brief time left, I would like to discuss a few of the advances that have been made beyond quasilinear theory and then indicate some new directions that I think are necessary for continued success of anomalous transport applications. The references and names are not close to being complete, and are meant to be indicative of typical approaches.

<u>Advances Beyond Quasilinear Theory</u>

Resonance Broadening	Dupree[23]/Galeev[24]
	Weinstock[25]
	Davidson, Caponi[26]...
Renormalized Turbulence Theory	
Direct Interaction Approx.	
	Orszag[27]/Kraichnan[28]
	Martin, Siggia, Rose[29]
	Krommes, Kleva[30]...
Generic Effects	Taylor[31]
	Manheimer, Finn[32]
	Chu[33]
	Krall, McBride[34]
	.
	.
	.

A. Resonance Broadening

The most widely explored of these advances is that of resonance broadening. Resonance broadening is in fact not really a departure from quasilinear theory at all; it simply uses the quasilinear dielectric and the quasilinear diffusion but includes in the orbits the effect of the quasilinear diffusion on the particle orbits themselves.[23,24] Thus, the linear dielectric is replaced by a nonlinear dielectric which includes these orbit effects.

$$\chi(k,\omega) \to \chi^{N.L.}[k,\ \omega + i\Delta\omega_k(v)] \quad , \quad \Delta\omega_k = k^2 D(k,\omega) \tag{23}$$

One recent example was given by Huba and Papadopoulos,[35] applying resonance broadening theory to the lower-hybrid-drift wave discussed earlier in the present talk. In this case, replacing the electron dielectric by its nonlinear extension, one can again calculate from the dispersion relation an equation for the resonance broadening in terms of ω and k in steady state, steady state meaning when the growth rate of the instability equals zero because of the effect of the resonance broadening term.

$$1 + \chi_i + \frac{2\omega_{pe}^2}{k^2 v_e^2}\left[1 - \int_0^\infty ds \, \frac{2s \exp(-s^2)\Lambda J_0^2(\sqrt{2}\,\mu s)}{\omega - kV_E - k\overline{V}_B s^2 + i\Delta\omega_k(s)}\right] = 0 \quad ,$$

$$s = v_\perp/v_e \quad , \quad \Lambda = \omega - kV_E - kV_{de} \quad . \tag{24}$$

Secondly, the diffusion equation itself gives the resonance broadening contribution in terms of the level of the field fluctuations

$$\Delta\omega_k = \frac{\omega_{pe}^2}{\omega_{ce}^2}\,\frac{T_i}{T_e}\left(k^2 v_e^2 \int_0^\infty ds \, \frac{i\ s \exp(-s^2)J_1^2(\sqrt{2}\,\mu s)}{\omega - kV_E - k\overline{V}_B s^2 + i\langle\Delta\omega_k\rangle_{k=k_m}}\right)\frac{\epsilon_F}{nT_i} \quad . \tag{25}$$

Combining the two expressions for $\delta\omega$ gives a determination of the fluctuation level and therefore a determination of the diffusion coefficient.

Huba and Papadopoulos only calculate the level of fluctuations given by this consistent treatment of marginal stability due to orbit diffusion, but it is fairly easy to extend their calculation, using the definition of resonance broadening, to determine the transport. Clearly, in order to produce marginal stability, the theory will give a resonance broadening frequency of order the linear growth rate. Since the resonance broadened frequency must be comparable to the linear growth rate in order to give the cancellation that leads to a stationary state, and since the resonance broadened frequency is proportional to the diffusion coefficient, it follows that the diffusion coefficient according to the resonance broadening theory (at least in the lower-hybrid-drift mode) is closely equal to the value $D \simeq \gamma/k^2$, which you will note is precisely the relation given by Kadomtsev, et al.,[1,2] in the earliest days of anomalous diffusion theory. I do not know what to make of this, exactly, except that there is often more to guesswork than meets the eye.

I emphasize again that there are many other examples besides the one given on application of resonance broadening including, for example, the work of Davidson and Caponi on resonance broadening of acoustic waves and so on.[26] I emphasize also that the resonance broadening theory is actually equal to a quasilinear theory of diffusion with the level of fluctuations determined by stabilization of the wave due to orbit modification by the fluctuations themselves. I had several other examples which time does not permit me to give, but they all follow the same trend. The linear and quasilinear equations are used to give the diffusion due to a specific mode and some model is used to estimate the fluctuation level. It is also a general trend that considerable attention is given to the specific mode which drives the turbulence, and the stability properties are quite well worked out. On the other hand, in general, there is not nearly as systematic an effort to determine the fluctuation level. Generally, there seems to be plausible mechanisms which would certainly limit the growth of the waves and these are taken in providing estimates. There are few cases in which an effort as elaborate as those involved in the linear stability theory is made to determine which of various competing mechanisms would provide, in a specific case, the fluctuation level.

B. Renormalized Turbulence Theories

When I was preparing this talk, it was my intention to go into some depth on the direct interaction approximation and renormalized weak turbulence theory,[27-30] but on closer examination of the literature it seemed to me that these theories, while important, have not yet reached a stage where their impact on anomalous diffusion theory can be felt. A primary contribution of this work is to set on a consistent and systematic basis the various nonlinear effects which have been invoked in other theories. Clearly, the nonlinear treatments should include the quasilinear theories[4] which are both plausible and tested in many cases, but should also include the orbit modifications and other nonlinear wave and wave particle interactions. The earliest approaches in turbulence are based on the reasonable technique of expanding the fluctuations of the particle distribution function as a power series in the fluctuating electromagnetic fields, $\delta = [E^2/8\pi]^{\frac{1}{2}}$.

The quasilinear equations truncate the expansion to first order, treating the fluctuations as linear. The associated background distribution function consists of two parts: a resonant part which evolves in time according to a diffusion equation, with rate coefficients proportional to the fluctuation intensity, and a nonresonant part which describes the sloshing motion of the particles in the waves. In the usual weak turbulence theory the fluctuations are expanded to third order and the fluctuation spectrum is constructed to fourth order using the random phase approximation.[36,37] The associated equation for the evolution of the plasmon density N_k,

$$\frac{\partial N_k}{dt} \sim 2\gamma_k N_k + \sum_{k_1} M_{k,k_1} N_k N_{k_1}$$

$$\cdot\ \delta(\omega_k - \omega_{k_1} - k\cdot v + k_1\cdot v) + \sum_{k_1 k_2} M_{k_1 k_2 k} N_{k_1} N_{k_2} N_k \;,$$

$$\cdot\ \delta\left(\omega_{k_2} - \omega_{k_1} - \omega\right)\, \delta(k_2 - k_1 - k) \tag{26}$$

contains the linear growth term, the first RHS term of Eq. (26), the induced scattering and nonlinear Landau damping terms which are the second terms of RHS Eq. (26), and three wave interaction terms, the third term of RHS Eq. (26). Such equations have been used successfully in describing the evolution and saturation of a large number of plasma instabilities. Despite this history of success, the weak turbulence theories are now recognized to be deficient in a variety of respects.[30]

1. This theory is generally correct only for a continuous spectrum. If the spectrum is discrete because of finite spatial boundaries or because the system is immersed in a magnetic field, the steady-state, quasilinear diffusion operator formerly involves a series of delta functions at each of the wave particle resonances. This is because the diffusion coefficient involves force correlations which in linear theory do not decay asymptotically to zero but

rather recur on a wave time scale. Nonlinearly, in many cases however, the correlations do decay because of either stochasticity arising for example from island overlaps, or other statistical effects. These decay mechanisms have only recently been discussed, so it is really not practicable to go into much detail here on their effect. The important thing, however, is that it appears that stochastic effects lead to test particle diffusion in phase space, which affects both the background distribution and the fluctuating distribution. The quasilinear theory only predicts the effect of this diffusion on the background distribution $<f>$.

2. Diffusion is basically a nonanalytic process. This is because it has elements of Compton scattering, which is well known to be divergent in the case of linearly resonant particles. The Compton scattering process is one in which a particle absorbs a plasmon and then emits another plasmon because the waves cause particle jitter about their free orbits. The divergence of Compton scattering in the case of linearly resonant particles is because the actual particle orbit is not a free orbit but should more correctly include the perturbation of the orbit by the presence of all waves except the test wave. Statistically, such orbit perturbations can be described by a diffusion process. You can see the elements of resonance broadening in this kind of effect.

3. The resonance broadening theories have been a very important advance both because they fit within the framework of quasilinear theory and thus are tractable in producing specific results, but also because they have the elements of self-consistency, namely, the effect of the waves in the orbits are included and so they begin to nibble at the edges of a truly consistent treatment of the turbulence problem. However, they have their flaws; in particular, the resonance broadening formulations in general do not conserve energy. It is easy to see why. The particles respond to a test wave and eventually, by orbit diffusion, cause

the wave to damp. The truth is, of course, that the background wave distribution is not an infinite sink for energy but must conserve energy. Therefore the interaction of the test waves through the particles on the background should also be considered. Formulations of resonance broadening in this way would produce energy conservation and may alter the present prediction of the formalism. Doing this sort of thing properly amounts to a renormalization of the plasmon propagater, but the systematology of the approaches so far taken is not particularly clear; it is clear they are fairly tedious, and at present I am not able to extract a prediction of these more consistent looking theories to compare with the predictions of the nonenergy conserving resonance broadening theories. However, in the case of primary resonances, $\omega_k - \vec{k}\cdot\vec{v} \simeq 0$, where the simplest weak turbulence theories may not be valid, the direct interaction approximations do give a formalism that contains terms that can be identified with appealing physical processes, giving some hope that there will be practical consequences in the models. Such processes for example are: a diffusion of the shielded test particles due to stimulated emission and absorption of fluctuations, resonance scattering of the test particle by the plasmons, a "pondermotive" renormalization of the background distribution due to the emission of fluctuations in the previous process, drag terms due to polarization associated with the stimulated emission and absorption waves and, lastly, associated pondermotive effects. In stochastic acceleration problems, where the potential is specified externally, only the diffusion term remains in the simplest orbit diffusion or resonance broadening theories.

Where these theories now really stand is that they provide an organized and convenient starting point for systematic derivations of turbulence in various approximations. What approximations will be developed remains to be seen.

C. Global/Generic Analyses

Lastly, I would like to consider a couple of examples of what might be called generic calculations; that is, calculations that do not rely on a specific model for stability or turbulence but produce results which are somewhat model independent. Some of this work is really based on the success that J. B. Taylor[31] has had with his models of conservation of helicity in reversed field pinches. Theories of this sort (as Taylor's, which predicts profiles in terms of states to which a plasma may relax, without specifying the mechanism for relaxation or without specifying the efficiency of competing mechanisms) are very powerful. They have gaps, of course, in that it is not always easy to determine exactly whether they should apply, but nonetheless, as a guidance tool they prove particularly valuable in analyzing RFP's.

In the spirit of Taylor, Chu[33] has provided me with a preprint of a paper which takes the following approach: In reversed field pinch, there will be fluctuations, but there will be a tendency the system to relax toward Taylor states. The possibility exists that there will be a continuous inpouring of energy or interaction between the walls of the system and the plasma, and that there will be an excited set of magnetic states which will satisfy

$$\nabla \times \delta B = \frac{4\pi ne\delta V}{c} \tag{27}$$

where $\delta B \equiv B_s e^{i\vec{k}\cdot\vec{r}}$ is a fluctuating magnetic field and the density of these "magnetors" will be distributed according to photon statistics

$$n_s = \frac{1}{\exp(k_S/k_T) - 1} \quad .$$

Now, none of this is really particularly important to the basic argument of Chu. Consider magnetic fluctuations of the form given in Eq. (27); a velocity or current arises in response to these fluctuations and the drifts corresponding to the fluctuations can therefore be written in the following form:

$$V_D = \sum_{s'} \frac{ck_s}{4\pi ne} B_s e^{i\vec{k}_s\cdot\vec{r}} \quad . \tag{28}$$

Diffusion can be calculated from the particle drifts by using a correlation theory in which the correlation time is assumed to be dominated by the diffusion itself.

$$D = \int_0^\infty \langle V_D(t)V_D(t+\tau)\rangle d\tau = \int_0^\infty |V_D|^2 \exp[-Dk_s\tau]d\tau \qquad (29)$$

Thus Eq. (29) is an integral equation for the diffusion coefficient, D. Now using the simplest models for the drift velocity, V, you can see that multiplying the right-hand side, top and bottom, by D, the diffusion coefficient itself will be proportional to only the first power of the magnetic fluctuations, since the drift velocity itself is proportional to the first power of the magnetic fluctuations.

$$D \sim \frac{c^2}{\omega_p^2} \frac{e}{mc} \left[\sum |B_s|^2\right]^{\frac{1}{2}} \propto \delta B \qquad (30)$$

Now there is not much specific here since it is not easy to decide what the actual excitation level δB should be. Also the correlation time is assumed to be simply given by the diffusion coefficient D; no growth time or oscillation time appears in that equation. Nonetheless, this is a rather tantalizing result in that it is the only one I have seen in which the diffusion coefficient is proportional to the square root of the fluctuation energy rather than to the fluctuation energy itself. Also, this result says that if you have a model for the fluctuation energy, a specific scaling on density and so on is predicted. For example, if it turned out in fact that the fluctuation energy was independent of density, this diffusion coefficient would be proportional to $1/n$, which is a result often measured in tokamak. The reader is invited to check with Dr. Chu for further details.

A second example of a generic calculation is due to Manheimer and Finn,[32] based on a quasilinear comparison of the spinup of a plasma in response to fluctuations with the diffusion of a plasma in response to fluctuation. The rate of change of the poloidal velocity in terms of the plasma fluctuations is

$$\frac{\partial}{\partial t} nv_{i\theta} + \bar{v}\cdot\langle u_i u_i\rangle\Big|_\theta = \frac{ne}{m_i}\left[E_\theta - \frac{v_r B_z}{c}\right] + \frac{e}{m_i}\langle\delta n\delta E_\theta\rangle \tag{31}$$

where it is assumed of course that quasilinear theory will be used to provide the density and field fluctuations. Now in the Vlasov equation itself, assuming that the system is stationary, the right-hand side of Eq. (31) vanishes. This gives the rate of spinup proportional to the velocity components

$$\frac{\partial}{\partial t} nv_{i\theta} = -\nabla\cdot\langle u_i u_i\rangle\Big|_\theta = -\frac{1}{r}\frac{d}{dr} r\langle u_{ir}u_{i\theta}\rangle - \frac{\langle u_{ir}u_{i\theta}\rangle}{r} \tag{32}$$

which in general are produced by turbulence

$$\langle u_r u_\theta\rangle \sim \frac{\langle u_\theta \delta E_\theta \delta f\rangle}{2B} \quad . \tag{33}$$

The input to Eq. (33) is provided by multiplying the Vlasov equation by various powers of velocity and integrating over velocity. In the case of the lower-hybrid-drift wave, for example, the velocity components in (33) can be evaluated explicitly

$$\langle u_\theta \delta E \delta f\rangle = \frac{e}{m_i}\sqrt{\frac{\pi}{2}}\,\frac{nV_\theta^{\,2}}{4k_\theta v_i^{\,3}}\,\delta E^2$$

$$\eta = \sqrt{\frac{\pi}{2}}\,\frac{\delta E^2}{2m_i k_\theta n v_i^{\,3}}$$

$$V_\theta = -(cT_i/eBn)(dn/dr) \tag{34}$$

and one notes directly that this matrix element is proportional to the plasma resistivity itself. This is not restricted to lower-hybrid waves, and the result predicted by Manheimer and Finn is that the plasma should spinup in a time comparable to the resistive diffusion time produced by the fluctuations.

Now I emphasize that this result is taken from published work and is not my own. In related work,[34] I have either tended to take the system as quasi-stationary in which the spinup time would be treated as being a very long time scale compared to resistivity time, or taken the system to be responsive, that is, the spinup time can be of the same order as resistivity in which case it is not a good approximation to set the right-hand side of Eq. (31) equal to zero; rather it would be necessary to self-consistently solve the set of equations. So I am not convinced automatically by the predictions of this theory that consistent with weak turbulence theory the plasma will begin to rotate and that the time required to start rotation will be comparable to the resistive diffusion time. (There are, however, other mechanisms to relate diffusion time to spinup time.[38]) Nonetheless, this shows the extent to which one can get model independent results. These generic calculations are extremely appealing when trying to analyze systems as complex as reversed field pinches or reversed field configurations.

V. NEW DIRECTIONS

So that is where we stand, at least in my view, and a reasonable question is where should we be going. For one thing, it should be clear to anyone who has attended these sessions over the last three days that compared to the increasingly and elaborate numerical work on resistive MHD in 1, 2, and more dimensions, at a large variety of institutions, anomalous transport theory is both scarce and fragmented. I have shown work by three or four groups who are in fact not being represented at this meeting. Most of the work on anomalous transport theory is simply adapted from previous applications or is developed by researchers working fairly independently of the experimental programs en passant, while performing other research.

This is not a particularly promising situation. It would not really occur to anyone to take a MHD simulation of a stellarator performed ten years ago, simply redraw the curves, and then claim that they apply to the field reversed configuration. Nonetheless, we are often forced to take model results from theta pinch theory, for example, or tokamak theory, and apply them in the hopes that they dominate the behavior of the devices we are talking about. This is simply because relatively little systematic work is going on in developing turbulence theories for specific application to reversed field configurations, compact torus, and the like. In order that the new applications of anomalous diffusion should be as successful as the applications of several years ago, a number of obvious things must be considered:

- Geometry
- Particle Orbits, e.g., trapping, $\Delta\omega_k \cdots$
- Steady-State $\chi^{N.L.}$ $(k, \omega, \Delta\omega)$
- Nonlocal Theories
- Corona Models and Boundary Conditions
- Other Modes
  - low frequency drift
  - high beta magnetic

- drift Alfven
- others

The reason for these particular needs emerge from material quoted during this review, when you look at what was required to make the theories applicable in previous cases.

Geometry is important - the particle orbits respond to the geometry. The geometry affects both linear growth rates, the nonlinear development, the nonlinear processes which cause diffusion, resonance broadening effects, and so on.

The particle orbits which respond to the geometry enter directly into the linear stability theory, in the sense that turbulence theory is so responsive to the plasma dielectric.

Inclusion of nonlinear effects on the dielectric are obviously important. The obvious effect, of course, is diffusion due to waves including resonance broadening or development of islands which may overlap, or spread of turbulence to adjacent rational surfaces, but also may include things like detrapping which could be a mechanism of killing one of the stabilization mechanisms for the wave.

The need for nonlocal theories is clear in the cases where sharp sheaths tend to develop. In cases where properties change rapidly over a plasma profile, it is interesting and important to know whether a local instability really has sufficient nonlocal influence that it can be treated as operating over a range which includes some substantial changes in geometry.

The boundary conditions or the conditions outside the plasma are quite important. In the case of the field reversed configurations, the loss from the inside of the plasma is much determined by the boundary layer, because continuity across the boundary brings the effect of particle loss on open field lines into direct contact with the diffusion across field lines from inside the plasma. Indeed in the case of the FRX, it can be shown that a substantial change in the assumption as to how plasma is lost after it crosses the separatrix produces substantial changes in predictions for confinement time.

The reason that other modes are required should be obvious by now. The lower-hybrid wave by no means is a universally important mode. It arose in importance to begin with because in theta pinches, where it had previously been assumed that ion acoustic waves were dominant, experiments soon showed that the electron temperature was not substantially higher than the ion temperature and ion acoustic modes in those situations simply did not exist. Lower-hybrid modes had the virtue that they were more nearly independent of T_e/T_i, so they emerged in importance; however, in cases where profiles become very flat, low frequency modes should become increasingly important and these have never been properly included in the modelings. In the case of reversed field configurations, high beta modes, and high beta effects and magnetic fluctuations are particularly important. Drift Alfven waves have been cited as important in the context of field reversed configurations, and this is only the beginning.

If you want a reasonable result, you have to have a reasonable input and I think the inputs that are required are clear. I have not included a major alteration of weak turbulence theory because the present efforts seem to be to put the present weak turbulence theories on a more sound and self-consistent basis and there is no indication at present that the results of weak turbulence theories will be much modified by the present work.

REFERENCES

1. B. B. Kadomtsev and O. P. Pogutse, Nuclear Fusion 11, 67 (1971).
2. Status and Objectives of Tokamak Systems for Fusion Research, WASH-1295, UC-20 (1973).
3. N. A. Krall and A. W. Trivelpiece, Principles of Plasma Physics (McGraw-Hill, New York, 1973).
4. R. C. Davidson and N. A. Krall, Nuclear Fusion 17, 1313 (1977).
5. R. D. Bengston, S. J. Marsh, E. A. Robson, and C. A. Kapetanakos, Phys. Rev. Lett. 29, 1073 (1972).
6. P. C. Liewer and N. A. Krall, Phys. Rev. Lett. 30, 1242 (1973).
7. N. A. Krall, et al., in Plasma Physics and Controlled Nuclear Fusion Research, Vol. II, p. 483 (IAEA, Vienna, 1979).
8. I. Hening, T. Jarboe, J. Marshall, and A. Sherwood, Proc. 3rd High-Beta Workshop, ERDA-76/108 (1975).
9. A. Sherwood (private communication).
10. S. Hamasaki and N. A. Krall, Phys. Fluids 20, 229 (1977).
11. S. Hamasaki (private communication).
12. S. Hamasaki and N. A. Krall, JAYCOR Report J510-81-071 (1981).
13. W. T. Armstrong, R. Linford, J. Lipson, D. A. Platts, and E. G. Sherwood, Phys. Fluids (in press).
14. J. Lipson, et al., Applied Phys. Letters 39, 43 (1981).
15. S. Knox, et al., Phys. Fluids (to be published).
16. R. C. Davidson and N. T. Gladd, Phys. Fluids 18, 1327 (1975).
17. P. C. Liewer and R. C. Davidson, Nuclear Fusion 17, 85 (1977).
18. W. M. Manheimer, Phys. Rev. Lett. 45, 1249 (1980).
19. A. Buffa, et al., Proc. Reversed Field Pinch Workshop, LANL, April 1980.

20. D. F. Duchs, D. E. Post, and P. H. Rutherford, Nuclear Fusion 17, 565 (1977).

21. W. Horton, Jr., H. Okuda, C. Cheng, Y. Koo, W. Lee, Y. Matsuda, and M. True, Plasma Physics and Controlled Nuclear Fusion Research (IAEA, Vienna, 1979).

22. H. H. Klein, M. Cotsaftis, N. Krall, and J. McBride, Phys. Rev. Lett. 42, 1144 (1979).

23. T. H. Dupree, Phys. Fluids 9, 1773 (1966).

24. A. A. Galeev, Phys. Fluids 10, 1041 (1967).

25. J. Weinstock, Phys. Fluids 12, 1045 (1969).

26. M. Z. Caponi and R. C. Davidson, Phys. Fluids 17, 1394 (1974).

27. S. A. Orszag and R. H. Kraichnan, Phys. Fluids 10, 1720 (1967).

28. R. H. Kraichnan, J. Math. Phys. 2, 124 (1961).

29. P. C. Martin, E. D. Siggia, and H. A. Rose, Phys. Rev. A 8, 423 (1973).

30. J. Krommes and R. Kleva, Phys. Fluids 22, 2176 (1979).

31. J. B. Taylor, Phys. Rev. Lett. 33, 1139 (1974).

32. W. Manheimer and J. Finn, Phys. Fluids 24, 1865 (1981).

33. C. Chu, GA-A16320 (1981).

34. N. Krall and J. McBride, Nuclear Fusion 17, 713 (1977).

35. J. Huba and K. Papadopoulos, Phys. Fluids 21, 121 (1978).

36. A. A. Vedenov, E. P. Velikhov, and R. Z. Sagdeev, Nucl. Fusion 1, 82 (1961).

37. W. E. Drummond and D. Pines, Nucl. Fusion Suppl. Pt. 3, 1049 (1962).

38. S. Hamasaki and R. Linford, Bull. Am. Phys. Soc. 24, 1081 (1979).

MeV and GeV Prospects for Producing a Large Ion Layer Configuration for Fusion Power Generation

J. Rand McNally, Jr.
103 Norman Lane
Oak Ridge, TN 37830

Injection of multi-MeV molecular hydrogen ions into a magnetic mirror or magnetic mirror well can lead to the production of an Ion (or proton-E) Layer with prospects for fusion power generation. This involves: 1). "slow" (exponential or Lorentz) trapping of protons from dissociation and/or ionization of H_2^+ ions; 2). electron cyclotron drive of the electronic temperature to reduce the electron stopping power; 3). production of an Ion-Layer, E-Core plasma configuration having prospects for cold fuel feed with in situ axial acceleration of say D_2^+ ions in the negative E-Core; 4). ignited advanced fuel burns in the resulting high beta plasma with excess (free) neutrons available for energy multiplication or fissile fuel breeding; 5). development of a nuclear dynamo with fuel feed, plasma energy, and Ion-Layer current maintenance by fusion products; and 6). a natural divertor end loss of ashes with charge separation permitting a natural direct electrical conversion prospect.

The 100 mA cw H_2^+, 5-MeV FMIT-prototype and the 20/35 MeV FMIT accelerators under design and/or construction at Los Alamos National Laboratory will provide adequate H_2^+ beam power to generate small plasmas capable of demonstrating the principles of proton density buildup via the exponential process at 5-MeV and the Lorentz process at 20 or 35 MeV. For fusion reactor core evaluation a LAMPF size or larger (1 mA, 800 MeV H_2^{+*}, $\rightarrow$ 10 GeV) accelerator would be required to develop a GeV Ion-Layer of 1 $\rightarrow$ 5 m radius. Microwave power at 60-120 GH_z of up to about 100/1000/10,000 kw cw for the 5/20 or 35/$\gtrsim$ 800 MeV injection cases to provide buildup conditions via programmed electron cyclotron heating (ECH) in magnetic fields of about 20 to 40 kG at the midplane of the 2/1 magnetic mirror.

The basic $n\tau$ conditions for ion containment against ion-ion scatter and ion-electron slowing down are:

$$n\tau_{ii} \simeq 2 \times 10^{10}\, T_i^{3/2} / \sqrt{1-\beta}$$
$$n\tau_{ie} \simeq 6K \times 10^{11}\, T_e^{3/2} / (1- T_e/T_i),$$

with n in cm^{-3}, τ in s, T in keV, and K determined by the number of e-folds permitted in ion slowing down. Instabilities will be ameliorated by the broad velocity spectrum of the slowed down and scattered ions and their large Larmor radii; however, a magnetic well may be initially needed until beta exceeds a few percent (partial field reversal). Appropriate programming of ECH power will adjust the electron temperature and minimize the plasma potential effects as the ion density grows until an Ion-Layer is generated. During reactor core evaluation with programmed cold fuel feed into the multi-mega Joule energy plasma, the ECH power level can be reduced and perhaps even turned off when a full scale ignition of plasma occurs. It should be noted that the 300 keV protons in the DCX-1 mirror experiment were remarkably quiescent shortly after beam turn-off indicating the beam-on instability was driven by a few well-ordered, recently trapped protons.

Following generation of the Ion-Layer cold D-T or primed D-D ($\sim 1\%$ T, $\sim 8\%$ ^3He) can be fed axially into the E-Core with D_2^+, T_2^+, DT^+, $^3He^+$, and /or $^6Li^+$ ions formed by plasma reactions being accelerated into the E-Core. *Dissociation or ionization* of these ions then results in irreversible trapping of these second generation ions unless upscattering doubles their energy in the axial direction. Coulomb and nuclear elastic scattering of fuel ions as well as fusion reactions will result in large, magnetic cross-field, radial excursions of these ions leaving the electrons behind to maintain the E-Core. The charged fusion reaction products will contribute to partial or complete sustainment of the Ion-Layer.

The poloidal pinch current will satisfy the relation

$$I^2 \sim 200\, P \pi a^2 \sqrt{a/R} \sum n_o T_o,$$

where P is of order unity but depends on the particular plasma profiles of density and temperature, I is in amperes, a and R are the **minor** and major radii in cm, and $\sum n_o T_o$ is the plasma energy density in ergs. Since most of the plasma density will be resident in the ions *($T_i \sim 2T_e \gtrsim 200$ keV at $r = 0$) in a fully* catalyzed reacting D-D plasma core the ion pressure will drive an ion dominated current flow ($J \times B = -\nabla p$) which may replace in part the GeV injection beam requirements for sustaining the Ion-Layer. The charged fusion reaction products with initial ion energies up to about 15 MeV will provide a seed current to permit possible drive of the pressure gradient driven bootstrap current.

The reacting configuration will operate as a nuclear dynamo with self generation of electric and magnetic (except for external **mirror** coils) field provided appropriate fueling and ash removal can be performed. Electrons leaving the system axially at small radii and ions departing the system at larger radii will provide some direct electrical conversion prospects primarily as a result of the natural divertor action of the Ion-Layer, E-Core configuration.

This Ion-Layer, E-Core fusion reactor core offers an optimal fusion configuration for burning the advanced fuels (D-D, D-^3He, and/or D-^6Li) **for** breeding fusile (T, ^3He) fuels or fissile (^{233}U or ^{239}Pu) fuels, for direct electrical conversion, or for thrust prospects.

*References: "Prospects of a Multi-MeV H_2^+ Injection-*Accumulation Experiment", ORNL/TM-3207 (November,1970); Nucl. Fusion 11, 191 (1971); "Fusion Chain Reactor Prospects and Problems", ORNL/TM-4575 (July, 1974); "Simplified Approach to Attaining a Proton E-Layer," ORNL/TM-4965 (July,1975); "A Double Quantum Jump in CTR", ORNL/TM-4967 (July, 1975); "Physics of Fusion Fuel Cycles", Nuclear Technology/Fusion (January, 1982).

PROPAGATION OF INTENSE CHARGE-NEUTRAL
ION BEAMS IN MAGNETIC FIELDS

S. Robertson, H. Ishizuka, W. Peter, and N. Rostoker
University of California, Irvine, California, U.S.A., 92717

We present the results of theoretical and experimental investigations of the motion of intense space-charge-neutral ion beams in applied magnetic fields. The motivation for the research is to show that intense beams can be propagated into magnetically confined plasma for the purposes of heating[1] or of driving currents. First we have considered the motion of a beam incident upon a transversely oriented magnetic field. This geometry corresponds to a beam incident on the outermost magnetic surface of a tokamak or spheromak. The motion is determined by the value of $(\omega_{pi}/\Omega_i)^2 = \epsilon - 1$, where ω_{pi} is the ion plasma frequency, Ω_i is the ion cyclotron frequency, and ϵ is the plasma dielectric constant. We show that the beam penetrates into the field by transverse polarization if ϵ is sufficiently large. Second, we have considered the motion of a beam incident upon a longitudinal field. This geometry corresponds to a beam incident upon the major axis of a spheromak, linear solenoid, or magnetic mirror. We show that for a beam having a magnetic skin depth $c/\omega_{pe} \leq$ the beam radius r_o, the magnetic field is excluded from the beam and the beam is magnetically compressed.

If a semi-infinite slab beam is of finite dimensions transverse to a magnetic field, electrons and ions are deflected toward opposite surfaces of the slab and create a polarization electric field. According to Schmidt's capacitor model,[2] $\epsilon_o E_y = n_o e y_e$ where y_e is the displacement of the electrons. The y-equation of motion for the electrons is $m_e \ddot{y} = - eE_y - ev_x B_z$ or $\ddot{y} = -\omega_{pe}^2 y - \Omega_e v_x = -\omega_{pe}^2 (y + \Omega_e v_x/\omega_{pe}^2)$. The solution within the field is harmonic oscillations about a mean displacement $(\Omega_e v_x/\omega_{pe}^2)$ giving mean electric field of $E_y = - v_x B_z$. This field exactly cancels the force of the magnetic field and thus the beam continues undeflected. (The particles in the polarization layers are lost, but the rate appears acceptable for most applications.[1]) Solutions to a more exact model which includes the longitudinal forces have been obtained which show that v_x is only slightly diminished.[3-5] It has also been shown that unless $\epsilon >> (m_i/m_e)^{\frac{1}{2}}$ a virtual anode is formed and the beam is reflected.[5-8]

The experimental apparatus[5] is shown in Fig. 1. A charge-neutral proton beam is generated by an annular (11.25 cm id x 15 cm od) magnetically-insulated ion diode attached to a Marx generator delivering 140 - 180 kV. At a point 30 cm downstream a uniform beam of 12 A/cm^2 is incident upon a transversely oriented field of 0 - 6 kG. The beam current density is measured by biased Faraday cups and the beam floating potential is measured by a Langmuir probe having an internal voltage divider. Without an applied field, damage patterns (Fig. 2) taken at the downstream field boundary show a circular beam of 15 cm dia. With a field of 1400 G which should deflect single ions by 14 cm we observe a much smaller deflection of 2 cm. The beam diameter is reduced to 12 cm perhaps due to the loss of the polarization layers. A shorting metal plate inserted transverse to the field lines increases the deflection to the single-ion value. By means of the Langmuir probe, the peak potential at points along a diameter transverse to the field was determined. From the slope of a potential plot (Fig. 3) the field E_y was determined to be approximately the value given by $E_y = - v_x B_z$ up to a field of 1000 G ($\epsilon \geqslant 600$). Above 1000 G E_y did not increase, perhaps due to the required peak potential becoming large compared to the accelerating potential.

The propoagation of an intense ion beam axially into a magnetic field is similar to the injection of a gun produced plasma into a magnetic mirror. Artsimovich[9] has pointed out that the latter experiments are theta pinches when viewed from the beam frame. If $c/\omega_{pe} << r$, the magnetic field is excluded from the beam channel and the magnetic pressure gradient causes the beam to be compressed at the snowplow velocity until the increasing transverse pressure of the beam balances the magnetic pressure. Beam compression[10] by a magnetic field has been demonstrated experimentally with the apparatus shown in Fig. 4. The beam propagates into a 25 cm dia. $\times$ 1 m lucite drift tube in which dipole magnetic field is generated by a circular coil located 55 cm from the upstream end. Damage patterns taken at four depths within the field (Fig. 5) indicate that the radial collapse velocity increases with distance. The beam diameter (FWHM) is reduced from 20 cm to 6 cm and the beam current density is increased by approximately a factor of four.

This result is consistent with the snowplow model and inconsistent with a model in which the particles follow field lines. The time-of-flight to the collapse location is 100 nsec which is near to the 75 nsec collapse time calculated from the snowplow model. In addition strong diamagnetic signals are observed confirming exclusion of flux from the beam channel.

This research was supported by the United States Department of Energy.

REFERENCES

1. E. Ott and W. Manheimer, Nucl. Fusion 17, 1057 (1977).
2. G. Schmidt, Phys. Fluids 3, 961 (1960).
3. K. D. Sinel'nikov and B. N. Rutkevich, Zh. Tekhn. Fiz. 37, 56 (1967) [Sov. Phys.-Tech. Phys. 12, 37 (1967)].
4. W. Peter and N. Rostoker, to be published.
5. S. Robertson, H. Ishizuka, W. Peter, and N. Rostoker, Phys. Rev. Lett. 47, 508 (1981).
6. W. Peter, A. Ron, and N. Rostoker, Phys. Fluids 22, 1471 (1979).
7. S. Robertson and F. Wessel, Appl. Phys. Lett. 37, 151 (1980).
8. F. Wessel and S. Robertson, Phys. Fluids 24, 739 (1981).
9. L. A. Artsimovich, Controlled Thermonuclear Reactions, (Gordon and Breach, New York, New York, 1963), p. 368-369.
10. S. Robertson, to appear in Appl. Phys. Lett.

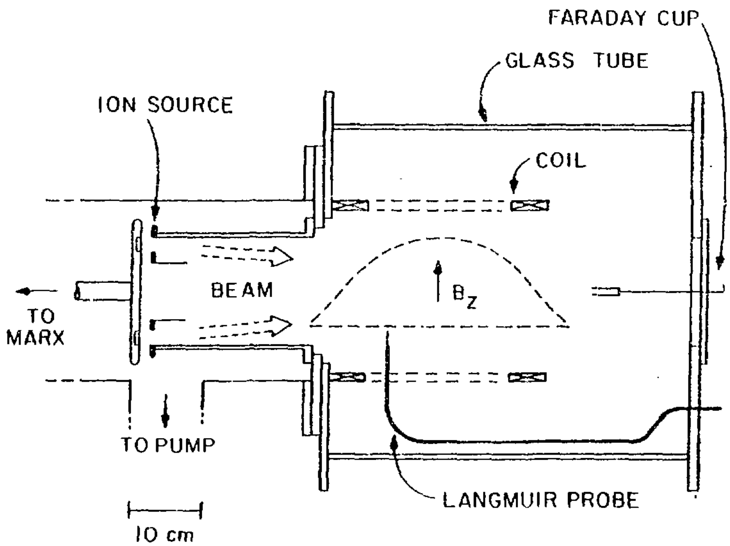

Fig. 1 Apparatus for cross-field propagation.

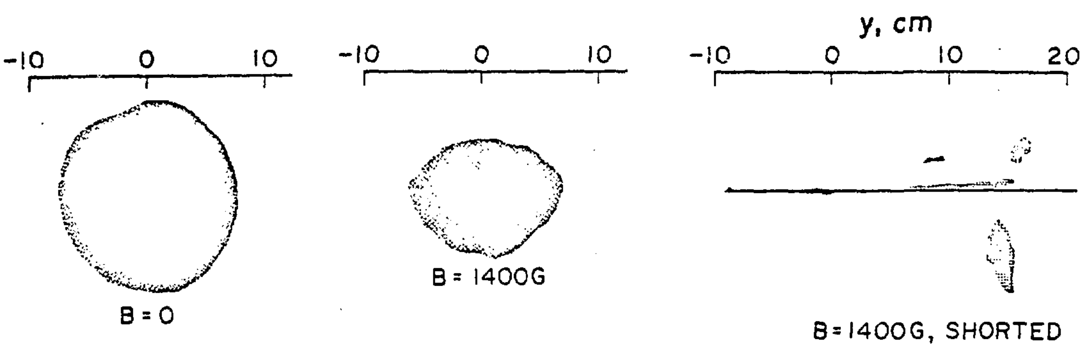

Fig. 2 Damage patterns at the downstream field boundary.

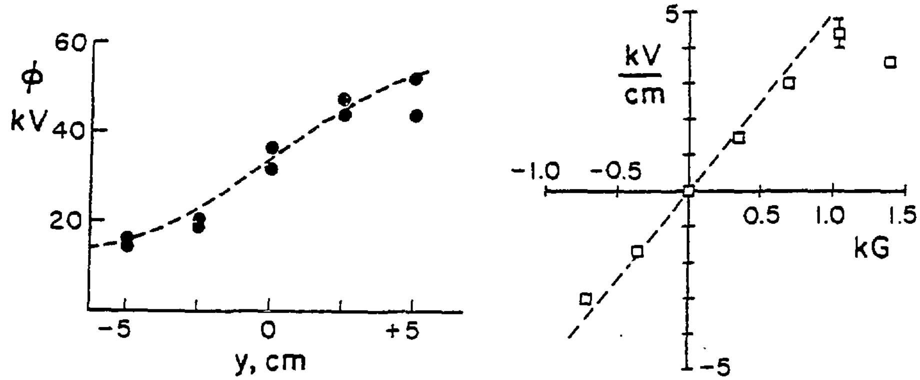

Fig. 3 Peak floating potential as a function of y (left) and peak electric field at y = 0 (left) as a function of B. The dotted line is E = - v X B.

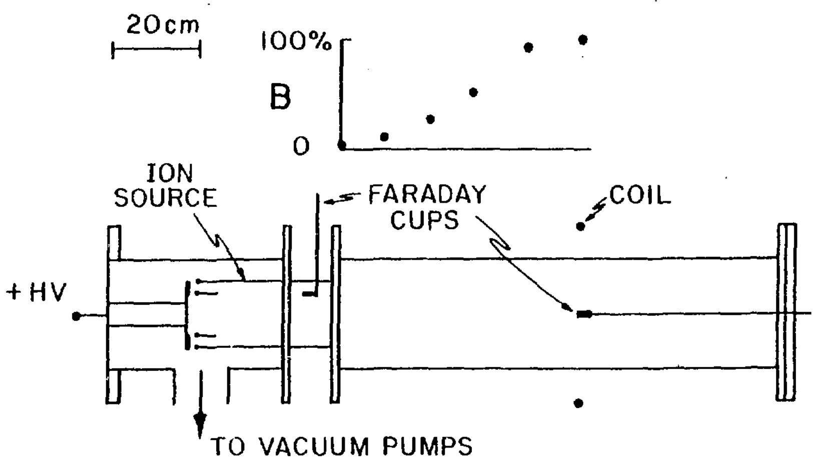

Fig. 4 Apparatus for beam compression.

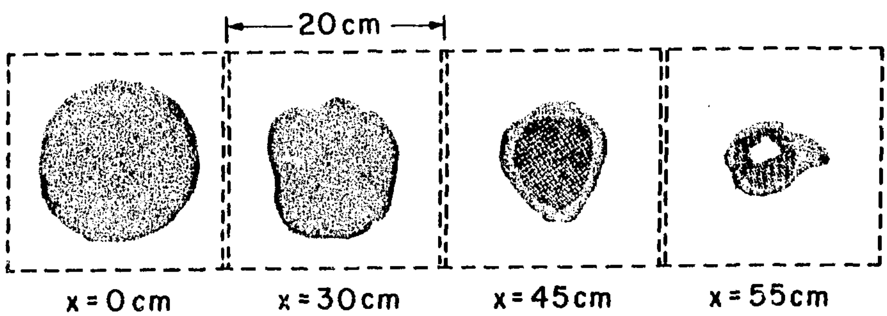

Fig. 5 Damage patterns at successsive distances into the field.

GENERATION OF A COMPACT TORUS WITH A μ-SEC ROTATING RELATIVISTIC ELECTRON BEAM

Gary Saenz
University of California, Irvine, California, U.S.A., 92717

ABSTRACT

We have observed field reversal up to 2.5 times the initial magnetic field in a plasma filled magnetic mirror by the use of a microsecond rotating electron beam. Hard X-ray measurements show the reverse fields are due to beam electrons rather than induced plasma currents.

There has been considerable interest in creating compact toroidal magnetic field geometries for confining hot plasma.[1,2] The principle advantage of a reactor design based on a compact torus or spheromak[3] is that the external magnetic field and associated plasma does not link the confinement geometry. The decay of 500 keV electron currents in a plasma density of $10^{14}/cm^3$, as calculated from the classical collision time, is on the order of 100 ms. This long lifetime together with the MHD stability of a compact torus makes the generation of this configuration with a relativistic electron beam worth investigating.

Early work at Livermore with rotating relativistic electron beams was directed toward creating stable reverse field configurations in magnetic mirrors by injecting a 200 ns burst of 600 A, 6 MeV electrons through a drift region into a magnetic well.[4,5,6] Although a trapping efficiency of 60% was achieved, field reversals of only 40% were obtained. The development of high current relativistic electron beam sources made it possible to inject single pulses of electrons (into mirrors filled with neutral gas) that contain over two orders of magnitude more charge than required for field reversal. Since then, field reversing rings have been trapped, and their lifetime extended to more than 1 ms.[7] Reverse fields from induced plasma currents have been observed when a rotating electron beam is injected into an initially neutral gas.[8] The lifetime of these configurations has been extended to 15 μs with field reversals up to 4 times the initial field. Changes in the magnetic field of 6 kG have been observed.[9]

When a rotating electron beam with rise time less than Alfvén time ($T_r << T_A$) is injected into a plasma, the induced plasma current is equal and opposite the azimuthal beam current. The plasma current is carried out of the beam channel by a magnetosonic or compressional Alfvén wave provided the Alfvén time is less than the diffusion time ($T_A < T_d$).[10] Here $T_A = V_A/r_b$, V_A is the Alfvén speed, r_b is the beam radius, $T_d = 4\pi\sigma r_b^2/c^2$, σ is the plasma conductivity and c the velocity of light. Magnetosonic oscillations have been observed when rotating beams are injected into plasma.[11,12] However, field reversal was achieved only at low plasma densities ($10^{13}/cm^3$) where the conductivity is anomalously low ($T_A >> T_d$)

and the return current decay is diffusive.[12]

In this paper we report observations of field reversal when a rotating electron beam with rise time greater than the Alfvén time ($T_r > T_A$) is injected into a plasma. When $T_r >> T_A$ we do not expect the return currents to develop and thus the reverse field will be due to the beam electrons.[13]

Figure 1 is a diagram of the experiment. A hollow electron beam is injected through a magnetic cusp to obtain a rotational energy component. It is reflected from a downstream mirror. The beam is created by a Marx generator connected to a 5 cm diameter hollow circular graphite cathode.[14] The anode foil is 25μ aluminized mylar located 5 cm from the cathode. The beam has a peak kinetic energy of 600 keV and current of 15 kA for about 1 μs. A coaxial plasma gun fills the interaction chamber with plasma prior to beam injection. $\dot{B}$ probes are located outside the beam channel at a radius of 7 cm and on axis (r=0). The hard X-rays from the beam electrons are measured by a collimated X-ray PIN diode. The plasma density is measured with a 2 mm microwave interferometer.

The change in the axial component of the magnetic field on axis and at a radius of 7 cm is shown in Fig. 2. The plasma density is 10^{14} cm^{-3}. As the rotating beam enters the system the on axis field decreases (note the polarity of the ΔB signals has been inverted) and the signal at the radius of 7 cm increases. At later times we observed oscillations that are characteristic of magnetosonic or compresional Alfvén waves. The hard X-rays last for approximately the same duration as the on axis diamagnetic signal. This is in contrast to observations with a short pulse beam, where the on axis diamagnetic signal lasts from 4 to 20 times longer than the X-ray signals.[9,12] In these experiments $T_r/T_A \simeq 1$, whereas in the short pulse experiments $T_r/T_A \simeq 0.3$. From this we conclude that the field reversal is due to the beam electrons as shown by Berk and Pearlstein[13] rather than induced plasma currents as in the short pulse experiments.

In Fig. 3 the ratio of the change in the magnetic field to the initial field at the minimum of the mirror is plotted. A peak field reversal of 2.5 is observed at a density of 3×10^{13} cm^{-3}. The shape of the curve in Fig. 3 is not yet well understood and will be investigated in future work. The peak of $\Delta B/B$ does not appear to correspond to the conditions for maximum energy transfer suggested by Chu et al.[10], namely that the beam duration equals the Alfvén time.

In summary we have observed field reversals up to 2.5 times the initial magnetic field in a plasma using a microsecond electron beam. The reverse magnetic field is due to the beam electrons, rather than induced plasma currents, as in shorter pulse beams.[11]

Work supported by the Department of Energy.

REFERENCES

1. W. C. Condit, T. Fowler, and R. Post, Status Report on Mirror Alternatives, L. L. Report UCRL-52008 (1976).
2. J. D. Sethian, K. A. Gerber, D. A. Hammer, D. N. Spector, and A. E. Robson, Bull. Am. Phys. Soc. 22, 649 (1977).
3. M. N. Bussac, H. P. Furth, M. N. Rosenbluth, 7th International Conference on Plasma Physics and Controlled Nuclear Fusion Research, Innsbruck, Austria 1978.
4. N. C. Christofilos, Phys. Fluids 9, 1425 (1966).
5. R. J. Briggs, G. D. Porter, B. W. Stallard, J. Taska. and P. B. Weiss, Phys. Fluids 16, 1934 (1973).
6. R. E. Hester, G. D. Porter, B. W. Stallard, J. Taska, C. W. Walker, and P. B. Weiss, Phys. Fluids 18, 96 (1975).
7. H. A. Davis, D. J. Rej, and H. H. Fleischmann, Phys. Rev. Lett. 39. 744 (1977).
8. C. A. Kapetanakos, W. M. Glack, and C. D. Striffler, Appl. Phys. Lett. 26, 368 (1975).
9. C. W. Roberson, D. Tzach, and N. Rostoker, Appl. Phys. Lett. 32, 214 (1978).
10. K. R. Chu, C. A. Kapetanakos, and R. W. Clark, Applied Phys. Lett. 27, 185 (1975).
11. C. A. Kapetanakos, W. M. Black, and K. R. Chu, Phys. Rev. Lett. 34, 1156 (1973).
12. C. W. Roberson, UCI Physics Department Report #77-68, to be published in Nuclear Fusion.
13. H. L. Berk and D. Pearlstein, Phys. Fluids 19, 1831 (1976).
14. F. Levine and A. Fisher, Bull. Am. Phys. Soc. 21, 1097 (1976).

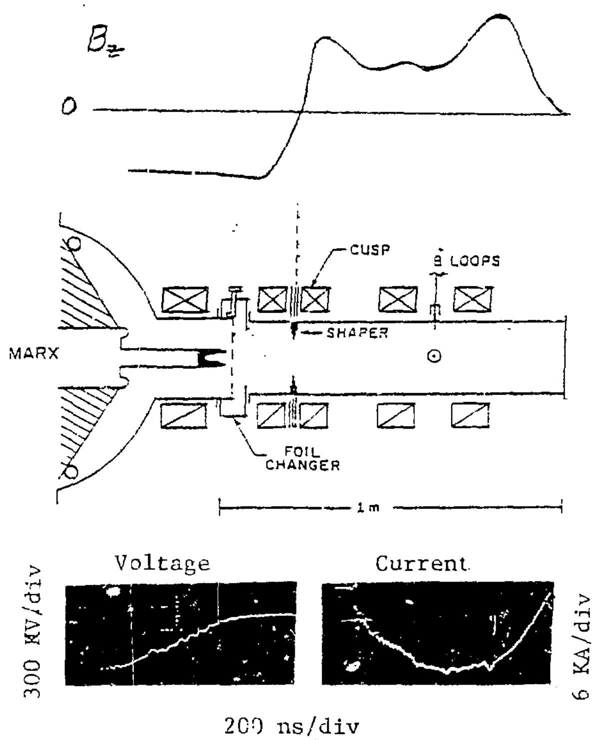

Figure 1. Diagram of Experiment

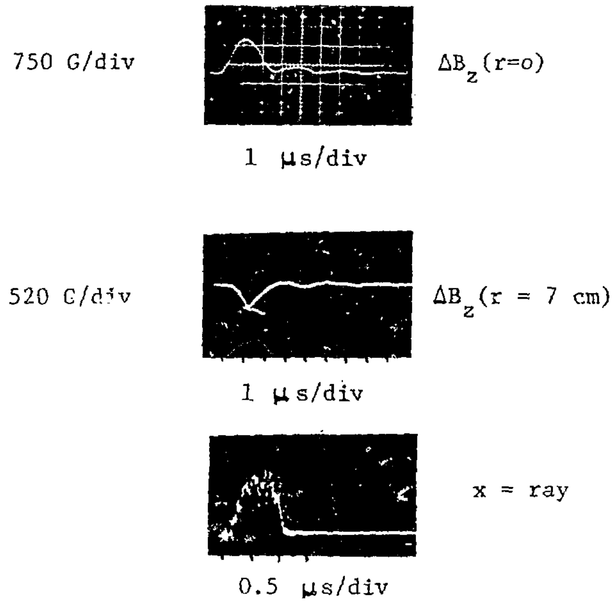

Figure 2. Scope traces; $n_p = 10^{14}cm^3$, $B_{oz} = 500$ G.

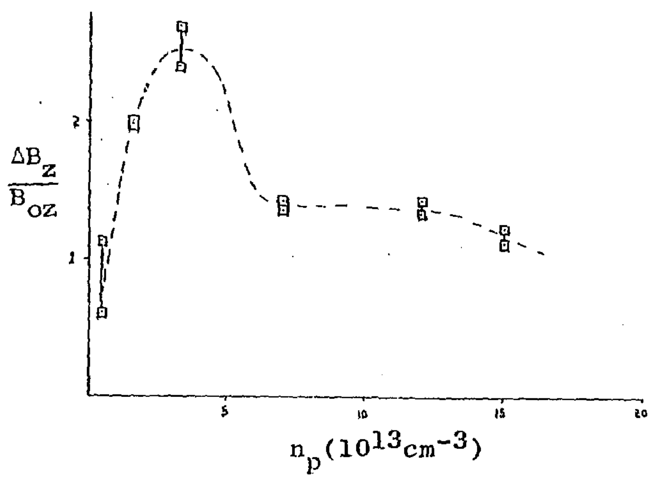

Figure 3. Change in B_z versus plasma density.

THE PROTOTYPE MOVING-RING REACTOR*

A. C. Smith, Jr., C. P. Ashworth, K. E. Abreu, D. M. Woodall†
Pacific Gas and Electric Company
San Francisco, California 94106

G. A. Carlson, W. S. Neef, Jr.
Lawrence Livermore National Laboratory, University of California
Livermore, California 94550

H. H. Fleischmann, W. Grossman, Jr.††, T. Kammash†††
Cornell University, Department of Applied and Engineering Physics
Ithaca, New York 14853

K. R. Schultz, C. P. C. Wong, D. K. Bhadra, R. L. Creedon, E. T. Cheng, G. R. Hopkins
General Atomic Company
San Diego, California 92138

Summary

We have completed a design of the Prototype Moving-Ring Reactor[1]. The fusion fuel is confined in current-carrying rings of magnetically-field-reversed plasma ("Compact Toroids"). The plasma rings, formed by a coaxial plasma gun, undergo adiabatic magnetic compression to ignition temperature while they are being injected into the reactor's burner section. The cylindrical burner chamber is divided into three "burn stations". Separator coils and a slight axial guide field gradient are used to shuttle the ignited toroids rapidly from one burn station to the next, pausing for 1/3 of the total burn time at each station. D-T-^{3}He ice pellets refuel the rings at a rate which maintains constant radiated power.

The first wall and tritium-breeding blanket designs make credible use of helium-cooling, SiC, and Li_2O to minimize structural radioactivity. "Hands-on" maintenance is possible on all reactor components outside the blanket. The first wall and blanket are designed to shut the reactor down passively in the event of a loss-of-coolant or a loss-of-flow accident.

Helium removes heat from the first wall, blanket, and shield, and is used in a closed-cycle gas turbine to produce electricity. Energy residing in the plasma ring at the end of the burn is recovered via magnetic expansion. Electrostatic direct conversion is not required for this design. The reactor produces a constant, net power of 90 MW(e).

Introduction

The objective of this work was to design a prototype fusion reactor based on fusion plasmas confined as "Compact Toruses." "Prototype" means an intermediate step between an experimental pilot plant and a lead commercial plant. We sought a design that shows promise for upgrade for commercial use.

The design calls for moving plasma rings with stationary burn cells for several important reasons: (i) The plasma burn chamber is separated from the ring-formation/heating and ring-exhaust/expansion sections. This minimizes the neutron fluence in regions outside the burner and physically segregates reactor functions, avoiding multi-purpose reactor component designs. (ii) The peristaltic and adiabatic magnetic compression brings the rings to ignition in a way which has the potential of being very efficient (and is insensitive to the low-energy ring formation efficiencies). (iii) Some variations in reactor power output can be accommodated by varying the number of identical burn modules. Because the rings are shuttled rapidly between burn stations, adjusting their "residency time" in each of the burn stations does not introduce significant time-varying thermal power to the walls. (iv) Use of multiple, moving plasma rings permits effective utilization of the ring generator and exhaust ring recovery equipment. (v) Moving the rings through the reactor greatly simplifies discharge of burn products. The reactor's linear geometry also provides an inherent divertor action.

A result of this work will be a set of physics, technology, and mechanical design criteria needed to make this concept attractive. These criteria can be used as targets for experiments and technology programs.

Six major criteria guided the prototype design. The prototype must: (1) produce net electricity decisively ($P_{net} > 70\%$ of P_{gross}), with $P_{net} \sim 100$ MW(e); (2) have small physical size (low project cost) but have a design that can be scaled up to an attractive commercial plant; (3) have all features required of commercial plants; (4) avoid unreasonable extrapolation of technology; (5) minimize nuclear issues substantially, i.e. accident and waste issues of public concern, and (6) be modular (to permit repetitive fabrication of parts) and be maintainable with low occupational radiological exposures.

The design succeeded in meeting all of these criteria except for small physical size.

General Reactor Overview

The Moving-Ring Reactor consists of three cylindrical in-line sections: a plasma ring generator and compressor; a central burner section; and a spent-ring exhaust section. Figure 1 shows the reactor.

Ring Generator, Compressor, and Expander

A hollow, coaxial plasma gun generates the compact toroids in the relatively low magnetic field (~0.26 T) 15.5 m beyond the first ring burn station. New rings are injected at ~ 2 s intervals. The hole through the inner gun electrode permits plasma diffusing from the burning rings to escape along field lines to the plasma dump and vacuum pumps located in the tank housing the gun.

The plasma rings are forced peristaltically into the 6.5 T magnetic field of the burner section by sequentially energizing compression "push coils" located between the plasma gun and the first burn station.

Compression scaling laws from MHD compact toroid equilibrium codes[2] were used to design the compressor. The principal scaling laws were $T_i \propto B$ and $\langle R_{ring} \rangle \propto 1/\sqrt{B}$. The design calls for 20 coils in the compressor. The coil radii range from 65 cm near the throat of the burner section to 320 cm near the plasma gun. The ring compression will require ~ 2-5 ms. Pulsed compressor coil currents range from 0.5 to 2.0 MA.

*Work performed for the Electric Power Research Institute under contract #RP-922.

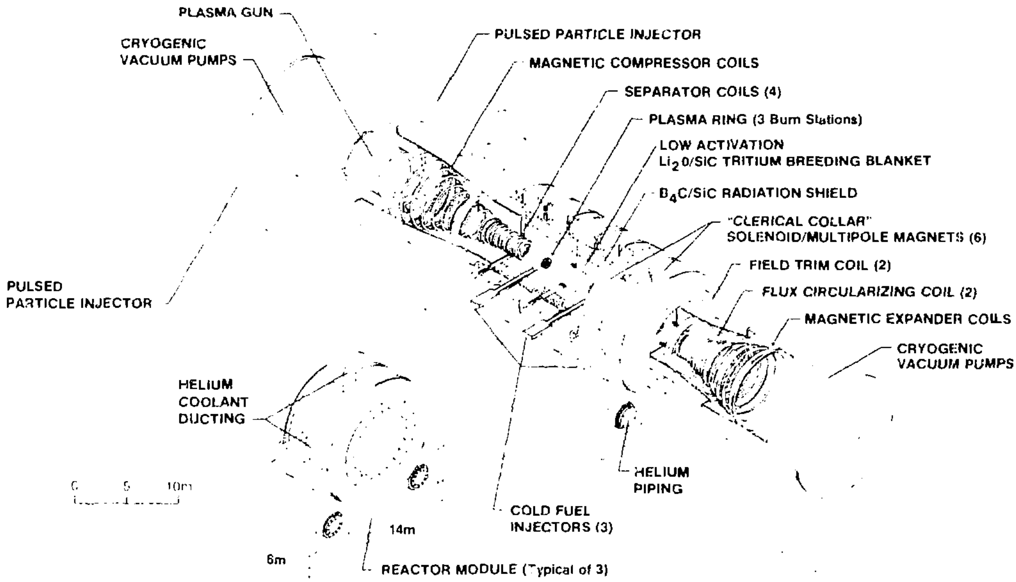

Figure 1: Overview of the Prototype Moving-Ring Reactor.

If the initial plasma temperature is assumed to be ~ 3 keV, the field compression ratio of ~ 25 will bring the plasma to the initial, ignition ion temperature of ~ 75 keV. Slotted, conducting walls are located just outside the compressor coils. These walls stabilize the plasma ring dynamically during compression against precessional/radial instabilities.

Rings of the type proposed in this reactor have been observed experimentally to "tilt" under some conditions. One of the schemes currently being considered to stabilize the tilt is to replace some of the ring's plasma current with axis-encircling particles, since this instability is not observed in purely astron-like experimental configurations. Therefore, this reactor design includes an option to "hybridize" the plasma ring with axis-encircling particles prior to the compression heating[3].

We assume that tilt-stabilization can be done with ~ 20% of the ring current carried by axis-encircling particles (i.e. "fast-particle" field-reversal ~ 40%). If protons are used, ~ 0.8 MJ beams of ~ 20 MeV particles would be required (assuming a generation/trapping efficiency of ~ 40%). The gun plasma combines with the particle ring in the region between the gun muzzle and the first compressor coil (see Fig. 1).

We calculate the overall injection and compression process efficiency (including the axis-encircling particles) to be ~ 70%.

Thermal and magnetic energy in the plasma rings at the end of the burn is recovered magnetically by 20 recovery coils in the expander section. We calculate the magnetic direct conversion efficiency to be ~ 75%.

Pulsed Plasma Burn Calculations

The 1-D Fokker-Planck transient plasma burn analysis used to model the fusion plasma has been described elsewhere[1]. We have assumed that the energy and particle confinement times are equal to the classical ion energy confinement time and that the electrons have an energy confinement time which is 1/10 of the ion energy confinement time.

The range of compact toroid characteristics which can be accommodated in the 2.5 m-bore prototype reactor is limited by first wall radiation loading and/or ring physical size. The reference design plasma is assumed to be a Field-Reversed Mirror type of plasma ring having some Spheromak-like imbedded toroidal magnetic field. We presume a magnetic/thermal energy ratio of 1/3 and an average $\langle\beta\rangle$ = 0.67 (peak β = 1.0). The supposed presence of the imbedded toroidal field permits credible investigation of a wide range of possible plasma sizes for use in the reactor.

The relative fraction of tritium in the plasma fuel mixtures was varied to investigate the increased direct-conversion output (for a given wall load) and the relaxed tritium breeding ratios possible with plasma burns "lean" in tritium. Reactor power balance considerations limited our scope of interest to ignited plasma burns lasting long enough to achieve Q = 40. As the relative fraction of tritium in the burns is decreased, the trade-offs are (1) whether the increased initial plasma sizes required for ignition lead to plasmas that no longer fit inside the first wall at the end of the burn and (2) increased total bremsstrahlung production because of higher temperatures and larger plasmas.

Based on these considerations, our burn model and assumptions predict that the prototype reactor could accommodate a burn with no less than 20% tritium. The reference design fuel mixture at the start of the burn is 20%T, 73%D, and 7%^{3}He. (The ^{3}He is in equilibrium recyclic concentration to maximize the charged particle production.) Initial plasma ion [electron] temperatures are 75 [50] keV, with an initial [final] plasma average radius of 39 [57] cm. The burn time (Q = 40) is 5.9 s. The fusion power per ring is ~ 105.5 MW.

The physical design of the reactor could accommodate poorer energy confinement than our base assumptions by up to a factor of 5 by increasing the initial tritium concentration in the burn to ~ 50%T. Under these conditions, fuel mixtures leaner than ~ 50% tritium would require plasma rings too big to fit in the 2.5 m reactor bore at the end of the plasma burn.

Axial Ring Transport

Electrically insulating materials are used throughout the first wall, blanket and shield. This greatly simplifies the plasma ring transport mechanism. An axial guide-field gradient of ~ 0.005 $T\text{-}m^{-1}$ provides force to move the rings. The rings are held in place at the burn stations (and stably separated from one another) using aluminum "separator coils" located at the midplane between burn positions.

Every ~ 2 s, each ring is rapidly (~ 0.01s-0.1s) shuttled to the next burn station (and the last ring exhausted into the expander) by sequentially tailoring the currents in the separator coils. This "musical chairs" ring translation permits the reactor to accommodate a wide range of plasma burn times without introducing the complication of time-varying wall loads.

There is an electromagnetic drag on the rings when they are moved. This arises from eddy currents induced in the superconducting coil cases and the metallic pressure vessel located radially just inside the superconductor coils. This drag has been calculated and is negligible.

Low-Activation First Wall, Blanket, and Shield

Materials. Silicon carbide was selected as the primary component of the first wall, blanket, and shield to (1) minimize induced radioactivities, (2) eliminate the possibility of first wall-blanket meltdown in the event of a loss-of-coolant accident, and (3) eliminate the presence of electrically-conducting materials near the rings to minimize the electromagnetic drag when the rings are translated. SiC is stable under neutron irradiation, has high thermal conductivity, and has low tritium permeability at temperatures below 1000 C.

Li_2O is the tritium breeding material.

High pressure helium (28 atm) is the high temperature coolant because of its chemical inertness and transparency to neutrons.

Mechanical Design. Twenty-four wedge-shaped lobes nest inside the cylindrical coolant pressure vessel to make up the first wall, blanket, and shield structure in each of the three 6 m-long burner modules (see Fig. 1). Figure 2 shows a cutaway view of one of the lobes.

The 1.4 m thick SiC/B_4C shield is secured to the pressure vessel. Penetrating through the shield into the front region of the lobe is a "forest" of small (2.1 cm diameter), concentric-feed, high-pressure SiC coolant tubes, 3.5 cm center-to-center. These tubes remove the heat from the Li_2O while an independent, 1 atm helium stream purges the tritium from the 0.6 m thick breeding zone. The blanket-shield assembly is encased in a SiC "bathtub" clamped at its base to the pressure vessel. The "bathtub's" curved, first wall surface is 0.6 cm thick; the sidewalls thickness is 2.0 cm. Using ceramics in this fashion is credible because the large SiC structure supports little load beyond its own weight.

The 1.4 m SiC/B_4C shield thickness is more than adequate to protect the superconducting magnet through

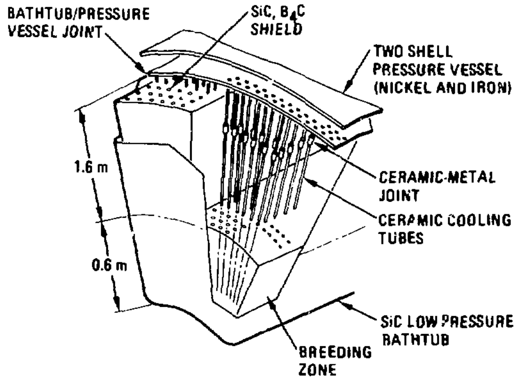

Figure 2. Low-activation blanket/shield module.

the reactor life. Occasional annealing of the Cu-stabilizer is not necessary.

Helium coolant ducts loop over the axial sections of the clerical collar guide field coils to provide the coolant routing to the main helium piping located in the base of each reactor module.

Neutronics. The Li_2O/SiC breeding zone is 0.6 m thick with a 0.2 m thick SiC reflector. The Li_2O high temperature zone has a volume fraction of ~ 57%. The total blanket energy multiplication is 1.19 while the tritium breeding ratio is 1.09 (considerably more than the 0.9 T/n required for the 20% tritium plasma burn).

The impurity level in the materials was assumed to be ~ 1 ppm. The average wall load of 1.7 $MW\text{-}m^{-2}$ results in a dose rate just outside the breeding zone of ~ 0.4 $mrem\text{-}hr^{-1}$ and a dose rate just outside the shield of << 2.5 mrem-hr one day after shut-down. Therefore, "hands-on" maintenance is possible on all components outside the blanket. The dose rate inside the vacuum chamber is ~ 0.2 $rem\text{-}hr^{-1}$, making contact maintenance in this region impossible.

Magnetic Field Design

The graded, axial guide field in the reactor's burner section is produced by a set of 6 NbTi superconducting coils. A radial magnetic well is produced by adding a set of eight alternating bends to the coils. We've dubbed the resulting shape the "Cleric Collar" coil. The rectangular superconductor current bundles are 0.45 m × 1.74 m and the average coil radius is 5 m. The 1.9 m longitudinal segments used in this design provide the radial magnetic well. With the separator coils energized, the radial well depth is ~ 0.4% at ~ 1 m. The axial field is nominally 6.5 T, with an axial gradient of ~ 0.005 $T\text{-}m^{-1}$.

The elliptical magnetic flux bundles leaving the reactor are circularized by auxilliary superconducting coils located at each end of the guide field coil set.

The four separator coils which maintain the plasmas in their burn positions have an average radius of 1.5 m. The water-cooled conductor bundles are 18 cm × 18 cm. The coils are encased in a 25 cm-thick SiC neutron shield to prevent afterheat meltdown of the aluminum-alloy conductor in the event of a LOCA/LOFA.

Vacuum System

Arrays of liquid-helium-cooled cryopanels vacuum-pump the reactor. These panels, located in the two end tanks, are specially designed to pump helium as well as deuterium and tritium. The hydrogen isotopes are cryocondensed. The helium is cryotrapped in argon sprayed directly onto the cryopanels.

Different amounts of pumping are required at the two ends of the reactor. The refueled plasma rings are ignited and confine the fusion fuel well. Large amounts of gas will be released in the exhaust end of the reactor as the rings complete their burns. On the other hand, the injector end of the reactor must pump only half of the effluent which has diffused out of the rings during the burn.

We calculate the molecular gas loads to be 2 and 15 torr-liter-sec^{-1} at the injector and exhaust ends of the reactor, respectively. The optimum argon spray rate for our design is ~ 30 argon atoms/helium atoms pumped. The total cryopanel areas required are 13 and 89 m^2 at the injector and exhaust ends, respectively. At any one time, 2/3 of the cryopanels are pumping while the remaining 1/3 are defrosting.

Pellet Refueling

The plasma rings are continuously refueled with D-T-^{3}He pellets at a rate which maintains constant total radiated power/ring (neutrons + bremsstrahlung). The relative concentrations of D-T-^{3}He in the refueling pellets are identical to the fuel composition of the plasma at the start of the burn. The average plasma density of ~ 5×10^{14} cm^{-3} and temperature of ~ 75 keV require a pellet velocity of ~ 10^7 cm-sec^{-1}. The 0.09 cm-radius pellets are accelerated by ablation using a CO_2 laser. The total refueling power is ~ 0.14 MW/ring.

Power Conversion System

Electricity is produced from the reactor's thermal output by a closed-cycle gas turbine. The thermal power cycle lends itself to dry-cooling without economic penalty. The hot, high-pressure helium (750 C, 28 atm) is ducted to the gas turbine located behind a shield wall inside the containment.

The reactor power flows are summarized in Figure 3. The reactor nets 90 MW(e) with an overall efficiency η ~ 25%. Clearly, slightly better performance (i.e. η ~ 30%) could be obtained by electrostatic direct conversion of the effluent plasma stream. However, since this does not turn out to be necessary for attractive performance of the commercial upgrade of this reactor, we decided not to add this feature (and complexity) to the design.

Reactor Safety Issues

Reactor safety played a major role in the prototype reactor design. The chief safety elements in the design are:

- First wall overheating from a LOCA/LOFA will terminate the fusion plasma burn by melting silicon safety plugs in SiC first wall.
- Meltdown of the first wall and blanket is precluded by design and choice of materials--even under total loss of convective cooling. Meltdown of the aluminum-alloy separator coils is avoided by the 25 cm-thick SiC radiation shield which completely encases the coils.
- Single, high-pressure SiC coolant tube failure will not cause chain failure during operation if coolant flow can be maintained. The resulting lobe pressurization can be handled by safety-release-and-shut-down systems.
- Hands-on maintenance can be performed outside the blanket of a removed burner module when plasma chamber end-shields are in place.
- SiC is an excellent tritium barrier for temperatures less than 1000 C.
- No high-level waste is produced.

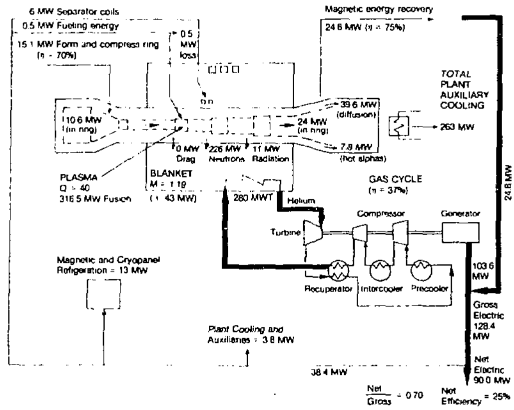

Figure 3. Prototype reactor power flows.

Reactor Design Summary

The prototype reactor met all of the design criteria except small physical size. With our present knowledge of materials, we could not satisfy simultaneously the needs for minimal radiological hazard in the reactor and small physical size.

Based on the current plasma burn model and assumptions, the initial fraction of tritium in the prototype plasma burn can be no less than 20% because of the dual constraints of permissible ring physical size and surface wall loading. We view this fuel mixture as a step toward larger bore commercial reactors. Fuel mixtures leaner in tritium may require direct cooling of the first wall to handle bremsstrahlung surface loading.

The current plasma burn model and assumptions indicate that acceptable prototype reactor performance requires near-classical confinement of the ion energy (assuming the electron energy confinement is no worse than 1/10 × classical ion energy confinement).

The step-wise translation of the plasma rings allows the reactor to accommodate a wide range of plasma burn characteristics (such as burn time and β).

The reactor design achieves several features of importance to potential users: (i) The ~ 90 MW(e) net output is a reasonable stepping-stone reactor size in a development program leading to a larger commercial upgrade plant; (ii) It minimizes nuclear issues (minimial component radioactivity, no possibility of meltdown, no high-level wastes); (iii) The commercial upgrade has the potential of increased direct-conversion output for a given thermal size; (iv) Use of dry-cooling in the thermal power cycle permits reactor siting flexibility; (v) The direct gas cycle cuts containment building pressure by a factor of ~ 10; (vi) The reactor's linear, modular design simplifies maintenance.

References

†University of New Mexico, Albuquerque, NM 87131
††New York University, New York, NY 10012
†††University of Michigan, Ann Arbor, MI 48109

[1] A. C. Smith, Jr., et al., The Moving-Ring Reactor, EPRI Final Project Report, Contract RP922 (1981) [to be published].
[2] W. Grossman, Jr., et al. (to be published).
[3] H. H. Fleischmann, et al., Joint U.S./Japan Symposium on Compact Toroids, Princeton, NJ (1979).

REVIEW OF JAPANESE CT STUDIES

Kenji WATANABE

Course of Electromagnetic Energy Engineering
Faculty of Engineering, Osaka University
Yamada-oka 2-1, Suita, Osaka 565, Japan

1) INTRODUCTION

At present, studies of the CT plasma are being carried out by nine groups in Japan. Number of studying groups is increasing. Works are listed in the Table. As is well known, fundamental studies of plasma in Japan have been carried out 25 years by rather small groups of many universities except a few institutes, so the CT study is also the case because the study is still a fundamental one. Study program in Japan has not yet arranged on gathering and systematizing various groups.

Historical point of view, which helps understanding group character for study in long time, gives the following study trend of various groups: Group (A), (B) and (C) in the Table are working on the reversed field theta pinch, mainly studying the rotational instability and sometimes trying an inclusion of toroidal magnetic field in addition to the poloidal one. Group (D) came from a collision and compression experiment of conical theta pinch gun plasmas and is now working on the CT plasma formation in a flux conserver by injecting the magnetized coaxial gun plasma. Group (E) has been working on a SPAC series of new type torus plasma generation, mainly using the REB technique, and now is making the SPAC VI DR experiment of beam ring plasmas and their merging. Theoritical and/or simulation works on spheromak physics and its reactor by Group (F) and (G) are considered to be in the preliminary stage and working on a double spheromak plasma merging in close collaboration with Princeton peoples. On the other hand, however, a working group named Group (J) of the moving ring reactor design is proceeding forward for two years supported by the Grant-in-Aid for fusion research by MOE Japan. A work by Group (I) contributes to the working group, just described. It is also noticed that a trial of getting exact solutions of CT equilibrium with finite p in a drum-type flux conserver are proceeded by Group (H).

By the way, the view point of CT reactor concept does not control present experiments as a whole, but is recognized to point out important factors to be studied in a proceeding of experiments. Every experiments are carried out rather in a fundamental plasma physics itself, far observing the possibility to get the fusion plasma with the same plasma configuration as the tokamak. Nevertheless, the CT study is recognized as a study of the tokamak reactor-core plasma improvement from the feedback-collaboration between tokamak reactor core and the associated reactor technologies, i.e., a plasma study corresponding to the need from the associated technologies in order to simplify the tokamak reactor installation without toroidal facilities.

2) Study Proceeding and Results

The CT studies are conveniently classified in two groups, the first being on the toroid with both toroidal field, B_t, and poloidal field, B_p, and the second being on the prolate toroid with only B_p, that is, the reversed field theta pinch.

i) Studies of compact toroid with B_t and B_p, carried out recent one year in Japan, is considered concentrated on a merging of two CT plasmas, although they have not previously arranged with one another. Three works are summarized here, one is simulation and another two are experiments.

The simulation work by Groups (F) and (G), which is presented in the poster session[1], concerns with a merging of double spheromak plasma. Let's consider that a pair of spheromak facilities are arranged separated a distance apart in the symmetric axis, and is additively set the third conducting current core between them. The third one supplies a poloidal field which separates apart the two growing spheromaks in the initial stage, and then decreases to merge two completely-grown spheromaks with each other. Simulation is carried out by a twodimensional MHD code with the finite Alfven velocity. The results show that the same two spheromaks, each with poloidal and toroidal fluxes, Φ_p and Φ_t, are really merged, and results in the one with the doubled toroidal flux, $2\Phi_t$, and unchanged poloidal flux Φ_p. The case is also studied that initial spheromaks have different Φ_p's with each other. It is also found that the merging process depends strongly on the plasma resistivity.

A reactor consideration based on the spheromak merging is given.

The first work of the merging experiment by Group (D), which is presented in poster session too[2], is carried out using the CT formation method by the magnetized coaxial gun-plasma injection into the flux conserver. Two CT plasmas are produced successively in time in the identical conserver and merged with each other: A magnetized plasma gun is operated succesively two times in 80 μs. The first operation produces the normal, single CT in the flux conserver as the usual way, employed by Osaka, LANL and LLNL groups. 80 μs is long enough for the CT to reach the fundamental mode equilibrium state. This is considered as the target plasma, onto which the second gun plasma is injected. The result of magnetic field measurements shows that the merging is really observed and core parts of both plasmas take rather long time, i.e., about 100 μs for the merging to be completed, although the periphery parts of them merge together quickly. The merged state observed is estimated showing that the poloidal flux is unchanged and the toroidal field results in doubled, being consistent with the simulation result described above. This experiment, however, could not result in any further heating of the first CT, unfortunately.

The second experiment by Group (E), is now installing a large apparatus, called SPAC VI DR, which makes two beam-plasma-ring transportations and their merging with controlled relative velocities. The machine is expected to start operation next March. Preliminary experiments of plasma ring production has successfully been made with REB. This work is recognized as a fundamental experiment of the moving ring reactor.

A design calculation by Group (I) gives a result of the conveyer type moving ring reactor. A 600 MWt reactor is designed with the envisaged overall efficiency of about 35 % including efficiencies of ring formation and the magnetically coupled energy recovery of the ring at the reacter end.

ii) As for the reversed field theta pinches without B_t, a summary of works by (A), (B) and (C) groups is given in the poster session[3]. The rotational instability has not been understood enough yet, so a scaling law study is attempted upon experimental results, on including an idea from the tokamak scaling. The result, that τ_s is proportional to $nr_s l_p L$, seems plausible, where τ_s, r_s, l_p, L are the stable time, the separatrix radius of plasma column, the plasma column length and the length of compression coils, respectively.

REFERENCES

1) M. Katsurai et al., A17 in Poster Session of this symposium,
2) K. Watanabe et al., ibid., B3,
3) Y. Nogi et al., ibid., A3.

ACTIVITIES OF CT-STUDY GROUPS IN JAPAN

	Members	Present work	Future planning
(A) Nihon University	H.Yoshimura S.Hamada S.Shiina K.Yokoyama Y.Nogi S.Shimamura K.Saito Y.Osanai	Reversed field theta pinch (Rotational instability, Inclusion of toroidal magnetic field in addition to the poloidal one)	Operation of theta pinch machine to confirm L^2 - scaling
(B) Institute of Plasma Physics, Nagoya	K.Hirano Y.Aso S.Himeno S.Yamaguchi	Reversed field theta pinch with end magnetic field (Rotational instability)	
(C) Osaka University Plasma Physics Lab.	H.Ito T.Ishimura S.Ohi S.Goto Y.Ito S.Okada M.Tanjo T.Minato	Reversed field theta pinch (Rotational instability)	Translation of theta pinch plasma
(D) Osaka University Course of Electro-magnetic Energy Eng.	K.Watanabe T.Uyama M.Nishikawa N.Satomi A.Ozaki K.Ikegami	CT plasma formation in a flux conserver by injecting the magnetized coaxial gun plasma Merging experiments of two CTs	Behavior of plasma injected to cryo-conserver by the magnetized gun with cryo-electrodes
(E) Institute of Plasma PHysics, Nagoya	A.Mohri K.Narihara Y.Tomita T.Tsuzuki M.Hasegawa	Plasma ring formation by beam injection	Merging experiments of two rings (SPAC-VI DR)
(F) Hiroshima University Inst. Fusion Theory	T.Sato	Physics of spheromak merging	
(G) University of Tokyo Dept. of Electronic Eng.	M.Katsurai K.Katayama T.Sato	Spheromak fusion reactor using merging operation	
(H) University of Tokyo Dept. of Applied Physics	S.Kaneko	Trials of getting exact solution of MHD equilibrium in CT	
(I) Kyoto University Inst. Atom. Energy	K.Yoshikawa M.Ohnishi H.Murashima H.Matsuoka	Conceptual design study of a moving reactor	
(J) Reactor Design Group supported by Grant-in-Aid for fusion research by MOE Japan		1st step of design on moving ring reactor	

CONFERENCE ATTENDEES

Amherd, N. A., EPRI
Anderson, D. V., LLNL
Armstrong, W. T., LANL
Auerbach, S. P., LLNL
Bailey, V. L., PSI
Barnes, C. W., LANL
Bartsch, R. R., LANL
Bellan, P., Caltech
Boyd, J. K., LLNL
Brandenburg, J. E., LLNL
Bruhns, H., Univ. of Maryland
Cary, J. R., Univ. of Heidelberg
Cayton, T. E., LANL
Chrien, R., LANL
Chu, C. K., Columbia Univ.
Cochrane Jr., J. C., LANL
Cohen, B. I., LLNL
Condit, W. C., Westinghouse Electric Co.
Devoto, R. S., LLNL
DiMarco, J., LANL
Dobrott, D. R., Science Applications, Inc.
Dove, W. F., USDOE
Finn, J., Naval Research Lab.
Fisher, A., Univ. of California, Irvine
Fleischmann, H. H., Cornell Univ.
Gerwin, R., LANL
Goldenbaum, G. C., Univ. of Maryland
Greenly, J. B., Cornell Univ.
Hameiri, E., New York Univ.
Hammer, J. H., LLNL
Harned, D. S., Univ. of California, Berkeley
Hartman, C. W., LLNL
Hayworth, M., LANL
Henins, I., LANL
Hewett, D. W., LANL
Hoffman, A. L., Mathematical Sciences Northwest, Inc.
Hoida, H. W., LANL
Janos, A., PPPL
Jarboe, T. R., LANL
Jardin, S. C., PPPL
Jaykumar, R., Cornell Univ.
Jensen, T. H., Public Service Electric and Gas Co.
Katsurai, M., Univ. of Tokyo
Kerbel, G. D., LLNL
Killeen, J., LLNL
Kim, J-S., LBL
Knox, S. O., LANL
Koloc, P. M., Prometheus II, Ltd.
Krall, N. A., Jaycor
Langford, J. M., USDOE-SAN
Lewis, H. R., LANL
Lilliequist, C., LANL
Linford, R. K., LANL
Lipson, J., LANL
Morikawa, G., N.Y. Univ.
Marshall, J., LANL
McCoy, M. G., LLNL
McKenna, K. F., LANL
McNally Jr., J. R.
Milroy, R. D., Mathematical Sciences Northwest, Inc.
Mirin, A. A., LLNL
Mohri, A., Nagoya Univ.
Moses, R. W., LANL
Munson, C., PPPL
Nogi, Y., Nihon Univ., Tokyo
Paul, S., PPPL
Pickles, W., LLNL
Pietrzyk, Z. A., Univ. of Washington
Platts, D. A., LANL
Post, D. E., PPPL
Post, R. F., LLNL
Prono, D. S., LLNL
Rej, D. J., LANL
Ribe, F. L., Univ. of Washington
Robertson, S., Univ. of California, Irvine
Robson, A. E., Naval Research Lab.
Saenz, G., Univ. of California, Irvine
Sato, T., Hiroshima Univ.
Schnack, D., LANL
Schwarzneier, J. L., LANL
Sessler, A. M., LBL
Sethian, J. D., Naval Research Lab.
Sevillano, E., Univ. of Washington
Seyler, C. E., Cornell Univ.
Sgro, A. G., LANL
Shearer, J. W., LLNL
Sherwood, A. R., LANL
Shestakov, A. I., LLNL

Shumaker, D. E., LLNL
Siemon, R. E., LANL
Smith, A. C., PG&E
Spencer, R. L., LANL
Steinhauer, L. C., Mathematical Sciences Northwest, Inc.
Sun, Y. C., PPPL
Tang, W., PPPL
Teofilo, V. L., Physics International Co.
Turner, W. C., LLNL
Tuszewski, M. G., LANL
Uyama, T., Osaka Univ.
Vlases, G. C., Univ. of Washington
Watanabe, K., Osaka Univ.
Wright, B. L., LANL
Wysocki, F., PPPL
Yamada, M., PPPL
York, T. M., Pennsylvania State Univ.

Work performed under the auspices of the U.S. Department of Energy by the Lawrence Livermore National Laboratory under Contract W-7405-Eng-48.

Technical Information Department · Lawrence Livermore Laboratory
University of California · Livermore, California 94550